Characterization of Atg18p and its role in cellular trafficking in *Saccharomyces. cerevisiae*.

By

Samira Khaliq

0914181

A thesis submitted to the University of Birmingham for the degree of DOCTOR OF PHILOSOPHY

School of Biosciences
College of Life and Environmental Sciences
University of Birmingham
B15 2TT

Oct 2012

Supervisors: Dr Stephen K. Dove, Dr F. Michelangeli and Professor Robert H. Michell

ABSTRACT

Phosphoinositides are a group of signaling lipids in eukaryotic cells, which mediate trafficking through various cargo specific pathways, stress responses, autophagy and pathogen detoxification via spatio-temporal regulation of effector proteins.

PtdIns3*P* serves as a precursor to PtdIns(3,5)P_2 and in *S. cerevisiae* one type III, PI 3-Kinase (Vps34p) and one PI(3)*P*-5 Kinase (Fab1p) have been identified. Though it has been some time since the discovery of PtdIns(3,5)P_2 yet it's cellular role I not completely understood. The synthesis and degradation of PtdIns(3,5)P_2 is highly regulated and is known to affect vacuolar morphology and trafficking pathways converging at the yeast vacuole in multiple ways. Recent findings also link PtdIns(3,5)P_2 turnover with PtdIns5*P* synthesis, and therefore some of the functions associated with PtdIns(3,5)P_2 may invariably be PtdIns5*P* functions.

A number of PtdIns3*P* and PtdIns(3,5)P_2 binding effector proteins have been identified and Atg18p, a yeast PROPPIN, is one such protein which is relatively uncharacterized.

This study focuses on characterization of Atg18p in order to gain insight into its functions. It shows through investigations of *in vivo* localization of GFP tagged Atg18p and Vac7p, that Vac7p might be one of the factors which contributes towards Atg18p *in vivo* localization and therefore Atg18p localization is under the dual control of lipid binding as well as protein interactions.

In vivo and *in vitro* study of Atg18p mutants (in the highly conserved lipid binding domain) indicates that Atg18p lipid binding is slightly distinct from *K. lactis* Hsv2p lipid binding. In addition, Fourier transform ion cyclotron resonance mass spectrometery (FT-ICR-MS) data reveals that Atg18p-lipid binding could be affected through possible modifications. These modifications putatively alter the localization via affecting lipid binding in a specific signal mediated manner.

The experiments carried out in this research also show that Atg18p binds Vps41p and Apl5p independently, through particular sites which overlap its lipid binding domain and hence offers a plausible explanation for *in vivo* localization of Atg18p during various processes e.g salt stress and autophagy.

This study also suggests a plausible role of PtdIns(3,5)P_2 in multi-vesicular body (MVB) sorting, retrograde trafficking from the vacuole to pre-vacuolar endosome (PVE) and regulation of vacuole morphology via mediating Doa4p, Vac7p and Atg18p localizations.

Hence Atg18p localization seems to be a highly regulated process, affected by both lipid binding and protein-protein interactions.

Acknowledgements

I would like to express my sincere gratitude to the following (in order of descend).

- All Mighty Allah for giving me this opportunity and helping me to cope through all the stresses and making me resilient.
- Mrs S.Khaliq, my Mother, for all her patience, upbringing and for giving me half of her genes and Mr A.Khaliq (late), my Father, for all his love and affection and of course, the second set of genes.
- Mr M.Kashif, my Brother, for all his enthusiasm, motivation and generous support.
- Dr F.Michelangeli, Dr S.K.Dove, and Prof R.H.Michell, my supervisors, for all the wonderful things they helped me to learn and also for their patience with me.
- HEC and UOB, the funding agencies, which helped pay all the bills.
- All my friends and colleagues for their never ending support.
- And Cookie (my cat) not mine any longer; loves my mom now.

DEDICATION

To my beloved parents, brother and all my teachers!

CONTENTS

Standard yeast nomenclature is used in this dissertation. Examples of abbreviations used are as follows:

Gene (dominant)	*ATG18*
Gene (recessive)	*atg18*
Point Mutation	H244R (where H is the amino-acid residue in the wild-type protein while R is the substituted amino acid in the mutant).
Protein (wild type)	Atg18p
Protein (mutant)	$Atg18p^{H244R}$
Gene knockout (deletion-Marker)	*atg18::KANMX6*
Gene Knock In (Tag-Marker)	*ATG18-3HA:HIS3*

Standard lipid nomenclature is used in this dissertation. Numbering of phosphate groups on Inositol head group in PPINs are as follows:

D3: Inositol head phosphorylated at 3 position e.g PtdIns3*P*

D3 and D5: Inositol head phosphorylated at postions 3 and 5 e.g PtdIns(3,5)P_2

List of Abbreviations

Abbreviation	Definition
α-SNAP	Alpha N-ethylmaleimide-sensitive factor attachment protein
AKT	AK (mouse strain) Thymoma (named after)
ALP	Alkaline Phosphatase
Amp	Ampicillin
ANTH Domain	AP180 N-Terminal Homology domain
AP 1 Pathway	Adaptor 1 pathway
AP 2 Pathway	Adaptor 2 pathway
AP 3 Pathway	Adaptor 3 pathway
APS	Ammonium per sulphate
ATP	Adenosine tri phosphate
BAR Domain	Bin–Amphiphysin–Rvs domain
BSA	Bovine Serum albumin
C2 Domain	Cell membrane / Ca^{++} domain
$CaCl_2$	Calcium chloride
CCT domain	Constans CO-like, and TOC1 domain
Chmp	Chloramphenicol
CMT syndrome	Charcot-Marie-Tooth disease
Co-IP	Co-immunoprecipitation
CORVET complex	Class C core vacuole/endosome tethering complex.
CPS Pathway	Carboxypeptidase S Pathway
CPY Pathway	Carboxypeptidase Y Pathway
CVT	Cytosol to vacuole transport/trafficking
DAG	Diacylglycerol
dATP	deoxy adenosine tri phosphate
dCTP	deoxy cytosine tri phosphate
dGTP	deoxy guanosine tri phosphate
DIC	Differential interference contrast
DMSO	Dimethyl Sulfoxide
DNA	Deoxy ribonucleic acid
dNTP	deoxy nucleotide tri phosphate
DTT	Dithiothreitol
dTTP	deoxy thymidine tri phosphate
DUBs	De ubiquitination enzymes
E.coli	*Escherichia coli*
ECL	Enhanced Chemiluminescence
EDTA	Ethylenediaminetetraacetic acid
EEA	Early Endosome antigen
EGF	Epithelial Growth Factor
EGFR	EGF receptor
ENTH Domain	Epsin N-Terminal Homology domain
ER	Endoplasmic reticulum
ESCRT	Endosomal Sorting Complex Required for Transport
FM4-64	N-(3-triethylammoniumpropyl)-4-(4-diethylaminophenylhexatrienyl) pyridinium dibromide
FPLC	Fast Protein Liquid Chromatography
FYVE Domain	Fab1-YOTB-VAC1-EEA1 (named after the 4 proteins first identified with this domain)

g	Grams
x g	Gravitational force
G418	Geneticin
GFP	Green fluorescent protein
GRAM Domain	Glucosyltransferases, myotubularins and other membrane-associated proteins (named after)
GST	Glutathione S transferase
GTPase	Guanosine tri phosphatase
HA	Hemagglutinin
HEAT repeat domain	Huntingtin, elongation factor 3 (EF3), protein phosphatase 2A (PP2A), and the yeast PI3-kinase TOR1 (first identified in)
HEPES	4-(2-hydroxyethyl)-1-piperazineethanesulfonic acid
HOPS	Homotypic fusion and protein sorting
HPLC	High performance liquid chromatography
Hr	Hour
HRP	Horse radish peroxidase
IMPase	Inositol mono phosphatase
IP_3	Inositol 1,4,5-trisphosphate
IP_4	Inositol 1,4,5,6-tetrakisphosphate
IP_5	Inositol 1,3,4,5,6-pentakisphosphate
IP_6	Inositol 1,2,3,4,5,6-hexakisphosphate
IP_7	Diphosphoinositol pentakisphosphate (“PP-IP5 ”)
IP_8	Bis-diphosphoinositol tetrakisphosphate (PP)2-IP4
IPs	Inositol polyphosphates
IPTG	Isopropyl β-D-1-thiogalactopyranosid
KAN	Kanamycin
KCl	Potassium chloride
K_d	Dissociation constant
KH_2PO_4	Potassium dihydrogen phosphate
KOH	Potassium hydroxide
LB	Luria-Bertani media
LC 3 compartment	Microtubule-associated protein light chain 3
LC-CID-FT MS	Liquid chromatography-Collision induced dissociation-Fourier transform-Ion cyclotron resonance-Mass spectrometry
M6R	Mannose 6 receptor
MAPK	Mitogen-activated protein kinase
MES	2-(N-morpholino)ethanesulfonic acid
$MgCl_2$	Magnesium chloride
MHC 1	Major Histo-compatibility complex 1
min	Minutes
MTMR	Myotubularin related protein
mTOR	Mammalian target of Rapamycin
MVB	Multi-vesicular body
myc	Protein tag derived from *c-myc* protein
Na_2HPO_4	disodium hydrogen phosphate
NaCl	Sodium chloride
NADPH	Nicotinamide adenine dinucleotide phosphate
NaOH	Sodium hydroxide

$(NH_4)_2SO_4$	Ammonium sulphates
NLS	Nuclear localization signal
NSF	N-ethylmaleimide sensitive factor
OD_{600nm}	Optical density at 600nm
ORF	Open Reading frame
PA	Phosphatidic Acid
PAGE	Poly acrylamide gel electrophoresis
PAS	Pre Autophagosomal structure
PBS	Phosphate buffered saline
PBST	Phosphate buffered saline with Tween 20
PCR	Polymerase chain reaction
PEG	Polyethyleneglycol
PH Domain	Pleckstrin homology domain
PI / PtdIns	Phosphatidylinositol
PIP_2	Phosphatidylinositol bis phosphate
PIP_3	Phosphatidylinositol tris phosphate
PKB	Protein kinase B
PLC	Phospholipase C
PM	Plasma Membrane
PMN	Peacemeal nucleophagy
PMSF	Phenylmethanesulfonyl fluoride
POPC	1-*palmitoyl*-2-oleoyl-glycero-3-phosphatidyl Choline
POPE	*Palmitoyl-oleoyl*-phosphatidyl Ethanolamine
PPIn	Polyphosphoinositide
PROPPINs	β-propellor phosphoinositide binding proteins
PIPs	Phosphoinositides
PtdIns(3,4)P_2	Phosphatidylinositol 3,4-bisphosphate
PtdIns(3,4,5)P_3	Phosphatidylinositol 3,4,5-trisphosphate
PtdIns(3,5)P_2	Phosphatidylinositol 3,5-bisphosphate
PtdIns(4,5)P_2	Phosphatidylinositol 4,5-bisphosphate
PtdIns3*P*	Phosphatidylinositol 3-phosphate
PtdIns4*P*	Phosphatidylinositol 4-phosphate
PtdIns5*P*	Phosphatidylinositol 5-phosphate
PTEN	Phosphatase and tensin homolog
PVC	Pre-Vacuolar Compartment
PVE	Pre-Vacuolar Endosome
PX Domain	Phox homology domain
RFP	Red fluorescent protein
RNA	Ribonucleic acid
RS-ALP	Reverse sorting-alkaline phosphatase
S. cerevisiae	*Saccharomyces cerevisiae*
SC media	Synthetic complete media
SDS	Sodiumdodecylsulphate
SDS-PAGE	SDS polyacrylamide gel electrophoresis
SH2 Domain	*Src* Homology 2
SNARE	Soluble N-ethylmaledimide-sensitive factor attachment protein receptor
SOB	Super optimal broth
SOC	Super optimal broth with catabolite repression
ssDNA	(Salmon sperm) single stranded DNA

STAM	Signal transducing adaptor molecule
TAE	Tris-acetate EDTA
Taq-Polymerase	*Thermococcus aquatiqus* polymerase
TBS	Tris buffered saline
TBST	Tris buffered saline with Tween 20
TEMED	N,N,N', N'-tetramethylethylenediamine
Tgo-polymerase	*Thermococcus gorgonarius* polymerase
TGN	trans Golgi network
TNSF	Tumor necrosis factor
TOR	Target of rapamycin
Tris	Tris(hydroxymethyl)aminomethane
Tris HCl	Tris(hydroxymethyl)aminomethane hydrochloride
Triton X-100	Polyethylene glycol octylphenol ether
Tween-20	Polyoxyethylene sorbitan monolaureate
UBD	Ubiquitin binding domain
UIM	Ubiquitin interacting motif
V-ATPase	Vacuolar adenosine tri phosphatase
WD Repeat proteins	Tryptophan-aspartate repeat protein
WIPI Proteins	WD repeat domain phosphoinositide-interacting protein
VPS	Vacuolar protein sorting
Wt/WT	Wild type
yEGFP	(Yeast optimized codon) enhanced green fluorescent protein
YEPD	Yeast extract peptone dextrose
YETD	Yeast extract tryptone dextrose
YNB	Yeast nitrogen base

List of Figures

1.1 Chapter 1; Introduction

Lipids are an essential component of all membranes; about 1000 different lipid species are present in the distinct membranes marking the boundaries of organelle matrix in eukaryotes (Stahelin 2009).

These lipids can be classified into 2 main categories; 1) structural lipids which are highly abundant e.g phosphotidylcholine (PtdCho) and Phosphotidylethanolamine (PtdEth) and contribute towards physiochemical properties of the membrane and 2) signaling lipids which are normally maintained at low levels and can be highly varied in response to a stimulus e.g phosphoinositides (Lemmon 2003; Balla 2005; Behnia and Munro 2005; Chang-Ileto, Frere et al. 2012).

Biochemical, electrophysiological, and molecular work has shown that these latter lipids, actively control many cellular processes, including membrane trafficking (Corvera, D'Arrigo et al. 1999; Cote and Vuori 2009), cell signaling (Payrastre, Missy et al. 2001), regulation of actin cytoskeleton (Takenawa and Itoh 2001), production of second messengers (Dove, McEwen et al. 1999; Dove and Michell 2009; Dong, Shen et al. 2010) and regulation of intrinsic properties of transmembrane proteins such as ion channels, which are usually coupled to various aspects of Ca^{++} signaling (Balla and Catt 1994; Balla, Szentpetery et al. 2009), and vesicle fusion machinery (Odorizzi, Babst et al. 2000).

Dynamic lipid-protein interactions have instigated research in the area of lipid mediated cellular physiology as some lipids are generated and/or degraded within a few seconds in response to a stimulus. Both the generation and termination of the lipid signal is a highly

regulated process and many effector proteins are identified to participate in such a regulation.

One of the first examples of this 'lipid signaling' to be recognized was the formation of 1-steroyl, 2-arachidonyl diacylglycerol (DAG) during signal transduction from many types of G-protein coupled receptors (GPCRs) (Gilman 1987). This specific species of DAG was later found to specifically bind, recruit to the plasma membrane and activate the classical isoforms of Protein Kinase C (cPKCs) that are essential to events downstream of Ca^{2+} signaling in animal cells (Nishizuka 1995; Nakamura, Hamada et al. 2005). This simple example illustrates the first paradigm of lipid signaling because the interaction between DAG and cPKCs not only changes the steady-state localization of the enzyme from the cytosol to the plasma membrane, but also activates it to phosphorylate target proteins (Irvine and Dawson 1980; Irvine, Letcher et al. 1984).

Many lipid signals are thought to work in a broadly similar way, despite the fact that many of these lipid signals and their cognate binding sites display very disparate stereochemistry.

1.2 Phosphoinositides

Arguably one of the most important groups of signaling lipids are the Phosphoinositides (PPIns). The parent phosphoinositide, Phosphatidylinositol (PtdIns) is a negatively charged glycerophospholipid which forms a minor component of the inner lamina of most eukaryotic membranes. PtdIns consists of a phosphatidic acid (PtdOH) backbone linked to a *myo*-inositol head group via a phosphodiester group (Figure 1.1). This molecular architecture confers a unique stereochemical identity upon each of the other 5 hydroxyl

groups on the inositol ring; suggesting why evolution selected this molecule as the basis for a family of lipid signals.

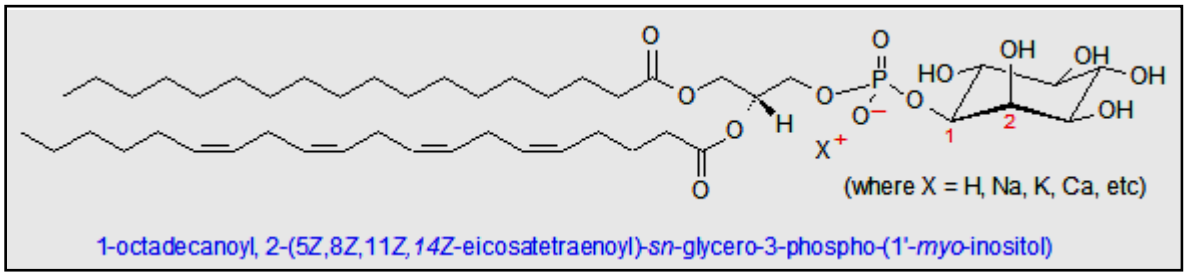

Figure 1.1: Structure of Phosphotidyl-Inositol (PI) AOCS lipid library.

In mammalian cells PtdIns is normally synthesized in the ER but is primarily present on the cytosolic leaflet of most eukaryotic membranes (Helmkamp 1990); once PtdIns is synthesized, it is transported to other membranes via vesicular transport or through lipid transfer proteins (Liscovitch and Cantley 1995).

Mable and Lowell Hokin *et al* first identified that PtdIns can be phosphorylated at numerous positions to give rise to PIP, and PIP_2 (Hokin and Hokin 1958). Later studies identified regio-isomers of both PIP and PIP_2 and another highly phosphorylated PIP_3, however phosphorylation of hydroxyls D2 and D6 of the Inositol ring are not observed in any naturally occurring PPIns; though the D6 position is known to form a diester link during synthesis of GPI-anchored proteins (Ikezawa 2002).

Phosphoinositides are one of the most acidic lipids and are found in all eukaryotic cells in varying concentrations, with the exception of PIP_3 which is not found in plants or fungi. None of the bacteria, except actinobacteria, are known to synthesize PtdIns or PPIns, although it is believed that archaeal ether lipids may serve similar functions (Corda, Iurisci et al. 2002).

PPIns are not abundant lipids; PtdIns comprises only 5-20% of total lipid in a typical membrane and the total mass of all the other polyphosphoinositides is likely to be less than 4% of the level of PtdIns (Hope and Pike 1996). Hence it's difficult to individually analyze PPIns quantitatively *in vivo* using chemical methods. Therefore the most commonly used method to detect and quantify phosphoinositides is to radioactively label cells with $[^{32}P]PO_4^{2-}$ or $[^{3}H]$Ins and then extract, deacylate and quantify each radiolabelled PPIn species by anion exchange HPLC (Dove, Lloyd et al. 1994; Dove, McEwen et al. 1999).

Steady state levels of each phosphoinositide species are maintained through continuous phosphorylation and dephosphorylation; by the action of phosphoinositide phosphatases and ATP-dependent phosphoinositide kinases. It is hypothesized that this dynamic cycling is necessary for rapid concentration changes in PPIn, though the exact reason has never truly been explained. The phosphoinositide kinases and phosphatases responsible for this cycling and for synthesis and degradation are so specific, that many are sensitive to phosphorylations at positions on the inositol ring that are not their substrate sites in PPIn. For example, type I 'PI 3-kinases' will only phosphorylate PtdIns(4,5)P_2 *in vivo* at the D3 hydroxyl of the inositol ring (Boronenkov, Loijens et al. 1998), whereas a related enzyme, Vps34p will carry out exactly the same reaction, but will only use PtdIns as a substrate (Herman and Emr 1990; Hickinson, Lucocq et al. 1997). This substrate specificity, together with the sub-cellular localization of these lipids and their cognate kinases and phosphatases, is the biochemical basis for the well-defined pathways of phosphorylation and dephosphorylation of PPIn that are characteristic of all eukaryotes.

The complexity of regulation of phosphoinositide synthesis is indicated by the fact that some 18 phosphoinositide interconversions mediated by 19 phosphoinositide kinases and 28 phosphoinositide phosphatases have been identified in mammals to date and many clinical conditions are linked to malfunction of this system (Figure 1.2) (Kuksis 2003).

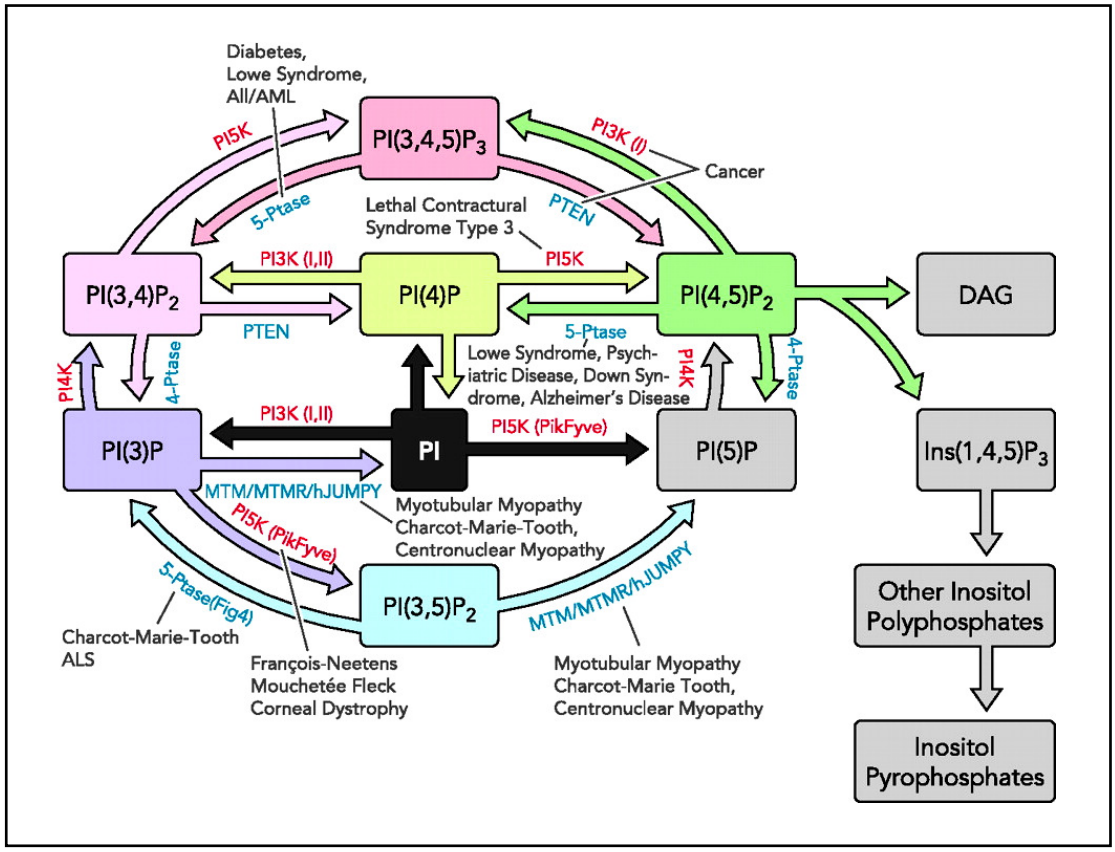

Figure 1.2: Interconversions of Phosphoinositides and the diseases linked to perturbations in the synthesis/degradation of each of these Phosphoinositides (McCrea H J , De Camilli P Physiology 2009;24:8-16)

Indeed, recent work suggests that PPIn may actually be part of the way that a cell 'signals' compartment identity (Lawe, Patki et al. 2000; Balla 2005), as certain PPIn are intimately associated with certain organelles; e.g. PtdIns(4,5)P_2 with the plasma membrane (Strachan and Read 1999) and PtdIns4*P* with the Golgi (Choudhury, Hyvola et al. 2005).

This makes a great deal of sense from a cell biological and evolutionary standpoint since the phosphor-monoesters on the PtdIns 'stem' can be rapidly remodeled in a way that allows the cell to change compartment identity during endo-membrane flow. Indeed it may not be by chance that PPIn evolved at precisely the same point in evolution as the endo-membrane system first appeared.

The basis of phosphoinositide signaling comes from using pre-existing low abundance molecules and altering their levels rapidly via synthesis or degradation in order to generate a signal. This is exemplified with the classical PtdIns(4,5)P_2 mediated IP3/DAG pathway. PtdIns(4,5)P_2 is present in plasma membrane in low concentrations and is synthesized from PtdIns4P by the action of type I phosphatidylinositol 4 phosphate 5 kinases e.g Mss4p. Upon activation by membrane receptors like α1 adrenergic receptors, PtdIns(4,5)P_2 is broken down by PLC into inositol 1,4,5-triphosphate (InsP_3; IP3) and diacylglycerol (DAG), both of which function as second messengers. DAG remains on the cell membrane and cascades the activation of cPKCs, which in turn phosphorylate numerous other cytosolic proteins while IP3 enters the cytosol and triggers Ca^{2+} signaling via activation of IP3 receptors in the ER. Both DAG and IP3 signaling is terminated by reversing the activity of PLC by phosphatases like Slj1p or by removing the stimulus to the α-receptors (Oancea and Meyer 1998; Stauffer, Ahn et al. 1998) (Figure 1.3).

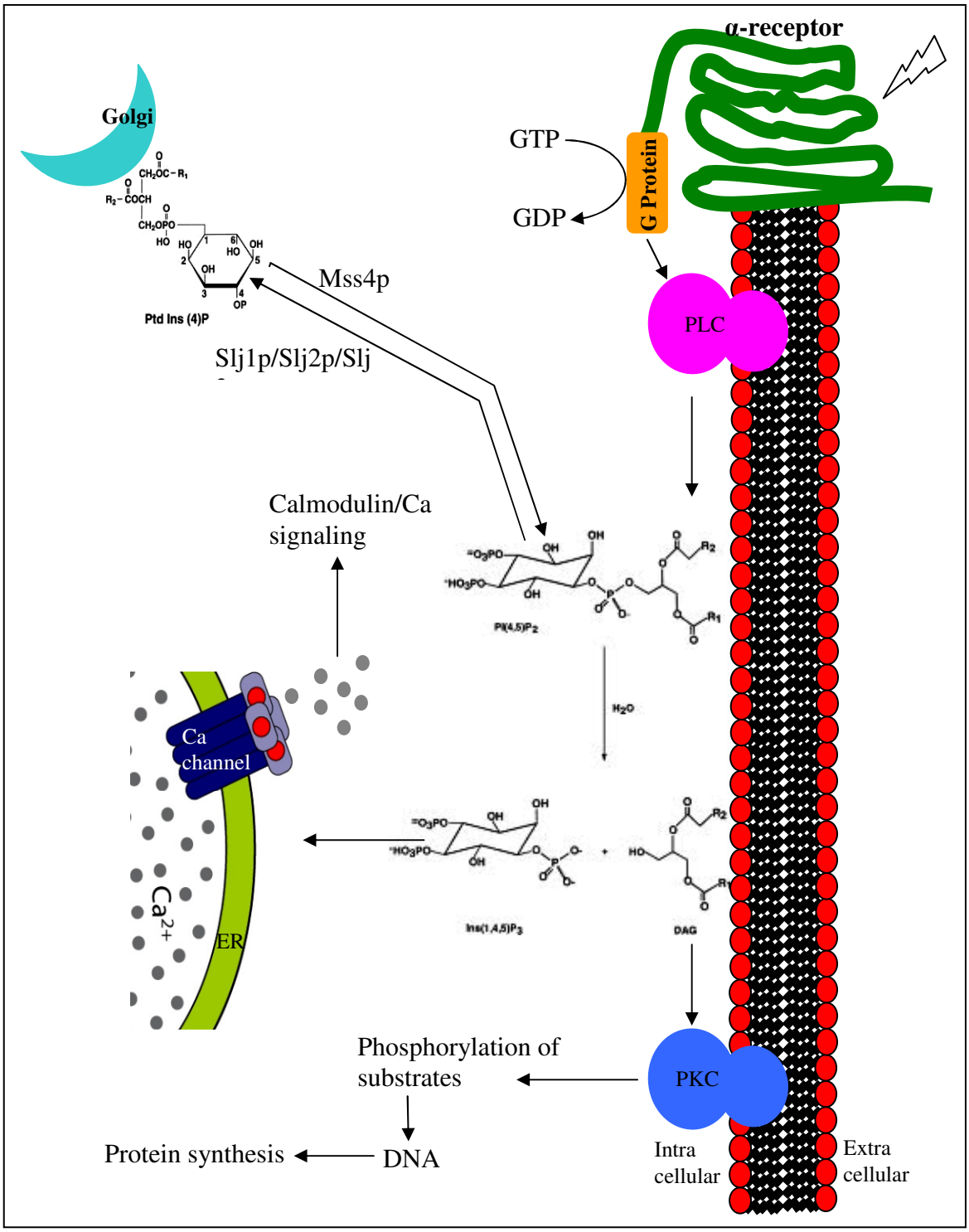

Figure 1.3: Phosphoinositide signaling exemplified by DAG/IP3 pathway.

1.3 Constitutive PPIn signaling and membrane trafficking

Constitutive membrane trafficking is the process where by membrane lipids, integral membrane proteins, and the soluble protein content of membranous organelles are

transported from its site of synthesis, the ER, to where they function. This process requires selection of specific proteins and lipids that should move from those that do not. This usually is in the form of transport intermediates mostly as small vesicles, which originate through fission from source membrane and are actively moved on to their destination membrane where they fuse and deliver the cargo (Springer, Spang et al. 1999; Jordens, Marsman et al. 2005). This swiftly operates as a cycle, and the direction of movement can be altered rapidly in response to stimulus generated 'signals'. This later "regulated" membrane traffic also uses much of the same machinery and principles as constitutive traffic but differs in the context of response to the stimulus and regulatory elements.

Since the identification of phosphoinositides they have been implicated in constitutive as well as regulated membrane trafficking (Herman and Emr 1990; Yamamoto, DeWald et al. 1995). The origin of phosphoinositide metabolism and membrane trafficking have been traced back to similar period in evolution. Although it is not known whether multiple PPIns species originated first as a mechanism to 'sense' the external environment or was it the trafficking machinery which evolved first, but the basic underlying strategy is quite similar.

PPIns serve as a means of stringent regulation via complex feedback loops which ensure that actions such as vesicle budding or fusion do not occur unless multiple conditions are satisfied, and vesicles do not normally form unless they contain cargo and do not fuse unless they have reached the correct destination.

This is best exemplified by clathrin mediated endocytosis; peripheral clathrin adaptor, AP-2 is recruited to the plasma membrane, which subsequently binds cytosolic clathrin and epsin (all of which bind PIP_2). These protein-protein interactions result in shaping the invagination which is acted upon by the cytosolic GTPase, dynamin, to 'pinch off' the neck. The process is completed by modifying the membrane phosphoinositide by synaptojanin, consequently terminating the process as AP-2, epsin, and dynamin proteins 'drop off' the membrane (Cremona and De Camilli 2001; Luthi, Di Paolo et al. 2001; Lee, Wenk et al. 2004). Hence in each distinct trafficking event, the phosphoinositide and the adaptor molecules may differ yet the process remains similar.

Currently a lot is known about the involvement of phosphoinositides at individual membrane trafficking events, however how a single species performs diverse functions at assorted loci within a cell is ambiguous.

PtdIns3*P* is one such constitutively produced lipid which is enriched on Trans Golgi network (TGN) and the endosomes *in vivo* (Emr and Malhotra 1997; Cooke, Dove et al. 1998; Gary, Wurmser et al. 1998; Dove and Michell 2009) and it is maintained at constant levels by the activity of Vps34p. Vps34p was first identified as a protein required for normal function of the VPS pathway in *S. cerevisiae* and together with its sub-cellular localization was later acknowledged for its role in PtdIns3*P* synthesis (Whitman, Downes et al. 1988; Herman and Emr 1990; Schu, Takegawa et al. 1993; Vanhaesebroeck and Waterfield 1999).

If total level of PtdIns3*P* (0.04% of total membrane phospholipids) is averaged across the endosomal pathway (endosomes and lysosomes roughly make up 2% of cellular

membranes) its level (4%) becomes comparable to PtdIns(4,5)P_2 (Roth 2004) and mediates constitutive membrane trafficking in the endo-lysosomal compartments.

Screening of mutants defective for membrane trafficking has lead to the identification of common, yet specific phosphoinositide binding modules. This validated the role of phosphoinositides in membrane trafficking and assigned regulatory roles to these phosphoinositide binding 'effector' proteins.

One such domain which binds PtdIns3*P* is the FYVE domain. 27 FYVE domain proteins in humans, 15 in *C. elegans*, and 5 in *S. cerevisiae* have been identified to date (Stenmark, Aasland et al. 2002).

FYVE domain proteins are known to function in endocytosis (Corvera 2000), in growth factor signaling (Stenmark, Aasland et al. 2002), and in regulation of the actin cytoskeleton. Most FYVE domain proteins localize to endosomes and plasma membrane according to their function, respectively (Wurmser, Gary et al. 1999). As these proteins contain numerous other domains, and their PtdIns3*P* binding specificities also vary, it is evident that they work in multi-protein complexes.

A possible explanation for assembly of such multi-protein complexes and a role for PtdIns3*P* in such membrane trafficking events come from the finding that inhibition of PtdIns3*P* synthesis via wortmanin restricts fusion of the incoming vesicles. Fusion requires Rab5p and studies indicate that the inhibited step is downstream of the guanine nucleotide exchange on Rab5 (required to deliver Rab5 to the membranes (Jones, Mills et al. 1998).

Numerous Rab5 effector proteins e.g EEA1 bind PtdIns3*P* (Simonsen, Lippe et al. 1998) and are mis-localized in Δ*vps34* cells indicating that EEA1 binds to membranes through a combination of interactions with PtdIns3*P* and other proteins (Dumas, Merithew et al. 2001), nonetheless Rab5 is present on membranes regardless of PtdIns3*P* or EEA1 (Lawe, Chawla et al. 2002). Thus PtdIns3*P* acts as tag for fusion of incoming vesicles to give directionality to trafficking (Rubino, Miaczynska et al. 2000) by assisting in the assembly of a protein complex on the endosomes that tethers the incoming vesicle and also participates in fusion reaction. This is also depicted by the fact that the incoming endocytic vesicles lack PtdIns3*P* and PtdIns3KIII only generates PtdIns3*P* on the incoming membrane once the vesicle has budded (Vieira, Botelho et al. 2001). The same is also true for the PAS directed PtdIns3*P* synthesis eventually leading to the fusion of autophagosome with the vacuole/lysosome (Hu, Hacham et al. 2008; Obara and Ohsumi 2011; Obara and Ohsumi 2011).

Hence by the activity of various binding partners/effector proteins, a single lipid like PtdIns3*P* can act to bring about a common process e.g fusion amongst various membranes in the endo-lysosomal compartments.

1.4 Signaling by 'housekeeping' PPIn.

The first PPIn signals recognized were the 'acutely regulated' lipids like PtdIns(3,4,5)P_3, whose mass, when averaged across the cell, changes many fold during various regulated cellular events; most notably during growth factor and GPCR signaling (Wymann and Schneiter 2008). However, many other lipid signals, including most PPIn (e.g PtdIns3*P*) are maintained at fairly constant levels when averaged across a whole cell, because they regulate constitutive trafficking via the formation of multimeric protein complexes.

Indeed these constitutive lipids often regulate multiple processes in the same cell, at the same time, but somehow independently of each other. How can this be the case if PPIn work simply by recruiting effector proteins to membranes, since if this were the case then all of the effectors of PtdIns3*P* would be recruited to every compartment in which this lipid is found; in complete contrast to what is observed.

Infact the binding proteins for the constitutive PPIn are actually 'co-incidence detectors' that require the presence of both their cognate PPIn ligand and a protein binding partner or partners in the same compartment, before the process will proceed. Biochemically, this comes about because the affinity of the effector protein for each of its protein and lipid ligands is individually too weak to sustain a stable interaction with the membrane. Hence stable membrane association is only achieved through avidity effects via multiple weak interactions. Indeed the paradigm from constitutive PPIn signaling is all about the formation of specific protein complexes that are mediated by many weak interactions, each contributing fractional binding and stabilized by a PPIn. The corollary to this is that the complex can also be disassembled rapidly when required, simply by removing or adding phosphates to the PtdIns 'stem'.

Hence PPIns signaling is robust and the levels can vary substantially within minutes in response to a stimulus, recruiting effector proteins to the sites of their synthesis/breakdown. Yet lipids like PtdIns(3,5)P_2 act in dual capacity, regulating trafficking at lower levels while acting as a signal at higher levels.

It is also important to note that although many of the phosphoinositides are inter-convertible yet discrete localization of the phosphatases and kinases limits their synthesis

and degradation to particular loci within a cell e.g PtdIns(4,5)P_2 is a component of the plasma membrane and can be synthesized from PtdIns4*P* and/or PtdIns5*P* by the activity of two distinct but related phosphoinositide kinases; Phosphatidylinositol 5-phosphate 4-kinase (PIP4K) (EC 2.7.1.149) phosphorylates PtdIns5*P* at 4-position, whereas phosphatidylinositol 4-phosphate 5-kinase (PIP5K) (EC 2.7.1.68) phosphorylates PtdIns4*P* at 5-position to form PtdIns(4,5)P_2 (Walker, Dougherty et al. 1988; Whitman, Downes et al. 1988; Ishihara, Shibasaki et al. 1996). As the cellular level of PtdIns4*P* is approximately ten times higher than that of PtdIns5*P*, the major synthetic pathway for the formation of PtdIns(4,5)P_2 is probably through the activity of PIP5Ks.

Although PIP5Ks can also phosphorylate PtdIns, PtdIns3*P* (Ishihara, Shibasaki et al. 1996; Anderson, Boronenkov et al. 1999) and PtdIns(3,4)P_2 at D-5 to generate PtdIns5*P*, PtdIns(3,5)P_2 and PtdIns(3,4,5)P_3 respectively (Clarke, Letcher et al. 2001; Halstead, Roefs et al. 2001) albeit to a lesser extent. This raises a question as to what determines which synthesis pathway is carried out *in vivo*?

PIP5K proteins exist as isoforms and all isoforms have a well-conserved central region (the kinase catalytic domain) and a sub-domain within the catalytic domain called the activation loop, which differs in sequence between the PIP5K and the PIP4K family. This loop determines substrate specificity, as substitution of specific amino acids in this domain of PIP5K to the corresponding amino acids in PIP4K switches its substrate specificity from PtdIns4*P* to PtdIns5*P* in order to synthesize PtdIns(4,5)P_2. The sub-cellular localization of the mutant PIP5K (with PIP4K activation loop) is also different, which suggests that the substrate specificity and sub-cellular localization of PIP5K are intimately linked to substrate and pathway specificity (Kunz, Wilson et al. 2000).

Local production of Ins(1,4,5)P_3 and PtdIns(3,4,5)P_3 from PtdIns(4,5)P_2 and synthesis of PtdIns(4,5)P_2 itself as a second messenger also indicates that the levels of PtdIns(4,5)P_2 are not uniformly distributed in the cell, but are rather distributed in various pools which are temporally and spatially regulated. This is achieved by regulated degradation or synthesis, possibly through specific regulation of the activity of PIP5K isoforms.

The beauty and precision of PPIns signaling also comes from the formation of complexes, each subset being explicit for a specialized function only e.g. PtdIns3*P* synthesis in the endocytic pathway drives normal endocytic trafficking (Gillooly, Morrow et al. 2000) and is regulated by the formation of Vps34p complex II (Ohsumi 2001; Obara, Sekito et al. 2006; Obara, Noda et al. 2008; Obara and Ohsumi 2011) highlighted by the presence of Vps38p in the core complex whereas the directed synthesis of PtdIns3*P* at the PAS is regulated via Vps34p complex I comprising of core complex and Atg14p (Kihara, Noda et al. 2001; Vieira, Botelho et al. 2001).

Many pathogenic species interefere with PIP turnover in their hosts; this facilitates invasion and survival within the host cell (Figure 1.4).

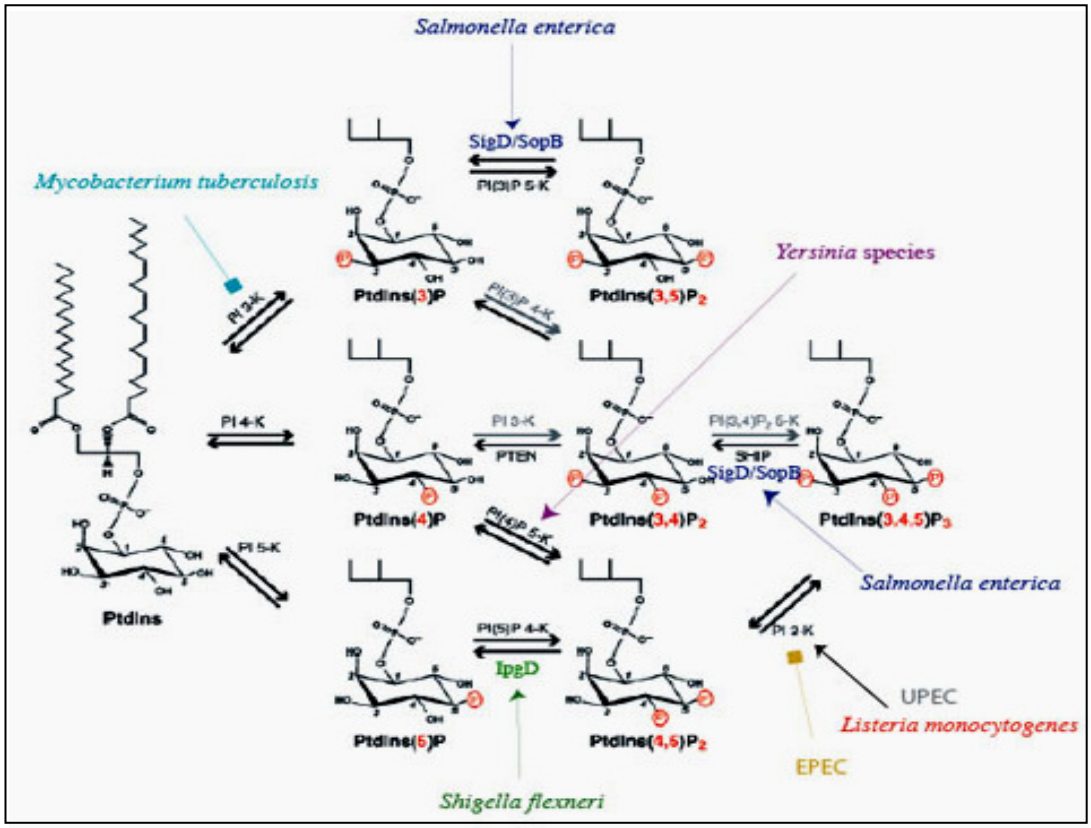

Figure 1.4: Known Phosphoinositide kinase and phosphatase targets during pathogenecity (Pizarro-Cerda and Cossart 2004).

Studies on phosphoinositide binding proteins have revealed that the majority of lipid-binding occurs through specific protein domains which contain cationic surfaces. These motifs are typically 50–120 amino acids long and fall into a few common protein folds. Among the modules that have been characterized to bind Inositol lipids are: pleckstrin-homology (PH), Phox (PX), C2, SH2, protein tyrosine binding (PTB), FYVE, PHD, GRAM, BAR, ENTH/ANTH and a novel domain in PROPPINs. These domains collectively represent some of the largest families of domains within the proteome (Dove and Michell 2009).

However it's quite uncertain as to how many of these proteins must associate with the membrane to obtain physiological activity and membrane remodeling in processes such as endocytosis.

Nonetheless it is observed that clusters of basic amino acid residues interact with the acidic head group of the lipid, initially through electrostatic interactions later giving way to specific binding so as to increase the membrane residence time. On the contrary some modules are nonspecific and associate with a membrane, based on its physical properties such as charge or curvature only (Takenawa and Itoh 2006).

Their affinities for the target Phosphoinositides are also different from being very strong to very weak. There are also examples of synchronized, merged interactions of various modules producing a coincidence detector, capable of being activated by combination of lipids/Proteins (Michell, Heath et al. 2006; Dove and Michell 2009).

Significantly some of the lipid binding modules also bind the water-soluble Inositol phosphates, like the PH domain of PLCδ binds PtdIns(4,5)P_2 and its head group Ins(1,4,5)P_3 with high specificity. This strongly indicates that due to such additional binding affinity, another layer of regulation is enabled (Razzini, Brancaccio et al. 2000).

In order to function correctly, the effector proteins bind cognate PPIns and another ligand which is mostly a resident protein of a specific compartment within the cell; e.g EEA1 (endosomal regulator with a FYVE domain) binds PtdIns3*P* but only becomes active when it interacts with GTP-Rab5p on the early endosome (Dumas, Merithew et al. 2001; Mishra, Eathiraj et al. 2010). Therefore any increase/decrease in a particular

phosphoinositide level leads to recruitment or relocation of specific proteins within the cell assuring a spatio-temporal mode to signaling biology (Stahelin 2009).

1.5 Lipid (phosphoinositide) kinases

The molecular diversity coupled with rapid and reversible phosphorylation of the inositol head group makes phosphoinositides ideal signaling candidates. The synthesis of phosphoinositides is carried out by phosphoinositide kinases which are also critical for phosphoinositide isomer-specific localization and functions, making it ever so important to understand their functioning in order to realize the balance between normal cell physiology and growing list of human diseases associated with malfunction of these enzymes.

Phosphatidylinositol phosphate kinases (PIPK) are widely classified into 3 groups:

- Type 1 PIPK phosphorylate D-3 position e.g convert PtdIns4*P* to PtdIns(3,4,)P_2 and hence are known as PI3Ks.
- Type II PIPKs phosphorylate D-4 position e.g convert PtdIns3*P* to PtdIns(3,4)P_2 and are known as PI4Ks,
- Type III PIPKs phosphorylate D-5 positions e.g convert PtdIns3*P* to PtdIns(3,5)P_2 and are known as PI3*P* 5-Ks.

Each class is further grouped according to its iso-forms. PI3Ks have 8 known isoforms in mammals which are distinguished according to their homology, regulatory domains and activation cascades.

Each of these sub classes share significant homology but differ in their substrate specificities, localization and function and (Anderson, Boronenkov et al. 1999) are regulated precisely via accessory proteins.

Most enzymes are hetero-dimeric protein complexes, comprising of catalytic and regulatory domains e.g class Ia-PI3Ks has an N-terminal domain which binds regulatory proteins, a RAS binding domain, a C2 helix and the catalytic domain (Fry 1994).

In humans there is one class I PI3K, 3 class II PI3Ks and one class III PIK, where as yeast cells are characterized by a single class III PI3K i.e Vps34p; nonetheless Vps34p requires the curial association of Vps15p and Vps30p for its normal activity (Rothman, Howald et al. 1989; Herman, Stack et al. 1991). PI4Ks also are subdivided into type II (e.g PI4K2A) and type III (PI4KCA), the later shares homology with PI3Ks and together form the largest phosphoinositide kinase family.

On the contrary PIP5K/PIP kinases do not share homology with either PI3Ks or PI4Ks, yet mammalian and yeast PIP5K show conserved sequences. In mammals 3 PIP kinases have been identified, designated as type I, II, and III. Both type I and II are homologous to yeast Mss4p (Homma, Terui et al. 1998) while a third recent addition is PIKfyve (mammals) (Shisheva 2008) or Fab1p (yeast) (Efe, Botelho et al. 2005).

Both Fab1p and PIKfyve are known to associate with accessory proteins like Vac14p, which is hypothesized to act as a scaffold for the assembly of Fab1p complex (Dove, McEwen et al. 2002; Jin, Chow et al. 2008). The activity of Fab1p is decreased

substantially in absence of any one of the complex components which emphasizes the fact that it is tightly regulated.

The substrate specificity of type I and II PIP kinases is largely dependent upon their C-terminal 22-27 amino-acid activation loop and its interaction with the catalytic site. It is interesting to note that when the activation loop of type I is swapped with type II, the substrate specificity changes in the chimera (Kunz, Wilson et al. 2000) accordingly.

Malfunction of many of these enzymes is linked to diverse disease etiologies ranging from various forms of cancer, diabetes and heart disease. Gain of function mutations in PI3KA are found to be highly frequent in colon, gastric and brain cancer which have lead to investigations of several inhibitors as potential anti-cancer drugs (Workman, Clarke et al. 2010).

1.6 Lipid (Phosphoinositide) phosphatases

There are many Phosphoinositide specific phosphatases comprising several large families; over 35 various phosphatases have been identified in mammalian cells. Phospholipase-independent mechanisms of phosphoinositide degradation are executed by dephosphorylation of phosphoinositides at the D-3, D-4 and/or D-5 positions and the responsible phosphoinositide phosphatases are highly conserved throughout the eukaryotic kingdom.

In yeast seven known groups of phosphoinositide phosphatases exist which are further divided into three subgroups on the basis of their catalytic domain properties as follows:

- The SAC-domain phosphatases (Hughes, Woscholski et al. 2000; Minagawa, Ijuin et al. 2001),
- The inositol polyphosphate 5-phosphatase domain enzymes (Ooms, Fedele et al. 2006), and
- The myotubularins ortholog Ymr1 (Parrish, Stefan et al. 2004).

Mammalian phosphatases are classified into two superfamilies:

- The protein tyrosine phosphatase (PTP) superfamily (Denu and Dixon 1998) and
- The inositide polyphosphate phosphatase (IPP) superfamily (Acharya, Labarca et al. 1998).

PTP carry out a double-displacement reaction i.e. they displace the leaving inositol group with an active-site nucleophile and phospho-enzyme intermediate, whereas members of the inositol polyphosphate 5-phosphatase family catalyze direct displacement of the inositol leaving group via nucleophilic water.

Nonetheless both types are known to carry out catalysis at extreme proficiency; the reaction rates are 17-20 orders of magnitude over spontaneous rates, the catalysis being carried out at sub-second time scales (Matthews, Bowne et al. 1992).

The significance of each phosphoinositide specific phosphatase has been highlighted by the finding that mutations in each of the MTM genes has been found to correlate with a genetic disorder and of the 10 mammalian 5-phosphatases identified, each one is individually known to regulate hematopoietic cell proliferation, synaptic vesicle recycling, insulin signaling, and embryonic development in its own right (Mruk and Cheng 2011).

INPP5E and OCRL, the 2 known 5-phosphatases in mammals are known to be mutated in Lowe and Joubert syndrome respectively (Lichter-Konecki, Farber et al. 2006; Erdmann, Mao et al. 2007; McCrea, Paradise et al. 2008) whereas SHIP2 (SH2 (Src homology 2)-domain inositol phosphatase), and SKIP (skeletal muscle- and kidney-enriched inositol phosphatase) are known to negatively regulate insulin signaling and glucose homeostasis; SHIP2 polymorphism is known to render increased resistance to glucose and SHIP1 is found to be mutated in some leukemias, but INPP4B (inositol polyphosphate 4-phosphatases) is known to act as a tumor suppressor in breast cancer (Blero, De Smedt et al. 2001; Sasaoka, Hori et al. 2001; Wada, Sasaoka et al. 2001).

The Sac-phosphatases being non-specific, degrade multiple mono-phosphoinositides as well as PtdIns(3,5)P_2. One such example of Sac domain phosphatase is Fig4p, which is known to be mutated in degenerative neuropathy (Chow, Zhang et al. 2007; Chow, Landers et al. 2009; Lenk, Ferguson et al. 2011; Ferguson, Lenk et al. 2012).

1.6.1 PTEN (Phosphatase and Tensin homolog)

The importance of PTEN was brought to light when it was noted that this gene was mutated in multiple advanced cancers and was postulated to be a candidate tumor suppressor gene located on human chromosome 10q23 (Myers, Pass et al. 1998). PTEN was mistook for a protein phosphatase initially because of the signature CX5RT/S phosphatase catalytic motif similar to many members of the protein tyrosine phosphatase superfamily, but later biochemical analysis revealed very poor protein phosphatase activity *in vitro* (Myers, Pass et al. 1998; Lee, Yang et al. 1999; Chu and Tarnawski 2004; Mund and Pelham 2010) and a much significant phosphoinositide phosphatase activity

that targets the D-3 phosphate of PtdIns3*P*, PtdIns(3,4)P_2 and PtdIns(3,4,5)P_3 as substrates.

Later it was found out that PtdIns(3,4,5)P_3 is the preferred substrate *in vitro* and the primary substrate *in vivo*. Nonetheless protein and phosphoinositide phosphatase activities of PTEN can be uncoupled. The G129E missense mutation alters the phosphoinositide binding pocket and selectively eliminates PTEN phosphoinositide phosphatase activity *in vitro* (Myers, Pass et al. 1998; Lee, Yang et al. 1999; Chu and Tarnawski 2004).

It is also hypothesized that PTEN catalyzes an auto-dephosphorylation reaction in order to promote the conformational transitions required for the priming of PTEN C-terminal domains for physiologically important protein binding functions (Vazquez, Ramaswamy et al. 2000; Vazquez and Sellers 2000; Vazquez, Grossman et al. 2001).

PTEN knock-out mice exhibit elevated levels of PtdIns(3,4,5)P_3 and an activated Akt (Stambolic, 2000; Sun,1999) indicating links between regulation of cell proliferation and apoptosis. This is over emphasized by the fact that besides p53, PTEN is the most commonly mutated gene in human cancer, and the most deleted/mutated phosphatase in human sporadic and hereditary cancer syndromes such as Cowden's disease, glioblastoma, prostate and endometrial cancers, Bannayan – Zonana syndrome, and Lhermitte – Duclos disease, among others (Stambolic, 2000;Li, 1997).

1.6.2 MTM Family of phosphatases

The significance of MTMs was revealed when it was discovered that mutations in MTMs cause X-linked myotubular myopathy (MTM1) and Charcot-Marie-Tooth disease Types 4B1 and 4B2 (MTMR2, MTMR13) (Clague et al, 2005; Liu et al, 2010; Nile et al, 2010).

In mammalian cells myotubularins (MTMs) are highlighted for their 3-phosphatase activity and PtdIns5*P* production (Blondeau, Laporte et al. 2000) but later it was pointed out that they were able to dephosphorylate both PtdIns3*P* and PtdIns(3,5)P_2. This trait coupled with their localization as peripheral membrane proteins of endosomal compartments is consistent with their involvement in regulation of the PtdIns3*P* and PtdIns(3,5)P_2 signaling and with the trafficking defects associated with MTM null mutants.

14 MTMs have been identified, but not all are known to be catalytically active. Both catalytically active and inactive MTMs are conserved through out the eukaryotes (Begley, Taylor et al. 2003; Kim, Vacratsis et al. 2003) except for *S. cerevisiae* where a single active MTM1 homolog Ymr1p (Yeast Myotubularin-Related 1), has been identified and no catalytically-inactive members are found (Parrish, Stefan et al. 2004).

There also exists a lack of understanding regarding which MTM phosphatase homologue targets each pool of its substrate, and how does loss of MTM phosphatases cause multiple diseases, keeping in mind that most of them appear to have redundant functions.

One possibility is that perhaps MTMs are a general PtdIns disposal facility, allowing lipid recycling, membrane neutrality and/or termination of lipid signaling. Yet another more

plausible scenario could be the requirement of multiple monomeric active and inactive units to associate with each other forming heteromers and hence keeping the activity of MTMs in check; confiding with the requirement of multiple MTMs.

1.6.3 Sac-like Phosphatases

As the name implies, Sac1-like phosphoinositide phosphatases are characterized by yeast Sac1p like domain (Cleves, Novick et al. 1989; Chung, Sekiya et al. 1997). They are further divided into 2 subgroups; 1) Sac domain proteins e.g Sac1p and Fig4p and 2) Sac1-like-phosphatase domain with an adjacent 5-phosphatase domain e.g mammalian synaptojanins 1 and 2, and the cognate yeast phosphatases Inp51/Sjl1, Inp52/Sjl2, and Inp53/Sjl3 (Stolz, Kuo et al. 1998; Hughes, Woscholski et al. 2000)

The ability to hydrolyze a number of PtdIns in these enzymes is rendered by the 5-ptase and *Sac1*-like domains (Brice, Alford et al. 2009). There are several gene products designated to be *Sac1*-like, including three in mammals and four in budding yeast (Hughes, Cooke et al. 2000; Hughes, Woscholski et al. 2000).

They are capable of dephosphorylating PtdIns(4,5)P_2, PtdIns(3,5)P_2 and PtdIns(3,4,5)P_3 (5-ptase substrates), along with PtdIns3*P*, PtdIns4*P*, and PtdIns(3,4)P_2 (*Sac1*-like substrates) (Hughes, Cooke et al. 2000; Zhong, Hsu et al. 2012).

Although the Sac1-like activities are non discriminating but observation of selective elevations in PtdIns4*P* and PtdIns(3,5)P_2 in Δ*sac1* and Δ*fig4* (*S. cerevisiae*) mutants,

indicate that individual proteins may prefer distinct lipid substrates in cells (Nemoto, Kearns et al. 2000; Gary, Sato et al. 2002).

Sac1 is a type II integral membrane protein which localizes to the membranes of the endoplasmic reticulum and Golgi, anchored to the membranes via two C-terminal transmembrane domains (Cleves, Novick et al. 1989; Whitters, Cleves et al. 1993) which are essential for optimal catalytic activity *in vivo* (Foti, Audhya et al. 2001). Δ*sac1* leads to cold-sensitivity for growth, cell wall abnormalities, and assorted ER-associated defects (Cleves et al., 1989; Novick et al.,1989) which are correlated to elevated PtdIns4*P* levels observed in Δ*sac1* cells.

Sac1p-mediated mechanisms for coupling membrane trafficking to growth factor is hypothesized to be dependent on homo-oligomerization of Sac1 in a much regulated manner; timely COPII-mediated exit of the phosphatase from the ER, and disassembly of the complexes in the Golgi complex to promote timely COP1-mediated retrieval of the phosphatase back to the ER (Mayinger, Bankaitis et al. 1995; Kochendorfer, Then et al. 1999; Schorr, Then et al. 2001; Wiradjaja, Ooms et al. 2007; Blagoveshchenskaya, Cheong et al. 2008; Knodler, Konrad et al. 2008; Blagoveshchenskaya and Mayinger 2009; Mayinger 2009).

Fig4p is a sac-like phosphatase required for normal actin polarization in response to mating pheromone (Erdman, Lin et al. 1998; Overmeyer, Erdman et al. 1998) and regulation of PtdIns(3,5)P_2 synthesis. Its primary phosphoinositide phosphatase specificity is towards D-5 phosphoester bond of PtdIns(3,5)P_2, and localizes to the

vacuolar membranes (Botelho, Efe et al. 2008). Δ*fig4* cells are defective in vacuole fission and retrograde trafficking accompanied by slightly enlarged vacuoles (Gary et al., 2002;Michell et al., 2006;Michell and Dove, 2009).

Paradoxically, Fig4p is also required for activation of the Fab1p and replete PtdIns(3,5)P_2 synthesis (Rudge, Anderson et al. 2004; Duex, Tang et al. 2006) although the physiological rationale for such a paradoxical coupling between a phosphatase and a kinase remains obscure.

This phosphoinositide kinase-phosphatase coupling is signified by the fact that defects in this enzyme are associated with Charcot–Marie–Tooth peripheral neuropathies (CMT) that affect motor and sensory nerves and cause progressive distal muscle weakness and atrophy (Nicot and Laporte 2008). It is also recently identified that expression of Fig4p in neurons is necessary to prevent spongiform degeneration (Ferguson, Lenk et al. 2012).

1.7 Phosphoinositides present in eukaryotes

Myo-inositol forms the head group of PPIns, which can be phosphorylated at 3, 4, and/or 5 positions through the activity of specific kinases. This results in generation of seven distinct species namely PtdIns3*P*, PtdIns4*P*, PtdIns5*P*, PtdIns(3,4)P_2, PtdIns(3,5)P_2, PtdIns(4,5)P_2, and PtdIns(3,4,5)P_3. A brief description of the 7 phosphoinositides is as follows:

PtdIns3*P* is produced by phosphorylation of D-3 position of PtdIns by PI 3-kinases. PI3 kinases phosphorylate D3 position and acts on a number of substrates generating PtdIns3*P*, PtdIns(3,4)P_2, PtdIns(3,5)P_2 and PtdIns(3,4,5)P_3.

In *S. cerevisiae*, Vps34p is the sole PI 3-kinase which requires Vps15p (serine/threonine kinase) to be recruited from the peripheral pool to the TGN; where it is acknowledged to be involved in protein sorting from TGN to the vacuole, besides its role in autophagy (Stack and Emr 1994). Mammalian Vps34p also performs similar functions.

There are a number of putative pathways for down regulation of PtdIns3*P* via a number of kinases and/or phosphatases;

- Generation of PtdIns(3,4)P_2 via PI 4-kinase, but needs much investigation.
- Generation of PtdIns(3,5)P_2 via PI 5-kinase, exemplified by Fab1p/PIKfyve.
- Generation of PtdIns via PI 3-ptases, exemplified by MTMs.

FYVE domain was amongst the first to be identified as a PtdIns3*P* binding domains and a basic motif (R/K)(R/K)HHCR is known to be critical for PtdIns3*P* binding (Hurley, Boura et al.). However the binding affinity of FYVE domain for the lipid is very low indicating that other protein interactions are required for increased membrane residence.

PX domain is also known to bind PtdIns3*P* and some 15 (in yeast) and 54 proteins (in mammals), are known PX-domain containing proteins (Yu and Lemmon 2001) and are known to have varying lipid affinities; the ones with low affinities form part of multi-unit complexes. PX domain of p47 is the only one known to bind PtdIns(3,4)P_2 preferentially rather then PtdIns3*P* (Bravo, Karathanassis et al. 2001; Ellson, Davidson et al. 2006).

PtdIns4*P* is synthesized by PI 4-kinases type I and II and is further acted upon by PI P-kinases type I to generate PtdIns(4,5)P_2 and together the 2 lipids contribute 10% of the total cellular Phosphoinositide pool. Besides this canonical pathway, an alternate elusive pathway is also hypothesized to exist which uses type II PI-3kinases to produce PtdIns(3,4)P_2. PtdIns4*P* is richly found on TGN while its phosphorylation product PtdIns(4,5)P_2 is enriched on the plasma membrane and together form the highest constitutive PPIns. PtdIns4*P* is known to recruit epsinR, oxysterol binding protein (OSBP), the clathrin adaptor AP-1 and the four phosphate-adaptor protein 1 and 2 (FAPP 1 and 2) to TGN and required for secretory pathway (Godi, Di Campli et al. 2004; Hirst, Miller et al. 2004; Robinson 2004).

PtdIns5*P* is the latest addition to the list of signaling lipids present in eukaryotes, although it's very low abundance is proving resistance in identifying its functions. It is synthesized by PI 5-kinases e.g PIKfyve/Fab1p or PI 3-ptases e.g MTM (Walker, Urbe et al. 2001; Sbrissa, Ikonomov et al. 2002; Schaletzky, Dove et al. 2003). It can also be used as a substrate by type II PI P-kinases for PtdIns(4,5)P_2 synthesis (Rameh, Tolias et al. 1997) and PTEN like ptases which are specific for PtdIns5*P* (Pagliarini, Worby et al. 2004) however, how each pool is regulated and maintained remains to be investigated. PtdIns5*P* levels are known to rise upon thrombin stimulation (Morris, Hinchliffe et al. 2000) and osmotic stress (Sbrissa, Ikonomov et al. 2002; Sbrissa, Ikonomov et al. 2002). It is also known that IpgD (*S. flexneri* ptase similar to PI 4-Kinase) targeted synthesis of PtdIns5*P* at the pathogen entry sites causes membrane ruffles (decreasing membrane rigidity) which is vital for virulence (Allaoui, Menard et al. 1993).

It is also known that a decrease in PtdIns5*P* (by the type II PtdInsP-kinase b) leads to a decreased Akt/PKB activity in response to insulin (Carricaburu, Lamia et al. 2003) while an increase (by type II PtdInsP-kinase b) has an opposing effect. This is hypothesized to be due to negative regulation of PtdIns(3,4,5)P_3 and the subsequent activation of Akt. *In vitro* studies report that PtdIns5*P* binding to PTEN (Pagliarini, Worby et al. 2004) and MTMs increases their activity (Schaletzky, Dove et al. 2003), possibly through allosteric regulation.

ING2 (inhibitor of growth protein 2) a PHD domain protein is identified as a nuclear receptor of PtdIns5*P* (Gozani, Karuman et al. 2003). This seems to be very interesting as ING2 is a known tumor suppressor and induces apoptosis in a p53 dependent manner, yet how the lipid is synthesized in the nucleus and the relevance of PtdIns5*P* binding to ING2 needs much investigations. It is also believed to be involved in trafficking from the late endosomes to the plasma membrane and cytokinesis.

PtdIns(3,4)P_2 is a minute component of the plasma membrane after receptor activation but acts as an important second messenger and is involved in recruiting a number of protein phosphatases and kinases to the plasma membrane, thereby regulating their activity (Lemmon 2008).

PtdIns(3,5)P_2 is the least abundant of the Phosphoinositides under normal conditions but its levels increase 30 fold when yeast cells are under osmotic stress. It is enriched on the vacuole membrane and/or the late endosomal membranes (Cooke, Dove et al. 1998; Gary, Wurmser et al. 1998).

PtdIns(4,5)P_2 is synthesized by type I PtdIns4*P* 5-kinase and is found on the plasma membrane where it acts as a substrate to PLC and triggers DAG/IP_3 signaling. DAG remains on the plasma membrane while IP_3 diffuses into the cytosol and is involved in regulation of Ca^{++} channels on ER membranes (Irvine 1987; Irvine 1987; Irvine 1992; Balla and Catt 1994).

PtdIns(3,4,5)P_3 is synthesized by class I PtdIns 3-kinases and is primarily involved in regulation of down stream signaling events of anabolic pathways like cell proliferation and growth, the most prominent being the AKT pathway. It is involved in recruiting phosphatases like PTEN and PH domain proteins like AKT1/PKB1 and PDK1 to the plasma membrane and is involved in regulation of processes like cell survival and proliferation (Whitman, Downes et al. 1988).

As the primary aim of this project was characterization of Atg18p which selectively and specifically binds PtdIns3*P* ad PtdIns(3,5)P_2 hence these 2 lipids will be discussed in detail hereafter.

1.7.1 PtdIns3*P*/ PI(3)*P*

PtdIns3*P* is one of the 7 PPIns enriched on the inner (concave) surfaces of the isolation membrane, autophagosomes, in ambiguous structures juxtaposed to the elongating tips of isolation membranes, endosomes, MVBs, and the TGN (Stack, DeWald et al. 1995; Obara and Ohsumi 2008).

Hence as indicated by its localization, PtdIns3*P* is found to be involved in regulating a number of signaling events in most eukaryotes, the most prominent one being endocytosis; vesicle mediated transport to and from the vacuole and autophagy (Herman and Emr 1990). PtdIns3*P* level within the cells also does not vary immensely hence it acts to localize proteins and facilitates in formation of protein complexes rather than being an actual signal for the event.

In yeast cells, class III PI-3Kinase, Vps34p is involved in the synthesis of PtdIns3*P* and it is known to form at least 3 complexes. The core complex is formed between Vps34p, Vps15p and Vps30p. In addition to this core machinery, Complex I is formed when Atg14p targets the core complex towards PAS while Complex II is formed when Vps38p targets the core complex to the endosomes (Kihara, Noda et al. 2001). (Figure 1.5)

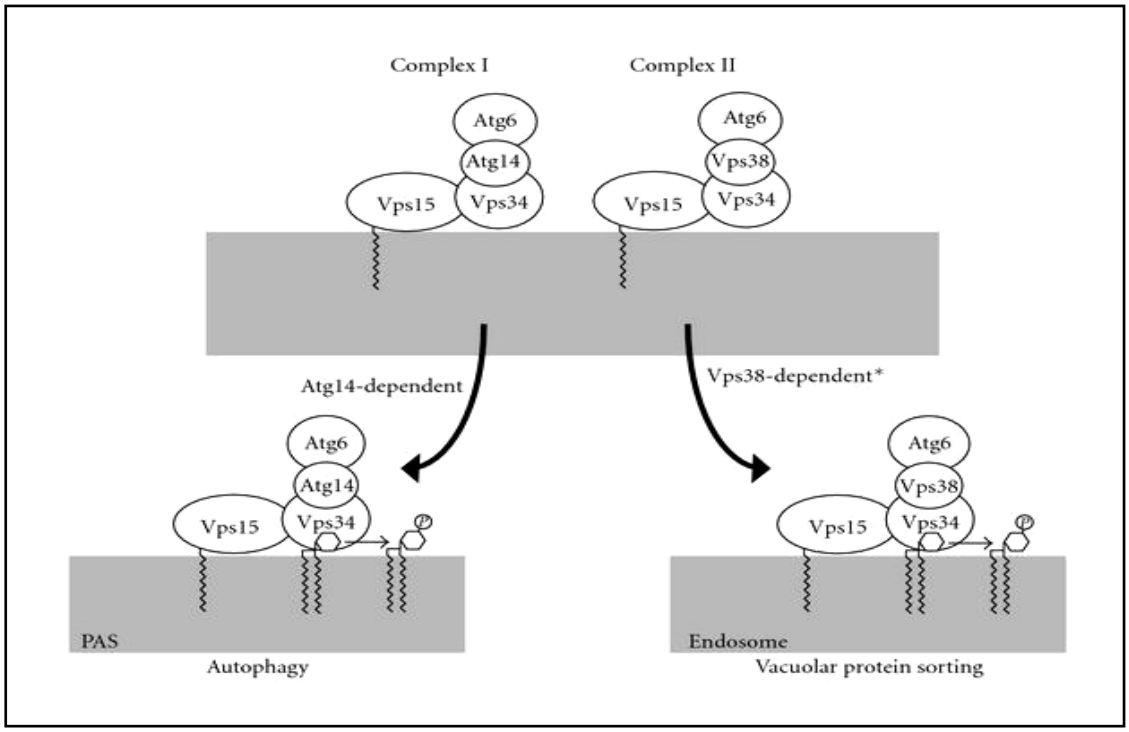

Figure 1.5: Vps34 complexes (Obara and Ohsumi).

Over expression of *VPS38* does not rescue autophagy defects in Δ*atg14* cells and vice versa indicating that each complex is distinct and does not overlap in functions (Obara and Ohsumi 2011). The regulation of the two processes i.e autophagy and VPS pathway by PtdIns3*P* synthesis is also hence quite discrete although the function of the lipid in either pathway is general i.e to localize effector proteins.

Vps34p, Vps15p and Vps30p homologues are found through out eukaryotes and Δ*vps34*, Δ*vps15* and Δ*vps30* mutants are characterized by substantial decrease in PtdIns3*P* levels leading to enlarged vacuoles and defects in VPS pathway and autophagy (Volinia, Dhand et al. 1995).

Studies on cellular fractions indicate that Vps15p associates with the cytosolic side of TGN (Herman, Stack et al. 1991) and forms a complex with Vps34p. Vps15p is known to have a protein kinase domain and an N-terminal sequence which serves as an attachment site for myristic acid (Stack, DeWald et al. 1995; Budovskaya, Hama et al. 2002). 2 distinct regions in Vps15p namely protein kinase domain and 3 tandem repeats (similar to HEAT repeat motif) are essential for its interaction with Vps34p, while a C-terminal 28 amino-acid motif in Vps34p is crucial for such an interaction, whereas Vps34p kinase domain is not required for this interaction (Budovskaya, Hama et al. 2002).

Mutations, D165R and E200R in the highly conserved kinase domain (Herman, Stack et al. 1991) or short C-terminal deletions of Vpsl5p result in inactivation of Vps15p and consequently Vps34p, with a rapid, severe and highly specific, temperature-conditional defect in vacuolar protein delivery (Herman, Stack et al. 1991). This is believed to be due

to Vps15p mediated phosphorylation of Vps34p; considered to act as switch for regulation of soluble protein sorting either towards the vacuole or towards the secretory pathway.

Vps30p/Atg6p, another Vps34p accessory protein, is a peripheral protein which binds to the cytosolic side of the membranes. Its interaction with Atg14p hints its involvement in autophagy more then in the VPS pathway. It is involved in retrieval of Vps10p (CPY receptor) from the late endosome to the TGN and retromer function (Cowles, Snyder et al. 1997; Seaman, Marcusson et al. 1997) but details of specific interactions are much awaited (Kametaka, Okano et al. 1998).

Δ*vps34* cells are characterized by a large vacuole and defects in endocytosis, autophagy and osmotic stress response (Stack and Emr 1994; Kihara, Noda et al. 2001; Burda, Padilla et al. 2002), but AP-3 pathway (alternate adaptin dependent pathway from TGN to the vacoule) is not affected (Stack, DeWald et al. 1995; Odorizzi, Cowles et al. 1998).

By using the genetically tractable Dictyostelium, it was shown that lithium suppresses PtdIns3*P*-mediated trafficking and its effects can be reversed by over expression of inositol monophosphatase (IMPase), which is consistent with the inositol-depletion hypothesis (King, Teo et al. 2009). *Δvps34* cells also have undectable levels of PtdIns(3,5)P_2 which will be discussed later.

Of the number of domains that are found to bind PtdIns3*P* with much specificity, FYVE domain followed by the PX domain is the most prominent. There are also reports which suggest that PH domain binds PtdIns3*P* with much lesser affinity in its polymeric forms (Razzini, Brancaccio et al. 2000).

An interesting observation is that although the FYVE domain specifically binds PtdIns3*P*, but surprisingly GFP tagged Fab1p (PtdIns3*P*-5 kinase), which is known to have a FYVE domain, resides on the vacuole instead of the endosome (Michell, Heath et al. 2006).

1.7.2 PtdIns(3,5)P_2/PIP(3,5)P_2

The presence of PtdIns(3,5)P_2 in Eukaryotic cells was first identified around 1999 and since then investigations have shown that it controls several membrane trafficking events and is crucial for cellular response to hyper-osmotic stress in yeast (Dove, Cooke et al. 1997; yamamoto et al 1995; gary et al 1998, 2002; Jeffries et al 2004).

There are no reports of presence of PtdIn(3,5)P_2 in Eubacteria and Archae bacteria, but almost all of the eukaryotic cells maintain low (>0.1%) yet constant levels of PtdIns(3,5)P_2 mostly enriched at the vacuole and the late endocytic compartments. An increase of up to 30 folds (in yeast), and 6 folds (in plants and some animals) which peaks within seconds, is observed when the cells are hyper-osmotically stressed (Dove, Cooke et al. 1997; Michell, Heath et al. 2006).

Nonetheless generation of minute amounts of PtdIns(3,5)P_2 from PtdIns3*P*, distinguishes a cell compartment by recruiting a number of regulatory proteins to the locale (Cooke, Dove et al. 1998; Gary, Wurmser et al. 1998). However how cells regulate PtdIns(3,5)P_2 synthesis in response to hyper-osmotic shock in particular and stress in general (Dove, McEwen et al. 1999), remains unexplained largely due to very low endogenous levels and lack of sensitive quantitative and qualitative techniques.

Although it has proven to be an elusive molecule, there has been quite advancement in its characterization in the past decade.

Fab1p is the sole known kinase (in yeast) (Gary, Wurmser et al. 1998) and PIKfyve (in mammals) which uses PtdIns3*P* (as a precursor) for PtdIns(3,5)P_2 synthesis. This is an intriguing aspect that in most species only a single kinase serves to make several functional pools of PtdIns(3,5)P_2 within cells for different purposes.

The common canonical pathway for PtdIns(3,5)P_2 synthesis within cells is as follows:

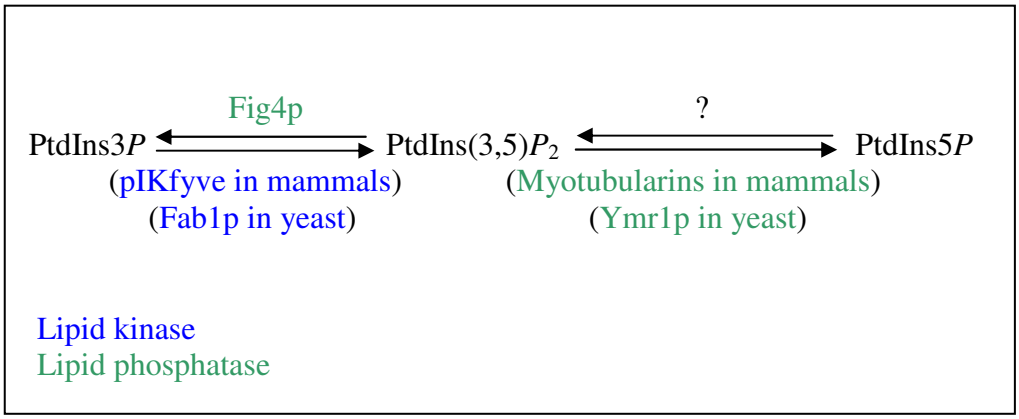

Figure 1.6: Canonical pathway for PtdIns(3,5)P_2 turnover.

Most of PtdIns(3,5)P_2 is enriched on the membranes of the endocytic compartments correlating with the localization of Fab1p/PIKfyve at the same loci (McEwen, Dove et al. 1999). A highly enlarged vacuole, defects in VPS, MVB, vacuole acidification, growth at restrictive temperature, and failure to respond normally to osmotic stress are some of the trade mark characteristics of cells lacking PtdIns(3,5)P_2 (Gary, Wurmser et al. 1998; Gary, Sato et al. 2002; Efe, Botelho et al. 2005).

As Δ*fab1* cells display a number of defects it is quite obvious that PtdIns(3,5)P_2 regulates several pathways through its interaction with various effector proteins, each group being specific for a particular event.

Partially active Fab1p mutants are able to rescue some of the defects associated with null mutants which suggests that some of the pathways have an absolute requirement (membrane trafficking and osmotic stress response) for the lipid while others are partially dependent (vacuole acidification) (Gary, Sato et al. 2002).

All eukaryotic PtdIns3*P* 5-kinases carry an N-terminal FYVE domain, a regulatory CCT domain and C-terminal kinase domain. Recently a mutation in CCT domain of PIKfyve has been identified to cause corneal dystrophy (Kotoulas, Kokotas et al. 2011).

Although mouse PIKfyve can rescue yeast *Δfab1* defects and vice versa (Ikonomov, Fligger et al. 2009), interestingly the use of YM201 636, a novel inhibitor of PIKfyve does not affect Fab1p under similar conditions (Jefferies, Cooke et al. 2008). This could be reasoned due to structural differences or more probably due to differences in regulation of the two enzymes.

It could also be argued that a second unidentified route exists for PtdIns(3,5)P_2 synthesis in yeast or it could be possible that Fab1p does not require its FYVE domain for the synthesis of PtdIns(3,5)P_2. The later is supported by the finding that FYVE domain truncation in Fab1p does not have a profound effect on Fab1p activity or localization (Botelho, Efe et al. 2008) which raises questions to the hypothesis that Fab1p uses

PtdIns3*P* as a substrate. However if this would be true then the level of PtdIns(3,5)P_2 should be normal in *Δvps34* mutants, which is certainly not the case indicating that indeed PtdIns3*P* is the precursor molecule and the substrate for PtdIns(3,5)P_2 synthesis but nonetheless it is crucial to develop sensitive assays and markers for PtdIns(3,5)P_2 identification, both *in vitro* and *in vivo*.

Another possibility is that Fab1p-FYVE domain binds PtdIns5*P* as an allosteric activator/inhibitor. Although it is hypothesized that the binding pocket of FYVE domain could possibly interact with 5-phosphate in a similar fashion as 3-phosphate of PtdIns3*P* (Misra and Hurley 1999) yet studies on such a possibility are missing.

Another possibility is hinted in the ability of Fab1p to make PtdIns5*P* from PtdIns *in vitro* (Dove, McEwen et al. 1999), and a similar ability of PIKfyve both *in vitro* and *in vivo* to synthesize PtdIns5*P* (Shisheva 2008).

Over expression of kinase dead or mutant PIKfyve (able to produce PtdIns5*P* but unable to produce PtdIns(3,5)P_2) causes extensive vacuolation of cells which can be rescued by exogenous PtdIns(3,5)P_2 but not PtdIns(5)*P* (Ikonomov, Sbrissa et al. 2002) indicating that vacuolar fission is regulated by the levels of PtdIns(3,5)P_2 but less likely by PtdIns5*P*. This is also supported by the finding that PtdIns5*P* levels decrease upon hypo-osmotic shock. Hence it can be argued that both PtdIns5*P* and PtdIns(3,5)P_2 individually regulate vacuole morphology, and although the presence of PtdIns5*P* in yeast is highly likely, it is not yet clear if Fab1p demonstrates such an ability *in vivo* and needs much investigation.

The use of *fab1-1* mutant could reveal valuable information in this regard. This mutant carries a G864E mutation in the highly conserved CCT domain and the vacuole fails to fragment under hyper osmotic stress in such mutants (Gary, Sato et al. 2002; Botelho, Efe et al. 2008). CCT domain in PtdIns3*P* 5-kinases is known to play a significant role in regulation of effector proteins, as this site is mapped for association of Fab1p effector proteins like Vac7p and Atg18p. Another example is of CCT domain of Group II chaperonins, which is known to interact with actins, tubulins and WD40 β-propellers (Ohtaki, Noguchi et al. 2010). Hence it is quite possible that Fab1p dependent PtdIns(3,5)P_2 and/or PtdIns5*P* synthesis directs remodeling of cytoskeleton under specific conditions. This could also hold true since Fab1p activity is crucial for vacuolar fission and more so since Fab1p is known to interact with a WD β-propeller namely Atg18p which in turn binds Vac17p (Efe, Botelho et al. 2007) (a myosin receptor) and functions in vacuole inheritance. Enigmatically, a kinase-dead version of Fab1p (*fab1*^{D2134R}) replicates most of the defects of Δ*fab1* mutants (Cooke, Dove et al. 1998; Dove, McEwen et al. 1999; Botelho, Efe et al. 2008) indicating that the kinase activity is a pre-requisite for normal vacuole morphology but does not shed light on whether it is PtdIns(3,5)P_2 or PtdIns5*P* or both lipids that are required for such processes.

Another intriguing aspect is that over expression of Fab1p does not significantly increase intracellular PtdIns(3,5)P_2 levels even in case of constitutively active mutants (*fab1-5*) (Gary, Sato et al. 2002; Botelho, Efe et al. 2008), indicating that Fab1p is auto-inhibited; hypothesized to be regulated through its C-terminal, CCT domain and autophosphorylation but the dexterity between 'on' and 'off' Fab1p and the synthesis and degradation of PtdIns(3,5)P_2 is not yet completely understood. However a recent study suggests that PIKfyve is not auto-inhibited but phosphorylated by PKB in response to

signaling cascades (Hill, Hudson et al. 2010).

Nonetheless, Fab1p is found to associate and form a complex with Vac7p (a trans-membrane protein), Vac14p (HEAT repeat scaffold protein), Fig4p (sac-domain phosphatase) and Atg18p (WD β-Propeller effector protein) (Bonangelino, Catlett et al. 1997; Bonangelino, Nau et al. 2002; Dove, McEwen et al. 2002; Dove, Piper et al. 2004; Rudge, Anderson et al. 2004; Duex, Tang et al. 2006; Efe, Botelho et al. 2007) Although interestingly most eukaryotes have Vac14p, Fig4p and Atg18p homologues but Vac7p is only exclusive to fungi (Bonangelino, Catlett et al. 1997) (Figure 1.7).

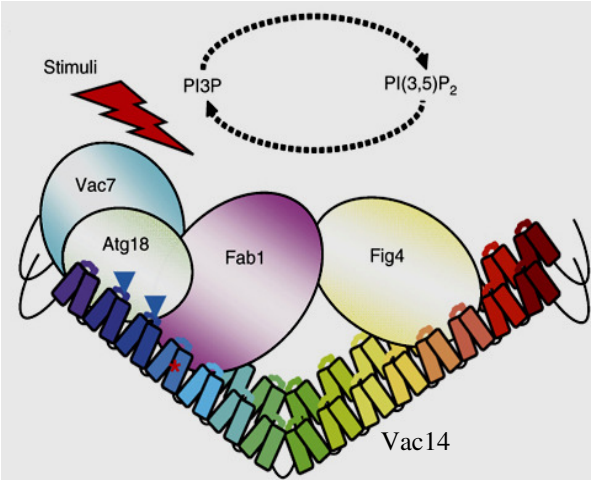

Figure 1.7: Fab1p complex

A diagrammatic representation of the Fab1p complex, where Fig4p comes in contact with Fab1p after an initial stimulus. Although Atg18p and Vac7p do not come in contact with Fig4p yet they are a part of the complex required for the PtdIns(3,5)P_2 synthesis on the vacuole after the induction of osmotic stress (Jin, Chow et al. 2008).

A null mutant of any one of these proteins results in a highly enlarged vacuole, trafficking defects and discrepancies in PtdIns(3,5)P_2 levels (Dove and Michell 2009). As most of these null mutants exhibit similar trafficking defects so it seems likely that the key event is a failure of PtdIns(3,5)P_2 synthesis rather than absence of such machinery (with the exception of Atg18p, discussed later).

Both mammalian and yeast Vac14p is composed entirely of HEAT repeats and *VAC14* mutants are known to functionally impair the scaffold protein at the heart of the Fab1-complex and hence result in an aberrant PtdIns(3,5)P_2 level (Rudge, Anderson et al. 2004).

It is also reported that the mouse mutant *Ingls* (infantile gliosis) results from a missense mutation in *VAC14* that prevents the association of Vac14p with Fab1p resulting in the generation of a partial complex, leading to non-viability linked to neurodegenerative conditions (Jin, Chow et al. 2008). Interestingly Δ*vac14* cells show some redundant PtdIns(3,5)P_2 levels and can be rescued by Vac7p over-expression (not true vice versa) (Rudge, Anderson et al. 2004) indicating that the requirement for Vac14p can be bypassed by Fab1p-Vac7p association and hence proving that indeed Vac14p is required as a scaffold which provides stability to Fab1p complex.

Fig4p forms a complex with Vac14p which is postulated to act independently of Fab1 complex (Duex, Tang et al. 2006). Δ*fig4* cells have an overall 20% increase in PtdIns(3,5)P_2 level proving it to be a bonafide PtdIns(3,5)P_2 phosphatase. But Δ*vac7* cells over expressing Fig4p have x7 PtdIns(3,5)P_2 levels (as compared to Δ*vac7* cells alone) while PtdIns3*P* and PtdIns4*P* levels plunge 40% and a double null mutant, Δ*vac7*Δ*fig4*, has normal levels of PtdIns(3,5)P_2 (Gary, Sato et al. 2002) which makes it ambiguous to function solely as a specific PtdIns(3,5)P_2 phosphatase but puts it in a position as a regulatory element in the PtdIns(3,5)P_2 synthesis machinery (Gary, Sato et al. 2002); although the mechanistic dexterity between the kinase and phosphatase in the same complex is not yet known, although it is postulated that such an association of a kinase

and a phosphatase in the same complex allows rapid lipid turnover and helps maintain compartment identity (Ikonomov, Sbrissa et al. 2007) (Figure 1.8).

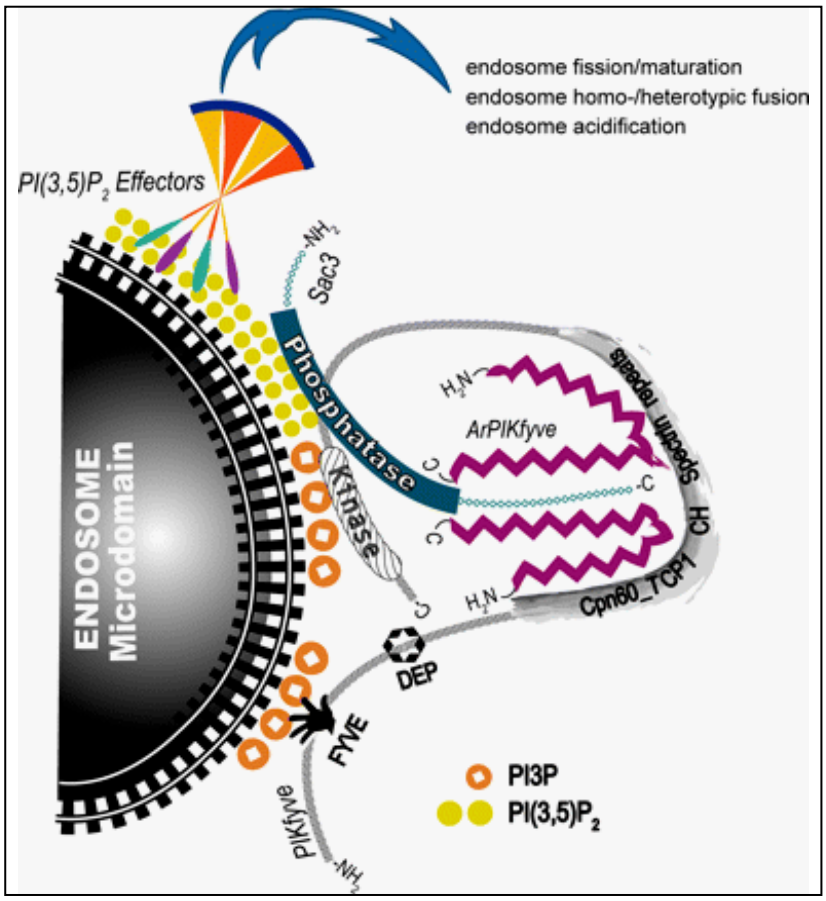

Figure 1.8: Association of PIKfyve (Fab1p), ArPIKfyve (Vac14p) and Sac3 (Fig4p) for PtdIns(3,5)P_2 turnover (Ikonomov, Sbrissa et al. 2007).

Vac7p is an integral vacuole membrane protein and Δ*vac7* cells replicate most of Δ*fab1* defects. *fab1-5* mutants are able to rescue Δ*vac7* cells indicating that CCT domain of Fab1p is crucial for its regulation and possibly Vac7p (which binds Fab1p within CCT domain) is required as an activator (Duex, Tang et al. 2006). Most of the disease associated mutations in Fab1p (in humans) are also in the CCT domain region indicating the involvement of regulatory auto inhibition of Fab1p to be crucial for normal functioning of this pathway (Gary, Sato et al. 2002).

Vac7p is also known to effect the vacuolar localization of Atg18p (Efe, Botelho et al. 2007), one of the PtdIns(3,5)P_2 effector proteins named as PROPPINs (discussed separately).

Other PtdIns(3,5)P_2 effector proteins identified till date are Vps24p (Whitley, Reaves et al. 2003), Ent3p, Ent5p (Friant, Pecheur et al. 2003),TOR1 (Bridges, Ma et al. 2012),TRPL ion channel (Rohacs 2007; Rohacs and Nilius 2007) and Tup1p (Han and Emr 2011).

Studies have only revealed that Ent3p and Ent5p are clathrin adaptors and co-operate in different ways to sort proteins between TGN and the endosomes (Costaguta, Duncan et al. 2006). They bind PtdIns through their ENTH domains but their selectivity both *in vitro* and *in vivo* for PPIns gives a vague idea of their exact function in the cell (Friant, Pecheur et al. 2003). Although both proteins are associated in AP1 dependent trafficking of Chs3p, but Ent3p is also known to be an endosomal PtdIns(3,5)P_2 effector required for protein sorting into MVB but not for the internalization step in endocytosis (Friant, Pecheur et al. 2003; Eugster, Pecheur et al. 2004; Costaguta, Duncan et al. 2006). Interestingly, Δ*ent3* and Δ*ent5* is redundant but Δ*ent3*Δ*ent5* shows MVB sorting defects similar to Δ*vps34* (Friant, Pecheur et al. 2003).

Vps24p is a member of the ESCRT complex III and is involved in MVB sorting of the cargo. Its binding to PtdIns(3,5)P_2 is attributed to a lysine in its N terminal but the K_D of Vps24p (>50 μM) indicates otherwise. Nonetheless over expression of N terminal of Vps24p in rat cells causes defects similar to the ones observed in over expression of

kinase dead PIPkIII which is why it is designated to be a PtdIns(3,5)P_2 effector protein (Whitley, Reaves et al. 2003).

Two Sec14 domain containing proteins from plants, the PX-domain-containing mammalian sorting nexin Snx1p (Zhong, Lazar et al. 2002) and the trafficking protein Ivy1p (Lazar, Scheglmann et al. 2002) are also among the PtdIns(3,5)P_2 binding proteins with unestablished functions.

The most recent additions to PtdIns(3,5)P_2 effector proteins is Tup1p and Cti6p. Both these proteins are found to be involved in chromatin architecture-modulation that is dependent on endosomal PtdIns(3,5)P_2 levels (Han and Emr 2011).

None of these PtdIns(3,5)P_2 effectors are known to effect local concentrations of their PIP ligands but the possibility of such a control cannot be ruled out as indicated by studies on Atg18p (discussed later). Besides, very little knowledge of how known PtdIns(3,5)P_2 effector proteins function, it is also plausible that there are many other unidentified effector proteins. In addition, very little is known regarding PtdIns(3,5)P_2 involvement in cellular trafficking and the exact concentration of the lipid signal necessary to elicit a basal physiological response. Recently the implication of PtdIns(3,5)P_2 in formation of PtdIns5*P* has accentuated to rethink about its physiological relevance and functions (Meijer, Berrie et al. 2001; Sbrissa, Ikonomov et al. 2012). Hence there is a lot to be understood and learnt about this elusive yet very interesting molecule. The known functions associated with PtdIns3*P* and PtdIns(3,5)P_2 till date, are highlighted in Table 1.1.

PtdIns3*P*	PtdIns(3,5)P_2
PtdIns3*P* is found to be involved in safingol-induced autophagy (Coward, Ambrosini et al. 2009). It is critical for cell growth and survival by activating PKB/Akt pathway (07Bhaskar and Hay 2007); (08Yap, Garrett et al. 2008). Nerve myelination as indicated by CMT disease and X-linked myotubular myopathy (Chow, Zhang et al. 2007). Autophagy(08Hu, Hacham et al. 2008). Cell migration (Domin, Harper et al. 2005). Endosome fusion (Simonsen, Lippe et al. 1998) Receptor sorting and internalization via MVBs (Katzmann, Odorizzi et al. 2002). Translocation of glucose transporter protein (Berwick, Dell et al. 2004) Dynamic regulation, maturation and signaling of APPL endosomes (09Zoncu, Perera et al. 2009). Retrograde trafficking (98Bryant, Piper et al. 1998).	Vacuole fragmentation in response to osmotic stress (97Dove, Cooke et al. 1997). Retrograde membrane trafficking from lysosomal and late endosomal compartments (Bryant, Piper et al. 1998). Cvt Pathway (02Nice, Sato et al. 2002). MVB sorting (98Odorizzi, Babst et al. 1998) Trafficking of some membrane transporters to cell surface in animal cells e.g, SGK1 and chitin synthase (Chs3p) in *S. Cerevisiae* . Regulation of Vacuole/lysosome size, shape and acidity (97Dove, Cooke et al. 1997). Neuro-secretion (Jin, Chow et al. 2008). Response to insulin (09Baek, Kim et al. 2009). Inheritance of the endosome/lysosome(05Efe, Botelho et al. 2005). Epigenetic regulation of GAL1 promoter (Han et al. 2011). Regulation of retromer complex (Jefferies et al. 2008).

Table 1.1: Some of the known PtdIns(3,5)P_2 and PtdIns3*P* mediated cellular processes.

1.8 The role of Phosphoinositides in MVB sorting

Vps34p and Fab1p, are the two kinases involved in the synthesis of PtdIns3*P* and PtdIns(3,5)P_2, respectively and both these Phosphoinositides are involved in maturation of MVB; PtdIns3*P* signaling initiates the MVB sorting by recruiting Hse1p-Vps27p followed by recruitment of ESCRT-I (Vps23p, Vps28p and Vps37p), ESCRT-II (Vps22p, Vps36p and Vps25p) and ESCRT-III (Vps2, Vps20, Vps24p and Snf7p) which is thought to be a downstream event. A number of these proteins are known to bind phosphoinositides e.g Vps27p binds PtdIns3*P* (Stahelin, Long et al. 2002) while Vps24p binds PtdIns(3,5)P_2 (Whitley, Reaves et al. 2003) which points out that possibly PtdIns3*P* (Vps27p/ESCRT-0) is required at the initial steps in MVB sorting while PtdIns(3,5)P_2 (Vps24p/ESCRT-III) probably acts at a later stage.

Hence it is logical to believe that MVB sorting defects in Δ*vps34* cells (lacking PtdIns3*P*) are due to the lack of recruitment of the ESCRT proteins to the MVB but it could also be due to subsequent low levels of PtdIns (3,5)P_2 which is not yet clear. A number of other proteins like Rsp5p (Ubiquitin ligase) also bind Phosphoinositides (Blondel, Morvan et al. 2004) which ties cargo ubquitination and membrane localization and partly explains how might Δ*fab1* have a distinct phenotype from other null mutants of the ESCRT proteins.

Involvement of Fab1p/PtdIns(3,5)P_2 in MVB sorting was first pointed out through mis-localized GFP-Phm5p on the vacuole membrane, in Δ*fab1* cells (Odorizzi, Babst et al. 1998) which could be due to defects in;

- Cargo Ubiquitination.
- MVB maturation i.e defects in Ubiquitinated cargo packaging into ILVs.

- Cargo deubiquitination, which occurs prior to its insertion, and is a pre-requisite for ILV formation.
- Subsequent fission of ILVs.
- Defects in fusion of the mature MVB with the vacuole.

Cargo ubiquitination is not affected in Δ*fab1* cells (Katzmann, Sarkar et al. 2004) while a defect in cargo packaging into ILVs is not likely, as ESCRT-0 complex acts upstream of PtdIns(3,5)P_2 signaling but binding of Vps24p (ESCRT III) with PtdIns(3,5)P_2 could act as a possible clue to link PtdIns(3,5)P_2 dependent fission of ILVs with ESCRT-III dependent activity of Vps4p. This is also highlighted by the finding that Δ*vps4* (AAA-type ATPase) cells exhibit a very similar phenotype as Δ*fab1* cells in terms of defective MVB sorting (Katzmann, Babst et al. 2001). It is postulated that disruption of *VPS4* leads to a block in MVB formation also exemplified by an ATPase deficient form of Vps4p which behaves as a dominant negative (Babst, Wendland et al. 1998).

One in yeast and at least 2 isoforms of Vps4p have been identified in humans (McDonald and Martin-Serrano 2009). Numerous references indicate that Vps4p oligomerizes into a dual hexameric ring assembly and goes through rounds of ATP stimulated oligomerization, oligomerization stimulated rigorous ATP hydrolysis and subsequent disassembly to monomeric form (Babst, Wendland et al. 1998). This process requires effector proteins and binding of Vps4p through its amino terminal MIT (Micro Tubule Transport/trafficking) domain with the ESCRT-III complex.

It is also noted that an ATPase deficient *VPS4* mutant is found to be associated with circular protrusions caused by over expression of Snf7p (ESCRT-III component) unable

to generate force for fission of the membrane, suggesting that ATP hydrolysis is crucial for membrane incision (Wemmer, Azmi et al.). Hence it could be possible Vps24p binding to MIT domain of Vps4p is PtdIns(3,5)P_2 dependent via coincidence detection of other effector proteins.

A study also points out that alkaline pH enhances the binding of Snf7p to all the ESCRT proteins except Vps4p (which remains unaffected) (Weiss, Huppert et al. 2009) therefore ESCRT complexes are more stable in an alkaline pH and probably vesicle budding (ILV formation) through Vps4p, requires an acidic environment. Hence an acidification defect in Δ*fab1* cells could also be one of the factors effecting Vps4p function and MVB sorting.

Cargo deubiquitination could also not be ruled out as the steady state turn-over of Ubiquitin in Δ*fab1* mutants is similar to a Δ*doa4* mutant, also supported by the fact that irreversible deubiquitination of cargo bypasses the requirement for PtdIns(3,5)P_2 in MVB sorting (Reggiori and Pelham 2001). One such scenario could be the requirement of the lipid for localization of the deubiquitinating machinery, which is in consistence with the requirement of most constitutive phosphoinositides in formation of such complexes; nonetheless very little is known regarding the formation of such complexes, let aside the lipid mediated functioning.

Some of the PtdIns3*P* is also reported to be down regulated via entering the vacuole lumen along with the ILVs, how this effects the MVB sorting process in general and PtdIns(3,5)P_2 signaling in particular, is not yet clear although logically it fits into a negative feedback loop for MVB sorting.

Figure 1.9 is a diagrammatic representation of key steps in MVB sorting and the proteins involved in regulation of each step.

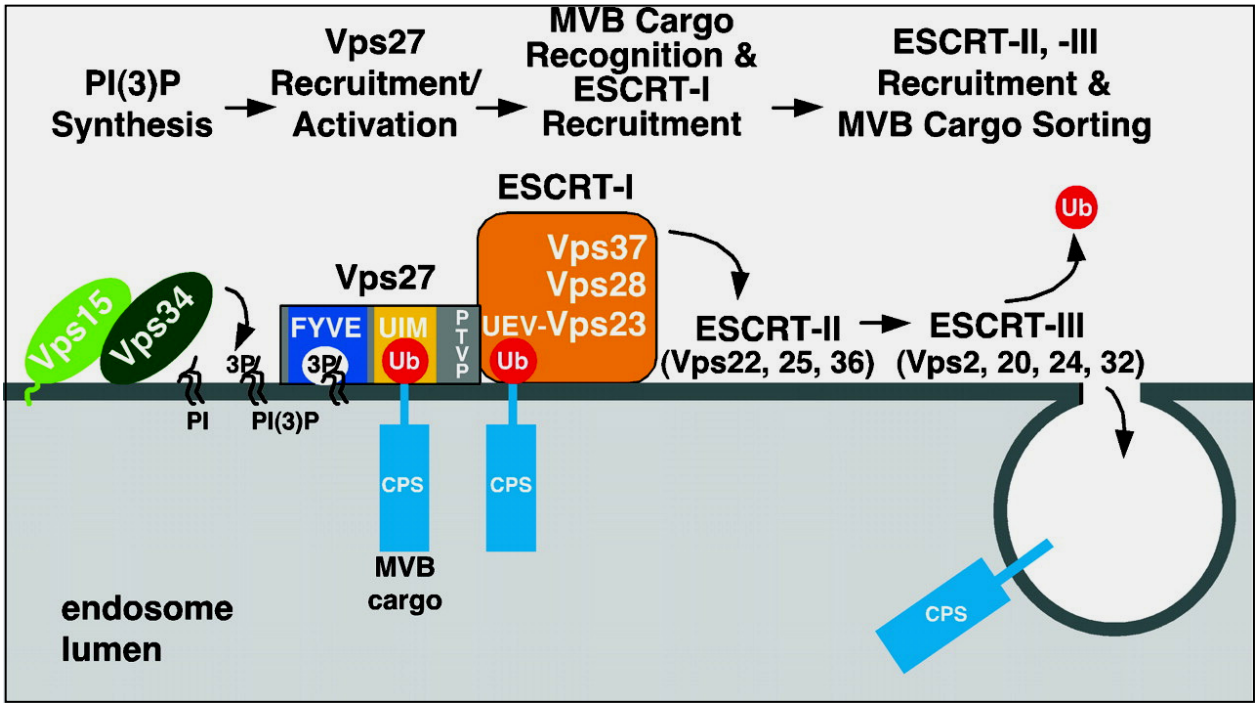

Figure 1.9: PtdIns3*P* mediated assembly of ESCRT complexes and MVB sorting of CPS (Katzmann et al 2003)

1.9 The role of Phosphoinositides in regulation of Vacuole morphology and trafficking.

Membranes are constantly exchanged between organelles in the form of vesicles which ensures apt cellular trafficking following changes in phosphoinositide levels. A number of pathways terminate at the vacuole and almost all the transport takes place through carrier vesicles. The membranes of these vesicles are marked by proteins specific for fusion with the vacuole. But continuous influx of materials into the vacuole results in an accumulation of the membrane which needs to be recycled back to the donor organelles. This is brought about through retrograde membrane trafficking and membrane fission. Besides,

these recycled membranes also need to be 'neutralized' before they are cast-off in order to retain identity of each compartment (Behnia, 2005 ; Jordens, 2005).

A number of trafficking pathways converging to yeast vacuole e.g VPS, Cvt and autophagy integrate PtdIns(3,5)P_2 and PtdIns3P signaling and hence defects in regulation of these lipids affects these pathways in multiple ways which are distinct yet overlapping and hence needs much investigation (Figure 1.10).

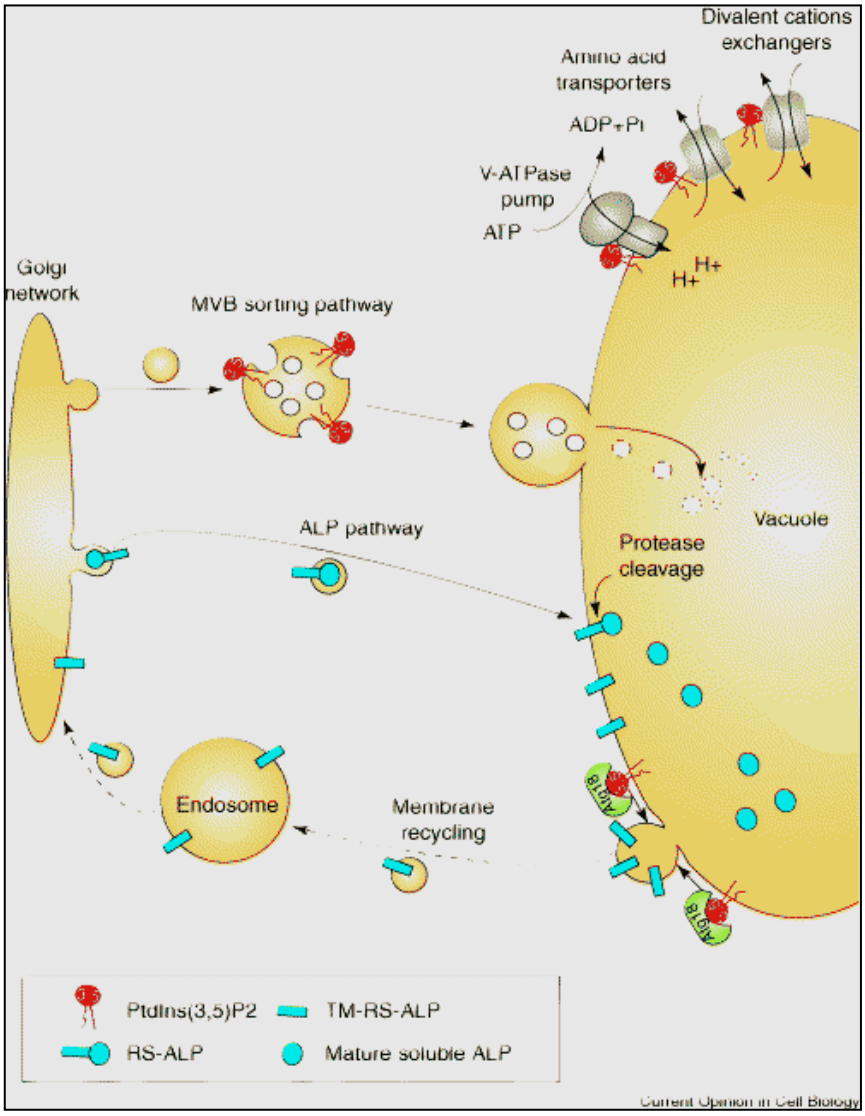

Figure 1.10: The role of PtdIns(3,5)P_2 in yeast vacuole trafficking and regulation of ion channels, nutrient channels and V-ATPase (Efe, Botelho et al. 2005).

There are two types of vacuolar fusions ; 1) Homotypic (self) fusion which is crucial for maintaining low numbers of the organelle and 2) Heterotypic (different) fusion which is the fusion of vesicles with the vacuole.

Both vacuolar fusion and fission require different sets of proteins of which known sets of proteins involved in fusion are: vesicle (v) or target (t) SNAREs, Rab GTPases, NSF, α-SNAP, HOPS/CORVET complexes and vacuolar H^+ ATPase (V-ATPase) (Karunakaran, Sasser et al. 2012). Ones involved in fission are: coat proteins such as COP I, COP II, clathrin, and GTPase dynamin (which binds PI through PH domain) (Ostrowicz, Meiringer et al. 2008).

SNAREs are integral membrane proteins which form stable *cis* (Homotypic fusion) or *trans* (heterotypic fusion) complexes which serve to anchor them to target membranes through their cytosolic facing coiled-coil loops. Yeast has 8 syntaxins (SNARE families) of which Tlg1 and Tlg2 are responsible for Late-golgi to early-endosome fusion (Bryant and James 2001) while Pep12p is a late endosome and Vam3p is a vacuolar syntaxin. These syntaxins in turn are targeted to their destined compartment through various but specific routes.Vam3p trafficking is through the AP-3 pathway (Darsow, Katzmann et al. 2001) while Pep12p is trafficked via GGA pathway where Pep12p interacts with clathrin for transport into the late endosome (Black and Pelham 2000).

Cells lacking endosomal syntaxins Pep12, Tlg1p, Tlg2p and Vam3p abolish late endosome formation. But in such cells Kex2p and V-ATPase accumulate in 2 different vesicles (Black and Pelham 2000) pointing to the fact that probably there are more then

one type of vesicle formation, each destined for a specific compartment and that disruption of any one pathway directly or indirectly effects the other pathways.

NSF/Sec18p, LMA1 and α-SNAP/Sec17p are involved in disassembly of *cis*-SNARE complexes which is considered to be essential for the docking of organelles rather than the actual fusion process. Organelle docking specificity comes from *trans*-interactions between Rab like GTPases, tethering factors and *trans*-SNAREs. Once the vesicles have tethered, the fusion or mixing of membranes is triggered by calcium signaling (Wickner and Haas 2000).

Yeast cells have 3 dynamin like proteins: Mgm1p and Dnm1p which function at the mitochondrial membrane, and Vps1p which was originally identified as a protein involved in vesicle formation at the Golgi. It has a role both in fission and fusion at the yeast vacuole, as it is a part of complexes formed during both these processes (Bryant, Piper et al. 1998).

Δ*vps1* cells exhibit both fission and fusion defects although VPS, actin organization and endocytosis are comparable to normal, illustrating its participation strictly confined to vesicle fission/fusion with the vacuole. Over expression of Vps1p results in tubulation of vacuoles under normal conditions which is much pronounced under hyper osmotic stress, where the vacuole is required to undergo fragmentation, a process requiring Ypt7p (Rab 7 homologue). On the contrary over expression of Dnm1p in wild type cells induces fission whereas over expression of Dnm1p in Δ*vps1* cells or vice versa does not rescue the defects. Hence it is postulated that Vps1p generates tubular structures of appropriate diameter and Dnm1p acts in subsequent scission (Jourdain, Gachet et al. 2009).

It is known that Vps1p couples several *t*-SNAREs together in its polymeric forms. At the on set of fusion, Sec18p/NSF (SNARE activating ATPase) and the *t*-SNARE depolymerize Vps1p which results in disassociation of Vps1p from the membrane (Peters, Baars et al. 2004). In accordance it is argued that Vps1p and Vam3p (t-SNARE) interact during fusion. The disassembly of Vps1p-Vam3p complex allows Vps1p to interact with Actin or Actin binding proteins and initiate fusion, after which it is released from the vacuole. Therefore the function and release of Vps1p depends on Sec17p-independent role of Sec18p (Collins, Thorngren et al. 2005).

The interactions between Rab GTPases and SNARE assembly were poorly understood until the identification of HOPS (homotypic fusion and vacuole protein sorting) and CORVET (class C core vacuole/endosome tethering) complexes which link the two processes.

Four class C VPS proteins namely Vps11p, Vps16p, Vps18p and Vps33p are shared amongst the 2 complexes. In addition, HOPS complex contains Vps41p/Vam2p and Vps39p/Vam6p, whereas CORVET complex has Vps8p and Vps3p (Peplowska, Markgraf et al. 2007). Strikingly, two additional intermediate complexes, Vps39-Vps8 and Vps41-Vps3 were also identified indicating that both these complexes exist in equilibrium and are interconvertable (Peplowska, Markgraf et al. 2007). They bind the PX domains of the SNARE proteins as well as act as Rab-GTPase effectors by binding Ypt7p (vacuolar Rab-GTPase) at the vacuole and Vps21p (endosomal Rab-GTPase) (Markgraf, Ahnert et al. 2009) at the endosome for SNARE assembly. Interestingly many units of the HOPS complex bind phosphoinositides specifically, PtdIns3*P*, PtdIns5*P* and PtdIns(3,5)P_2 (Boeddinghaus, 2002 ; Stroupe, 2006) . Hence it could be possible that the

lipid levels are required for recruitment of, or disassociation of such complexes from the vacuole membrane via protein-lipid interactions.

In cells, fission defects are epistatic to fusion defects and it is noted that the equilibrium between fission and fusion impinges on V-ATPase. Its physical presence is sufficient for fusion while fission requires its activity; demonstrated by a large single vacuole in mutants lacking V-ATPase, whereas pharmacological inhibition or conditional/constitutive mutants exhibit blocked vacuole fragmentation during hyper-osmotic stress (Baars, Petri et al. 2007) (Fig 1.11).

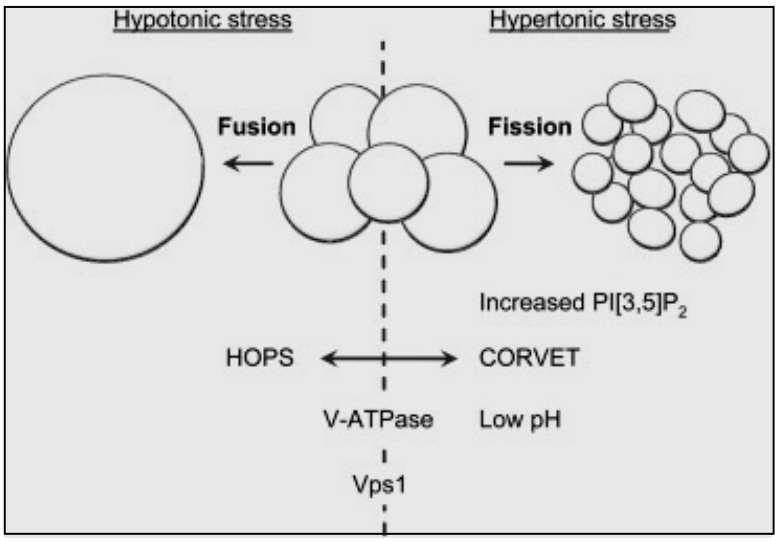

Figure 1.11: Regulation of Vacuole fission and fusion via PtdIns(3,5)P_2 (Richards,A 2010)

Although the mechanism behind such a regulation is hazy but studies have revealed that the two processes are coordinated via PtdIns(3,5)P_2 levels. Another possible link is the vacuole acidification which is essential for efficient fission/fusion and incidentally also defective in Δ*fab1* cells (lack PtdIns(3,5)P_2) (Baars, Petri et al. 2007; Lafourcade, Sobo et al. 2008).

Hence PtdIns(3,5)P_2 levels could actually intervene at numerous steps during fission/fusion of the vacuole but the underlying principle of lipid requirement essentially remains the same, i.e to act as a signal for initiation/assembly or termination/disassembly of such complexes (Xu and Wickner 2010).

In wild type cells the level of PtdIns(3,5)P_2 rises upto 30 folds under hyper osmotic stress whereas *Δfab1,* Δ*vac14* and Δ*vac7* cells which have none or very low levels of PtdIns(3,5)P_2 exhibit severe vacuole fragmentation defects under all conditions (Cooke, Dove et al. 1998; Bonangelino, Nau et al. 2002; Dove, McEwen et al. 2002; Gary, Sato et al. 2002; Efe, Botelho et al. 2005; Botelho, Efe et al. 2008; Dove, Dong et al. 2009).

Δ*atg18* cells also show vacuole fragmentation defects and are characterized by a large, single-lobed asymmetrical vacuole which is distinct from the *Δfab1* phenotype where the vacuole occupies nearly all of the cell's volume and is much more symmetrical. This difference becomes much pronounced when the cells respond to salt stress. *Δfab1* cells show no fragmentation when subjected to salt stress but Δ*atg18* cells show a decrease of vacuole fragmentation both under normal and salt stress conditions (Dove, Piper et al. 2004; Krick, Henke et al. 2008).

By using Phosphoinositide affinity matrices it was found out that many units of the V-ATPase interacted with PtdIns(3,5)P_2 (Catimel, Schieber et al. 2008) and consequently get enriched on micro-domains of docked vacuoles in order to interact with Ypt7p, Vam7p and other SNARE proteins. The concentration of HOPS complex at these sites was proposed to be crucial for coupling of Rab-GTPase and activation of SNARE assembly (Stroupe, Collins et al. 2006).

Hence a complete lack of vacuole fragmentation in Δ*fab1* cells could be explained on the basis of absence of PtdIns(3,5)P_2 synthesis and/or regulation of V_0-complex as well as HOPS complex. But 10 fold higher concentration of PtdIns(3,5)P_2 in Δ*atg18* cells and yet a large vacuole which fragments <20% under hyper-osmotic shock, cannot be explained on the basis of lipid concentrations alone, keeping in mind that Δ*atg18* cells do not have vacuole acidification defects (Efe, Botelho et al. 2007). This is only possible if there is an interaction of Atg18p with the vacuole fission/fusion machinery.

Fusion is known to be an extended, multi-step and comparatively slow process, which could be regulated at a number of points unlike fission which is thought to be a much rapid process. So it can be envisioned that the management of vacuole morphology through the intricate balance between fission and fusion could be more stringent by controlling fusion machinery where there could be many regulatory key points.
Hence if we assume that impaired fission accompanied by normal fusion is responsible for a large vacuole in Δ*atg18* cells then the key blocking point would rather be the initial stage and not the later process. So then does Atg18p act in triggering vacuolar fission, and how?

Besides the requirement of phosphoinositides for normal functioning of V-ATPase, actin depolymerization promotes PtdIns3*P* enrichment while repolymerization inhibits or displaces PtdIns3*P* at the vertex on the vacuole. PtdIns3*P* then promotes fusion and membrane remodeling via displacement of Vam7p (vacuolar t-SNARE), which is bound to the vacuole at the end of fusion and promotes uncoating of the vesicles (Cheever, Sato et al. 2001).

Sec17p enrichment is also known to reduce PtdIns3*P* levels while higher levels of Sec18p increase PtdIns3*P* on the vertex (Thorngren, Collins et al. 2004). A complex of Sec17p and Vam7p bind Sec18p at the vacuole, and later both are released for further activity. Therefore increased Sec18p activity would translate into elevated levels of PtdIns3*P* on the vacuole membrane leading to increased binding of HOPS complex and enhanced fusion, resulting in an increased release of the Vam7p. As PtdIns3*P* levels are much higher in the cell then PtdIns(3,5)P_2 therefore it is logical to believe that at any given time under normal conditions the rate of vesicle fusion is higher than vacuole fission or fragmentation.

Hyper expression of a FYVE domain in wild type cells is found to inhibit association of Vam7p with the vacuole (Cheever, Sato et al. 2001) therefore any protein with the ability to bind PtdIns3*P* or increase the availability of Sec17p at the vacuole could block the re-association of Vam7p, which could result in delayed fusion.

Atg18p binds both PtdIns3*P* and PtdIns(3,5)P_2 with much selectivity and specificity (Dove, Piper et al. 2004), hence it has the potential to block Vam7p re-association when PtdIns3*P* levels are high and block HOPS association when PtdIns(3,5)P_2 levels are high. This would give a dual control over vacuole fission/fusion machinery depending on the lipid levels.

If we assume that Atg18p regulates organelle fission/fusion in general via this mechanism, we can also explain its unidentified role in autophagy and Cvt pathway. It could be responsible for regulating fission/fusion in a likely manner in pathways

converging to the vacuole, e.g. fusion of the autophagosome with the vacuole or during processes like autophagosome formation.

In yeast, PtdIns3*P* and not PtdIns(3,5)P_2 is essential for autophagy and Cvt pathway (Krick, Tolstrup et al. 2006) but it is observed that cells with defective V-ATPase have a slowed autophagy and a blocked Cvt pathway (Kim, Kamada et al. 2001) indicating that PtdIns(3,5)P_2 mediated V-ATPase activity might be required for fusion of these vesicles with the vacuole rather than participating in the processes directly.

Vam7p association is also blocked by the ENTH proteins (PtdIns(3,5)P_2 and PtdIns(4,5)P_2 ligands) and SigD (PtdIns(4,5)P_2 5-phosphatase) (Cheever, Sato et al. 2001). On a similar trend it could be hypothesized that rate of fission could be increased in presence of PtdIns(3,5)P_2 ligands like Atg18p, which also happens to associate and regulate the PtdIns(3,5)P_2 5-Phosphatase; Fig4p. Hence Atg18p's involvement in vacuole fission/fusion could either be a direct one, or an indirect one.

1.10 Vacuole acidification and the role of Phosphoinositides

Organelle acidification is essential for the distribution and degradation of internalized ligands in the endocytic pathway, sorting of secretory proteins, regulation of post-translational modification, and vacuolar fission/fusion. As the pH of the ER is near neutral, the acidification increases progressively from the Golgi complex and is maximal at the lysosome/vacuole. Some brown and red algae have a vacuolar pH as low as 2, and values close to 0 have been reported in the vacuoles of ascidian cells. Figure 1.12 is a general representation of pH of various organelles.

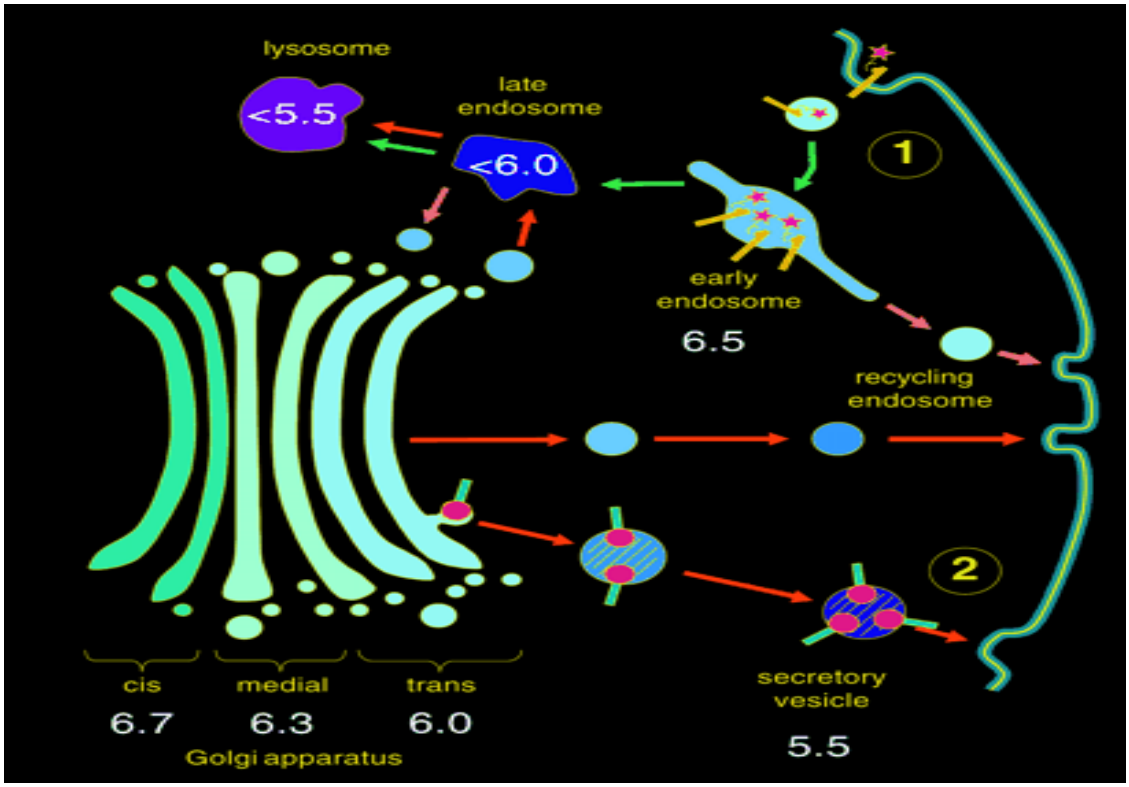

Figure 1.12: pH of various cellular organelles (Demaurex 2002)

It is postulated that maintenance of luminal acidification of the endocytic pathway and the vacuole are necessary for ligand-receptor dissociation, recycling of receptors and vacuolar protein degradation (Futerman and van Meer 2004).

A high pH in the endosome endorses endosome to Golgi influx (Nieland, Feng et al. 2004) while the low pH of the vacuole is essential for vacuolar fission as well as vesicle docking and fusion by SNARE proteins as exemplified by Bafilomycin A; an inhibitor of the V-ATPase known to inhibit fusion of the autophagosomes with the vacuole in rat hepatoma cell line (Yamamoto, Tagawa et al. 1998). Various pathways converging to the vacuole also show a perturbed vesicle transport in cells which have been incubated with Bafilomycin A, pointing out that lumenal pH of these compartments is at least one of the prerequisites for efficient vesicle transport. Although the organelle pH is essential yet

very little is known about the precise modes of regulation and the machinery involved in its maintenance.

One possible explanation could be that insertion, delivery, assembly and retrieval of Na^+-K^+-ATPases regulates the progressive differential pH of organelles at each step of the endocytic pathway. The gradient in acidification is achieved by a decrease in the passive H^+ permeability of the organelles, whereas the counter ion permeability remains high. This implies to the fact that the proton leak, rather than the counter ion permeability, sets the steady-state pH of secretory organelles. As the molecular identity of the proton leak is unknown, and the mechanism of proton conduction resembles that of voltage-gated proton channels (Demaurex 2002) it indicates that it is a highly regulated process.

Vacuolar pH is crucial for VPS pathway as well as autophagy and is maintained via Vacuolar-ATPase (V-ATPase), which is a multi-subunit transmembrane complex. It is composed of 2 multi-subunits; the transmembrane V_0 and the cytosolic V_1. The ratio between the 2 units varies and V_1 is relatively more abundant on the vacuole than the endosomes, explaining a much lower pH of the vacuole (Lafourcade, Sobo et al. 2008).

Vtc proteins were amongst the first identified set of proteins to affect the conformation of V_0 and consequently regulate the stability of the V-ATPase holoenzyme (Muller, Bayer et al. 2002). Later numerous other proteins were also recognized for their regulatory role e.g Vma21p, which is not a component of the V-ATPase yet V-ATPase subunits fail to localize to the vacuole membrane and instead accumulate in the cytosol in Δ*vma21* cells and the integral membrane unit is rapidly degraded (Hill et al 1994).

Several of V-ATPase sub-units bind PtdIns(3,5)P_2 which is also established by the fact that Δ*fab1* and Δ*vac7* cells have large neutral vacuoles. Besides yeast, such acidification defects are also observed in *C. elegans* and *D. melanogaster* cells where the Fab1 pathway is defective; but in complete contrast, the V-ATPase localization on these vacuoles is normal and does not seem to rescue the vacuole enlargement defect (Efe, Botelho et al. 2005). Hence it is not the localization or trafficking of V-ATPase but rather the function of V-ATPase via the effector proteins which is effected by PtdIns(3,5)P_2 levels.

Since lower concentrations of PtdIns(3,5)P_2 are required for vacuolar acidification then to restore normal vacuolar morphology, the acidification defects are less pronounced in mutants such as Δ*vac14*, where PtdIns(3,5)P_2 are not as low as Δ*fab1* cells and can be rescued by over expression of Fab1p (Dove, McEwen et al. 2002) indicating that either a second pathway exists for V-ATPase trafficking and/or such a pathway only requires low concentrations of PtdIns(3,5)P_2 which emphasizes on the necessity to establish the basal levels of PtdIns(3,5)P_2 *in vivo* and the effects of stress-induced accumulation of PtdIns(3,5)P_2 and its role in vacuolar acidification under such circumstances.

Δ*atg18* cells have very high levels of PtdIns(3,5)P_2 and do not show vacuole acidification defects, yet show a marked reduction in vacuole fragmentation under osmotic shock (Cooke, Dove et al. 1998). This validates the notion that Atg18p is a down stream effector protein which mediates vacuolar fission, but also indicates that normal vacuolar acidification alone cannot by-pass the requirement of Atg18p which possibly recruits other interacting partners to the vacuole for fission. This hypothesis is also in accordance

with the observation that hyper osmotic stress induces a rise in PtdIns(3,5)P_2 levels, subsequent vacuolar localization of Atg18p leading to vacuolar fragmentation.

1.11 Phosphoinositide binding protein domains / proteins

As nearly one-half of all proteins are located in or on membranes, it is not surprising that there is a variety of conserved phospholipid binding domains in eukaryotes. Some of these domain families rank in the top 15 modular domains in the human genome and are most often found in signal transduction and membrane trafficking proteins although a complete picture of how different cell types or disease states manipulate lipid signaling via protein recruitment is still awaited.

A number of predominant phosphoinositide binding protein domains are discussed here after.

1.11.1 FYVE Domain Proteins.

The FYVE domain is known to anchor the parent protein to the membrane via its insertion into PtdIns3*P* rich lipid bilayers and such membrane-mimetics are substantially increased in acidic conditions (Bryant, Piper et al. 1998).

The *EEA1* FYVE domain binds POPC/POPE/PtdIns3*P* vesicles with a Kd of 49 nM at pH 6.0, however associates approximately 24 fold weaker at pH 8.0. The decrease in the affinity is primarily due to much faster dissociation of the protein from the bilayer in basic media (Dowler, Kular et al. 2002). Lowering the pH enhances the interaction of the Hrs1p, Rufy1p, Vps27p and WDFY-FYVE domains with PtdIns3*P*-containing membranes *in vitro* and *in vivo*, indicating that pH-dependency is a general function of the

FYVE finger family (He, Vora et al. 2009). This indicates that other domains such as ENTH could also target membranes in a pH-dependent manner due to His protonation (Stahelin 2009).

The crystal structure of FYVE domain shows 2 anti parallel β-sheets and an α-helix, stabilized by 2 Zn^{++} binding clusters. The tip of FYVE domain is arranged such that it has basic and hydrophobic residues in order to achieve specificity towards PtdIns3*P* binding and avoid non specific binding (Misra and Hurley 1999).

Kular et al describes the PtdIns3*P* binding and membrane insertion of the FYVE domain through modulation of two adjacent His residues of the R(R/K)HHCRXCG signature motif. Mutation of either His residue abolishes the pH-sensitivity. Both, protonation of the His residues and nonspecific electrostatic contacts, stabilize the FYVE domain in the lipid-bound form, promoting its penetration and increasing the membrane residence time (Gaullier, Simonsen et al. 1998; Wurmser, Gary et al. 1999; Corvera 2000; He, Vora et al. 2009).

Although no substantial evidence is present in favour or against PtdIns5*P* binding of FYVE domain but it cannot be ruled out, because the crystal structure analysis of FYVE domain indicates that the PtdIns3*P* binding pocket can also accommodate PtdIns5*P* (Misra and Hurley 1999).

This becomes more exciting in light of the findings that the FYVE domain of MTMR3 is atypical in that it neither confers endosomal localisation nor binds PtdIns3*P*. Instead a deletion of FYVE domain in MTMR3 causes loss of PtdIns5*P* binding *in vitro* and *in vivo*

assays (Lorenzo, Urbe et al. 2005). Furthermore FYVE domain is not required for its catalytic activity, yet a mutation in catalytic site (C413S) leads to formation of ambiguous vacuolar structures (Walker et al., 2001) and combining this mutation with the one in the FYVE domain (C1174S) causes reduction in vacuole formation indicating the role of MTMs in PtdIns5*P*-dependent vacuolar phenotype (Lorenzo, Urbe et al. 2005).

1.11.2 PH Domain Proteins.

Pleckstrin-homology (PH) domains are modules of ~120 amino acids which are found in numerous signaling proteins involved in intracellular trafficking, cellular signaling and cytoskeletal remodeling (Lemmon, Ferguson et al. 1996).

Around 250 PH domain proteins in the human proteome have been identified. All PH domains consist of 7-stranded β-sandwich. The basic residues in the β1/β2 loop of the PH domain form a well-defined binding site with phosphoinositide head groups while the binding affinities vary from low to high (Lemmon, Ferguson et al. 1995) ($K_D > 1$ mM) (Bethoney, King et al. 2009).

Majority of PH domains have a conserved basic motif [K-X_n-(K/R)-X-R] in which the basic lysines and arginines play an important role in forming H-bonds with the head group of the PI. Other basic residues located within the domain vary from domain to domain and can provide a stronger binding affinity and create a unique binding pocket.

Two distinct members of the PH domain family, Tiam1p and Arhgap9p (Welch, Coadwell et al. 2003) that bind membranes through a site on the opposite side of the β1-β2 loop, suggest that there are still novel PH domains to be discovered within the genome. The

importance of PH domains and disease was recently highlighted in a study demonstrating that an E17K mutation in the Akt1p PH domain causes cancer (Scanga, Ruel et al. 2000).

The GRAM domain in MTMs is also postulated to be an overlap between a PH domain and the catalytic domain (Walker, Urbe et al. 2001), where it is postulated to bind PtdIns5*P* as an allosteric activator (Lorenzo, Urbe et al. 2005). PH domains are known to specifically bind to PtdIns(4,5)P_2 and/or PtdIns(3,4,5)P_3 (Lemmon, Ferguson et al. 1995).

1.11.3 PX Domain Proteins.

PX domain gets its name from Phox homology domain as it is a PIP binding structural domain first identified in proteins like NADPH Oxidase in the P40-phox and P47-phox domains. Other proteins like nexins, PtdIns 3-kinases and phospholipase D are also found to have a PX domain. Around 250 proteins have yet been identified to have a PX domain. It is approximately 120 amino-acids long and is believed to be involved in targeting of at least 47 known mammalian membrane proteins e.g the sorting nexins, and proteins involved in vesicle trafficking and phospholipid metabolism. Although PX is a structurally conserved domain yet there is very little homology in terms of amino-acid composition throughout the eukaryotes. PX domain primarily binds PtdIns3*P*, but is also reported to bind PA, PtdIns(3,4)P_2, PtdIns(3,5)P_2, PtdIns(4,5)P_2, and PtdIns(3,4,5)P_3 (Bravo et al 2001).

1.11.4 ENTH and ANTH Domain Proteins.

Ent and Ant are PIP binding proteins which were first identified to be involved in endocytosis and established to be PtdIns(3,5)P_2 binding (Eugster et al 2004). Typically,

ENTH and ANTH domains are composed of 8 α-helices connected through loops of varying lengths. Phosphoinositide binding takes place through a cleft of positively charged residues (Hyman, Chen et al. 2000). It is known that Ent proteins are required for cargo sorting between the TGN and vacuole, where Ent3p is found to be much crucial for GGA pathway whereas Ent5p functions in AP-1 pathway. It is also known that these proteins are involved in Chs3p recycling and associate with Vti1p (Copic et al 2007).

1.11.5 PROPPINS.

PROPPINs are WD repeat β-propellers and have homologues through out eukaryotes. They bind phosphoinositides especially PtdIns(3,5)P_2 and PtdIns3P with much selectivity and specificity. Most organisms have multiple PROPPINs which fold into 4-7 bladed propeller structures with an occasional loop between any of the blades (Dove, Dong et al. 2009). A typical β-PROPPIN is represented in Figure 1.13.

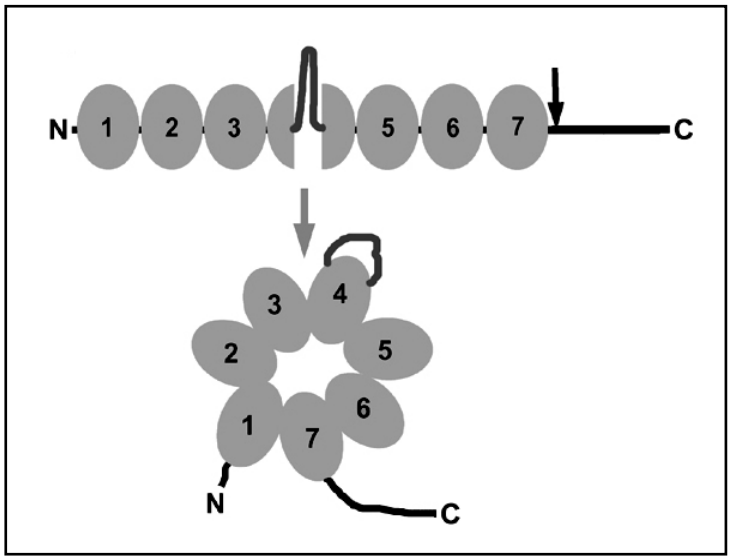

Figure 1.13: Structure of a typical β-PROPPIN (Dove, Piper et al. 2004)

There are four known PROPPINs in humans and yeast which fold into 7 bladed β-propellers. Table 2 outlines the PROPPINs in various organisms.

ORGANISM	NO OF PROPPINs	GROUP/TYPES NAMES	FUNCTIONS
S. cerevisiae	4	Atg18p	i) Fab1p/PtdIns3,5P_2 pathway ii) Autophagy iii) RS-ALP recycling out of the vacuole to the PVE. iv) Pexophagy. v) Cvt pathway.
		Atg21p	i) Autophagy particularly peroxisomes degradation. ii) Vaguely involved in Cvt pathway.
		Hsv2p	i) Cell wall formation during sporulation
		Tup1p	ii)Microautophagy. Modulation of transcription of *GAL* promoter.
Dictyostelium	4	1 representative of each group.	
Arabidopsis	5	4 belong to Hsv2 group and 1 is distinct.	
Metazoans	4 (two pairs)	Pair 1 is similar to Atg18p-Atg21p type Pair 2 is similar to Hsv2 type.	
Mammalian cells	4	WIPI I	Apoptosis, Autophagy and MP6R recycling.
		WIPI II	Apoptosis, autophagy.
		WIPI III	Membrane recycling.
		WIPI IV	Chromatin assembly, cell cycle control, RNA processing, apoptosis and vesicular trafficking.

Table 2: Known PROPPINs in various eukaryotic organisms.

PROPPINs bind PtdIns(3,5)P_2 with high affinity (*K*d 500 nM) and selectivity, and do not show significant binding to other PPln when assayed *in vitro*. The affinities of Atg18p and

Hsv2p for PtdIns(3,5)P_2 are similar to the affinity of the PH domain of PLCδ for PtdIns(4,5)P_2. However, PtdIns(3,5)P_2 is many-fold less abundant in unstressed cells than PtdIns(4,5)P_2, so it seems likely that additional protein–protein interactions might be needed to reinforce the recruitment of PROPPINs to membranes, in accord with the requirement of Vac7p for Atg18p vacuolar localization (Dove et al 2004; McEwen et al 1999).

'Lipid blot' assays suggest a preference of yeast Atg21p and human WIPI1 for PtdIns3*P* binding. The physiological meaning of this is not clear, since quantitative *in vitro* studies lead us to believe that the PtdIns(3,5)P_2 affinities of almost all PROPPINs is much more then PtdIns3*P* binding, except for DM3, a *Drosophila melanogaster* PROPPIN with equal affinities for PtdIns3*P* and PtdIns(3,5)P_2 (Lemmon 2008). Despite having a high K_D value for PtdIns(3,5)P_2 indicating specificity and selectivity, some *in vitro* assays, such as the lipid overlay assay, suggest otherwise. The apparent stronger binding of these proteins to PtdIns3*P* in such assays could simply be explained on the basis of hydrophobic/ hydrophilic properties of the 2 lipids i.e PtdIns(3,5)P_2 is much hydrophilic and tends to get washed off the nitrocellulose membrane more than PtdIns3*P* during the assay.

Expression of human WIPI1 is aberrant in cancer cells and is thought to be involved in regulation of apoptosis. Human WIPI1α has LXXLL signature motif for nuclear receptor interactions and binds androgen and estrogen receptors *in vitro*. Yeast PROPPINs namely Atg18p and Hsv2p show a striking similarity to human WIPI1 (Proikas-Cezanne et al 2004). Figure 6 represents the sequence homology of the hWipi-1α in the 7 WD domains in each blade of the propeller structure and a similar homology in yeast Atg18p and Hsv2p.

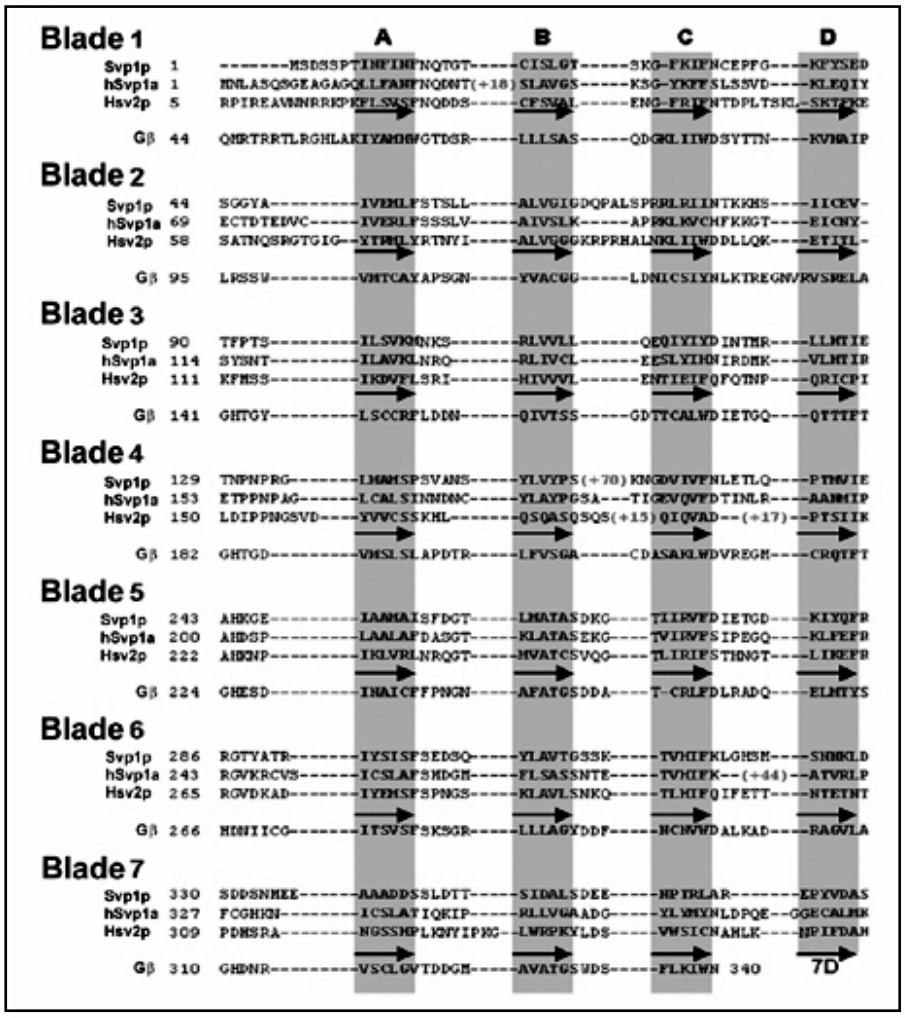

Figure 1.14: Homology between yeast β-PROPPIN (Dove et al 2004).

Atg18p, Atg21p and Hsv2p are not essential for cell survival and have independent functions. Δ*atg21* and Δ*hsv2* mutants show neither the retrograde-trafficking defect nor the abnormal accumulation of PtdIns(3,5)P_2 characteristic of Δ*atg18* cells (Dove and Johnson 2007). Δ*atg18* cells have enlarged vacuoles similar to Δ*vac7,* Δ*vac14* and Δ*fab1* cells but differ from them in having very high levels of PtdIns(3,5)P_2 and no vacuole acidification defects. Atg18p is known to physically interact with Fab1p C-terminal indicating that it might be involved in down regulation of PtdIns(3,5)P_2 synthesis (Efe et al 2007). Possibly Atg18p binding to Fab1p reverts it back to an auto-inhibited form. This

could also hold valid as Vac7p is known to recruit and interact with Atg18p on the vacuole (Efe, Botelho et al. 2007).

Hsv2p and Atg21p localize distinctively *in vivo*, and although the exact functions are not yet identified but most of the studies indicate their involvement in membrane trafficking and autophagy. Involvement of Atg18p, Atg21p and Hsv2p in vesicle fusion and membrane fission is also indicated by the finding that they are mis-localized in null mutants of some CORVET and HOPS subunits (Kane 2005) possibly influencing vesicle trafficking from the vacuole to the PVE in some fashion, promoting HOPS–CORVET subunit exchange.

Although no known phosphoinositide binding domain is mapped in these proteins but a central characteristic trait of this group is the ~75 amino-acid, highly conserved region which includes the proposed Phosphoinositide-interacting $^{Glu}/_{Gln}\psi$ Arg-Arg-Gly motif, spanning blades five and six (Michell, Heath et al. 2006) (Figure 1.13).

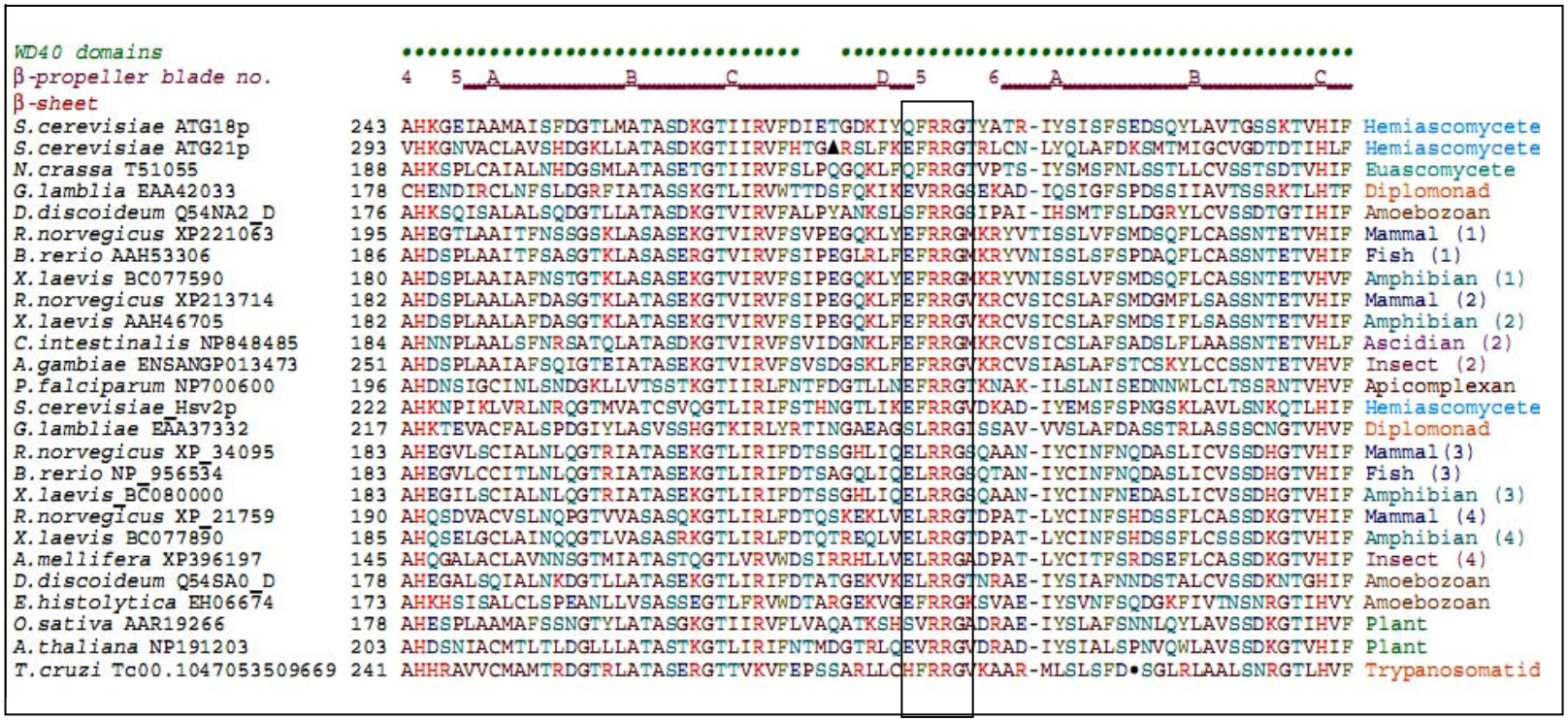

Figure 1.15: Homology between yeast and β-PROPPIN of the higher eukaryotes (Michell, Heath et al. 2006).

Mutation of Atg18p^{FRRG} to Atg18p^{FTTG} no longer binds Phosphoinositides *in vivo/vitro* and does not support retrograde vacuole-to-endosome trafficking and selective as well as non selective autophagy (Bryant et al 1998 ; Dove et al 2004) replicating the defects of the null mutant; hypothesized to be due to lack of lipid binding.

The role of Atg18p in autophagy is highlighted by the formation of an Atg18p-Atg2p complex. Surprisingly Atg18p^{FTTG} binds Atg2p, even in the absence of PtdIns3*P* binding. The cellular localization of this complex (Atg18p^{FTTG}-Atg2p) is not the same as in wild type, but is rescued by the insertion of 2xFYVE domain i.e Atg18p^{FTTG}2xFYVE. This indicates that PtdIns3*P*-binding of Atg18p is involved in directing the Atg18p-Atg2p complex to autophagic membranes but not the functioning of Atg2p or Atg18p. Atg18p^{FTTG}2xFYVE on the other hand neither restores vacuolar localization of Atg18p nor fragmentation defects under hyper osmotic shock indicating that PtdIns3*P* binding alone is not sufficient for normal function (Obara, Sekito et al. 2008).

Atg21p and Hsv2p are mis-localized from membranes in Δ*vps34* but not from Δ*fab1* cells, suggesting that PtdIns3*P* may be required for their localization *in vivo*, but why should lack of PtdIns3*P* mis-localize these proteins is yet unclear, keeping in mind that the affinity of these proteins for PtdIns3*P* is too low to be considered a key determinant. One explanation to this is that other proteins in such complexes require PtdIns3*P* (Dove et al 2004).

Tup1p is the newest addition to the list of PROPPINs found in yeast. It is shown to be involved in modulation of transcription of *GAL* promoter along with Cti1p. It binds PtdIns(3,5)P_2 with much specificity and selectivity both *in vitro* and *in vivo* (Han et al 2011).

1.11.6 Functioning of PROPPINs could be PtdIns(3,5)P_2 dependent or independent:

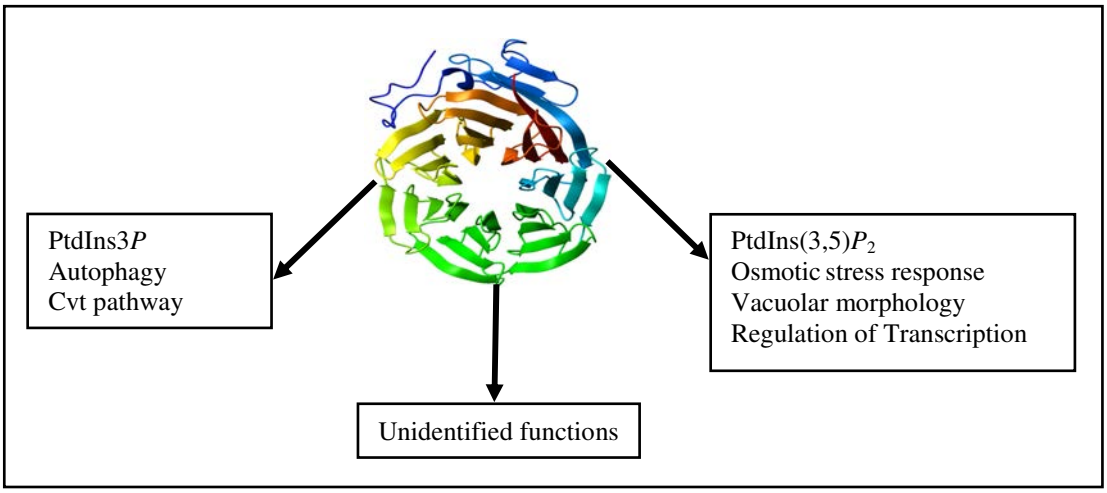

Figure 1.16: Functions of PROPPINs.

PROPPINs are known to have distinct and separable functions which are regulated by specific phosphoinositide binding. This is highlighted when Atg18p^{FTTG} (known to be defective for phosphoinositide binding) is fused with C-terminal of the vacuolar alkaline phosphatase and expressed in Δ*atg18* cells where it rescues Fab1 pathway defects but not Autophagy defects. On the contrary when Atg18p^{FTTG} is fused with FYVE domain, the autophagic defects are corrected but the Fab1 pathway defects persist (Krick, Tolstrup et al. 2006). This confirms that Atg18p autophagic functions are distinct and separable from Fab1p pathway. This also demarcates the requirement of Atg18p lipid binding for each function. However,

PtdIns(3,5)P_2 concentration in unstressed Δ*atg18* cells is 10-fold higher than in wild-type cells, indicating that feedback inhibition by PtdIns(3,5)P_2-ligated Atg18p normally limits PtdIns(3,5)P_2 synthesis at the vacuole.

In null mutants of other PROPPINs e.g Δ*hsv2* and Δ*atg21* the level of PtdIns(3,5)P_2 is normal indicating their lack of activity in regulation of lipid levels, nonetheless the autophagy related functions of these proteins are attributed to PtdIns3*P* binding while the vesicular trafficking is designated to intracellular PtdIns(3,5)P_2 levels.

Tup1p localization changes in response to PtdIns(3,5)P_2 levels and it is observed that it is redistributed to endosomes under hyper-osmotic shock while it is nuclear/ vacuolar/cytosolic under normal conditions. This is designated to impart Cti6p nuclear localization during Gal induction (Han et al 2011).

Thus PROPPINs have evolved to participate in a number of unrelated pathways and perhaps PIP binding is only required to localize the recycling machinery, with regard to various PIPs, each being specific for a typical membrane.

1.12 Atg18p

In 1990's Dove et al identified PtdIns(3,5)P_2 and its role in fragmentation of the yeast vacuole in response to hyper-osmotic stress (Dove, Cooke et al. 1997). PtdIns(3,5)P_2 levels in *Δfab1* cells are undetectable and a *fab1* null mutant exhibits a highly enlarged vacuole which fails to fragment even under 0.9M osmotic stress. In order to identify other proteins having similar aberrant vacuole morphology, a genetic screen was carried out by Dove et al (Dove, McEwen et al. 2002) and as a

result, a number of previously un-described proteins were identified to have a large vacuole phenotype. They were named *SVP1 (ATG18), SVP2 (VAC14),* and *SVP3* (Swollen Vacuole Phenotype 1-3) along with *HSV1* and *HSV2*.

It was later identified that these proteins were involved in standardizing PtdIns(3,5)P_2 levels with in the cell. Hence a large vacuole phenotype is a trait which appears when any of the Fab1p/PtdIns(3,5)P_2 pathway genes are disrupted which gave a direct indication that phosphoinositides play a crucial role in regulation of vacuole morphology.

Homology studies revealed that Svp1p was a previously identified protein namely Atg18p, which was described to play some unknown role in autophagy, while Svp2p was homologous to Vac14p. But no such alias was recognized for Hsv2p and Hsv1p although now there are a few references of them being involved in selective autophagy.

Atg18p, Atg21p and Hsv2p were collectively named PROPPINs due to their molecular configuration and PIP binding. They share some 70% homology amongst them and were later identified to be PtdIns(3,5)P_2 effector proteins and bind PtdIns3*P* and PtdIns(3,5)P_2 *in vivo* and *in vitro* assays with much selectivity and specificity (Dove, Piper et al. 2004). The exact mechanistic details of how these proteins regulate vacuole morphology and participate in autophagy are not clear and the extent of their involvement in other trafficking events is also not yet characterized.

Δ*atg18* cells have enlarged vacuoles, autophagy defects, trafficking defects, aberrant hyper-osmotic stress response, sporulation defects, block in pexophagy and the Cvt pathway, and growth defects on media containing glycerol as a sole C source as well as show reduced expression of RTG2 regulated genes even when unstressed (Kim et al 2001).

It is postulated that Atg18p and similar proteins have at least 2 known distinct roles, one which requires PtdIns3*P* binding (autophagy) and one which requires PtdIns(3,5)P_2 (Fab1 pathway) and hence may act in localizing/recycling of proteins to particular sites within the cell using lipid binding for localization (Guan, Stromhaug et al. 2001).

This is proved in studies where Atg18p binds to PtdIns3*P* for PAS localization (Abeliovich and Klionsky 2001) and PtdIns(3,5)P_2 for vacuolar localization (Dove et al 2004). PAS localized Atg18p is further involved in localization of Atg2p and recycling of Atg9p, while vacuolar Atg18p is required for retrograde trafficking from the vacuole to the late endosome (Bryant, Piper et al. 1998) and regulation of Fab1p.

In plants, staining with the autophagosome-specific fluorescent dye, monodansylcadaverine reveals that, unlike wild-type, *AtATG18a* RNA interference plants were unable to produce autophagosomes in response to starvation or senescence conditions. Hence *AtATG18a* induction, in Carbon/Nitrogen starvation and during senescence is required for complete autophagic response (Xiong, Contento et al. 2005).

As Atg18p and Atg21p are not known to initiate autophagosome formation neither over expression increases the total autophagic turnover (Krick, Muehe et al. 2008), it is possible that they function in preventing the premature cleavage of Atg8p-PE by regulating the access to the substrate; which is PtdIns3*P* dependent.

In Δ*atg18* cells, Atg8p-PE is recruited to the PAS in the normal fashion under starvation or nutrient rich conditions, but Atg21p/Hsv2p is required for correct Atg8p-PE targeting in nutrient rich conditions. Atg18p-Atg2p complex formation on the other hand does not require PtdIns3*P* for its formation (Kobayashi, Suzuki et al.). Therefore Atg18p is not solely required for Atg8p recruitment at the PAS, but possibly functions at a later stage. Hence Atg18p could participate in autophagy by recycling membrane proteins, which is probably blocked in Δ*atg18* cells resulting in exhaustion of autophagosome forming proteins.

Contrary to this, involvement of Atg21p/Hsv2p in Peacemeal-nucleophagy (PMN) (Krick, Henke et al. 2008) suggests that in nutrient rich medium Atg21p and Atg18p may be epistatic but these proteins do not have completely overlapping functions in terms of regulation of various types autophagy. Nonetheless, for an efficient autophagic response to starvation, Atg18p localizes at PAS through PtdIns3*P* binding (Obara, Sekito et al. 2008; Klionsky 2009) which does not have an allosteric effect but is required for membrane localization, and is not essential to take place through the native site for consequent function as well (Obara, Sekito et al. 2008; Klionsky 2009).

Vps34 forms 2 complexes for targeted PtdIns3*P* synthesis and interestingly, Atg18p is found to be involved in the processes regulated by both Vps34 complex I and II as well as regulation of vacuolar morphology (Kihara, Noda et al. 2001).

Another prominent function of Atg18p is to regulate the PtdIns(3,5)P_2 synthesis under stress and normal conditions, but the exact details are much awaited. Δ*fab1* cells exhibit a highly enlarged, single, symmetrical vacuole which shows the conFigureuration of an open 8 in dividing cells. This is linked to the requirement of PtdIns(3,5)P_2 in cytokinesis and vacuole inheritance. Δ*atg18* cells do not necessarily show open Figure eight morphology of the vacuole in some backgrounds, but it is known to localize at the elongating membrane tips during cell division, due to unexplained reasons (S. K. Dove, unpublished work). Nonetheless, Atg18p participates in regulation of vacuole morphology and to a lesser extent vacuole inheritance and membrane constriction events such as vacuole fission via regulating PtdIns(3,5)P_2 levels. Surprisingly PtdIns(3,5)P_2 levels in a *Δatg18* cells is 10 folds higher as compared to wild type cells, indicating its involvement in feedback inhibition of PtdIns(3,5)P_2 synthesis (Dove and Michell 2009) rather than its synthesis.

Under normal conditions Atg18p localizes to punctate structures juxta imposed to the vacuole and on the vacuole membrane. In Δ*fab1* cells, Atg18p loses its vacuolar association indicating that this could be due to PtdIns(3,5)P_2, but not the punctate localization. The vacuolar localization is also not dependent on a functional Cvt/Atg pathway, arguing against the possibility that Atg18 reaches the vacuole via Cvt vesicles or autophagosomes (Guan, Stromhaug et al. 2001).

Interestingly, the association of Atg18p with the vacuolar membrane is easily disrupted by osmotic lysis, but its binding to the peri-vacuolar punctate structure(s) is retained under the same conditions, suggesting that the nature of the association might be different.

Fab1p and Vac7p over expression can partially rescue Δ*atg18* cells indicating that a second PtdIns(3,5)P_2-dependent process, requiring Fab1p and Vac7p but not Atg18p, achieves some of the membrane exit from the vacuole, and that this process contributes to the vacuole enlargement in *fab1*Δ and *vac7*Δ cells besides low levels of PtdIns(3,5)P_2 (Duex, Tang et al. 2006).

One speculation would be the participation of the two other PROPPINs, Hsv2p and Atg21p in this process. However, single and double null mutants show no vacuolar defects, even though they bind PtdIns(3,5)P_2 avidly; although deletion of either of them partially reduces vacuole fragmentation in response to hyperosmotic stress (S. K. Dove, unpublished work).

WIPI-1 is a human homologue of Atg18p and folds as a β-propeller and functions to act as a PtdIns3*P* scaffold at the Phagophore (Puncta formation) (Proikas-Cezanne and Pfisterer 2009). One member of this family, WIPI 49, co localizes with MPR at TGN, endosomal membranes and clathrin coated vesicles (Jeffries, Dove et al. 2004).

Interestingly one study through RNAi, suggests that lack of PtdIns3*P* binding (mutant R221,222A) in WIPI 49 does not disrupt the MPR pathway but is essential

for normal endosomal organization and CI-MPR distribution (Jeffries, Dove et al. 2004). Such PtdIns3*P* binding deficient WIPI49 does not accumulate at the puncta indicating a role in regulation of compartment identity through membrane recycling, via lipid binding. This is also supported by the observations that WIPI-1 puncta-formation is inhibited by wortmannin and LY294002 (PIP III kinase inhibitors), and PtdIns3*P*-binding-deficient WIPI-1 (Proikas-Cezanne, Ruckerbauer et al. 2007).

On the other hand when autophagy is induced by rapamycin, gleevec, thapsigargin or amino acid deprivation, WIPI-1 accumulates at LC3-positive membrane structures as punctae. This is interesting as quantitative analysis of WIPI-1 puncta formation could be used to analyze basal and induced or inhibited levels of phagophore formation in mammalian cells.

1.13 Aims and objectives

The overall plan of the project was to define the cellular functions of Atg18p and by extension unravel the functions of other PROPPINs. This was undertaken by asking the following questions which were the primary aims of this project:

1. To resolve whether PtdIns(3,5)P_2 binding site and PtdIns3*P* binding site is the same in Atg18p? This was investigated by examining the localization and lipid binding of ATG18 mutants.
2. To examine if phosphorylation of the FRRGT motif can differentially affect PtdIns(3,5)P_2 binding versus PtdIns3*P* binding? What would be the phenotypic effects of mutating this possible phosphorylation site? This was investigated through FT-ICR-MS analysis.
3. Which trafficking pathways, to and from the vacuole is Atg18p involved in? This was investigated via studying the localization of various cargo proteins in Δ*atg18* background and GFP localization of Atg18p in various deletion backgrounds.
4. Does Atg18p bind adaptin AP-3? Atg18p has a very clear consensus sequence to bind the non-clathrin adaptin AP-3. Since mutation of other AP-3 binding proteins can affect Atg18p's localization, would it be possible that Atg18p binds/interacts with AP-3 *in vivo*? Tagging Apl5p, a subunit of AP-3 and directly measuring the binding to recombinant Atg18p *in vivo* via Co-IP was used to investigate this hypothesis.
5. Since Apl5p is known to interact with Vps41p, a HOPS subunit required for homotypic fusion, is it possible that Atg18p interacts with Vps41p? This was investigated via Co-IP of Atg18p with Vps41p *in vivo*.

Chapter 2; Materials and methods

2.1 Yeast and *E. coli* strains

BY4742 yeast wild type and null mutants were obtained from EUROSCARF (Germany) while wild type FY833 strain was purchased from ATCC (Manassas, USA).

Some yeast knock-ins and knock outs were from S.K.Dove lab (where specified) while others were made during this study (appendix 2).

All *S. cerevisiae* strains were grown in either yeast extract peptone/tryptone dextrose media (YEPD/YETD) or synthetic complete (SC) selective media (as specified) at 30/25°C.

E.coli TOP10 (Invitrogen) or BL21-star (DE3)-RIL (Stratagene) cells were used for sub cloning. *E.coli* cells were grown in LB media with appropriate antibiotics for selection.

2.2 Plasmids

pUG36 and pUG34 plasmids were gifted by Dr. J. H. Hegemann (Institut für Mikrobiologie, Germany). Plasmid pUG34 is a low copy centromeric yeast expression vector and was modified by Dr. Hegemann so that GFP is expressed as a C-terminal fusion to any gene cloned in frame into the multiple cloning sites (Niedenthal et al., 1996).

pUG36 (YCp, URA3, *p*MET25-yEGFP3-MCS-TCYC1 (Niedenthal et al., 1996) plasmid was used for green fluorescent protein (GFP) tagging and for microscopic analysis of localization of the protein of interest *in vivo*.

Cloning of genes in multiple cloning site of pUG36 allows the expression of yEGFP N-terminal fusion proteins under the control of methionine-regulated MET25 promoter (Mumberg et al., 1994).

pUG36-*ATG18*, pUG36-*ATG18*^{FTTG}, pRS316-ATG18^{FTTG}-GFP-FYVE, pUG36-*VAC7*, pUG36-*VPS41*, pRS423, pYM6 and pUR34-NLS were obtained from the Dove lab plasmid collection.

ATG18/atg18 site specific and random mutants were cloned into *Xho* I / *ECoR* I sites of pUG36 and pGEX-6P-K1.

Commercially available pGEX6P-1 (G.E.Biotech) plasmid was modified by Dr Dove and used for GST tagging of proteins. The modification was carried out by inserting protein kinase A phosphorylation consensus motif between GST and the protein of interest (pGEX6P-T1). Details pertaining these and other plasmids, which were received as gifts and used without modifications are listed in appendix 1.

2.3 Reagents and chemicals

All reagents and chemicals were purchased from Sigma and were Biotechnological grade or higher except Yeast extract, bacto peptone, bacto agar, yeast nitrogen base without amino acids and ammonium sulphate which were obtained from Difco Laboratories.

2.4 Site specific mutagenesis

Site specific/point mutations were created through PCR, using serial overlap extension (SOE) forward and reverse primers. Forward and reverse primers specific

for introducing the point mutation (shown in red) within the gene of interest were approximately 28-35 base pairs in size and are listed in table 2.1.

Mutation	Primer		Sequence		T_M °C
A263R	S001-SVP1-1-F	5'	ATGGCTACCAGATCTGATAAAGGTACTATCATCAG	3'	65.12
	S001-SVP1-1-R	3'	AAACTACCCTCTGATTACCGATGGTCTAGACT	5'	65.30
K266T	S002-SVP1-2-F	5	CCGCCTCTGATACTGGTACTATCATCAGG	3'	65.54
	S002-SVP1-2-R	3'	CCGATGGCGGAGACTATGACCATGATAG	5'	65.47
R271T	S003-SVP1-3-F	5'	GTACTATCATCACTGTCTTTGACATTGAAACGG	3'	64.11
	S003-SVP1-3-R	3'	CATGATAGTAGTGACAGAAACTGTAACTTTGCCC	5'	64.08
K280T	S004-SVP1-4-F	5'	TGAAACGGGTGATACTATCTACCAATTCAGGAG	3'	64.11
	S004-SVP1-4-R	3'	ACTTTGCCCACTATGATAGATGGTTAAGTCCTC	5'	64.11
H244R	S005-SVP1-5-F	5'	GGTCATCGAAGCTCGTAAGGGCGAGAT	3'	65.45
	S005-SVP1-5-R	3'	CCAGTAGCT TCGAGCATTCCCGC TCTA	5'	65.45
T268R	S006-SVP1-6-F	5'	GCCTCTGATAAAGGTCGTATCATCAGGGTCTTT	3'	65.3
	S006-SVP1-6-R	3'	CGGAGACTATTTCCAGCATAGTAGTCCCAGAAA	5'	65.3
Q283N	S007-SVP1-7-F	5'	GGGTGATAAGATCTACAAATTCAGGAGAGGGA	3'	65.3
	S007-SVP1-7-R	3'	CCCACTATTCTAGATGTTTAAGTCCTC TCCCT	5'	65.3

Table 2.1: Primers for Atg18p PCR based point mutants.

These primers were used to create site specific mutations using pUG36-*ATG18*^{Wt} as a template.

Expand High Fidelity PCR system (Roche) was used for creating point mutations in TECHNE TC-3000 (Staffordshire, UK) thermal block cycler. The desired fragment was amplified by a 2 step serial overlap extension PCR (Warrens, Jones et al. 1997). During the first round of PCR, pUG36-*ATG18*^{Wt} was used as a template with primers SOE-A1 and a reverse primer with the mutation site producing PCR fragment A. Simultaneously primer SOE-D1 with the forward primer with the

mutation site produced PCR fragment B. Both the PCR fragments A and B were then used for second round of PCR where they served as templates for primers SOE-A1 and SOE-D1. The resulting PCR product was a fragment of 2Kb housing the site specific mutation (Figure 2.1).

STEP 1

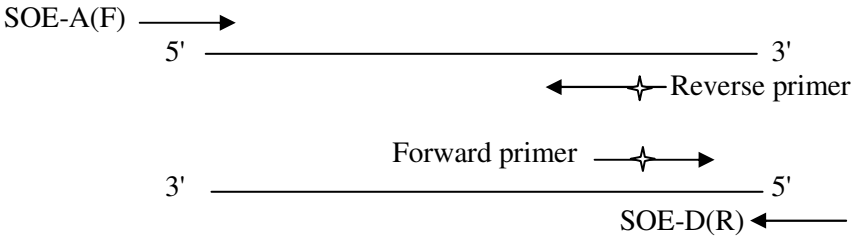

STEP 2

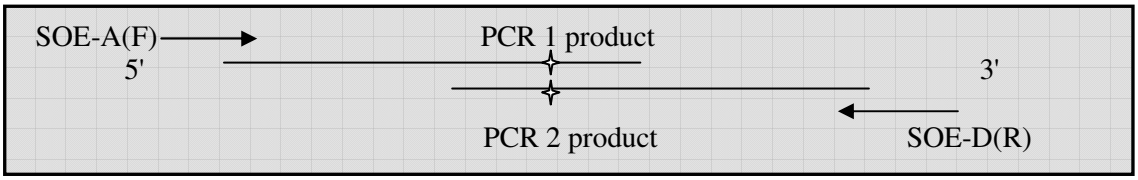

STEP 3

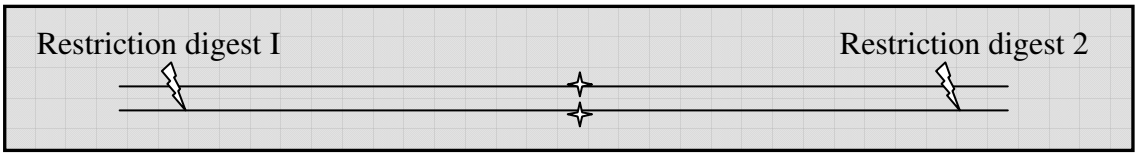

STEP 4

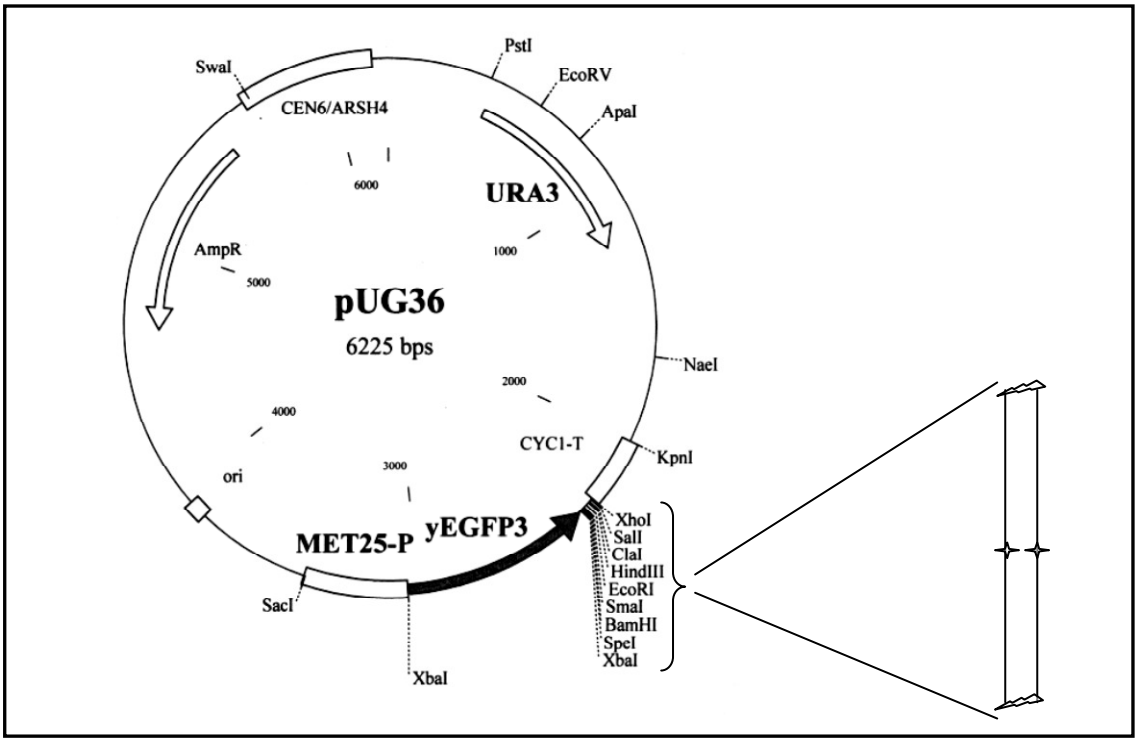

Figure 2.1: serial overlap extension (SOE A/D) PCR

PCR programme was as follows:

	PCR I	PCR II	Time in Min
Initial denaturation	94°C	94°C	2
Loop one;5 Cycles:			
Denaturation	94°C	94°C	1
Annealing	52°C	49°C	1
Template Extension	68°C	68°C	1.2
Loop two; 25 cycles			
Denaturation	94°C	94°C	1
Annealing	57°C	57°C	1
Template extension	68°C	68°C	1.2 (PCR I), 2.3 (PCR II)
Final elongation	68°C	68°C	10
Final hold	10°C	10°C	

Table 2.2: **PCR programme for site specific mutations in *ATG18*.**

The resulting 2 Kb fragment was digested with appropriate restriction enzymes (*EcoR* I / *Xho* I). The digested product was again run on 1% Agarose gel to recover 1.5Kb fragment which was used for ligation with the Vector (pUG36, for GFP tagging and pGEX6T1 for GST-tagging) using T_4 DNA ligase (New England Biolabs) at 16°C. The plasmid was transformed into *E.coli* and at least 5 colonies were grown overnight for Miniprep. The minipreps were redigested and checked for the right construct which was later verified through sequencing. Either Alkaline lysis or QIAquick spin Miniprep kit was used for *E.coli* plasmid minipreps. The point mutants created through this method are represented in Figure 2.2.

The PCR mix was made according to the following recipe;

	Concentration (stock solutions)	Volume used
Primer(s)	100 pmol	1.5 µl each
dNTPs	25 mM	1 µl
Tgo/*Taq* polymerase	3.5 Units/µl	1 µl
$MgCl_2$ Buffer	25 mM $MgCl_2$	10 µl
Template	≥400 ng	1.5 µl
Water		to make up 100 µl / reaction

Table 2.3: PCR mix

Mutant	Amino Acid (wild type)	Amino Acid (mutant)	Charge on Amino-acid Wt	Mutant
H244R	HIS	ARG	+	+
A263R	ALA	ARG	0	+
K266T	LYS	THR	+	0
T268R	THR	ARG	0	+
R271T	ARG	THR	+	0
K280T	LYS	THR	+	0
Q283N	GLT	ASP	0	0

Table 2.4: *ATG18* point mutations

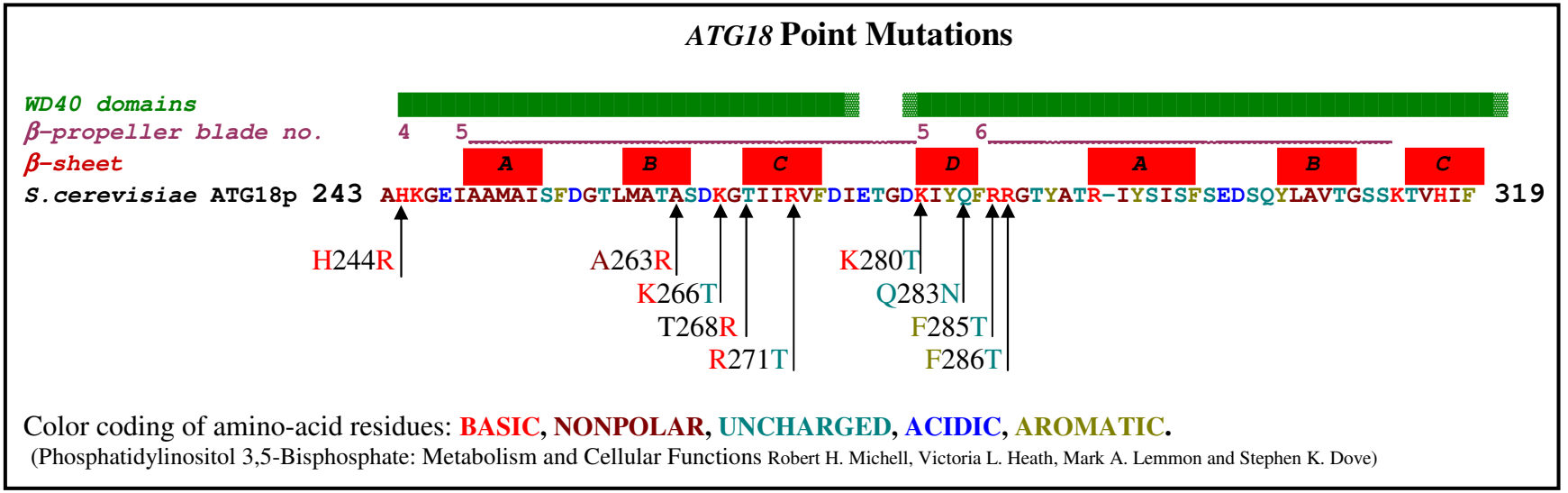

Figure 2.2: Point mutations created in ATG18 using SOE method.

2.5 DNA Sequencing

3 µl of sample, containing a minimum of 400 ng of DNA, was mixed with 1.6 µl (20 pmol, final concentration=3.2 pmol) of primer SOE-A1 or SOE-D1 (depending on the region of interest) and volume made up to 10 µl with double distilled deionized water.

This sample was sent to the Functional Genomics and Proteomics Unit, University of Birmingham (Birmingham, UK), which performed the sequencing of the samples, using ABI sequencing device. The device uses the 'big dye3 dideoxy' method and separates the dye labelled fragments by capillary electrophoresis. The sequencing data was analyzed in Chromas (version 1.45).

2.6 Cloning and Plasmid construction

'High fidelity polymerase', a mixture of *Tgo* and *Taq* polymerases (Roche) was used for creating site-specific mutations, and most of the other routine PCR products were used for cloning. Bioline Taq-polymerase was used for error-prone PCR and for some later genetic manipulations of yeast; to insert epitope tags into chromosomal genes. DNA restriction enzymes and T_4 DNA ligase were from New England Biolabs, Inc (Beverly, MA). Cloning was carried out using standard molecular biology techniques. PCR products were purified using ethanol precipitation method. Plasmid minipreps were performed using kits obtained from Qiagen Ltd. All PCR primers were synthesized by Alta Biosciences, University of Birmingham, UK.

2.7 DNA preparations

2.7.1 Genomic DNA preparation

50 ml of cell culture was grown to a cell density of 2 x 10^7 cells / ml in appropraite media. The cells were then spin down at 3000 xg for 5 minutes at 30 °C and the supernatant was discarded. The cell pellet was resuspended in 50 ml of 20mM Tris-Hcl, pH 8.9. It was then spin at 2000 xg at 30 °C for 5 minutes and the cell pellet was resuspended in 10 ml of 20mM Tris-Hcl, 10 mM EDTA, and 10mM DTT (freshly made) pH 8.9 and the cells were incubated in a water bath at 30 °C for 20 minutes. The cells were spin down at 2000 xg for 1 minute and the cell pellet was resuspended in 5 ml of 1M sorbitol, 50 mM K_2P0_4 pH 7.4 and zymolyase 20T (300 units) 1mg (final concentration) and incubated at 30°C for 30 minutes in a water bath.

The cells were then spin down at 1000 xg for 5 minutes and the supernatant was discarded. 10 ml of 1M sorbitol was added to the cell pellet and mixed gently and spin down at 1000 xg for 5 minutes. The supernatant was discarded carefully without disturbing the pellet.

5 ml of lysis buffer from Qiagen® genomic DNA preparation kit was added to the pellet along with 10 µl of RNAase A (25 mg / ml) and 100 µl of proteinase K (25 mg / ml) and after gentle mixing it was incubated at 50 °C for 40 minutes until the supernatant becomes clear. It was then spin at 4000 xg at 4 °C for 15 minutes and the supernatant was collected carefully.

This supernatant was passed through a pre-equiliberated column (100) under gravity flow. The column was washed once with wash buffer and the DNA was eluted in 2 ml TE buffer. The DNA was concentrated using ethanol precipitation.

2.7.2 Diagnostic DNA preparation (miniprep)

3 ml of cell culture was grown over night at 37 °C. The cells were spin down at 3000 xg and to the cell pellet, 250 µl of resuspension buffer from Qiagen® was added and mixed throughly. 250 µl of lysis buffer was added to the mixture and and mixed through inverting the tubes several times and left to stand for 5 minutes at room temperature. 300 µl of Neutralization buffer was then added and mixed throughly and the mixture was spin down at 13000 xg for 20 minutes at 4 °C. The supernatant was passed through the Qiagen column through centrifugation and washed once with wash buffer. The DNA was eluted in 500µl TE buffer and concentrated using ethanol precipitation.

2.7.3 Preparative DNA preparation (midi/maxi prep)

25 / 100 ml of cell culture was grown over night at 37 °C and the cells were spin down at 3000 xg. The cell pellet was resuspended in 4 / 12 ml of resuspension buffer and 4 / 12 ml of lysis buffer was added to the mixture and mixed gently by inverting the tubes several times. It was left at room temperature for 5 minutes and then 10 / 40 ml of neutralization buffer was added and mixed throughly.

It was then spin down at 15000 xg for 30 minutes at 4 °C and the supernatant was passed through a pre-equiliberated Qiagen tip (100) under gravity flow.

The column was washed once with 70 % ethanol and the DNA was eluted in 2 / 5 ml TE buffer and concentrated using ethanol precipitation.

2.8 Ethanol precipitation of DNA.

200 µl of DNA was mixed with 20 µl of 3M Sodium Acetate pH 5.2 and 400 µl ice-cold ethanol and mixed gently. It was then incubated on ice for 30 minutes and

centrifuged at 10000 *xg* for 20 minutes at 0°C. 250 µl of 70% ethanol was added to the pellet and after gentle mixing the sample was centrifuged again at 10000 *xg* for 10 minutes at 4°C. The supernatant was discarded while the pellet was left to dry and re-dissolved in double distilled deionized water.

2.9 *E. coli* Transformations.

100 µl of competent Top 10 *E.coli* cells (appendix 3) were thawed on ice for 10 min and 3-5 µl of the plasmid DNA was added to the cells. The cells were further incubated on ice for half an hour and then incubated at 42°C in a water bath for 90 sec. 1 ml of ice cold SOC (appendix 6.8) was then added and the cells left to recover for a further half an hour at 37°C in a shaking incubator at 90-100 rpm.

The cells were then harvested by centrifugation at 2000 *xg* for 5 min and spread on to appropriate selective media and incubated at 37°C for 14-16 hours.

2.10 Yeast transformations

Yeast strains were grown overnight in YEPD + 2% Glucose + selective antibiotic/ drop out amino acid, at 25/30°C to 0.5 OD_{600nm}. The cells were harvested by centrifugation at 3000 *xg* and the cell pellet washed with 1 ml 0.1M lithium acetate. Supernatant Lithium acetate was discarded after a quick centrifugation at 3000 *xg* and to the cell pellet the following reagents were added and mixed well in the exact order as listed below:

240µL 50% PEG

36 µL 1M Lithium acetate

50 µL 2mg/ml ssDNA (boiled)

03-15 µL Plasmid DNA / PCR product

Double distilled water to make up the volume to 350µL.

This mixture was mixed gently until the cell pellet was resuspended and then placed in the incubator at 30°C for 30-45 minutes. It was then subjected to heat shock at 42°C for 20 minutes. The temperature sensitive strains were left at 30°C over night and not heat shocked.

The reagents were then removed and the cells harvested through centrifugation at 1500 *xg*. 200 µl of double distilled water was added and the cells were mixed gently before they were spread onto SC selection medium and incubated at 25/30°C for 4 days.

2.11 Microscopy

Single colonies were picked with sterile pipette tips and cultures were grown over night in selective media at a suitable temperature. 200-400 µl of the over night culture was resuspended in 1 ml of fresh media and incubated at a suitable temperature for further 2-4 hours (depending on the strain background) to 0.5 OD_{600nm}. The cells were spun down at 1000 *xg* and resuspended in MES buffer pH 5.6. 2 µl of the cell culture was then used to prepare slides for microscopy. Nikon Eclipse E600 microscope with an XF100-3 filter cube (Omega Optical) and Nikon Plan Apo (100×/1.40 oil DIC H) projector was used to obtain images with ORCA digital camera (Hamamatsu, Japan) and processed in Adobe Photoshop. The magnification was x1000 and each image represents the phenotype exhibited by >90% of the cells.

2.12 Induction of autophagy through rapamycin

1 ml of cell cultures were grown overnight in appropriate media at a suitable temperature to an OD_{600nm} 0.6-0.7. The cells were washed once with fresh media

and resuspended in 1 ml of 1.7 % YNB + 2 % glucose and 0.2 µg /ml of rapamycin and incubated at an appropriate temperature for 4 hours. They were then examined microscopically either directly or resuspended in MES buffer pH 5.6 and then viewed using a GFP filter / RFP filter.

2.13 Cyclohexamide treatment

Cells were grown overnight in appropriate media to 0.6 OD_{600nm}. The cells were washed once in fresh media and once in 1.7% YNB with 2% glucose. The cells were then incubated in 1.7% YNB with 2% glucose and 200 µM cyclohexamide at 25 °C for 4 hours (Siegel and Sisler 1963). The cells were then washed once and resuspended in MES buffer pH 5.6 and examined microscopically.

2.14 FM4-64 Staining

100 µg of FM4-64 was dissolved in 10.3 µl of DMSO to make 16 mM FM4-64 stock solution.

1 ml of cell culture was grown to 0.6 OD_{600nm} and centrifuged at 1000 *xg*. The supernatant was discarded and the cell pellet resuspended in 200 µl of fresh media. 0.5 µl of 16 mM FM4-64 was added to 200 µl of pre-washed cell culture (40 µM final concentration of FM4-64) and incubated at 25°C or 30°C (depending on cell culture) in an orbital shaker for 1hour. The cells were then centrifuged at 1000 rpm for 1 minute and washed twice with fresh media. The cell pellet was then resuspended in 200 µl of MES buffer pH 5.6 + 2% glucose and examined microscopically using RFP filter (Vida and Emr 1995).

2.15 Co-localization

BY4741 strains with various RFP tagged organelle markers (Erin'O'Shea et al 2003) were used for co-localization with GFP tagged Vps41p, Vac7p, Fab1p, Vac14p Atg18p and Atg18p^{mutants} using standard yeast transformations. Each strain had a RFP tagged organelle marker as follows:

Strain	Marker	Organelle
BY4741	ANP1-RFP:KAN	TGN
BY4741	COP1-RFP:KAN	Golgi to ER
BY4741	CHC1-RFP:KAN	Golgi to vacuole (vesicles)
BY4741	PEX3-RFP:KAN	Peroxisomes
BY4741	SEC3-RFP:KAN	ER to Golgi
BY4741	SNF7-RFP:KAN	Late endosomes

Table 2.5: RFP tagged organelle markers used for co-localizations.

Each BY4741 cell culture with the specific RFP-tagged organelle marker was grown overnight in YEPD and G418 at 30°C. Standard yeast transformation protocol was used to transform these cells with GFP plasmids containing the genes of interest and grown on selective media. The successful transformants were grown to 0.5 OD_{600nm} and examined through fluorescence microscopy using GFP and RFP filters.

At least 60 cells from each cell culture were taken in to account for co-localization studies. The total number of red dots (punctae)/cell and green dots (punctae)/cell were counted individually for all 60 or more cells. Then the RFP and GFP images were merged using Photoshop software and the total number of overlapping dots counted for each cell for all the cells.

The total number of overlaps per cell were taken as a percentage of the RFP dots/cell and GFP/dots respectively. The percentage of the overlapping green dots and red dots were then calculated as a measure of the 2 individual percentages.

Total number of cells = ≥ 60

Total number of red dots/60 cells = X

Total number of green dots/60 cells =Y

Total number of green/red overlaps / 60 cells = Z

Percentage of red dots overlapping = X% of Z

Percentage of green dots overlapping = Y% of Z

Total percentage of overlaps = X% of Z ÷ Y% of Z

(Appendix 4)

2.16 Standard curve for cell OD

BY4742-wt and BY4742 Δ*atg18*::KAN cells were grown over night at 30 and 25°C respectively.

This cell culture was used for serial dilution from 10^1-10^{10}.

Number of cells for each dilution was counted by using a Neubauer's chamber, and a reciprocal OD_{600nm} was taken for each sample simultaneously. The OD_{600nm} versus the cell count was used to plot the standard curve (appendix 4.2).

2.17 Cell count using Neubauer's chamber

Cell culture(s) was grown over night in appropriate media with 2% glucose at 25/30°C. Cell OD_{600nm} was noted using Gene Quant Pro spectrophotometer.

The culture was then diluted and the dilution factor calculated as follows:

Volume of original cell culture used / total volume = dilution factor.

Example: When 250 µl of cell culture is added to 1000 µl of double distilled deionized water then the dilution factor is calculated as 250 / 1250 = 0.2.

The samples were mixed well before loading them into the prepared chamber. Approximately 10µl of each sample was used in the Neubauer's chamber and the total number of cells was counted in 4 squares using x100 lens on an Olympus light microscope. Each larger square comprises of 16 sub-squares (4x4). The total area covered by one large square is 1 mm^2 and the chamber depth is 0.1 mm, therefore each square has a volume of 0.1 µl (1 mm^2 x 0.1 mm= 0.1 mm^3 / 0.1 µl) (Figure 2.3).

The total number of cells in this volume was calculated as follows:

Total number of cells x dilution factor = X number of cells in 0.1 µl

Total number of cells in 1 ml = X number of cells x 1000 / 0.1 = number of cells / ml.

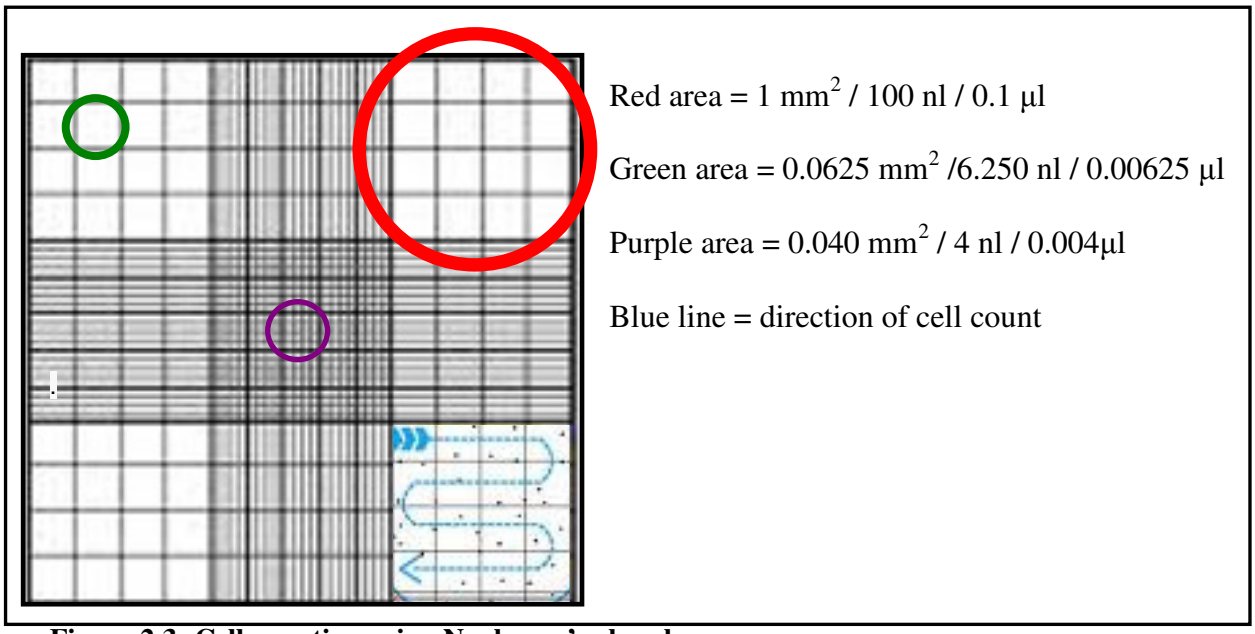

Figure 2.3: Cell counting using Neubauer's chamber.

2.18 Protein Expression and purification

Baker et al 1999 method for protein expression and purification was modified as follows:

Wild type or mutant genes were cloned into pGEX6T-P1 vector for GST tagging. The verified plasmids were transformed into BL21 cells and selected on chloramphenicol (34 μg/ml)/ Ampicillin (100 μg/ml) LB plates. The successful transformants were grown overnight in 10 ml LB (+ antibiotics) at 37°C to 1 OD_{600nm}. This culture was then transferred to 3 L of LB+100 μg/ml Ampicillin+34 μg/ml chloramphenicol and incubated at 37°C for 3-4 hours until the OD_{600nm} was 1. The culture was cooled by leaving it at 4°C for 20 minutes. Protein expression was induced with 0.1 mM IPTG at 30°C for 3 hours; 0.4 mM PMSF was added to decrease protein degradation. The cells were then centrifuged at 8000 *xg* (Beckman J2-MC, rotor JA18) for 20 min and washed once with wash buffer (appendix 5.16).

The cell pellet was resuspended in 40 ml ice cold lysis buffer (appendix 5.6) and incubated on ice for 1 hour. 1% Triton X 100 was then added and the mixture left on a suitable gentle shaker for further 1 hour. The lysed cells were then centrifuged at 8000 *xg* for 30 minutes at 4°C and the supernatant was again centrifuged at 15000 *xg* (Beckman L-70 ultracentrifuge, rotor Type 70 Ti) for 45 minutes at 4°C. The supernatant was filtered through 0.4 μm polyethylene sulphate (PES) filter disc (Millipore Ltd) syringe filters. The filtrate was added to 100 μl pre-washed and equilibrated glutathione sepharose beads 4B resin (GE Healthcare) (1.33 ml in 75% ethanol slurry) along with yeast protease inhibitor and incubated for 45 minutes at 4°C. The samples were then washed thrice with wash buffer and packed into a poly-prep chromatography column (Bio-Rad, #731-1550). The GST tagged protein was eluted from the column using 2.5 ml 30 mM glutathione elution buffer (appendix

5.4). Protein was quantified using SDS-PAGE and Bradford assay and stored at -20°C.

All GST tagged proteins used in this study were expressed using the above described method.

2.19 Bradford Assay

Biorad ready to use Bradford reagent was used for *in vitro* protein estimation. Each, 1-10 µl of 100 mg/ml BSA was added to 100 µl of the Bradford reagent in order to obtain a standard curve. They were mixed thoroughly and left for 5 minutes at room temperature. 1 µl of each fraction of the purified protein samples was added to 100 µl of the Bradford reagent simultaneously and left at room temperature for 5 minutes. Protein samples were analyzed against BSA standards.

2.20 Stability blots

10 ml of cell culture was grown overnight to 0.8 OD_{600nm} and centrifuged at 2000 *xg*. The cell pellet was washed once with double distilled deionized water. To the cell pellet, 300 µl of double distilled deionized water and 300 µl of 0.2 M NaOH was added and mixed thoroughly and left at room temperature for 5 minutes. It was then centrifuged and the supernatant removed completely. 50 µl of SDS-PAGE sample buffer was then added to the pellet, mixed thoroughly and boiled for 3 minutes at 90°C. 25 µl of this sample was then used to load on to 10% SDS-PAGE and the resolved proteins were transferred on to nitrocellulose membranes for further analysis (Kushnirov et al 2000, rapid and reliable protein extraction). This method was used to detect the stability of the constructs which was tested through the use of antibodies.

2.21 *APL5-9Myc* Tagging

APL5 was tagged with 9*Myc* using PCR amplification of the 9*Myc*-TRP cassette from the pYM6 plasmid using primers Apl5-R and Apl5-F.

The PCR mix and programme was set up as follows:

	Concentration (stock solutions)	Volume used
Primer(s)	100 pmol	1.5 µl each
dNTPs	25 mM	1 µl
Tgo/Taq polymerase	3.5 Units/µl	1 µl
$MgCl_2$ Buffer	25 mM $MgCl_2$	10 µl
Template	≥400 ng	1.5 µl
Water		to make up 100 µl / reaction

Table 2.6: PCR mix used for amplification of *9Myc-TRP1* cassette.

	Temperature °C	Time Minutes
Initial denaturation	94	2
Loop one;30 Cycles:		
Denaturation	94	1
Annealing	58	1
Template Extension	68	2.5
Final elongation	68	10
Final hold	10	

Table 2.7: PCR programme for amplification of *9Myc-TRP1* cassette.

The PCR product was ethanol precipitated and used for standard yeast transformation into (BY4742) *ATG18*-3HA:HIS3. Correct integration was verified through colony PCR using Primers APL5-cF and APL5-cR (Janke, Magiera et al. 2004).

APL5-F
5' 3'
AGAACCAAATGAAT TTCTTCGAGA CCAAAGCACTGACATTCGTACGCTGCAGGTCGAC

APL5-R
5' 3'
TCGCTGTCATTGAGAATTCACGACTTCGATTTTTTTATCG ATCGATGAATTCGAGCTCG

APL5-cF
5' 3'
AAAGGACAAGATTAATCTGAG

APL5-cR
5' 3'
ACTCAGCAGTGGTCATTGCCT

2.22 Co-Immuno Precipitation (Co-IP)

50 ml of cell culture was grown overnight to 1 OD_{600nm} and the cells were washed twice in wash buffer (appendix 5.16). The cells were spun down and resuspended in 100 µl of TNE buffer (appendix 5.13) with 1 µl of yeast protease inhibitor cocktail (P8215 Sigma). 100 µl of acid washed glass beads (400-625 µm) /sample were added to the culture and homogenized at 5000 *xg* for 1 min at 4°C. This was repeated 5 times (5 minutes) with consecutive breaks of 1 minute each and incubation on ice, between 2 successive rounds. The cells were then centrifuged for 5 min at 8000 *xg* and the supernatant collected in a fresh tube. 1% Triton X100 was added to a final concentration of 1% v/v and the lysates incubated on ice for 45 min, and then centrifuged at 8000 *xg*. The supernatant was collected in a fresh tube. 50 µl of the pre-washed anti body tagged protein G sepharose beads along with yeast protease inhibitor cocktail were then added to 100 µl of the cell lysates and incubated at room temperature for 1 hr. After an hour the protein G beads were

washed at least thrice with wash buffer (appendix 5.16) and the samples boiled for 3 minutes with 50 µl of SDS sample buffer (appendix 5.16). The samples were resolved on 10% SDS-PAGE (Phizicky and Fields 1995).

This method was used for detection of *in vivo* protein binding of FY833 *ATG18*-HA:HIS3-*APL5*-9*Myc*:TRP, and BY4742 *ATG18*-3HA:HIS3-GFP-*VPS41*. FY833 *ATG18*-HA:HIS3, BY4742 Δ*atg18*::KAN, BY4742 GFP-*VPS41* and BY4742^{WT} cell cultures were also grown and used as controls.

2.23 SDS-PAGE

Protein samples were boiled for 3 minutes with 30-50 µl x5 SDS-sample buffer and later resolved on 10% (w/v) SDS-PAGE in a Bio-Rad MiniProtean II xi Cell at 80V for approximately 2.5 hours. Biorad high / low molecular weight protein marker was used for qualitative purposes.

2.24 Coomassie blue staining

Proteins were visualized on 10% SDS gel using Coomassie brillant blue R250 (Sigma) in 50% (v:v) methanol and 7% (v:v) acetic acid. The working solution was made from 1 part ethanol to 9 parts Coomassie G250 solution.

SDS gel was immersed in deionized double distilled water and microwave for 1 minute. This was repeated thrice except for the third time when it was rinsed in cold water. Sufficient Coomassie Blue solution was added to the gel to completely cover it and microwave for 20 sec (x2) and later left at room temperature for further 5 minutes on gentle shaking. The gel was then washed thrice with double distilled water in order to visualize the protein bands.

2.25 Ponceau staining

The nitrocellulose membranes were immersed in Ponceau S (0.1% w/v in 5% Acetic acid) at room temperature, to identify successful transfer of the protein bands from SDS gel.

2.26 Western blotting

The samples were transferred onto Hybond-ECL nitrocellulose membrane (Amersham Biosciences) using Towbin buffer (appendix 5.14). The transfer was carried out at 400 milliAmp for 90 minutes.

The nitro-cellulose membrane was incubated with 3% milk protein in PBS (appendix 5.86) to block non specific binding at 4°C over night and then incubated with monoclonal primary antibody (1:3000 dilution) for 1 hour at room temperature with gentle shaking. The membrane was washed thrice with wash buffer (appendix 5.16) and then incubated with HRP-secondary antibody (1:5000 dilution) for further 1 hour at room temperature. It was then washed thrice and visualized using chemiluminescence reagents A and B (appendix 5.1), and AGFA photographic film. The photographic film was developed using AGFA Xograph developing system. Each sample was analyzed twice using primary antibodies for each of the tagged proteins in order to verify the results.

Protein detected	Primary antibody	Secondary antibody
Atg18p-3HA	Mouse monoclonal Antibody HA (Molecular Probes).	HRP-Goat Anti-Mouse (Invitrogen)
Atg18-GFP	Mouse monoclonal Antibody GFP-B2 (Santa Cruz).	HRP-Goat Anti-Mouse (Invitrogen)
Vps41p-GFP	Mouse monoclonal Antibody GFP-B2 (Santa Cruz).	HRP-Goat Anti-Mouse (Invitrogen)
Apl5p-9Myc	Mouse monoclonal Antibody 9E10 (Santa Cruz)	HRP-Goat Anti-Mouse (Invitrogen)

Table 2.8: Protein detection using monoclonal antibodies.

2.27 Lipid binding /Overlay assay

Nitrocellulose membrane spotted with Phosphoinositide lipids (~1 µg in chloroform:methanol:water mixture (400:56:4) were used for this assay. The membrane was blocked in 3% BSA in TBST or PBST (where specified) for 1 hr at room temperature and then 3-5 µl of the GST- tagged purified protein was incubated with the lipid dot blots at room temperature for further 1 hour. It was washed thrice with TBST (appendix 5.12) and monoclonal primary anti body was added to a final dilution of 1:1000 TBST and left for an hour at room temperature. After washing it thrice with TBST, the HRP-secondary anti body was added to a final dilution of 1:4000 and left with gentle shaking for another hour at room temperature. After a final washing the antibodies were detected using chemiluminescence reagents A and B (appendix 5.1) (Narayan and Lemmon 2006).

2.28 Analysis of ATG18^{Wt} and ATG18^{FTTG} phosphorylation through LC-CID-FT MS **(Liquid chromatography-Collision induced dissociation-Fourier transform-Ion cyclotron resonance-Mass spectrometry)**

BY4742 Δ*atg18*::KAN-pUG36*ATG18*^{Wt} and BY4742 Δ*atg18*::KAN-pUG36*ATG18*^{FTTG} cells were grown in 50 ml of SC-Met-Ura media with 2% glucose at 25°C. The cells were harvested through centrifugation at 1000 x *g* and washed once in double distilled deionized water. The cells were then resuspended in 500 µl TNE buffer + 2 µl protease inhibitor cocktail (Sigma) and lysed through mechanical shearing in a homogenizer, by the use of 100 µl of acid washed glass beads / sample. The samples were centrifuged at 1000 x *g* and the supernatant was incubated with 1% Triton X 100 (v/v) at 4°C for 15 minutes. The samples were then mixed with pre-equilibrated protein G sepharose beads (GE healthcare) at room temperature for 15 minutes. The samples were subsequently centrifuged at 2000 x *g* and supernatant was removed completely. The beads were washed twice with wash buffer (appendix 5.16) and supernatant discarded completely. To the pellet, 50 µl of 5 x SDS sample buffer was added and mixed thoroughly. This was then boiled at 90 °C for 5 minutes and 20 µl of the sample was run / well on 10% SDS-PAGE. The protein bands on the gel were visualized through Coomassie staining and GFP-Atg18p^{Wt} and GFP-Atg18^{FTTG} bands (approximately 75Kd) were cut from the gel using a sterile surgical blade.

These samples were then digested and later phosphor-enrichment was carried out. They were then analyzed through LC-CID-FT MS on LTQ FT Ultra, a hybrid device having an advanced Ion Trap and Fourier Transform Ion Cyclotron Resonance technology by Functional Genomics and Proteomics Unit, University of Birmingham (Birmingham, UK).

2.29 Yeast Knockouts.

2.29.1 Method 1 (*fab1::LEU2*)

Yeast genomic DNA from *fab1::*LEU2 strain was used to amplify the deletion cassette using primers designed upstream and downstream of the knockout.

Forward Primer

5' TGAAACTTTTGAAGTTAAAAGCTACATTTATGG 3'

Reverse Primer

5' CCATAAATGTAGCTTTTAACTTCAAAAGTTTCA 3'

The PCR conditions were as follows:

	Concentration (stock solutions)	Volume used
Primer(s)	100 pmol	1.5 µl each
dNTPs	25 mM	1 µl
Taq polymerase	3.5 Units/µl	1 µl
$MgCl_2$ Buffer	25 mM $MgCl_2$	10 µl
Template	≥400 ng	1.5 µl
Water		to make up 100 µl / reaction

Table 2.9: PCR mix used for amplification of *fab1::LEU2* cassette.

	Temperature °C	Time Minutes
Initial denaturation	94	2
Loop one;30 Cycles:		
Denaturation	94	1
Annealing	58	1
Template Extension	68	6
Final elongation	68	10
Final hold	10	

Table 2.10: PCR programme for amplification of *fab1::LEU2* cassette.

The PCR fragment was purified through ethanol precipitation and transformed into yeast strains using standard transformation protocol as mentioned earlier and grown

on selective media (Sc-Leucine). This method makes use of yeast genetics and integration of the deletion cassette takes place through homologous recombination resulting in a knock out of the target gene with *LEU2*. Five colonies of the successful transformants were used for colony PCR.

Colony PCR primers

5' TAAATATGCTTCAAGGCTTAGA 3'

5' TTCTTTGGCAAATCTGGAC 3'

Colony PCR programme

	Temperature °C	Time Minutes
Initial denaturation	94	5
Loop one;30 Cycles:		
Denaturation	94	1
Annealing	58	1
Template Extension	68	2
Final elongation	68	10
Final hold	10	

Table 2.12: PCR programme for colony PCR.

2.29.2 Method 2 *(apl5::HIS3)*

Marker cassette for *HIS3* was amplified from pRS423 plasmid using the following primers:

Apl5::HIS-F1

5' 3'

CGGCAAAGGTTACGTCCTTTTGGGTTTTTCTTTGAGAAATCACTAAAGGATTTGAT
TAAGGGT AGATTGTACTGAGAGTGCAC

Apl5::HIS-R1

5' 3'

ACTATAACTTCTTCAGTATCACTTAAATTATCCTTTTCATCTTTTACAATAAGATT
GGCCTCT CTGTGCGGTATTTCACACCG

These primers were designed such that they contain 40bp flanking regions up (start of the gene of interest) and down stream (end of the gene of interest) towards the 5′ end (represented in black) and 20 bp region homologous to the auxotrophic marker towards the 3′ end of the primer (represented in red). This would result in a deletion cassette with *HIS3* marker.

	Concentration (stock solutions)	Volume used
Primer(s)	100 pmol	1.5 µl each
dNTPs	25 mM	1 µl
Taq polymerase	3.5 Units/µl	1 µl
$MgCl_2$ Buffer	25 mM $MgCl_2$	10 µl
Template	≥400 ng	1.5 µl
Water		to make up 100 µl / reaction

Table 2.13: PCR mix for amplification of *HIS3* cassette.

	Temperature °C	Time Minutes
Initial denaturation	94	2
Loop one;30 Cycles:		
Denaturation	94	1
Annealing	58	1
Template Extension	68	2
Final elongation	68	10
Final hold	10	

Table 2.14: PCR programme for amplification of *HIS3* cassette.

The PCR product was purified through ethanol precipitation and transformed into yeast and grown on selective media (Sc-Histidine) at 25°C. Integration of the deletion cassette was through homologous recombination. Five colonies of the

successful transformants were used for colony PCR with colony PCR primers Apl5-his cF1/cR1.

Colony PCR primers

Apl5-his-cF1:
5' 3'
GGCAGTTGCCACAACCAGAAGAGCATAAC Tm 65.41

Apl5-his-cR1 (from HIS gene)
5' 3'
CCTTTGGTGGAGGGAACATCGTTGGTAC Tm 65.43

Colony PCR programme

	Concentration (stock solutions)	Volume used
Primer(s)	100 pmol	1.5 µl each
dNTPs	25 mM	1 µl
Taq polymerase	3.5 Units/µl	1 µl
$MgCl_2$ Buffer	25 mM $MgCl_2$	10 µl
Template	≥400ng	1.5 µl
Water		to make up 100 µl / reaction

Table 2.15: PCR mix for colony PCR.

	Temperature °C	Time Minutes
Initial denaturation	94	5
Loop one;30 Cycles:		
Denaturation	94	1
Annealing	58	1
Template Extension	68	2.5
Final elongation	68	10
Final hold	10	

Table 2.16: PCR programme for colony PCR.

Chapter 3: Results

Introduction

Almost all eukaryotic cells maintain low but constant steady-state levels of PtdIns(3,5)P_2 when measured at the level of the whole cell. The available evidence suggests that it is enriched at the vacuole and adjacent endocytic compartments. Although a number of signaling events require the presence of PtdIns(3,5)P_2 levels very little is known about the molecular details of these processes due to a number of ambiguities, namely;

- Only one PI 3-kinase (Vps34p) and one PI3P 5-kinase (Fab1p) have been identified to synthesize several functional pools of the PtdIns3*P* and PtdIns(3,5)P_2 and putatively PtdIns5*P* for numerous functions.
- Fab1p behaves slightly differently from its mammalian homologue PIKfyve.
- Vac7p, a vital component of PtdIns(3,5)P_2 synthesis core complex in *S. cerevisiae*, is exclusive to ascomycetes and its homologue has not been identified in any other eukaryotes (Bonangelino, Catlett et al. 1997). This creates ambiguities in understanding the regulation of Fab1p-like enzymes in yeast and other eukaryotes.
- The minimum requirement for PtdIns(3,5)P_2 explicit to a particular process seems to vary suggesting multiple independent binding proteins.
- Since PtdIns(3,5)P_2 now appears to be the source of most PtdIns5*P* in the cell, some of the original observations about PtdIns(3,5)P_2 function must be critically re-examined to determine if they are in fact functions of PtdIns5*P*.
- No *in vivo* markers for PtdIns(3,5)P_2 and PtdIns5*P* have been identified.

- PtdIns(3,5)P_2 and specifically PtdIns5*P* binding domains are ill defined.
- Only 6 PtdIns(3,5)P_2 effector proteins have been identified to date; namely the PROPPINs, Atg18p, Atg21p, Hsv2p and Tup1p, the ion channel Yvc1p/TRPML1 and one of the TOR complexes. Since these proteins are also known to have PtdIns(3,5)P_2 independent functions, it is difficult to clarify the precise influence of PtdIns(3,5)P_2 on these effectors.

Type III PtdIns3*P* 5-kinases, exemplified by Fab1p (yeast) and PIKfyve (mammals) (PtdIns3*P* 5-kinases) use PtdIn3*P* as a precursor for PtdIns(3,5)P_2 synthesis, therefore the localization of Vps34p (PtdIns 3-kinase) and Fab1p together with the effector proteins is critical in the regulation of these lipid regulated processes.

The Δ*fab1* null mutant exhibits a highly enlarged vacuole, with defects in hyper-osmotic stress mediated vacuole fragmentation, MVB sorting, vacuole acidification, vacuole inheritance and growth at restrictive temperatures. As most of these processes involve the vacuole membrane, it seems safe to postulate that most functions of PtdIns(3,5)P_2 occur on or near that organelle in yeast.

Normally the level of PtdIns(3,5)P_2 is 0.1% of the total cellular PtdIns but it increases to 30 folds (in yeast) during hyper osmotic shock. Over expression of Fab1p^{Wt} does not significantly increase intracellular PtdIns(3,5)P_2 levels except in the case of constitutively active mutant (*FAB1-5*). It is also hypothesized that Fab1p activity is regulated through an interaction between its C-terminal and CCT domains.

Both the effector Atg18p and activator Vac7p interact with each other as well as the Fab1p CCT domain, but how this binding is regulated is unknown. Other Fab1p modulators, Vac14p and Figure4p also bind Fab1p in this region but the details of how these proteins affect Atg18p and Vac7p binding are also not yet clear. Interestingly null mutant of any one of these genes partially replicates Δ*fab1* defects; some of which can be rescued by the over expression of other members of the complex.

As Δ*vac7* defects can only be rescued via *FAB1-5* mutant, Vac7p is postulated to be crucial for PtdIns(3,5)P_2 synthesis while Atg18p is hypothesized to be involved in PtdIns(3,5)P_2 down regulation because of the PtdIns(3,5)P_2 over production observed in Δ*atg18* cells. This strongly suggests that possibly Atg18p and Vac7p are responsible for antagonistically regulating PtdIns(3,5)P_2 levels, yet both Vac7p and Atg18p are relatively uncharacterized proteins. Hence an effort was made to extend our knowledge of PtdIns(3,5)P_2 mediated signaling by characterizing Atg18p; its localization, interactions, and lipid binding.

Chapter 3; Results

3.1: Atg18p Localization

Wild-type exponentially growing *S. cerevisiae* BY4742 cells display 4-7 small vacuoles clustered together when viewed using DIC (differential interference contrast) microscopy or stained with FM4-64 (a vacuole specific dye, (Vida and Emr 1995)) (Figure 3.1.1).

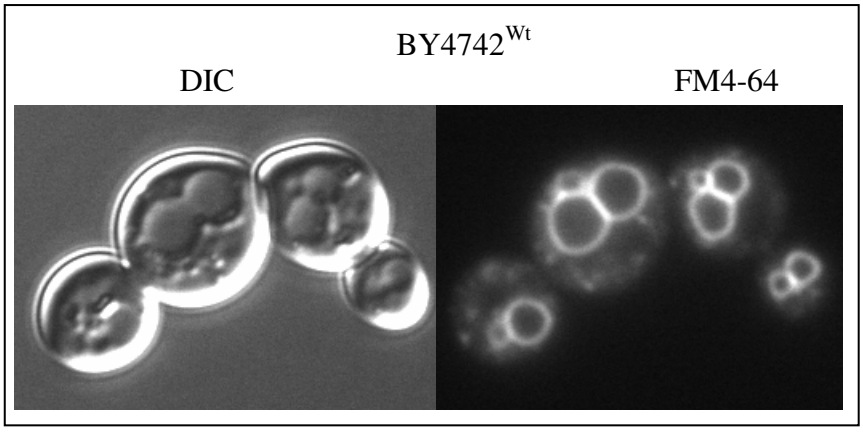

Figure 3.1.1: Vacuole morphology of wild type *S.cerevisiae* cells.

$BY4742^{Wt}$ cells were grown overnight to 0.5 OD_{600nm} in YEPD media with 2% glucose. The cells were washed with fresh media and resuspended in YEPD + 2 % glucose + 0.16 mM FM4-64 and incubated at 30°C for 1 hour. They were then washed once with fresh media and once with MES buffer pH 5.6 and resuspended in MES buffer pH 5.6 and viewed under the microscope using RFP filter.

In yeast, vacuole size is concomitant with the osmotic levels of the cytosol; hyper-osmotic stress results in vacuole fragmentation while hypo-osmotic shock causes it to become highly enlarged (Dove, Dong et al. 2009). Under basal conditions, regulation of vacuole morphology is stringent and affected by the many membrane proteins found to interact with each other at the vacuole membrane. These proteins can be categorized into 2 groups; ones which are integral membrane proteins and the ones which are peripherally attached.

Since the aim of this project was to characterize Atg18p (a peripheral membrane protein) and investigate its role in regulation of vacuole morphology with regard to phosphoinositide binding, it was most logical to trace the localization of Atg18p *in vivo* as a starting point.

Being a peripheral protein GFP-Atg18p is partly cytosolic, but is mostly enriched on punctate structures and the vacuole membrane. It is also occasionally observed on the segregation structure (during vacuolar division) in wild type cells (Figure 3.1.2A).

The localization is similar in Δ*atg18* cells (Figure 3.1.2B) indicating that presence or absence of endogenous Atg18p does not grossly affect the localization of exogenous GFP tagged Atg18p, although over-expression does cause vacuolation.

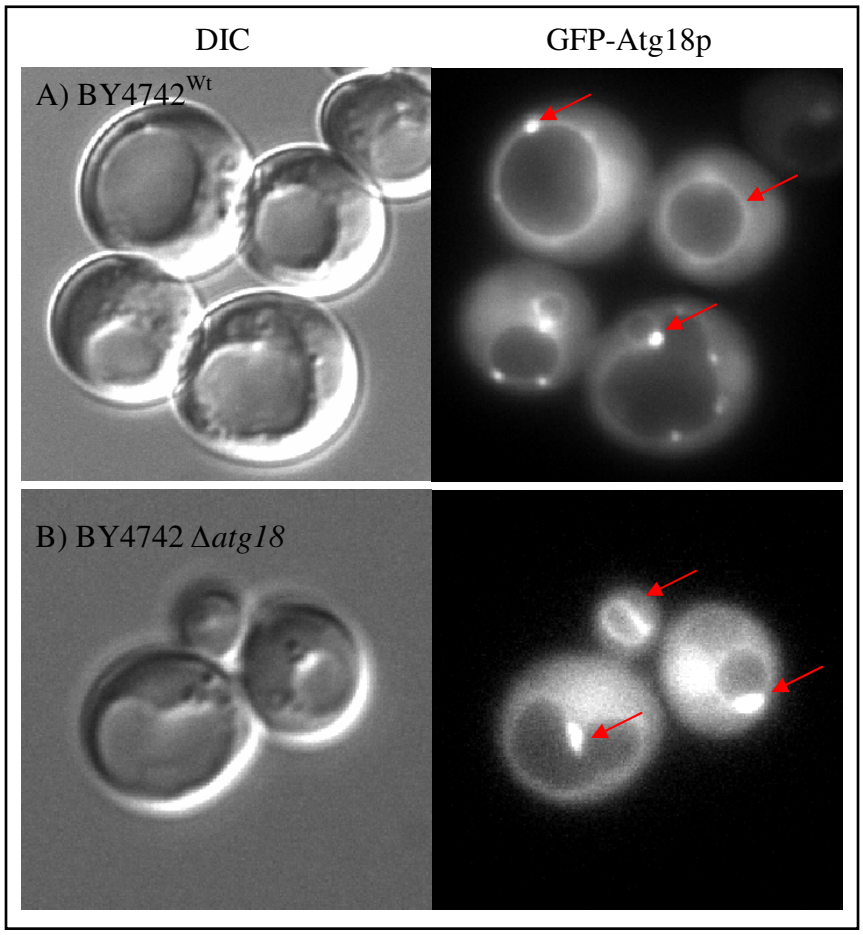

Figure 3.1.2: *In vivo* localization of GFP-Atg18p in wild type (A) and Δ*atg18* (B) cells.

A single colony of BY4742 pUG36-ATG18^{Wt} (Figure 1.2 A) and BY4742 *atg18*::KAN pUG36-*ATG18*^{Wt} (Figure 1.2 B) was grown overnight in SC-Ura-Meth with 2 % glucose. The cells were washed with fresh media and resuspended in 1 ml SC-Ura-Meth + 2% glucose and incubated at 25°C for 4 hours to OD_{600nm} 0.6. The cells were then resuspended in MES buffer (pH 5.6) and examined microscopically using GFP filter on a Nikon Eclipse E600 Microscope and processed using Photoshop. The localization of GFP-Atg18p in wild type / *atg18*::KAN cells is indicated by the arrows.

The vacuolar localization of Atg18p was confirmed with co-localization of GFP-Atg18p with FM4-64 staining (Figure 3.1.3) whereas GFP-Atg18p punctae were identified as pre-vacuolar endosome (PVE) through 44.9% co-localization with RFP-Snf7p, a PVE resident protein in yeast (yeast PVEs are comparable to Rab5p positive compartments of mammalian cells but infact are a hybrid of early and late endosomes; the vacuole being a likely hybrid of late endosome-lysosome) (Figure 3.1.4).

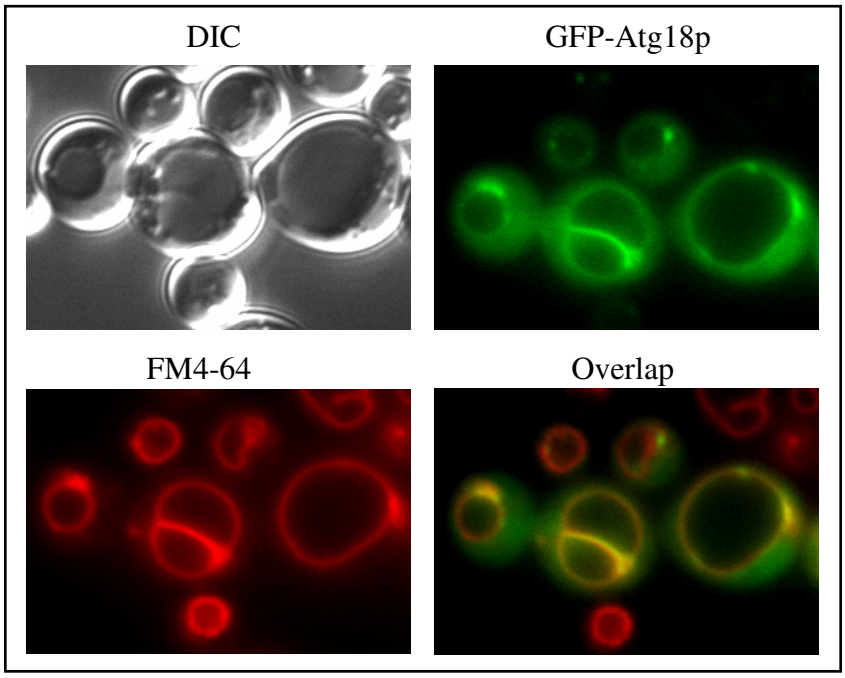

Figure 3.1.3: *In vivo* co-localization of GFP-Atg18p with FM4-64.

BY4742 *atg18*::KAN-pUG36-ATG18^{Wt} cells were grown overnight to 0.6 OD_{600nm} in Sc-Ura-meth with 2% glucose. The cells were washed with fresh media and resuspended in 1 ml Sc-Ura-Meth + 2% glucose and 0.16 mM FM4-64 and incubated at 25°C for 1 hour. The cells were then washed once with fresh media and once with MES buffer (pH 5.6) and resuspended in MES buffer (pH 5.6) and viewed under the microscope using RFP and GFP filters. The images were processed in Photoshop.

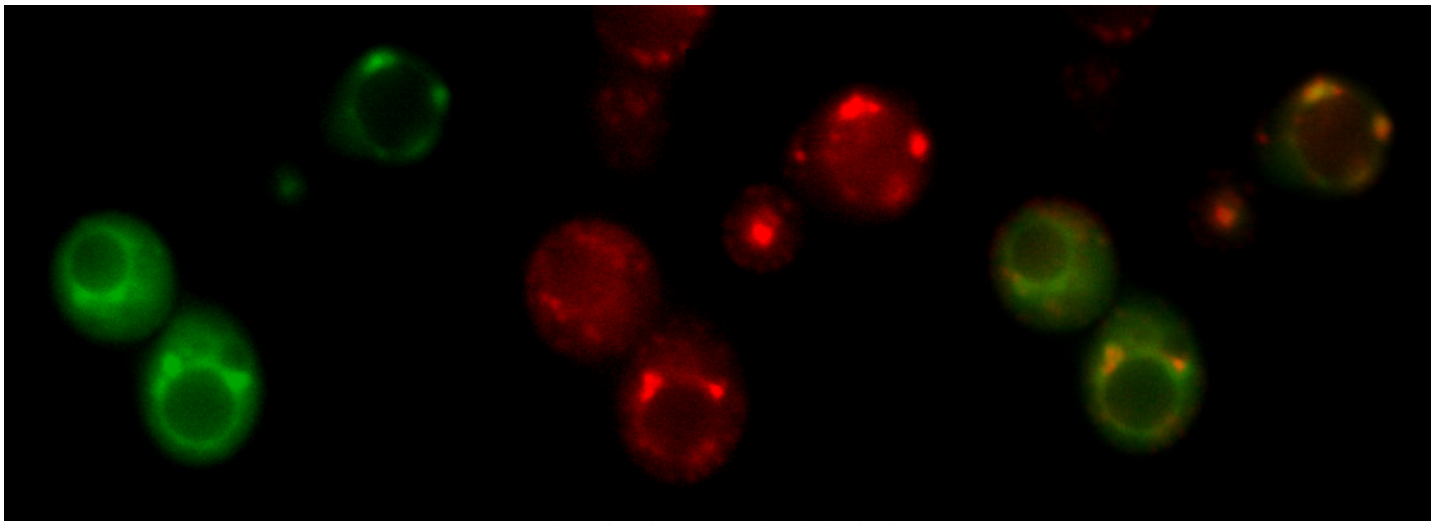

Figure 3.1.4: *In vivo* co-localization of GFP-Atg18p with RFP-Snf7p.

BY4741 RFP-*SNF7*:KAN-pUG36-*ATG18*^{Wt} cells were grown overnight to 0.6 OD_{600nm} in SC-Ura-Meth with 2 % glucose. The cells were washed with fresh media and resuspended in SC-Ura-Meth + 2 % glucose and incubated at 25°C for 4 hours. The cells were then washed once with fresh media and resuspended in MES buffer (pH 5.6) and viewed under the microscope using RFP and GFP filters. The images were processed using Photoshop.

Atg18p was identified as an autophagy related protein (consequently named *ATG18*) and for its role in regulation of vacuole morphology (consequently named *SVP1*; Swollen Vacuole Phenotype). It is also known that Atg18p enriches on the vacuole during osmotic shock (Figure 1.5 B) and as punctae during Nitrogen-starvation and the G_0 stage of the cell cycle (Dove, Piper et al. 2004; Obara, Sekito et al. 2008).

Since Rapamycin inhibits TOR and consequently induces autophagy (Tanemura, Saga et al. 2009), it was investigated whether use of Rapamycin would affect the localization of Atg18p in a similar fashion as nitrogen starvation; investigated by incubating BY4742 Δ*atg18* GFP-Atg18p cells in N-starvation media with (0.2µg/ml) Rapamycin or without Rapamycin (Figure 3.1.5 C/D).

Cyclohoxamide is a known inhibitor of protein synthesis and was used to block *de novo* synthesis of Atg18p, in order to see where the pre-existing pools of this protein localize under exponential growth and autophagy conditions (Figure 3.1.5 E/F).

(Together, these conditions were used as standard test conditions for all the later experiments).

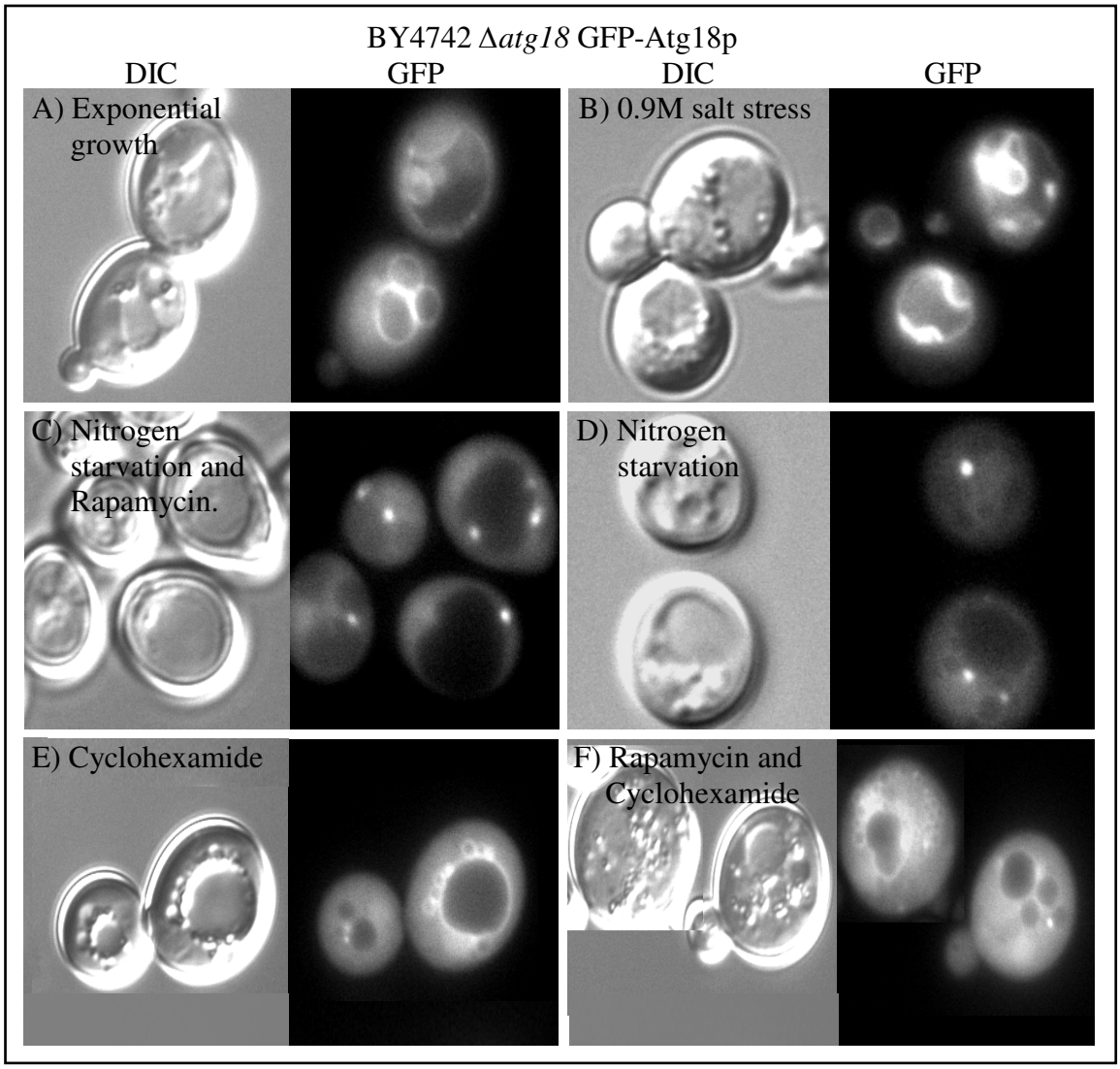

Figure 3.1.5: *In vivo* localization of GFP-Atg18p.

BY4742 *atg18::KAN* pUG36-ATG18^{Wt} cells were grown overnight in SC-Ura-Meth medium with 2% glucose to 0.6 OD_{600nm}. This cell culture was then split into 6 fractions. Fraction A was resuspended in MES buffer (pH 5.6) with 2% glucose, Fraction B was subjected to 0.9M salt stress, Fraction C was subjected to Nitrogen-starvation media without (0.2µg/ml) rapamycin, Fraction D was incubated with nitrogen starvation media + 0.2µg/ml Rapamycin, Fraction E was incubated in SC-Ura-Meth+2% glucose + 200µM/ml cyclohexamide and Fraction F was incubated in nitrogen starvation media with 0.2µg/ml Rapamycin and 200µM/ml cyclohexamide. All fractions were incubated at 25°C in the respective media for 4 hours each, except for Fraction B where the cells were visualized after 5 minutes of induction of osmotic shock. After each individual treatment the cells were washed once in fresh media and resuspended in MES buffer pH 5.6 (except Fraction B, which was visualized in saline) and all of these cells were then visualized microscopically using DIC and GFP fluorescence microscopy. The images were processed on Photoshop.

Figure 3.1.5 indicates, that in either case, i.e. in response to Nitrogen-starvation or rapamycin induction, GFP-Atg18p localization was very similar and it localized to punctate structures.

However, the use of cyclohexamide seems to increase Atg18p cytosolic distribution, both under exponential growth and autophagy conditions.

Interestingly, unlike wild type cells, the vacuole becomes large when incubated with cyclohexamide alone (Figure 3.1.5E) as compared to cells incubated with cyclohexamide and rapamycin (Figure 3.1.5F), indicating that cyclohexamide is possibly effecting the expression of some other protein/s involved in localization of Atg18p.

The next question addressed was whether GFP-Atg18p^{Wt} punctae formed during autophagy are different from the punctae formed under exponential growth conditions. Hence GFP-Atg18p punctae were quantified for their co-localization with Snf7p-RFP, under exponential growth and rapamycin induced autophagy conditions (Figure 3.1.6). The number of GFP-Atg18p punctae/cell were also quantified to test whether autophagy conditions redistributes the localization of Atg18p in the cell (Figure 3.1.7).

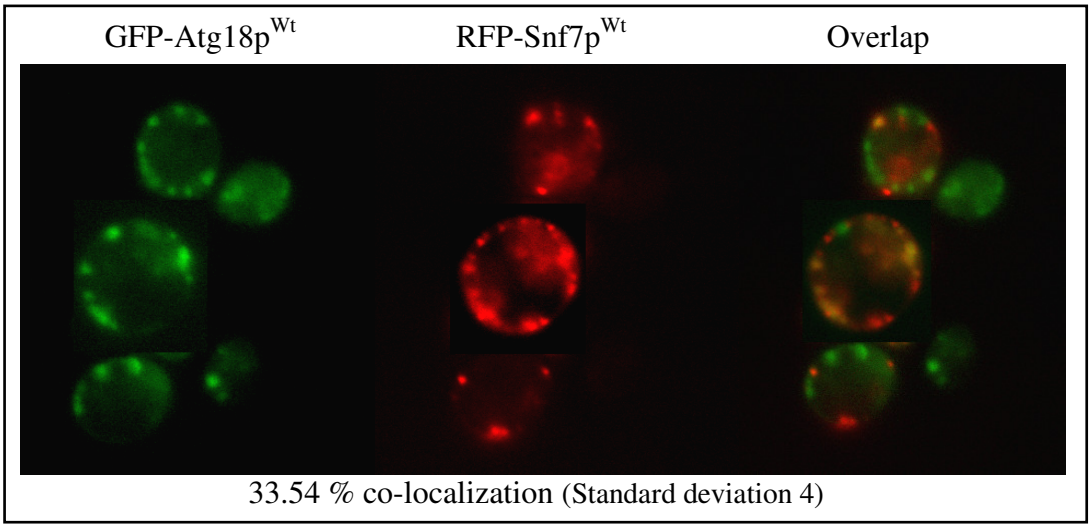

Figure 3.1.6: *In vivo* co-localization of GFP-Atg18p with RFP-Snf7p under autophagy conditions.

BY4741 *SNF7-RFP:KAN* pUG36-*ATG18*^{Wt} cell culture was grown overnight to OD_{600} 0.6 in SC-Ura-Met + 2 % Glucose at 25°C.The cells were harvested by centrifugation and resuspended in 1.7 % YNB + 2 % Glucose + 0.2 µg / ml Rapamycin, for 4 hours at 25°C and examined microscopically, using GFP and RFP filters mounted on a Nikon Eclipse E600 and the images were processed using Photoshop.

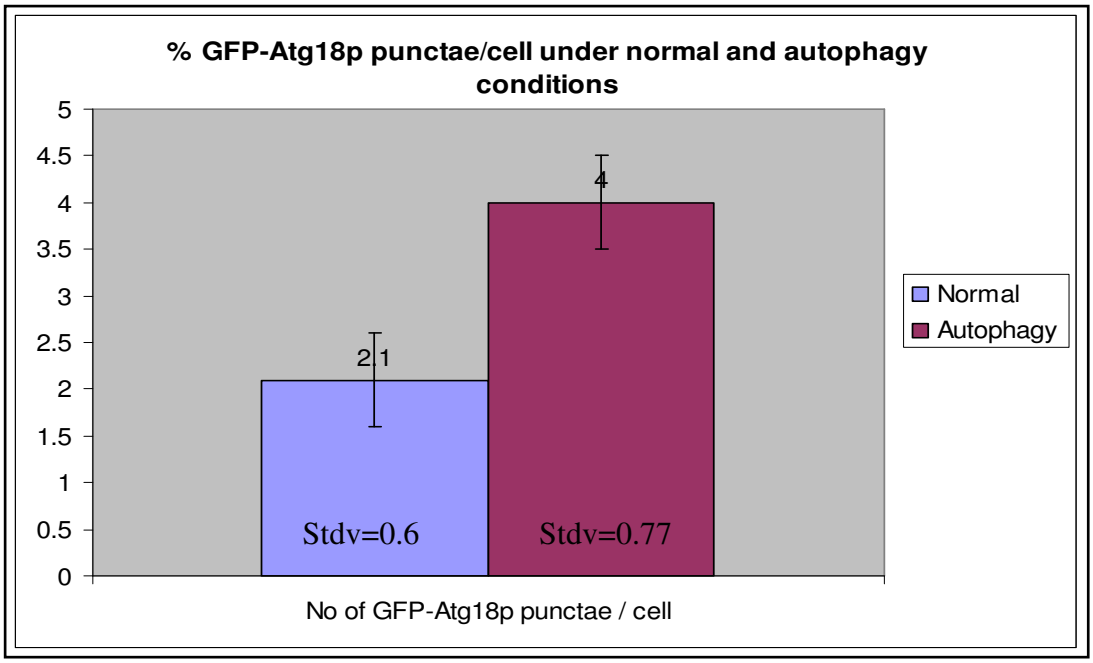

Figure 3.1.7: Quantification of GFP-Atg18p punctae under exponential growth and autophagy conditions.

BY4742 *atg18*::KAN pUG36-*ATG18*^{Wt} was grown overnight to OD_{600} 0.6 in SC-Ura-Met + 2 % Glucose at 25°C.The cells were harvested by centrifugation and half of the cell culture was suspended in 1.7 % YNB + 2 % Glucose + 0.2 µg / ml Rapamycin, for 4 hours at 25°C while the other half was resuspended in SC-Ura-Meth + 2% Glucose, for 4 hours at 25°C. Both cultures were washed once in fresh media and resuspended in MES buffer pH 5.6 and examined microscopically, using GFP and RFP filters mounted on a Nikon Eclipse E600. The numbers of punctae / cell were manually counted in ≥ 100 cells under exponential growth and autophagy conditions and plotted using excel.

The results show that the number of GFP-Atg18p^{Wt} punctae/cell increases, despite the fact the over all Snf7p-RFP/GFP-Atg18p co-localization decreases (from 44.9% to 33.54%) during autophagy. This suggests that there is a mixed population of GFP-Atg18p punctae (during autophagy), some of which are PVEs, while others are likely to be pre-autophagosomal structure (PAS). Hence a loss of Atg18p vacuolar localization accounts for its redistribution during autophagy and not alteration in expression level.

Nonetheless, the above does not yield any mechanistic information about how the shift from the vacuole to the punctate structures occurs during autophagy and vice versa during hyper osmotic stress.

Several studies have shown that Atg18p binds PtdIns3*P* and PtdIns(3,5)P_2 *in vivo* whilst biophysical *in vitro* analysis consistently show that PtdIns3*P* binding is 20-30 fold weaker than PtdIns(3,5)P_2 binding. It has also been postulated that localization of Atg18p during autophagy is largely PtdIns3*P* dependent, whilst vacuolar localization depends upon PtdIns(3,5)P_2 (Dove, Piper et al. 2004; Efe, Botelho et al. 2007). In order to verify this hypothesis, the localization of Atg18p in strains lacking Phosphoinositides, PtdIns3*P* and PtdIns(3,5)P_2 was investigated (Figure 3.1.8 A-D).

Fab1p is the only known PtdIns(3,5)P_2 5-kinase in *S. cerevisiae* while Vps34p is the sole type III PtdIns 3-kinase. Hence a cell with *fab1* knock out fails to synthesize PtdIns(3,5)P_2 while a Δ*vps34* cell fails to synthesize both PtdIns3*P* and PtdIns(3,5)P_2.

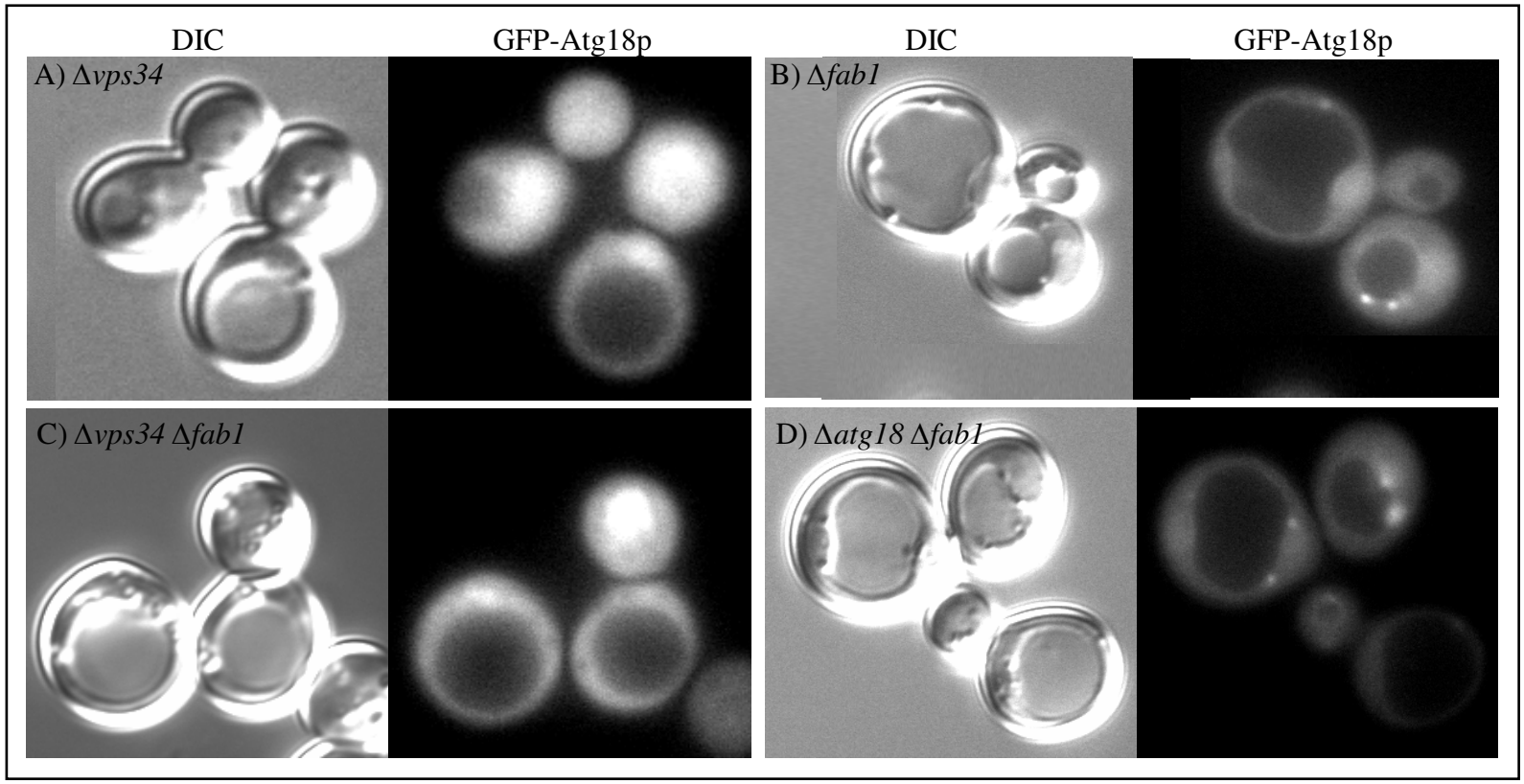

Figure 3.1.8: *In vivo* localization of GFP-Atg18p in Δ*vps34* and Δ*fab1* cells.

BY4742 *vps34*::KAN PUG36-*ATG18*^{Wt} , BY4742 *fab1::KAN* pUG36-ATG18^{Wt}, BY4742 *fab1*::LEU2 *vps34*::KAN pUG36-ATG18^{Wt} and BY4742 *fab1*::LEU2 *atg18*::KAN pUG36-ATG18^{Wt} cells were grown overnight in SC-Ura-Meth medium with 2% glucose to 0.6 OD_{600nm}. This cell culture was then resuspended in fresh SC-Ura-Meth with 2% glucose and incubated at 25°C for 4 hours to OD_{600nm} 0.5. Each culture was washed once in fresh media and resuspended in MES buffer pH 5.6 and visualized microscopically using DIC and GFP fluorescence microscopy. The images were processed on Photoshop.

In Δ*vps34* or *Δfab1Δvps34* cells Atg18p is mostly cytosolic which indicates that indeed Atg18p-lipid binding plays a crucial role in its *in vivo* localization. On the contrary, Atg18p only loses its vacuolar localization in Δ*fab1* cells, indicating that its punctate localization is not PtdIns(3,5)P_2 dependent.

We know that Atg18p loses its vacuolar localization in Δ*fab1* cells under exponential growth conditions, but does Fab1p affect the localization of Atg18p under salt stress and autophagy? (Figure 3.1.9)

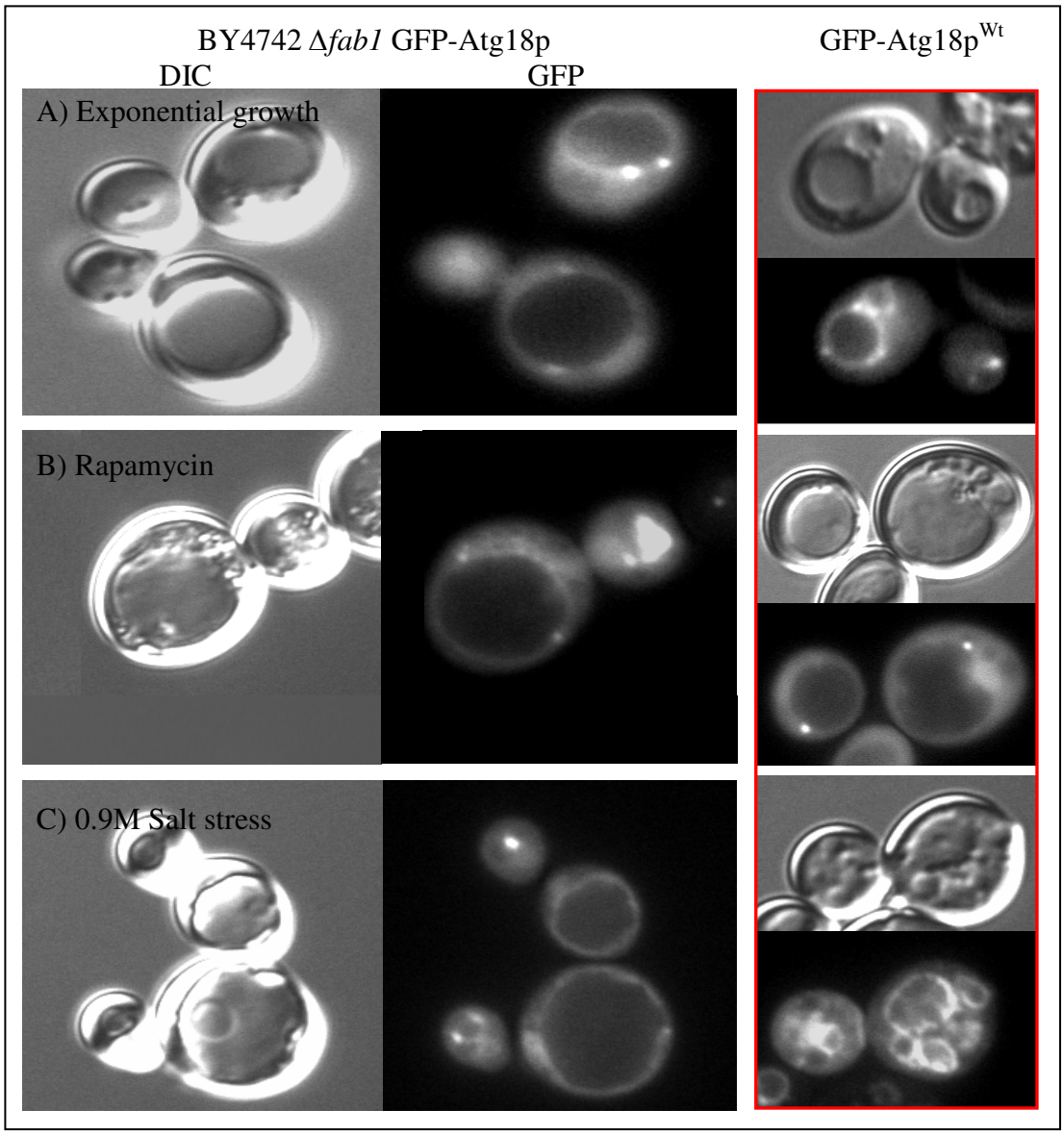

Figure 3.1.9: *In vivo* localization of GFP-Atg18p in Δ*fab1* cells.

BY4742 *fab1*::KAN pUG36-*ATG18*^{Wt} cells were grown overnight to 0.6 OD_{600nm} in SC-Ura-Meth with 2 % glucose. 200 µl of cells were added to 500 µl fresh media and incubated for further 4 hours at 25 °C and either examined as such (A) or examined after 0.9 M salt stress (C). 800 µl of the cell culture was resuspended in SC-Ura-Meth + 2 % glucose + 0.2 µg/ml rapamycin for 4 hours at 25 °C (B). Cultures A and B were resuspended in MES buffer (pH 5.6) for viewing under the microscope using GFP filters where as culture C was examined in saline. Photomicrographs in the left panel (highlighted by red) are only included as a reference to localization of Atg18p^{Wt} in Δ*atg18* cells, under specified conditions, but not to cell size.

Atg18p loses most of its vacuolar localization in Δ*fab1* cells under exponential growth conditions (Figure 3.1.9A). Localization of GFP-Atg18p in *Δfab1* cells, during autophagy is comparable to wild type (Figure 3.1.9B) pointing out that Atg18p role in autophagy is possibly independent of PtdIns(3,5)P_2-binding.

Under osmotic shock, GFP-Atg18p is seen to accumulate on the vacuole membrane (Figure 3.1.9C) however this is not sufficient to cause vacuole fragmentation. This is in accordance with Mayer et al (Zieger and Mayer), and suggests that besides lipid mediated localization, Atg18p also interacts with protein/s for its recruitment to a specific locale.

Nonetheless, Atg18p vacuolar recruitment largely depends on PtdIns(3,5)P_2 binding which was further verified by investigating the localization of Atg18p in Δ*vac7* and Δ*vac14* cells; known to have very low levels of PtdIns(3,5)P_2 (<10% and <25% respectively (Dove, McEwen et al. 2002; Rudge, Anderson et al. 2004)) (Figure 3.1.10).

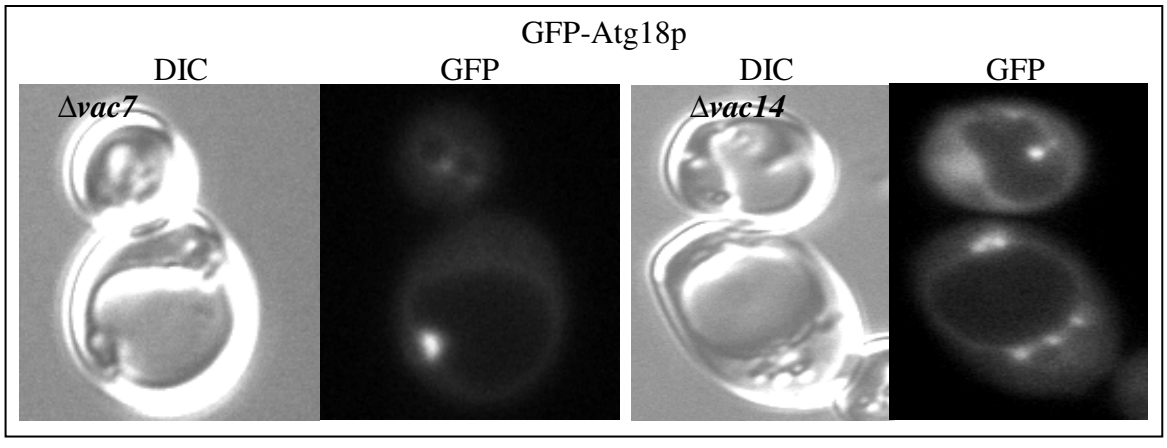

Figure 3.1.10: *In vivo* localization of GFP-Atg18p in Δ*vac7* and Δ*vac14* cells.

pUG36-*ATG18*^{WT} was transformed into BY4742 v*ac7*::KAN and BY4742 *vac14*::KAN cells and grown on selective media. A single colony was then picked and grown overnight to 0.6 OD_{600} in SC-Ura-Met + 2% Glucose. The cells were washed once with media and 500 µl of the culture was mixed with 500 µl of fresh media and incubated at 25°C for further 4 hours and then examined microscopically in MES buffer pH 5.6.

Although Atg18p is mostly punctae in Δ*vac7* and Δ*vac14* cells, yet very faint vacuolar localization in Δ*vac14* cells emphasizes Atg18p-PtdIns(3,5)P_2 binding specificity even under very low levels of the lipid or it could be due to PtdIns3*P*-binding as studies suggest that this latter lipid accumulate on the vacuole in cells lacking PtdIns(3,5)P_2 synthesis(Efe, Botelho et al. 2005).

However, after these observations, it becomes important to investigate whether Atg18p vacuolar localization is solely due to lipid binding as envisioned earlier or partly relies on some unidentified protein interaction/s?

Consequently this also gives rise to an important question; what factors bring about the shift in localization from the vacuole to the endosome during autophagy and vice versa during hyper osmotic stress? Furthermore what are the roles of PPIn kinases and phosphatases in these shifts?

PtdIns3*P* serves as a precursor to PtdIns(3,5)P_2 and is synthesized by the activity of Vps34p which is known to form at least two distinct complexes; VPS34 complex I comprising of Vps34p, Vps15p, Vps30p and Atg14p, forms and directs PtdIns3*P* synthesis at PAS while VPS34 complex II comprising of Vps34p, Vps15p, Vps30p and Vps38p, forms and synthesize PtdIns3*P* at the endosomal membranes (Kihara, Noda et al. 2001).

Since Atg18p is known to function in both autophagy and regulation of vacuole morphology, it was important to investigate the localization of GFP-Atg18p in Δ*vps34* (Figure 3.1.11), Δ*vps38* (Figure 3.1.12), Δ*atg14* (Figure 3.1.13), and Δ*vps38*

Δ*atg14* (Figure 3.1.14) cells under test conditions to check whether, 1) Atg18p punctae formation is PtdIns3*P* dependent and 2) PtdIns3*P* synthesis at a particular site effects Atg18p localization in any specific manner?

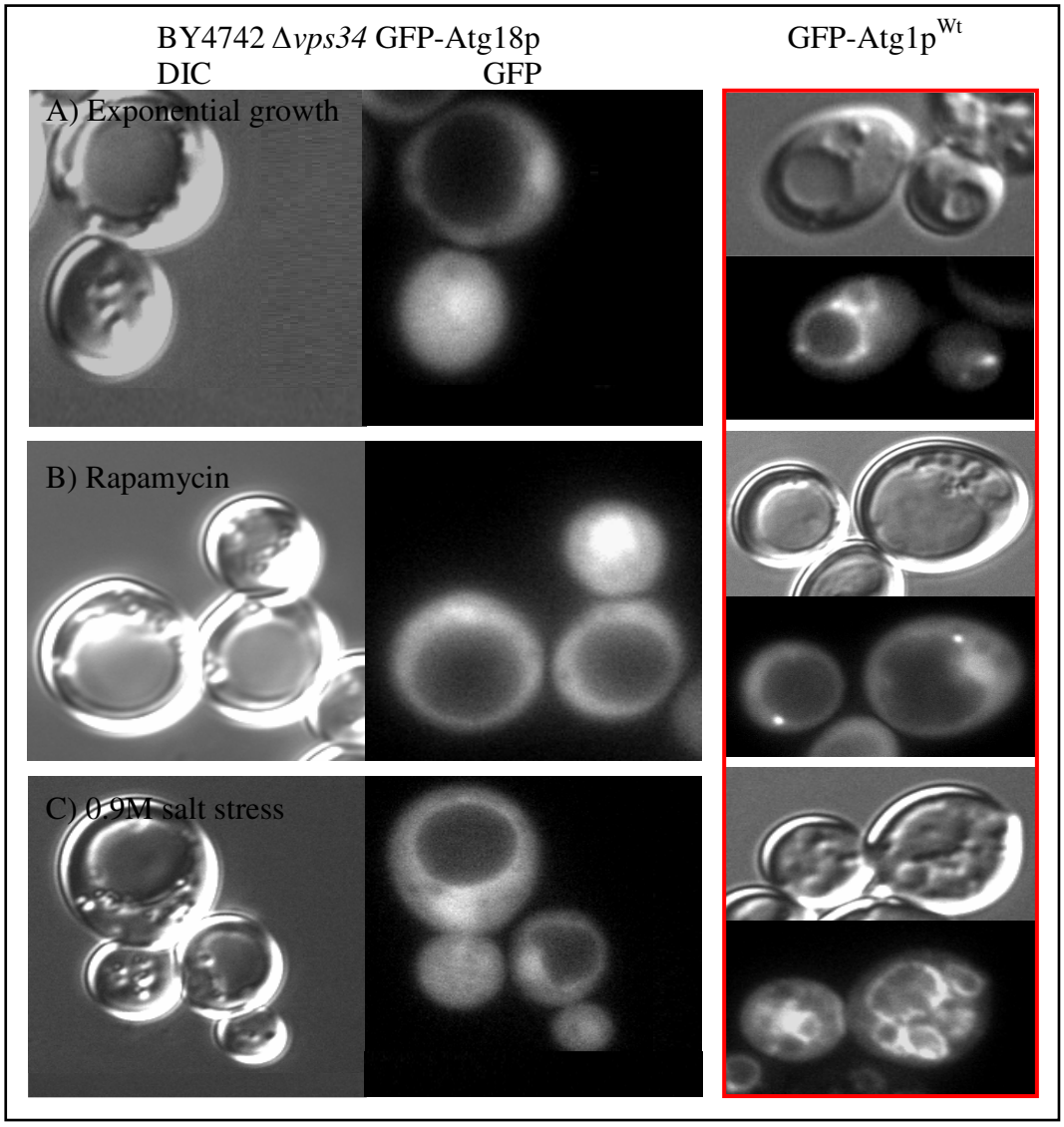

Figure 3.1.11: *In vivo* localization of GFP-Atg18p in Δ*vps34* cells

BY4742 *vps34::KAN* pUG36-ATG18^{Wt} cells were grown overnight in SC-Ura-Meth medium with 2% glucose to 0.6 OD_{600nm}. This cell culture was then split into 3 fractions. Fraction A was resuspended in MES buffer (pH 5.6) with 2% glucose, Fraction B was subjected to Nitrogen-starvation media with (0.2µg/ml) rapamycin and incubated at 25°C in the respective media for 4 hours each. Fraction C was subjected to 0.9M salt stress. All fractions A and B were washed once in fresh media and resuspended in MES buffer pH 5.6 while Fraction C was visualized in saline using DIC and GFP fluorescence microscopy. The images were processed on Photoshop. Photomicrographs in the left panel (highlighted by red) are only included as a reference to localization of Atg18p^{Wt} in Δ*atg18* cells, under specified conditions, but not to cell size.

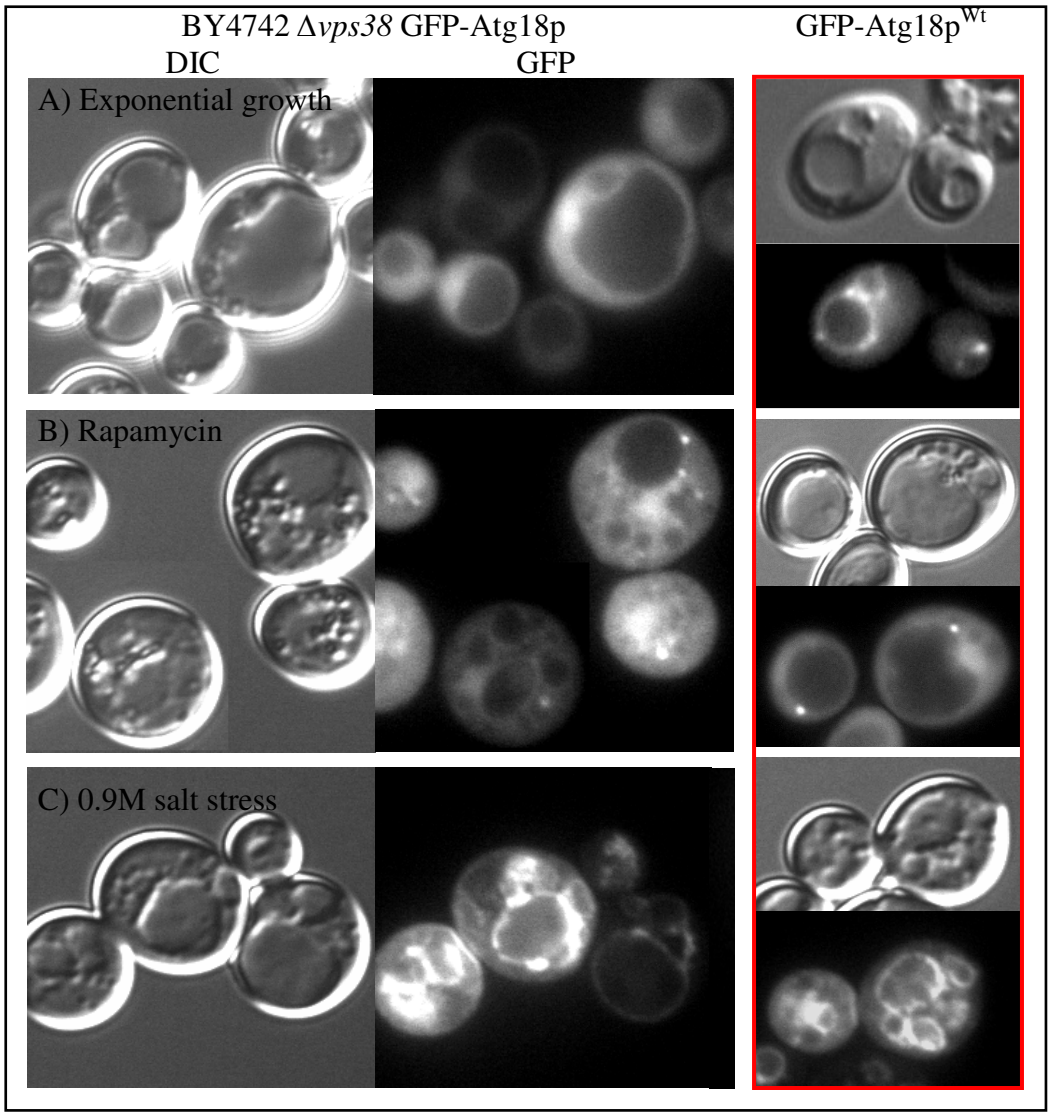

Figure 3.1.12: *In vivo* localization of GFP-Atg18p in Δ*vps38* cells

BY4742 *vps38::KAN* pUG36-ATG18^{Wt} cells were grown overnight in SC-Ura-Meth medium with 2% glucose to 0.6 OD_{600nm}. This cell culture was then split into 3 fractions. Fraction A was resuspended in MES buffer (pH 5.6) with 2% glucose, Fraction B was subjected to Nitrogen-starvation media with (0.2µg/ml) rapamycin and incubated at 25°C in the respective media for 4 hours each. Fraction C was subjected to 0.9M salt stress. All fractions A and B were washed once in fresh media and resuspended in MES buffer pH 5.6 while Fraction C was visualized in saline using DIC and GFP fluorescence microscopy. The images were processed on Photoshop. Photomicrographs in the left panel (highlighted by red) are only included as a reference to localization of Atg18p^{Wt} in Δ*atg18* cells, under specified conditions, but not to cell size.

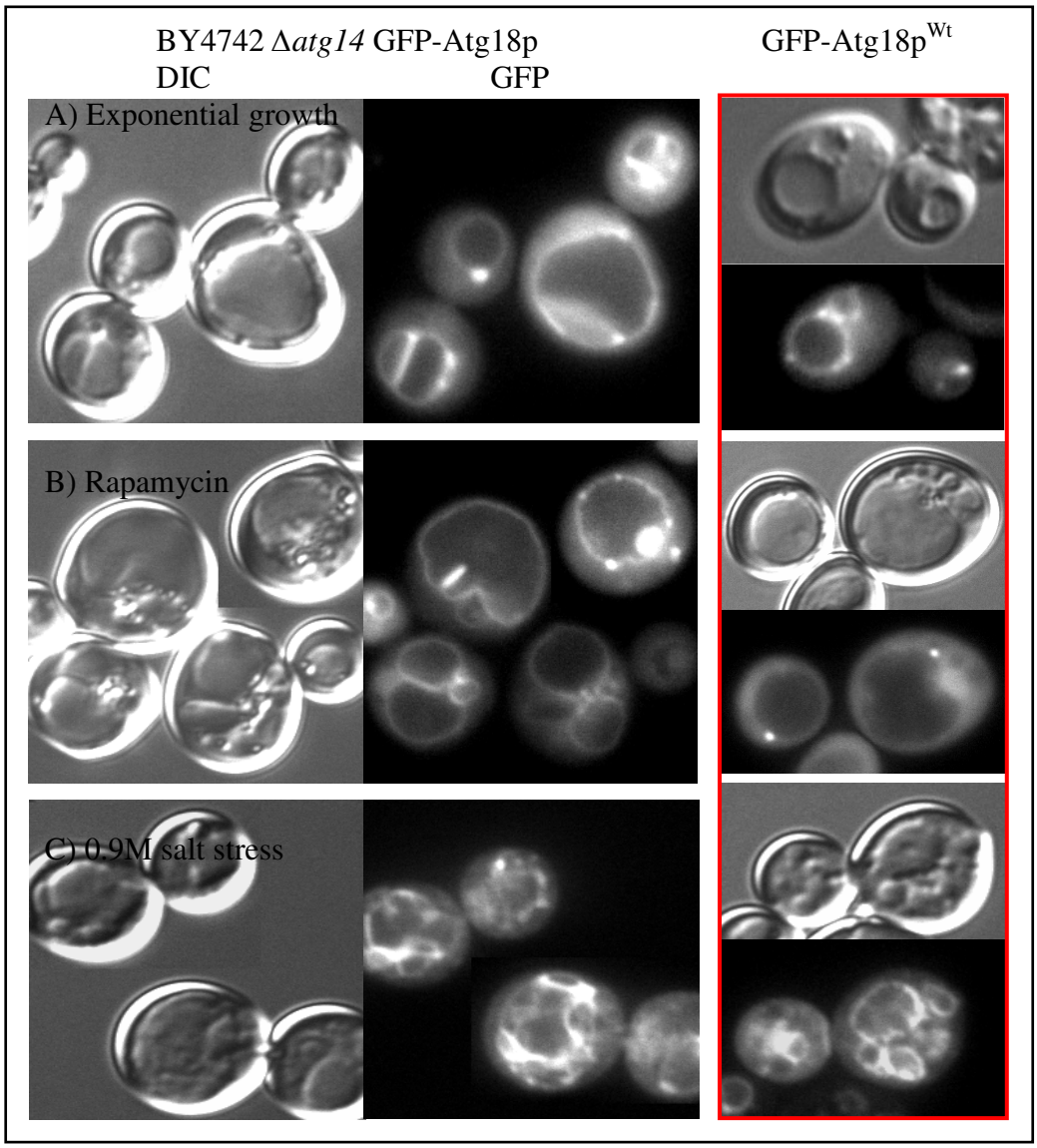

Figure 3.1.13: *In vivo* localization of GFP-Atg18p in Δ*atg14* cells.

BY4742 *atg14::KAN* pUG36-ATG18^{Wt} cells were grown overnight in SC-Ura-Meth medium with 2% glucose to 0.6 OD_{600nm}. This cell culture was then split into 3 fractions. Fraction A was resuspended in MES buffer (pH 5.6) with 2% glucose, Fraction B was subjected to Nitrogen-starvation media with (0.2µg/ml) rapamycin and incubated at 25°C in the respective media for 4 hours each. Fraction C was subjected to 0.9M salt stress. All fractions A and B were washed once in fresh media and resuspended in MES buffer pH 5.6 while Fraction C was visualized in saline using DIC and GFP fluorescence microscopy. The images were processed on Photoshop. Photomicrographs in the left panel (highlighted by red) are only included as a reference to localization of Atg18p^{Wt} in Δ*atg18* cells, under specified conditions, but not to cell size.

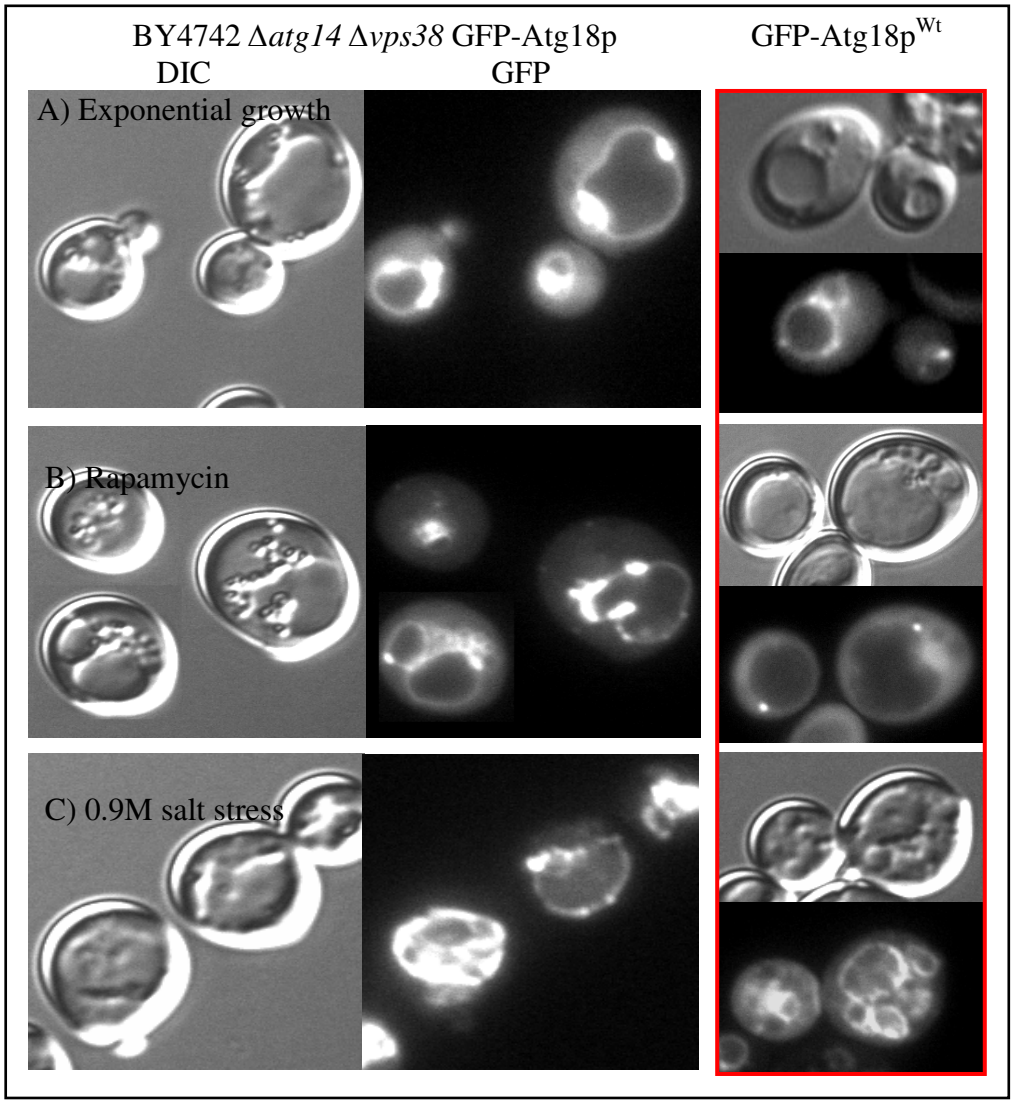

Figure 3.1.14: *In vivo* localization of GFP-Atg18p in Δ*vps38* Δ*atg14* cells.

BY4742 *atg18*::KAN *vps38::*HIS pUG36-ATG18^{Wt} cells were grown overnight in SC-Ura-Meth medium with 2% glucose to 0.6 OD_{600nm}. This cell culture was then split into 3 fractions. Fraction A was resuspended in MES buffer (pH 5.6) with 2% glucose, Fraction B was subjected to Nitrogen-starvation media with (0.2µg/ml) rapamycin and incubated at 25°C in the respective media for 4 hours each. Fraction C was subjected to 0.9M salt stress. All fractions A and B were washed once in fresh media and resuspended in MES buffer pH 5.6 while Fraction C was visualized in saline using DIC and GFP fluorescence microscopy. The images were processed on Photoshop. Photomicrographs in the left panel (highlighted by red) are only included as a reference to localization of Atg18p^{Wt} in Δ*atg18* cells, under specified conditions, but not to cell size.

It was observed that:

- Atg18p loses its localization in Δ*vps34* cells under all tested conditions (Figure 3.1.11) although it is novel to observe that there is very slight GFP-Atg18p vacuolar localization during salt stress. This further emphasizes that besides lipid dependent recruitment, Atg18p localization also partly dependent on its protein interactions.
- In Δ*vps38* cells (Figure 3.1.12), Atg18p substantially loses its localization under exponential growth conditions and although it does form a few punctae during autophagy but the vacuolar localization is not completely lost and the vacuole size does not increase as in wild type cells. Nonetheless, Atg18p vacuolar localization under salt stress conditions in such cells indicates that requirement of Vps38p can be bypassed during osmotic shock. However vacuole fragmentation defects despite Atg18p localization suggest that either Atg18p is unable to promote normal vacuole function during stress due to defects in recycling of a protein in a Vps38p/retromer dependent manner or the likely reduced pool of PtdIns(3,5)P_2 is unable to promote normal vacuole function during stress.
- In Δ*atg14* cells (Figure 3.1.13), Atg18p localizes normally under exponential growth conditions but does not form punctae under rapamycin induced autophagy conditions but instead remains vacuolar. This indicates that Atg18p localization during autophagy depends largely on Atg14p mediated PtdIns3*P* synthesis and that this is required for the Atg18p shift off the vacuole. The vacuole fragmentation and Atg18p localization is not affected by Δ*atg14* under osmotic shock.

- In Δ*atg14* Δ*vps38* cells (Figure 3.1.14) interestingly Atg18p localization is very similar to its localization in Δ*atg14* cells (under exponential growth, autophagy and salt stress) and Δ*vps38* cells (during salt stress). This indicates that 1) Vps34 core complex is capable of regulating PtdIns3*P* levels independently of Atg14p and Vps38p, 2) Vps34 complex II has more profound effects on the localization of Atg18p and 3) Atg18p localization is fine tuned by Vps34 complex I and II via maintenance of PtdIns3*P* levels.

This is reflected by 1) loss of Atg18p localization under exponential growth conditions in Δ*vps38* cells 2) defects in vacuolar fragmentation in Δ*vps38* cells under salt stress and 3) a large vacuole in Δ*vps38* cells under exponential growth conditions.

Recent work has highlighted a role for protein-protein interactions in control of Atg18p membrane binding (Baskaran et al 2012; Baskaran et al 2012; Krick et al 2012; Watanabe et al 2012). It was therefore logical to test if the redistribution of Atg18p observed during autophagy was a partial result of changes in such interactions. Hence Fab1p, Vac7p, Vac14p and Figure4p were considered potential candidates as their interactions with Atg18p on the vacuole were already known.

Vac7p is unique to fungi and is a trans-membrane protein, previously recognized for its role in activation of Fab1p for PtdIns(3,5)P_2 synthesis (Bonangelino, Catlett et al. 1997). Very little is known about the exact functions and trafficking of Vac7p, but it is reported that Atg18p interaction with Vac7p is partly responsible for vacuolar recruitment of Atg18p (Efe, Botelho et al. 2007). Therefore could it be

Vac7p which regulates Atg18p localization in addition to lipid mediated recruitment? Thus Atg18p *in vivo* localization was studied in Δ*vac7* cells (Figure 3.1.15).

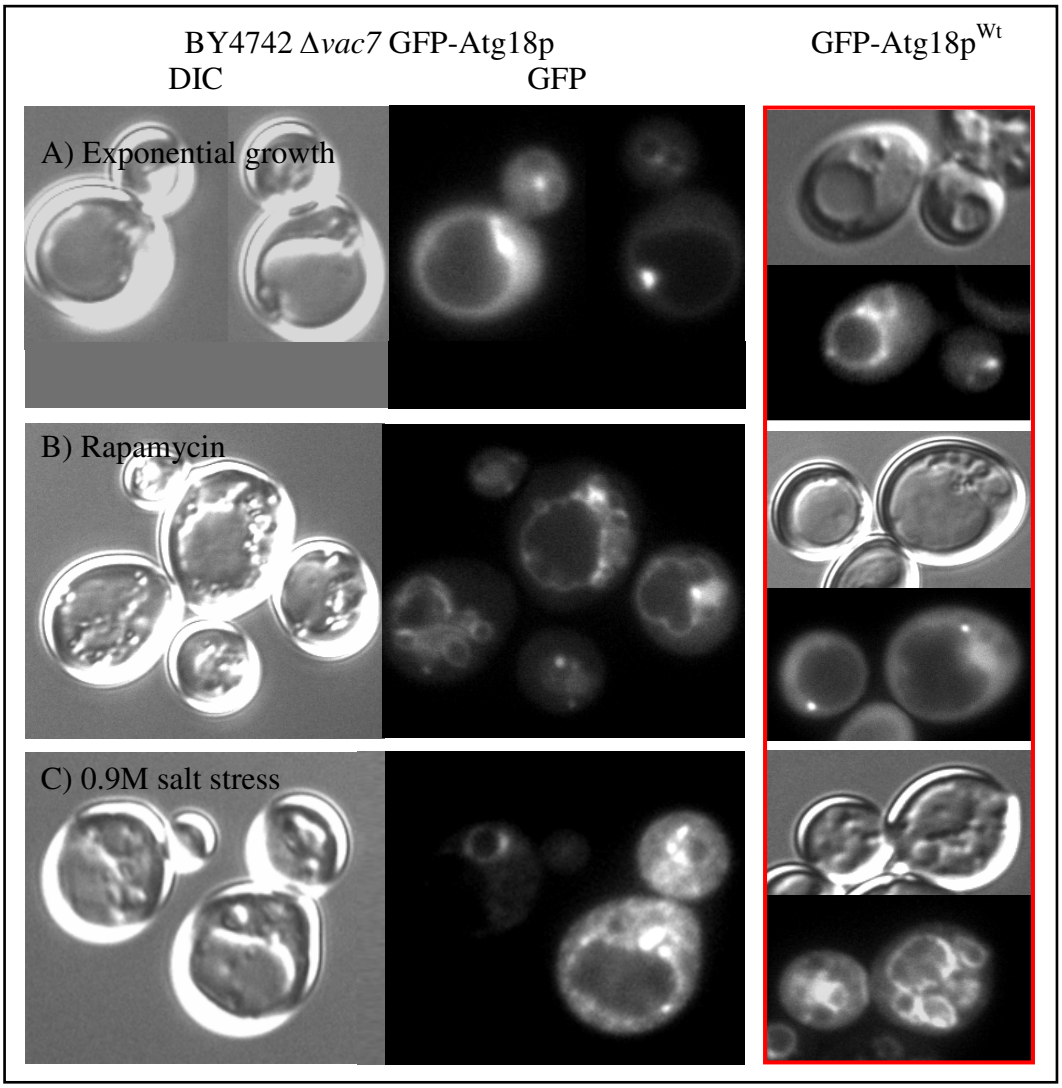

Figure 3.1.15: *In vivo* localization of GFP-Atg18p in Δ*vac7* cells.

BY4742 *vac7::KAN* pUG36-*ATG18*^{Wt} cells were grown overnight to OD_{600} 0.6 in SC-Ura-Met+2% Glucose at 25°C. The cells were harvested by centrifugation and resuspended in A) SC-Ura-Met + 2 % glucose, B) 1.7 % YNB + 2 % Glucose + 0.2 µg/ml Rapamycin and incubated at 25 °C for 4 hours whereas 100 µl of cell culture C) was incubated in 0.9 M salt + SC-Ura-Met + 2% Glucose and examined after 5 minutes of induction. Cultures A and B were spin down and resuspended in MES buffer pH 5.6 and examined microscopically using GFP filter mounted on a Nikon Eclipse E600. The images were processed using Photoshop. Photomicrographs in the left panel (highlighted by red) are only included as a reference to localization of Atg18p^{Wt} in Δ*atg18* cells, under specified conditions, but not to cell size.

Interestingly, besides loss of Atg18p vacuolar localization in Δ*vac7* cells under exponential growth conditions (Figure 3.1.15A), Atg18p also fails to localize correctly as punctae under autophagy conditions (Figure 3.1.15B) as well as the vacuolar membrane during salt stress (Figure 3.1.15C). Hence these results clearly indicate that Atg18p requires Vac7p for correct localization under all the tested conditions, but how does Vac7p affect Atg18p localization?

One possibility is that Vac7p itself could be changing localization; hence the distribution of this protein was examined.

Vac7p localizes to the vacuole in Δ*vac7* cells under exponential growth and salt stress conditions but as punctae during autophagy (Figure 3.1.16). This is significant because Fab1p is known to become deactivated during starvation, but the mechanism has never been uncovered; PtdIns(3,5)P_2 levels drop in wild-type cells during starvation/G_0 and the cells also fail to respond to hyper-osmotic stress with any increase in this lipid . This is the first report that Vac7p translocates from the vacuole during starvation and since Vac7p is absolutely required for Fab1p activity, this observation provides a mechanistic explanation for how Fab1p activity is regulated during autophagy.

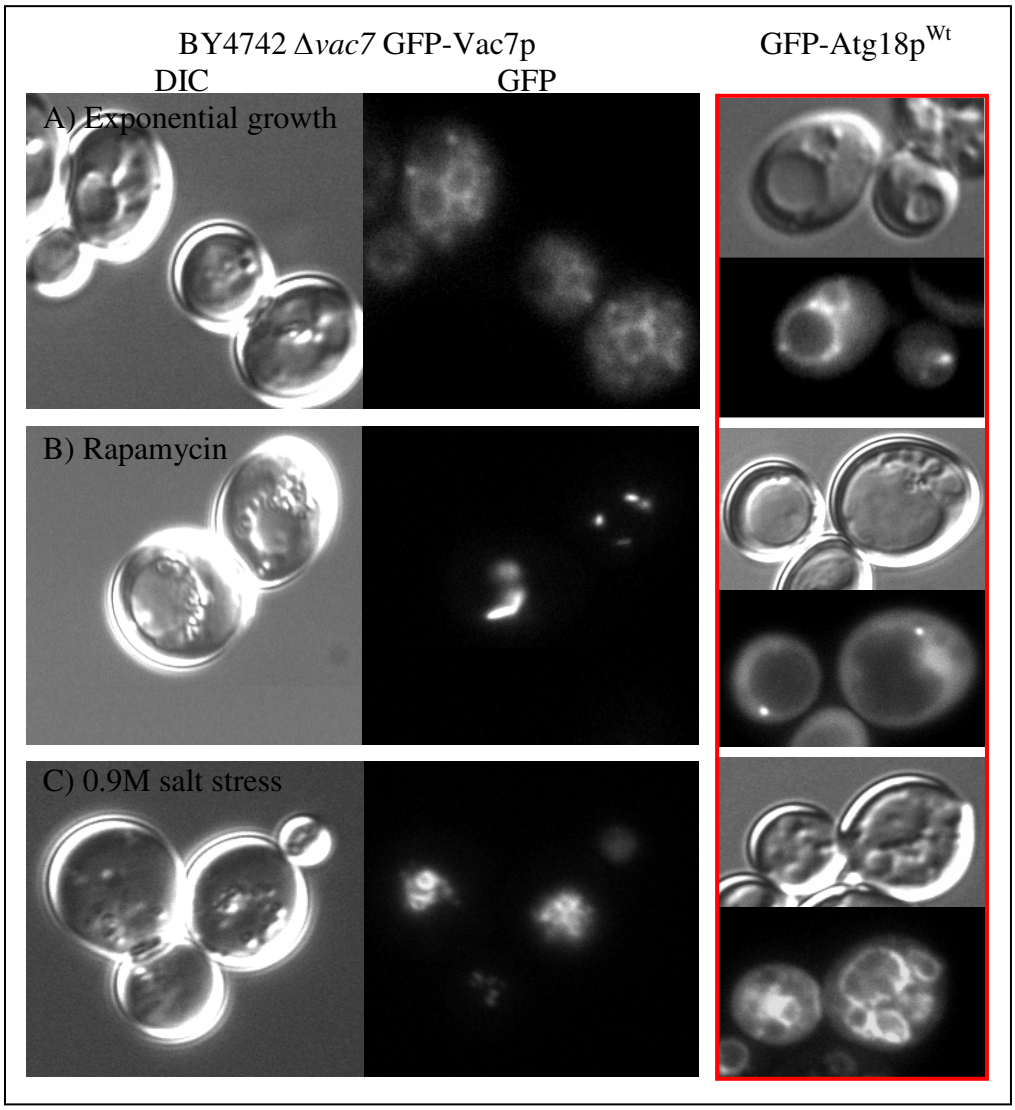

Figure 3.1.16: *In vivo* localization of GFP-Vac7p in Δ*vac7* cells.

BY4742 *vac7::KAN* pUG36-*VAC7*^{Wt} cells were grown overnight to OD_{600} 0.6 in SC-Ura-Met+2% Glucose at 25°C. The cells were harvested by centrifugation and resuspended in A) SC-Ura-Met + 2 % glucose B) 1.7 % YNB + 2 % Glucose + 0.2 µg/ml Rapamycin and C) 1.7 % YNB + 2 % Glucose + 0.2 µg/ml Rapamycin + 200 µM / ml cyclohexamide, and examined microscopically using GFP filter mounted on a Nikon Eclipse E600. The images were processed using Photoshop. Photomicrographs in the left panel (highlighted by red) are only included as a reference to localization of Atg18p^{Wt} in Δ*atg18* cells, under specified conditions, but not to cell size.

Since Vac7p localizes as punctae during autophagy, it is possible that this translocation not only results in loss of PtdIns(3,5)P_2 during starvation, displacing Atg18p from the vacuole, but also that the presence of Vac7p on punctae relocalises Atg18p to these organelles, via their well characterized direct protein-protein

interaction. In order to investigate this, it would be expected that some of the Vac7p punctae might be PAS and others might be Snf7p positive endosomes.

This was investigated by co-localization of GFP-Vac7p with RFP-tagged organelle marker proteins under autophagy conditions (Figure 3.1.17).

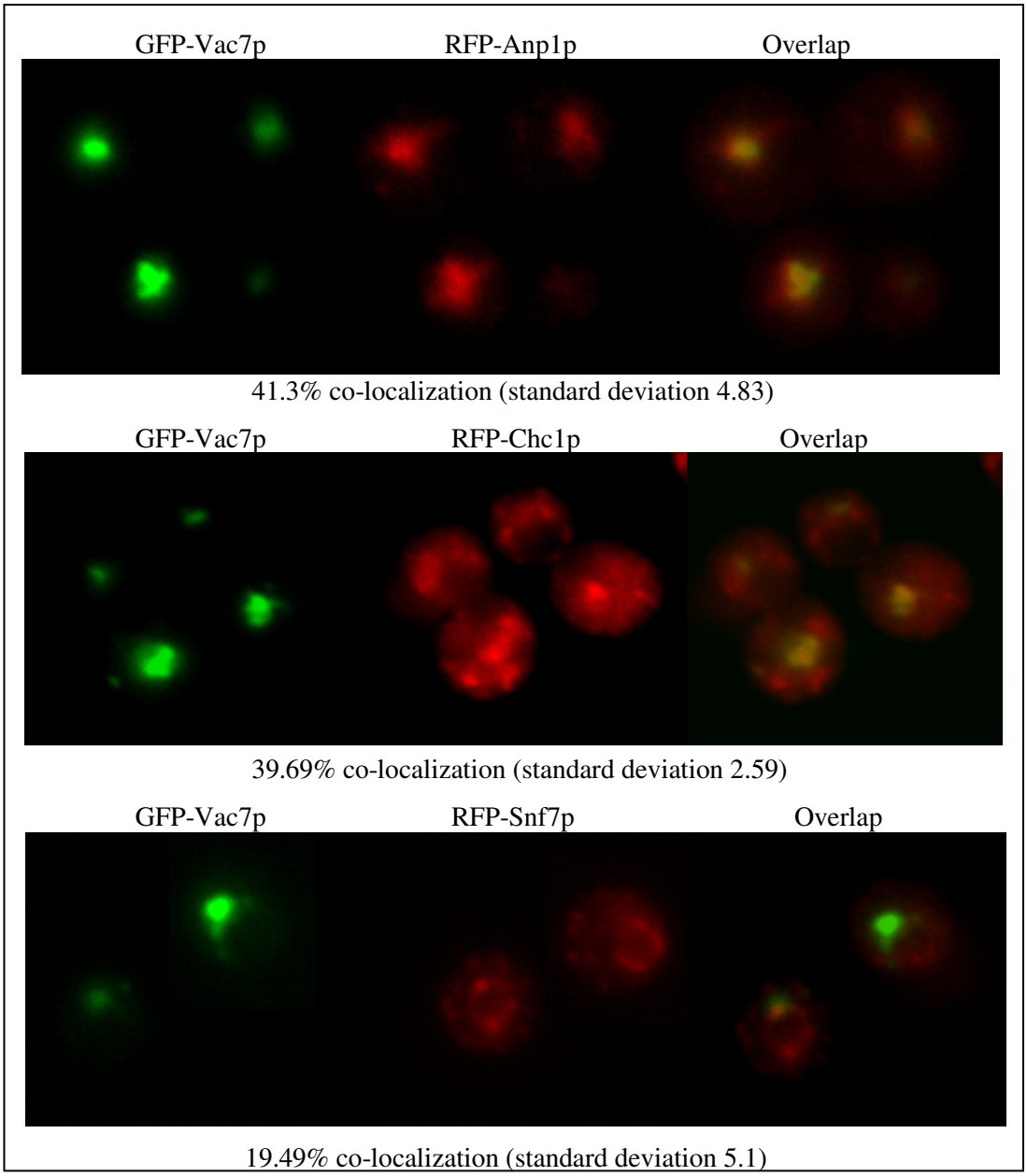

Figure 3.1.17: *In vivo* co-localization of GFP-Vac7p with RFP organelle markers (under autophagy conditions).

BY4742 RFP-tagged (Anp1p is a TGN marker and Chc1p is clathrin heavy chain, marker for clathrin coated vesicles) cells were transformed with pUG36-*VAC7*^{Wt} and grown on selective media at 25 °C. Successful transformants were grown in SC-Ura-Met + 2 % glucose overnight to 0.6 OD_{600nm}. The cells were spin down and resuspended in 1.7% YNB + 2 % Glucose + 0.2 µg/ml Rapamycin and incubated at 25 °C for 4 hours. The cells were washed once in MES buffer pH5.6 and then examined microscopically. The pictures were processed using Photoshop.

These results indicate that Vac7p punctae co-localize with Clathrin heavy chain and RFP-Anp1p (TGN marker) under autophagy conditions, both of which reside in the Golgi, although note that ~20% of GFP-Vac7p labeled punctae do not co-localize with any known marker, so a localization to the PAS cannot be ruled out.

Since Vac7p has a trans-membrane domain and such proteins are recognized to be transported from the TGN either via VPS pathway or the AP-3 pathway, it could be possible that Vac7p is either retained at the TGN during autophagy or is recycled back there from the vacuole, leading to an increase in overlap between GFP-Vac7p and RFP-Anp1p.

To distinguish between these possibilities, investigation of the *in vivo* localization of Vac7p in Δ*vps34* cells (no PtdIns3*P* synthesis) was crucial since the function of both the vacuole to PVE and retromer, that is required for trafficking from PVE to Golgi, depend upon this lipid (Figure 3.1.18).

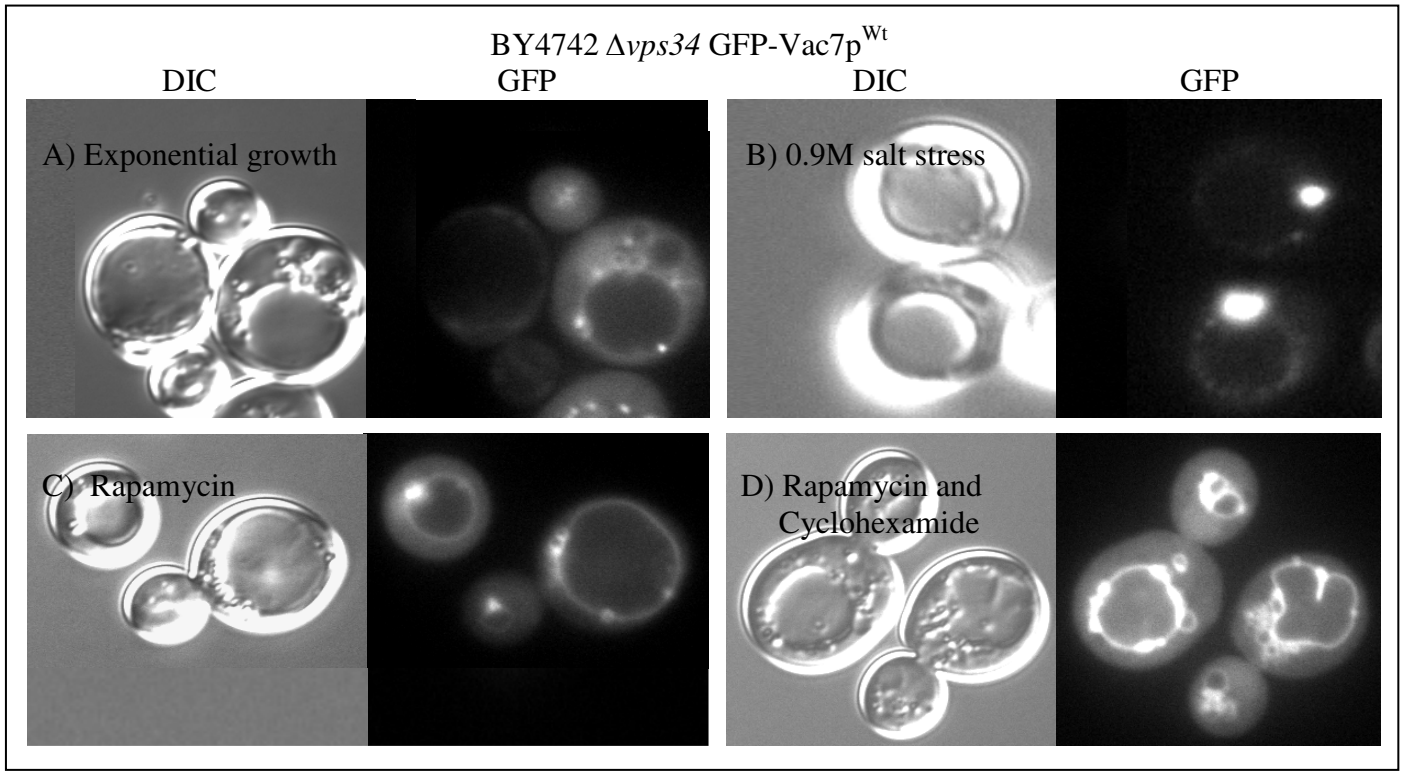

Figure 3.1.18: *In vivo* localization of GFP-Vac7p in Δ*vps34* cells.

BY4742 *vps34*::KAN pUG36-*VAC7*^{Wt} cells were grown overnight to OD_{600} 0.6 in SC-Ura-Met+2% Glucose at 25°C.The cells were harvested by centrifugation and resuspended in A) SC-Ura-Met + 2 % glucose B) 0.9M saline C) 1.7 % YNB + 2 % Glucose + 0.2 µg/ml Rapamycin and D) 1.7 % YNB + 2 % Glucose + 0.2 µg/ml Rapamycin and incubated for 3 hours and then 200 µM / ml cyclohexamide was added to this culture and left for further 1 hour. The cultures were then examined microscopically using GFP filter mounted on a Nikon Eclipse E600 and the images were processed using Photoshop.

Vac7p is observed to localize as punctae and partially on the vacuole membrane in Δ*vps34* cells under exponential growth conditions (Figure 3.1.18A) indicating no absolute requirement for PtdIns3*P* in Vac7p localization under fermentative growth; however, the relocation of Vac7p from vacuole to punctae during autophagy does appear to require PtdIns3*P* and/or PtdIns(3,5)P_2.

To investigate this, GFP-Vac7p localization was investigated in Δ*vps38* cells under test conditions (Figure 3.1.19).

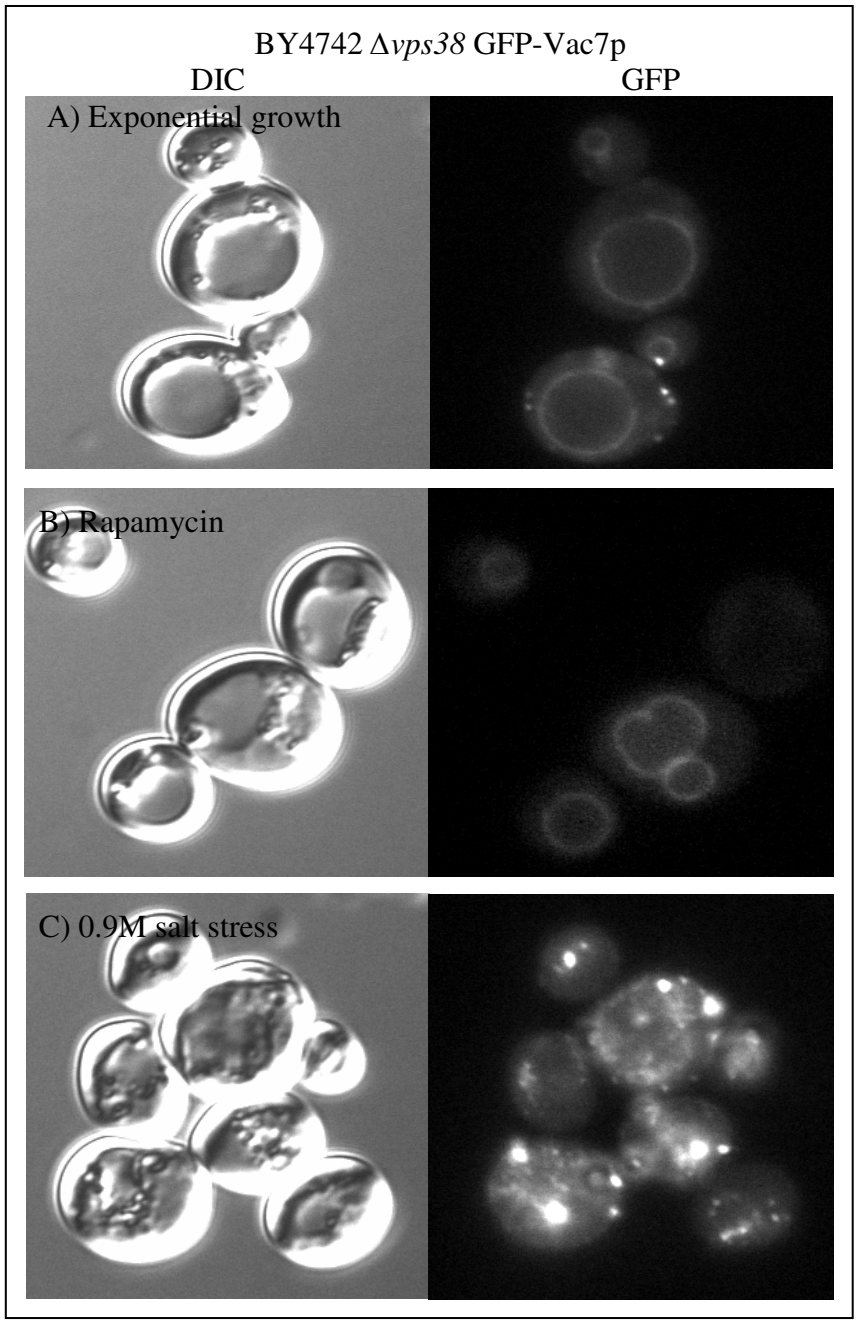

Figure 3.1.19: *In vivo* localization of GFP-Vac7p localization in Δ*vps38* cells.
BY4742 *vps38*::KAN pUG36-*VAC7*^{Wt} cells were grown overnight to OD_{600} 0.6 in SC-Ura-Met+2% Glucose at 25°C.The cells were harvested by centrifugation and resuspended in A) SC-Ura-Met + 2 % glucose B) 0.9M saline and C) 1.7 % YNB + 2 % Glucose + 0.2 µg/ml Rapamycin and incubated for 4 hours. The cultures were then resuspended in MES buffer except for culture used for induction of osmotic shock. The cultures were then examined microscopically using GFP filter mounted on a Nikon Eclipse E600 and the images were processed using Photoshop.

Vac7p localizes to the vacuole rim in both Δ*vps34* and Δ*vps38* cells under exponential growth and autophagy conditions, in contrast to Vac7p localization in wild type cells. This suggests that lipid dependent trafficking is important in the localization of Vac7p during autophagy; most likely both PtdIns3*P* and PtdIns(3,5)P_2 since 1) earlier data (see above) indicates that many of the punctae decorated by Vac7p under starvation conditions are Golgi and 2) PtdIns(3,5)P_2 and PtdIns3*P* are known to be absolutely required for vacuole to PVE and PVE to TGN trafficking respectively. Hence Vac7p would have to use both these pathways to return to the Golgi, in which case the requirement of PtdIns(3,5)P_2 and PtdIns3*P* can not be bypassed.

No strong evidence is available in favor of Fab1p dependent PtdIns5*P* synthesis in yeast, unlike its mammalian homologue PIKfyve. However a possible route of PtdIns5*P* synthesis exists via breakdown of PtdIns(3,5)P_2 by PtdIns 3-ptases; in yeast 3 such proteins are identified to date, namely Ymr1p, Inp51p and Inp52p.

Atg18p does not bind PtdIns5*P* but due to an emerging role of PtdIns5*P* in fission processes, the localization of Atg18p was investigated in Δ*ymr1* (Figure 3.1.20) and Δ*inp51* (Figure 3.1.21A/B) cells, in order to establish how Atg18p localization is affected a putative disruption in regulation of PtdIns(3,5)P_2 / PtdIns3*P* levels and/or PtdIns(3,5)P_2 / PtdIns5*P* levels.

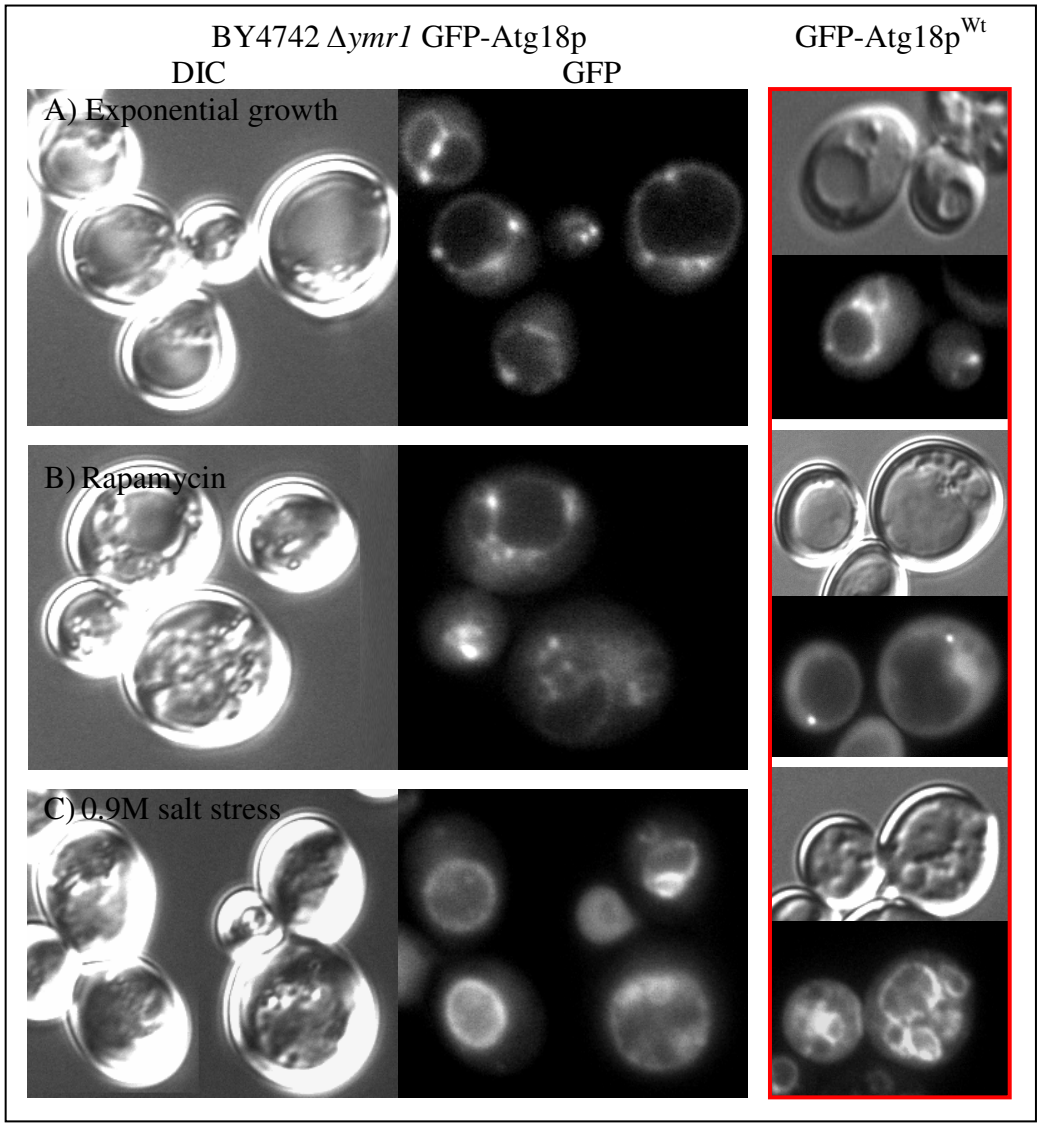

Figure 3.1.20: *In vivo* localization of GFP-Atg18p in Δ*ymr1* cells.

BY4742 *ymr1*::KAN pUG36-*ATG*^{Wt} cells were grown overnight to OD_{600} 0.6 in SC-Ura-Met+2% Glucose at 25°C.The cells were harvested by centrifugation and resuspended in A) SC-Ura-Met + 2 % glucose, B) 1.7 % YNB + 2 % Glucose + 0.2 µg/ml Rapamycin and C) 0.9M saline. Fractions A and B were incubated for 4 hours and then resuspended in MES buffer pH 5.6 and examined microscopically while fraction was examined in saline, using GFP filter mounted on a Nikon Eclipse E600. The images were processed using Photoshop.

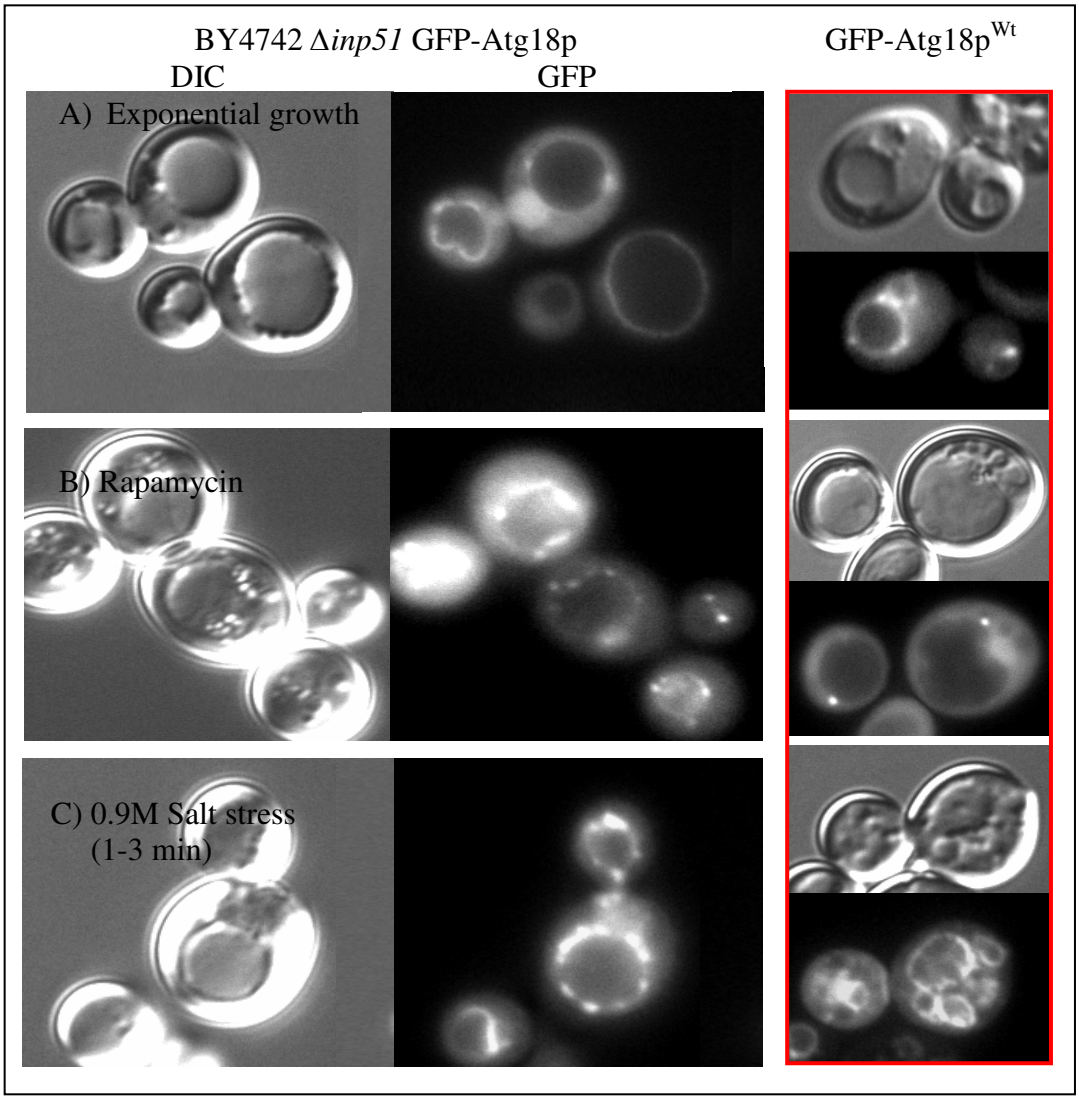

Figure 3.1.21A: *In vivo* localization of GFP-Atg18p in Δ*inp51* cells.

BY4742 *inp51*::KAN pUG36-*ATG*^{Wt} cells were grown overnight to OD_{600} 0.6 in SC-Ura-Met+2% Glucose at 25°C.The cells were harvested by centrifugation and resuspended in A) SC-Ura-Met + 2 % glucose, B) 1.7 % YNB + 2 % Glucose + 0.2 µg/ml Rapamycin and C) 0.9M saline. Fractions A and B were incubated for 4 hours and then resuspended in MES buffer pH 5.6 and examined microscopically while fraction was examined in saline, using GFP filter mounted on a Nikon Eclipse E600. The images were processed using Photoshop. Photomicrographs in the left panel (highlighted by red) are only included as a reference to localization of Atg18p^{Wt} in Δ*atg18* cells, under specified conditions, but not to cell size.

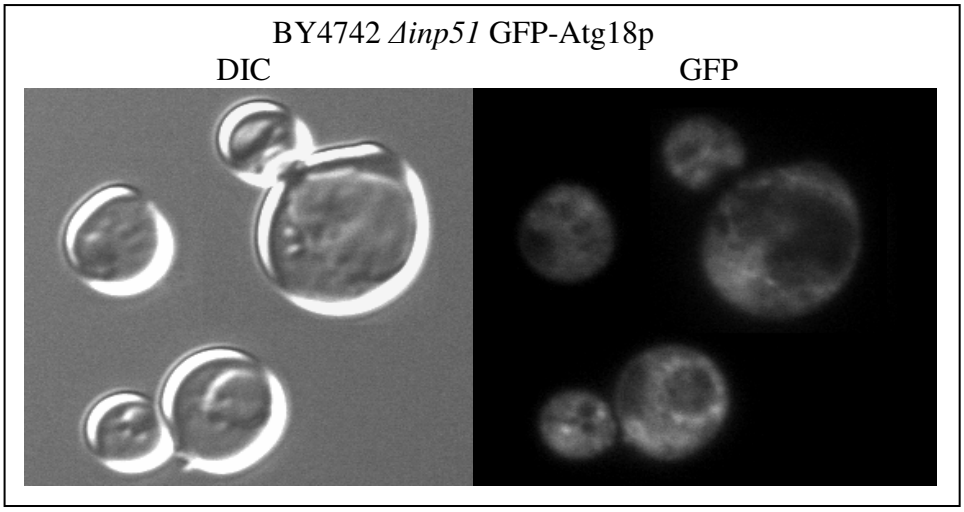

Figure 3.1.21B: *In vivo* localization of GFP-Atg18p in Δ*inp51* cells.

BY4742 *inp51*::KAN pUG36-ATG^{Wt} cells in 0.9M saline after 3-10 minutes if induction of salt stress. The fraction was examined in saline, using GFP filter mounted on a Nikon Eclipse E600. The images were processed using Photoshop.

Figure 3.1.20 shows that Ymr1p does not apparently affect Atg18p localization under normal conditions but it is interesting to note that despite vacuolar localization of Atg18p in Δ*ymr1* cells, the vacuolar fragmentation is very slow (if not blocked) and Atg18p does not completely lose its vacuolar localization during autophagy in Δ*ymr1* cells. It is also interesting to note that Atg18p punctae localization is much reduced in Δ*inp51* cells under exponential growth conditions. Whereas, during osmotic shock, such cells exhibit vacuole fragmentation defects and Atg18p loses its vacuolar localization after 3-10 minutes of induction of salt stress (Figure 3.1.21 A/B).

So in summary, both protein-protein and lipid interactions are essential for correct Atg18p localization; therefore it becomes important to investigate the lipid binding domain in Atg18p and investigate the effect of specific mutations on lipid binding and consequent localization.

Chapter 3; Results

3.2: Atg18p Lipid binding.

Although Atg18p is a PROPPIN protein, the properties of its lipid binding domain remain contentious, because some *in vitro* reports suggest it exclusively binds PtdIns(3,5)P_2 whilst *in vivo* data suggests that it binds PtdIns3*P* (Dove, Piper et al. 2004). The FRRG motif in PROPPINs is a highly conserved consensus motif and is recently identified to articulate PtdIns3*P* and PtdIns(3,5)P_2 binding (Baskaran, Ragusa et al.). Atg18p^{FTTG} lipid binding is decreased up to 40%. Hence the initial step was to investigate the lipid binding of Atg18p^{Wt} and Atg18p^{FTTG} mutant *in vitro* (Figure 3.2.1).

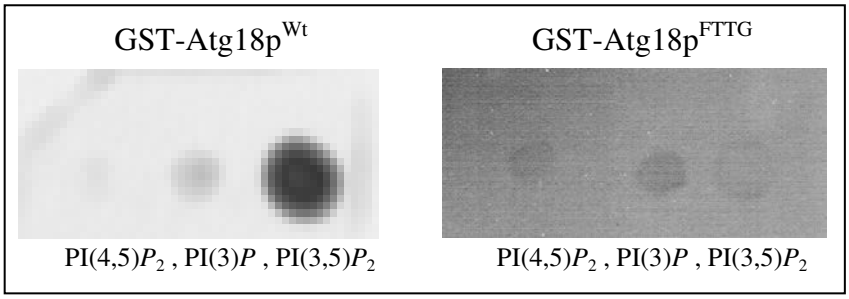

Figure 3.2.1: Lipid overlay assay; Atg18p^{Wt} and Atg18p^{FTTG}
ATG18p^{Wt} and Atg18p^{FTTG} were used for lipid dot blot assay and visuailized through chemiluminescence on photographic film.

Atg18p^{Wt} binds PtdIns(3,5)P_2 avidly while Atg18p^{FTTG} lipid binding is decreased substantially and hence the effect of this on *in vivo* localization of Atg18p^{FTTG} under various conditions was further investigated (Figure 3.2.2).

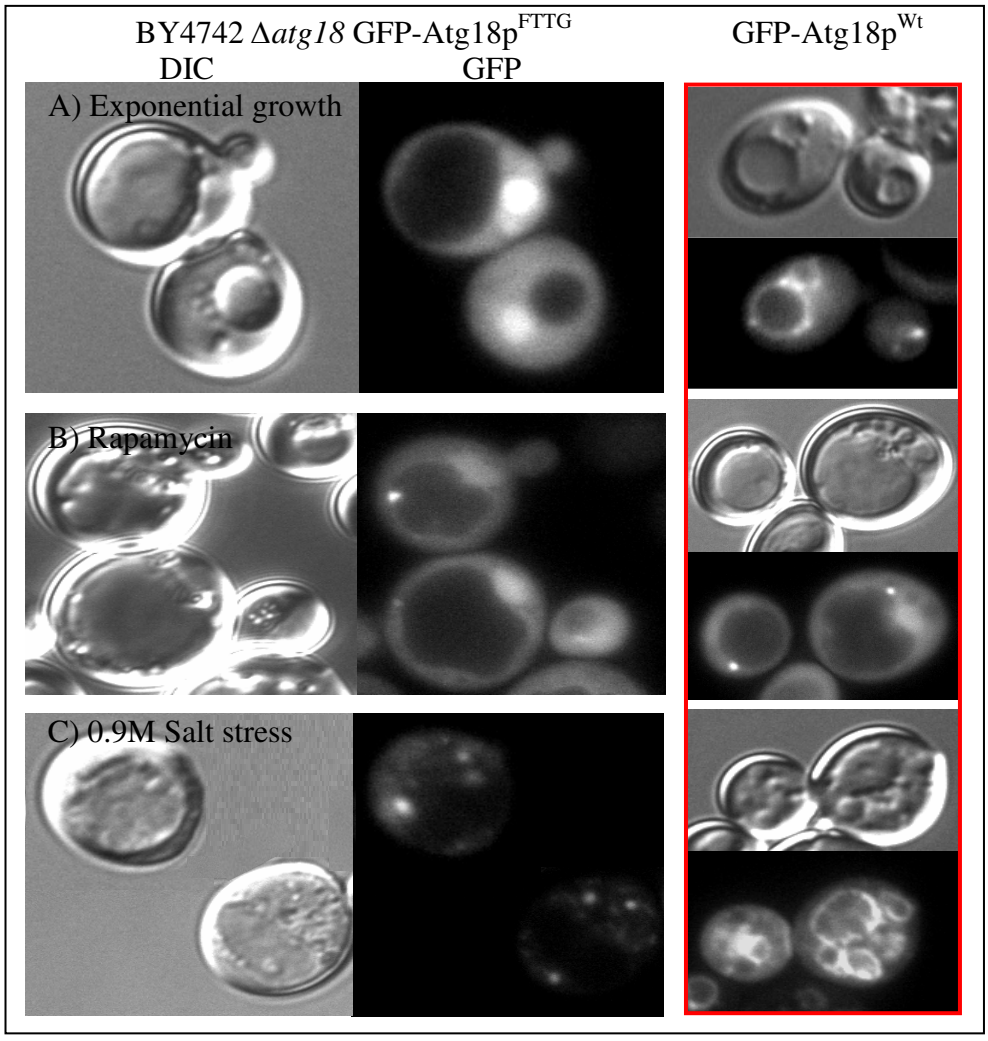

Figure 3.2.2: *In vivo* localization of GFP-Atg18p^{FTTG}

ATG18^{FTTG} was cloned into Xho1/ECoR1 sites of pUG36 and transformed into BY4742 *atg18*::KAN cells and grown overnight in Sc-Ura-Met + 2% glucose to an OD_{600} of 0.6. This cell culture was then divided into 3 fractions; Fraction A was suspended in SC-Ura-Met + 2 % Glucose, Fraction B was suspended in 1.7 % YNB + 2 % Glucose + 0.2 µg/ml Rapamycin whereas Fraction C was resuspended in 0.9M saline + SC-Ura-Meth +2% glucose. Fractions A and B were washed once with fresh media and then resuspended in MES buffer (pH 5.6). The cells were examined microscopically using GFP filter mounted on a Nikon Eclipse E600 and the images were processed using Photoshop. Photomicrographs in the left panel (highlighted by red) are only included as a reference to localization of Atg18p^{Wt} in Δ*atg18* cells, under specified conditions, but not to cell size.

Figure 3.2.2 shows that GFPAtg18p^{FTTG} is cytosolic and nuclear under exponential growth conditions and exhibits a large vacuole, whereas under autophagy conditions a few punctate structures are visible. It also localizes as punctae under salt stress but the vacuole fails to fragment.

The nuclear localization was confirmed via co-localization of Atg18p^{FTTG} mutant with RFP-NLS (RFP tagged nuclear localization signal) (Figure 3.2.3).

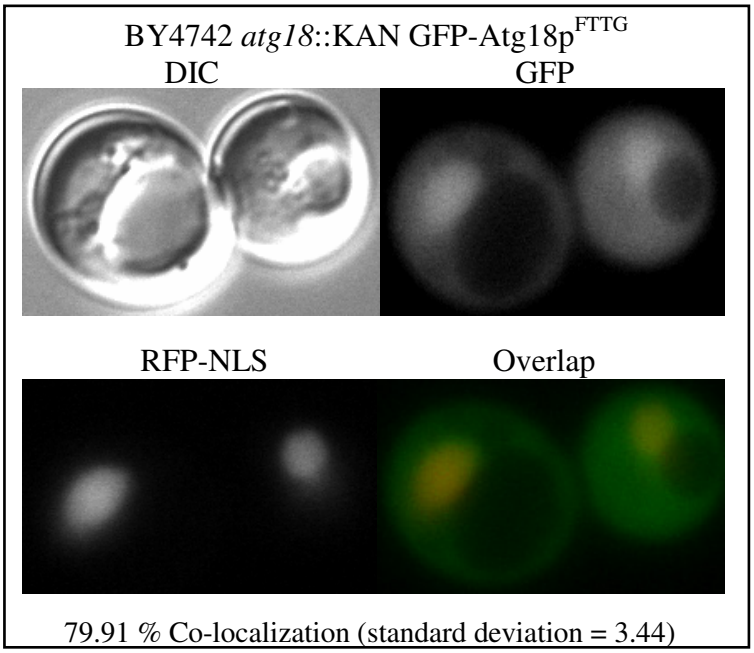

Figure 3.2.3: *In vivo* co-localization of GFP-Atg18p^{FTTG} with RFP-NLS.

BY4742 *Δatg18* GFP-Atg18p^{FTTG} was grown to an OD_{600} 0.5 in Sc-Ura-Met + 2% Glucose at 25°C and transformed with pUR34-NLS. The successful transformants were examined microscopically at an OD_{600} 0.6 in MES buffer pH 5.6 using GFP and RFP filters. The overlap was carried out using Photoshop.

Since many regulatory proteins are known to undergo modifications in order for them to gain or lose a function, and given that Atg18p^{FTTG} mutant loses its localization under test conditions, this mutant seemed to afford an excellent opportunity to determine whether Atg18p undergoes any modifications in response to various signals e.g in presence or absence of lipid binding?

This was investigated via LC-CID-FT-MS analysis of Atg18p^{Wt} and Atg18p^{FTTG} (Figure 3.2.4).

A high ion score for both fragments containing FRRG and SPRRLR motifs in $Atg18p^{Wt}$ indicate that these regions contain potential phosphorylation sites. However the ion score value for SPRRLR fragment decreases in $Atg18p^{FTTG}$ whereas FRRG fragment does not appear in these match results. Nonetheless, ion score for a third fragment VTSLLESSR is also high in $Atg18p^{Wt}$, which increases slightly in $Atg18p^{FTTG}$ mutant. This trend is also noticable in change in mass to charge ration [ΔM(ppm)] of VTSLLESSR fragment; ΔM(ppm) of this fragment increases in FTTG mutant. Hence this set of data suggests that modification of Atg18p through Phosphorylation may occur through multiple sites.

IC-MS data for Atg18p^{Wt}

Sequence	Activation Type	IonScore	Exp Value	Δ Score	m/z [Da]	MH+ [Da]	ΔM [ppm]	RT [min]
QPALSPRRRLR	CID	56	7.706E-05	1.00	496.27695	991.54662	4.77	15.85
FRRGTYATR	CID	56	0.0002396	1.00	823.43536	2468.29154	2.45	24.93
VTSLLESSR	CID	55	0.0003823	0.18	839.87628	1678.74529	2.97	14.76
NGDVIVFNLETLQPTMVIEAHK	CID	48	0.001912	1.00	839.38501	1677.76274	3.85	14.39
DDADPTSSnGGNSSIIK	CID	47	0.0026991	0.77	721.69720	2163.07706	4.31	17.86
DDADPTSSNGGNSSIIK	CID	47	0.0042153	1.00	786.34601	2357.02347	2.97	19.24
AHATTNNITLSVGGNTETSFK	CID	45	0.0042793		839.87628	1678.74529	2.97	14.76
DQQDAGHSDISDLDQYSSFTK	CID	41	0.0015348	0.63	508.81149	1016.61571	1.74	22.15
DDADPTSSNGGnSSIIK	CID	38	0.0109092	0.63	556.26782	1111.52837	3.80	18.92
TLGQIFPIK	CID	26	0.1173912	1.00	702.88635	1404.76543	4.26	14.56
LLHTIETNPNPR	CID	21	0.3189397	1.00	468.72672	936.44615	4.25	12.30

IC-MS data for Atg18p^{FTTG}

Sequence	Activation Type	IonScore	Exp Value	Δ Score	m/z [Da]	MH+ [Da]	ΔM [ppm]	RT [min]
VTSLLESSR	CID	60	3.016E-05	1.00	496.27667	991.54607	4.21	15.76
AHATTNNITLSVGGNTETSFK	CID	57	0.0002513	0.75	721.69653	2163.07505	3.38	17.86
DQQDAGHSDISDLDQYSSFTK	CID	52	0.0014214	0.65	786.34589	2357.02311	2.81	19.27
TLGQIFPIK	CID	34	0.0071129	0.53	508.81143	1016.61559	1.62	22.12
QPALSPRRRLR	CID	14	12.683605		823.37341	3290.47182	-0.86	23.40

Figure 3.2.4: LC-CID-FT-MS analysis of Atg18p^{Wt} and Atg18p^{FTTG} mutant.

Since various studies have demonstrated that phosphoinositide binding is only required for correct localization of Atg18p and if the requirement for phosphoinositide binding is bypassed by a chimeric ATG18^{FTTG}-RS-ALP (which correctly localizes to the vacuole membrane in Δ*fab1* cells) (Efe, Botelho et al. 2005) or ATG18^{FTTG}-FYVE (which correctly localizes to the endosomes/PAS) (Obara, Sekito et al. 2008), the functional abilities of Atg18p for vacuole morphology and autophagy respectively, can be partially restored. However none of these studies highlight the effect of Atg18p-PtdIns3*P* binding on Atg18p-PtdIns(3,5)P_2 binding or vice versa.

Atg18p^{FTTG} is not very useful in this regard since it loses both PtdIns3*P* and PtdIns(3,5)P_2 binding, hence the localization of GFP-Atg18p^{FTTG}FYVE chimeric protein was investigated to check if/how Atg18p-PtdIns3*P* binding effects vacuole morphology under various conditions (Figure 3.2.5).

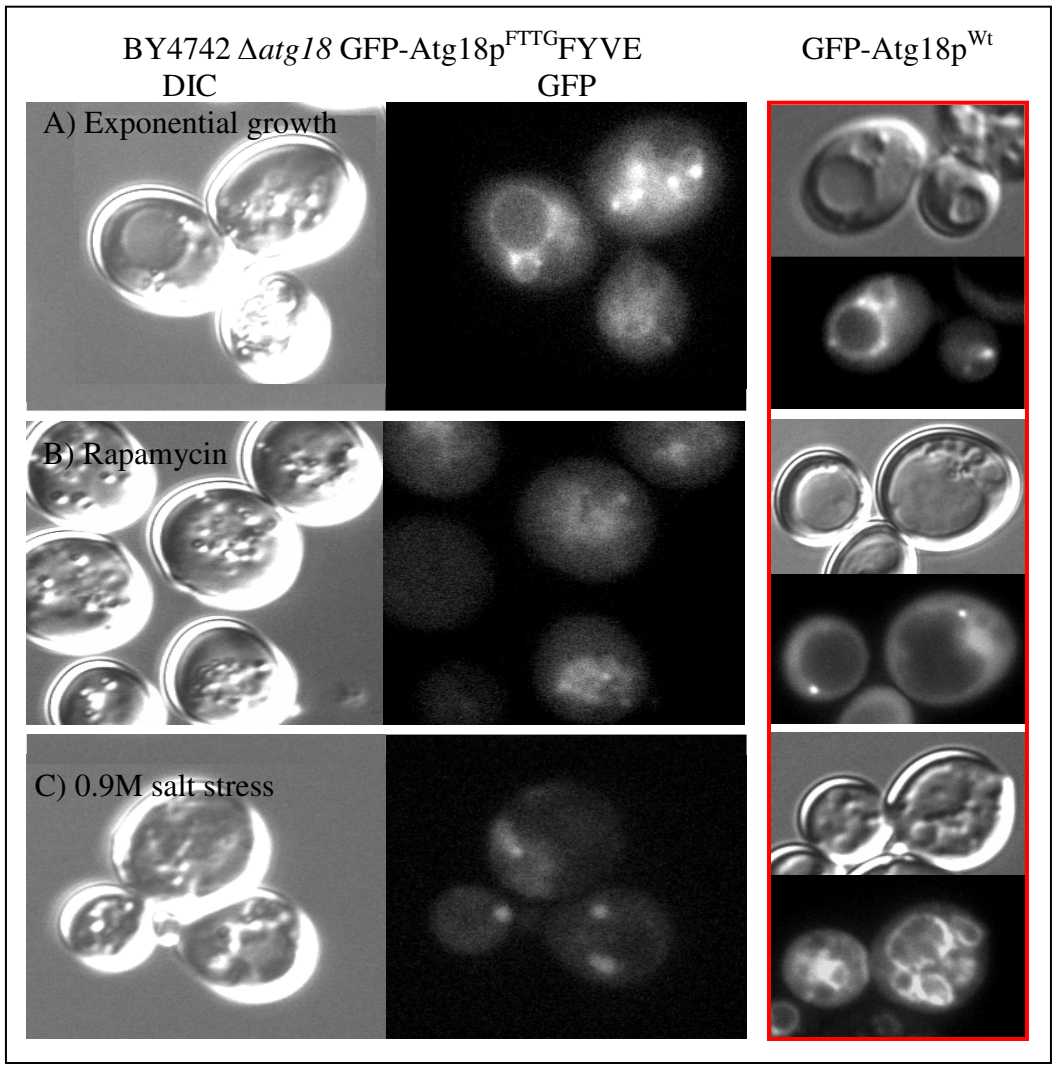

Figure 3.2.5: *In vivo* localization of GFP-Atg18p^{FTTG}FYVE.

BY4742 *atg18*::KAN GFP-Atg18p^{FTTG}FYVE cells were grown overnight in Sc-Ura-Met + 2% glucose to an OD_{600} of 0.6. This cell culture was then divided into 3 fractions; Fraction A was suspended in SC-Ura-Met + 2 % Glucose, Fraction B was suspended in 1.7 % YNB + 2 % Glucose + 0.2 µg/ml Rapamycin for 4 hours, whereas Fraction C was resuspended in 0.9M saline + SC-Ura-Meth +2% glucose. Fractions A and B were washed once with fresh media and then resuspended in MES buffer (pH 5.6). The cells were examined microscopically using GFP filter mounted on a Nikon Eclipse E600 and the images were processed using Photoshop. Photomicrographs in the left panel (highlighted by red) are only included as a reference to localization of Atg18p^{Wt} in Δ*atg18* cells, under specified conditions, but not to cell size.

Figure 3.2.5 shows that Atg18p^{FTTG}FYVE has a similar localization to Atg18^{Wt} under exponential growth conditions and the partial loss in vacuolar localization can be accounted for a loss in PtdIns(3,5)P_2 binding by this chimeric.

During rapamycin induced autophagy conditions, Atg18p^{FTTG}FYVE is visible as patches; as opposed to wild type, where it forms distinct punctae which could be mainly due to lack of disassociation of this chimeric from the membranes due to the FYVE domain. Another crucial difference in this regard is that unlike wild type cells, the vacuole size diminishes during autophagy in these cells.

It is also interesting to note that in response to osmotic shock, Atg18p^{FTTG}FYVE forms punctae and does not localize to the vacuole, which is similar to Atg18p^{FTTG} but not wild type. This confirms previous studies that demonstrated that Atg18p vacuolar localization during salt stress is dependent on PtdIns(3,5)P_2 binding; nonetheless Atg18p^{FTTG}FYVE localization is a good indicator of PtdIns3*P* pools during osmotic shock. It is also interesting to note that despite Atg18p^{FTTG}FYVE mis-localization, the vacuole fragmentation under osmotic stress is less defective than Δ*atg18* cells.

Since Atg18p^{FTTG}FYVE forms distinct patches during autophagy it was reasoned that these patches could be PAS sites and probably due to lack of lipid binding through its native sites, Atg18p^{FTTG}FYVE is unable to disassociate from these structures, giving it a patchy appearance.

Atg14p is involved in directing PtdIns3*P* synthesis to the PAS, and it is known that in absence of Atg14p, PAS formation is hampered.

Hence Atg18p^{FTTG}FYVE localization was investigated in Δ*atg14* cells in order to check whether this construct retains its ability to localize as patches, in which case it

would indicate that either these patches are not PAS and some other membranous structures and/or Atg18p punctae formation during autophagy is Atg14p dependent? And/or whether Atg18p-PtdIns(3,5)P_2 binding plays some role in its localization during autophagy? Figure 3.2.6 represents Atg18p^{FTTG}FYVE localization in Δ*atg14* cells under test conditions.

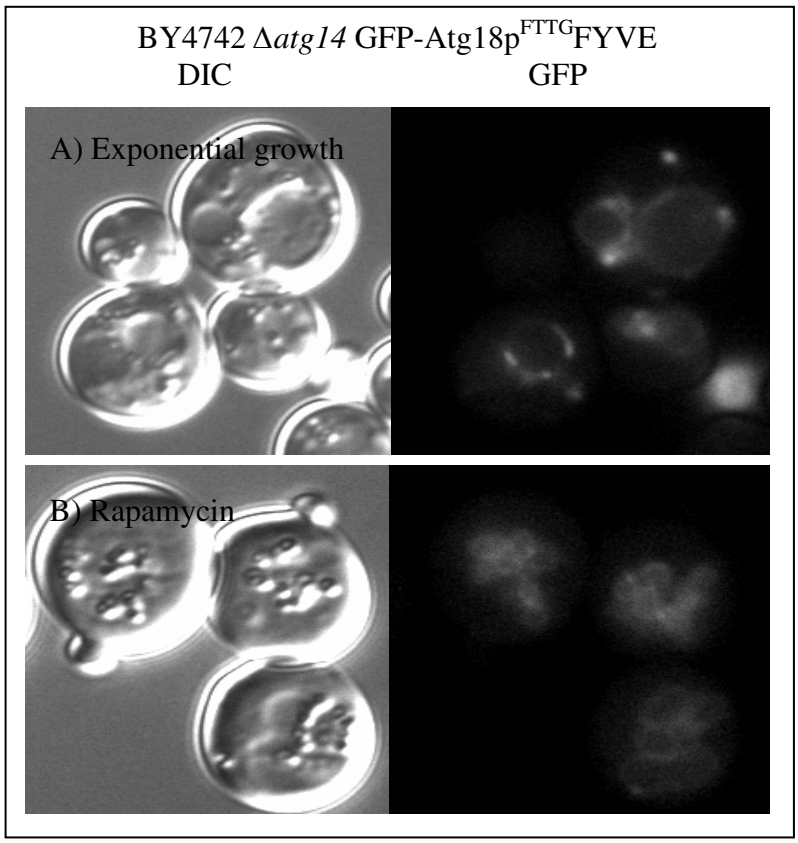

Figure 3.2.6: *In vivo* localization of GFP-Atg18^{FTTG}FYVE in Δ*atg14* cells.
pRS316-*ATG18^{FTTG}FYVE* was transformed into BY4742 *atg18*::KAN cells and grown overnight in Sc-Ura-Met + 2% glucose to an OD_{600} of 0.6. This cell culture was then divided into 2 fractions; Fraction A was suspended in SC-Ura-Met + 2 % Glucose and Fraction B was suspended in 1.7 % YNB + 2 % Glucose + 0.2 µg/ml Rapamycin for 4 hours. Both fractions were washed once and then resuspended in MES buffer (pH 5.6). The cells were examined microscopically using GFP filter mounted on a Nikon Eclipse E600 and the images were processed using Photoshop.

Atg18p^{FTTG}FYVE localization in Δ*atg14* cells is similar to its localization in Δ*atg18* cells under exponential growth conditions, but they become slightly different during

autophagy; although Atg18p^{FTTG}-FYVE is observed to be slightly patchy yet its localization to membranes becomes more prominent, unlike its phenotype in Δ*atg18* cells. This suggests that localization of Atg18p to PAS sites occurs after the initiation of phagosome formation via Atg14p mediated PtdIns3*P* synthesis nevertheless it could also be possible that this chimera is localizing primarily due to interaction/s of the attached FYVE domain and hence the interpretation of the data should be dealt with caution.

The SPRRLR motif in Atg18p is also suggested to be a putative lipid binding site, since Atg18p^{SPSSLS} mutant is observed to show a loss in its lipid binding abilities by 20% (Dove, Piper et al. 2004). Hence Atg18p^{SPSSLS} localization was also investigated under various test conditions (Figure 3.2.7).

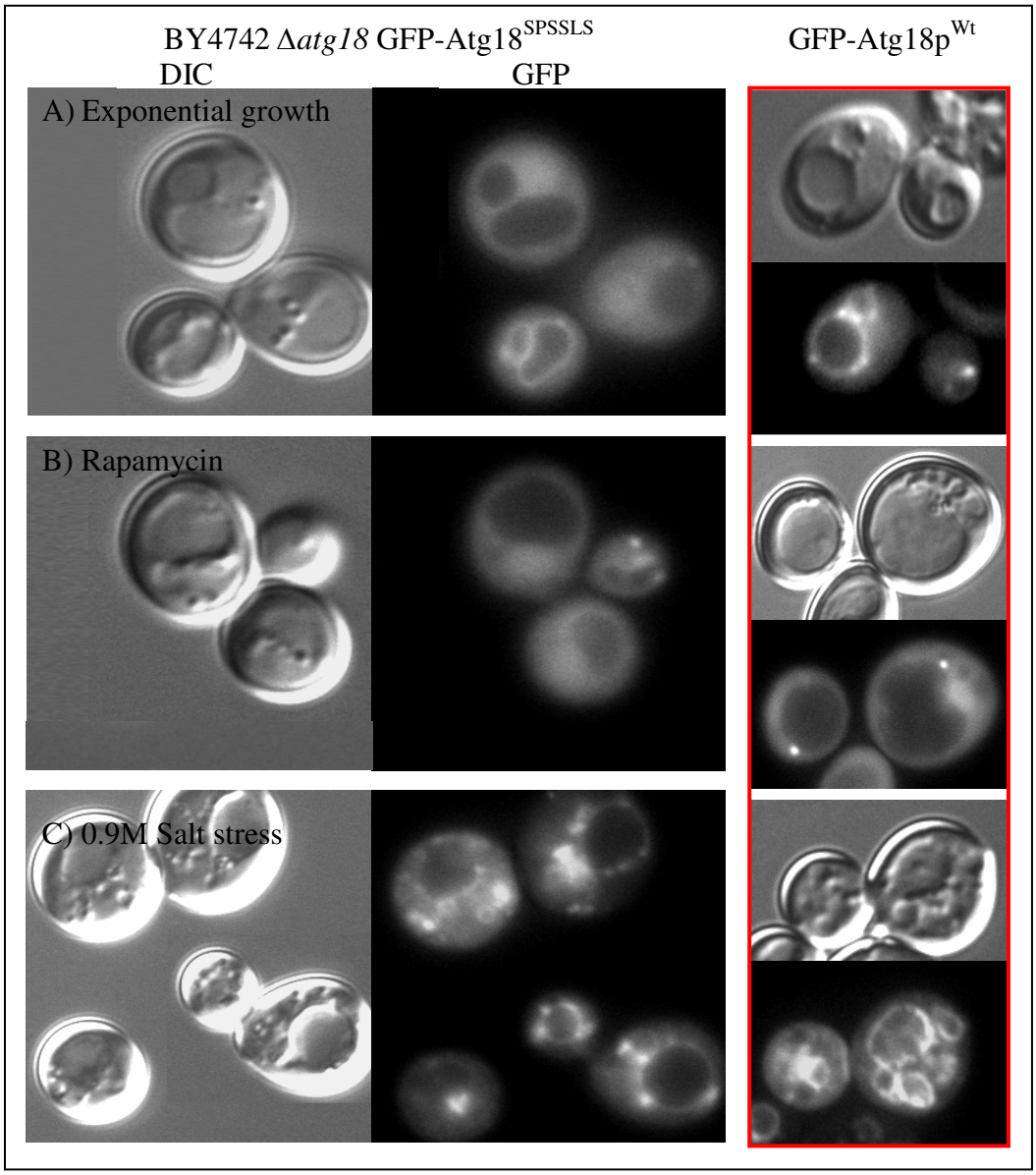

Figure 3.2.7: *In vivo* localization of GFP-Atg18p^{SPSSLS}.

pRS316-*ATG18*^{SPSSLS} was transformed into BY4742 *atg18*::KAN cells and grown overnight in Sc-Ura-Met + 2% glucose to an OD_{600} of 0.6. This cell culture was then divided into 3 fractions; Fraction A was suspended in SC-Ura-Met + 2 % Glucose, Fraction B was suspended in 1.7 % YNB + 2 % Glucose + 0.2 µg/ml Rapamycin and incubated at 25°C for 4 hours, whereas Fraction C was resuspended in 0.9M saline + SC-Ura-Meth +2% glucose. Fractions A and B were washed once with fresh media and then resuspended in MES buffer (pH 5.6). The cells were examined microscopically using GFP filter mounted on a Nikon Eclipse E600 and the images were processed using Photoshop. Photomicrographs in the left panel (highlighted by red) are only included as a reference to localization of Atg18p^{Wt} in Δ*atg18* cells, under specified conditions, but not to cell size.

Although most of the earlier reports on Atg18p^{SPSSLS} mutant infer their hypothesis based on its localization under exponential growth conditions, where its localization

is comparable to wild-type; it is quite obvious from this study that its localization under autophagy and salt stress are remarkably different. Atg18p^{SPSSLS} does not localize to the vacuole under salt stress and does not form the distinct punctae during autophagy, indicating that this motif does indeed play a crucial role in localization of Atg18p under osmotic shock and autophagy.

To further investigate the lipid binding of Atg18p, a number of PCR based point mutations were created in a region close to FRRG motif (the most highly conserved region) and were tagged with GFP and GST (Table 2.1); the GFP-tagged mutants were tested for their *in vivo* stability (Figure 3.2.8) and localization while the GST-tagged mutants were used for *in vitro* lipid binding analysis (Figure 3.2.9).

MUTANT	Amino-Acid Atg18p	Amino-Acid Mutant	Charge on A.A		Polarity of A.A	
			Atg18	Mutant	Atg18	Mutant
H244R	HIS	ARG	+	+	P	P
A263R	ALA	ARG	0	+	NP	P
K266T	LYS	THR	+	0	P	P
T268R	THR	ARG	0	+	P	P
R271T	ARG	THR	+	0	P	P
K280T	LYS	THR	+	0	P	P
Q283N	GLTM	ASP	0	0	P	P

Table 2.1: PCR based point mutations created in Atg18p.

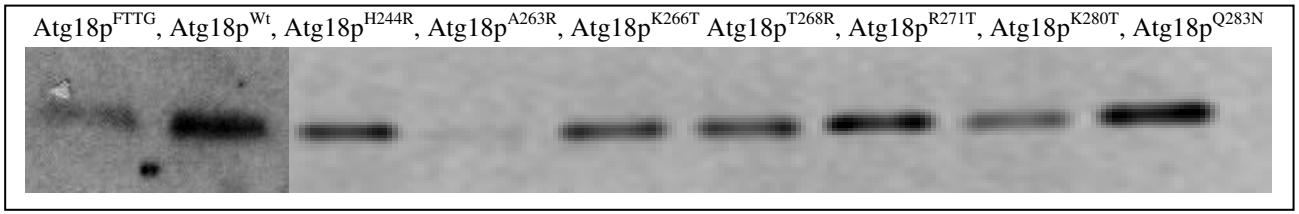

Figure 3.2.8: GFP stability blot of Atg18p (wild type and mutants).

Atg18p site specific mutants were GFP tagged in pUG36 expression vector and transformed into Δ*atg18* cells. All mutants were grown to an OD_{600nm} 0.6 and 3 ml of each culture was washed once with distilled water and then lysed through 0.1 M NaOH and the lysates used for SDS-PAGE. Anti GFP primary IgG was used to detect proteins in western blot.

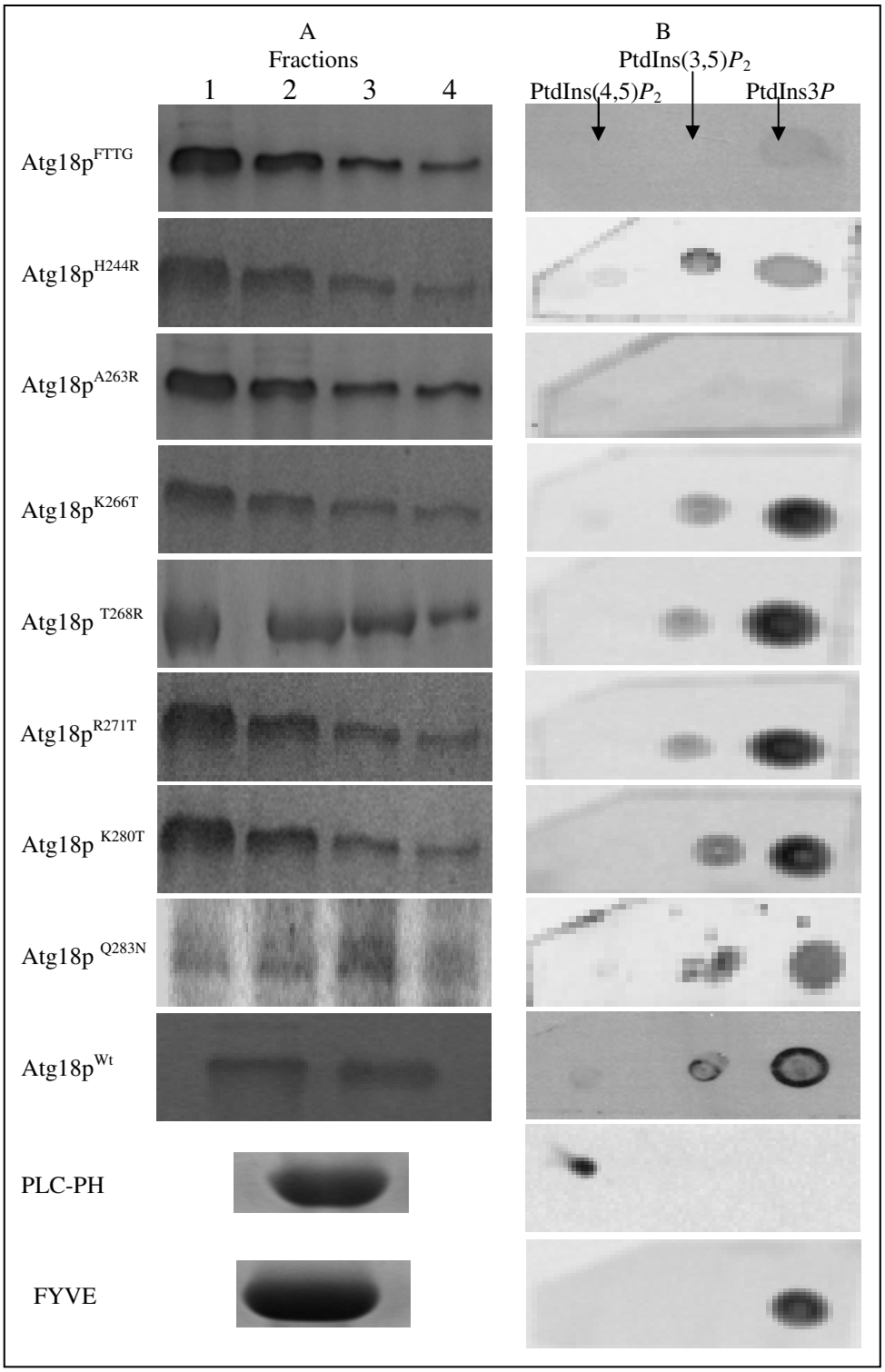

Figure 3.2.9: Fractions of Atg18p GST-tagged mutant proteins on SDS-PAGE and subsequent lipid dot blot assay.

(A) Atg18p mutants and wild type were expressed as GST-tagged proteins and resolved on SDS-PAGE (B) 3µl of each GST tagged Atg18p mutant protein was used for the *in vitro* lipid binding assay at pH 7.3 in TBST buffer.

The data in Figure 3.2.8 shows that the mutant proteins except Atg18p^{A263R} are stable, while the stability of Atg18p^{FTTG} is slightly decreased, as compared to wild type.

Figure 3.2.9 indicates that Atg18p^{A263R} loses lipid binding while Atg18p^{H244R} and Atg18p^{Q283N} may show decreased general binding; though as this *in vitro* assay is at best semi-quantitative, firmer conclusions would be unwise.

Therefore it becomes important to note the *in vivo* localization of all these mutants under various conditions (starting with Atg18p^{H244R}), which would be a much robust assay for Atg18p-lipid binding.

The localization of Atg18p^{H244R} mutant in Δ*atg18* cells, under various conditions (Figure 3.2.10).

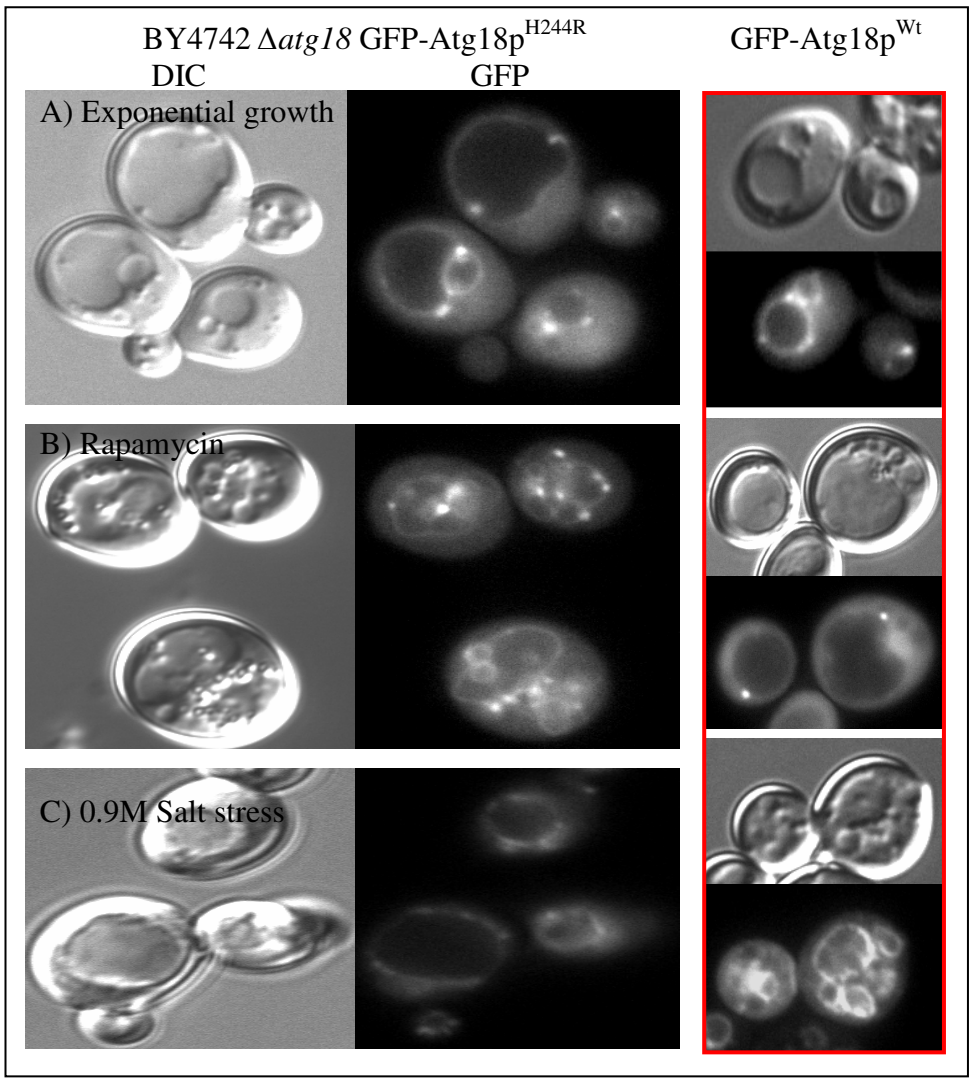

Figure 3.2.10: *In vivo* localization of GFP-Atg18p^{H244R}.

BY4742 *atg18::KAN* pUG36-*ATG18*^{H244R} cells were grown overnight in SC-Ura-Meth medium with 2% glucose to 0.6 OD_{600nm}. This cell culture was then split into 3 fractions. Fraction A was resuspended in MES buffer (pH 5.6) with 2% glucose, Fraction B was subjected to Nitrogen-starvation media with (0.2µg/ml) rapamycin and incubated at 25°C in the respective media for 4 hours. Fraction C was subjected to 0.9M salt stress. Fractions A and B were washed once in fresh media and resuspended in MES buffer pH 5.6 while Fraction C was visualized in saline using DIC and GFP fluorescence microscopy. The images were processed on Photoshop. Photomicrographs in the left panel (highlighted by red) are only included as a reference to localization of Atg18p^{Wt} in Δ*atg18* cells, under specified conditions, but not to cell size.

Although Atg18p^{H244R} mutant showed a substantial loss in *in vitro* lipid binding, yet it is punctae and only partially loses vacuolar localization indicating that its PtdIns(3,5)P_2 binding is much compromised. Hence it was important to establish the nature of these punctae since Atg18p punctae localization is associated with PtdIns3*P* binding.

GFP-Atg18p^{Wt} punctae co-localize with Snf7p, therefore GFP-Atg18p^{H244R} co-localization was investigated with RFP-Snf7p in order to verify if Atg18p^{H244R} punctae were similarly localized (Figure 3.2.11). In addition, the localization of this mutant was also investigated in Δ*vps34* cells (lacking both PtdIns3*P* and PtdIns(3,5)P_2) to check whether the localization is due to protein-protein interactions (Figure 3.2.12).

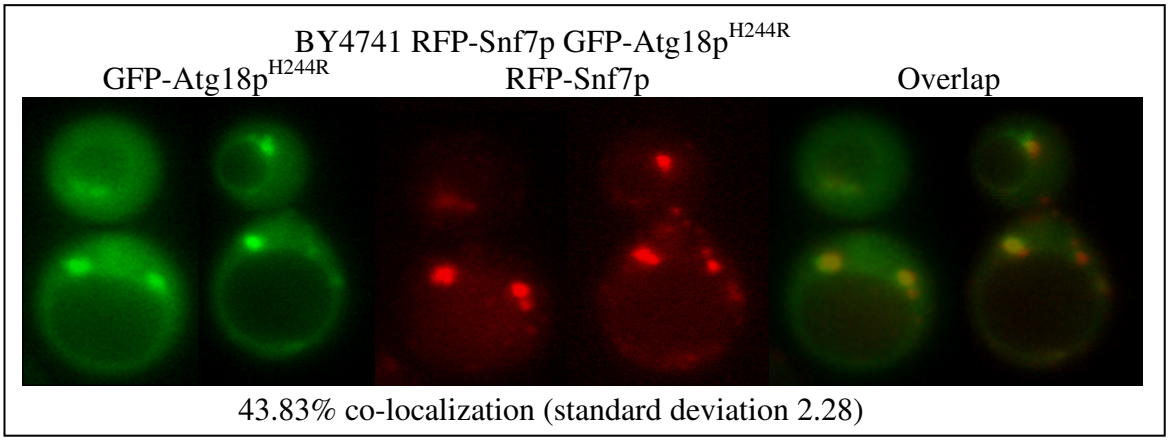

Figure 3.2.11: *In vivo* co-localization of Atg18p^{H244R} with RFP-Snf7p.

BY4741 *SNF7-RFP::KAN* pUG36-*ATG18*^{H244R} cells were grown overnight in SC-Ura-Meth medium with 2% glucose to 0.6 OD_{600nm}. This cell culture was then washed once in fresh media and resuspended in MES buffer pH 5.6 and visualized using RFP and GFP fluorescence microscopy. The images were processed on Photoshop.

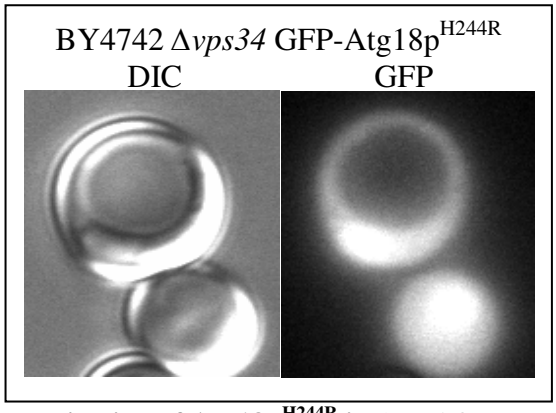

Figure 3.2.12: *In vivo* localization of Atg18p^{H244R} in Δ*vps34* cells.

BY4742 *vps34::KAN* pUG36-*ATG18*^{H244R} cells were grown overnight in SC-Ura-Meth medium with 2% glucose to 0.6 OD_{600nm}. The cells were washed once in fresh media and resuspended in MES buffer pH 5.6 and visualized using DIC and GFP fluorescence microscopy. The images were processed on Photoshop.

Atg18p^{H244R} punctae co-localize with Snf7p indicating that indeed Atg18p^{H244R} punctae are similar to Atg18p^{Wt} punctae; cytosolic localization of this mutant in Δ*vps34* cells (Figure 3.2.12) confirms that Atg18p punctae localization is PtdIns3*P* dependent as envisioned earlier.

The interaction of Atg18p^{H244R} with Vac7p appears normal as Atg18p^{H244R} is observed to localize to the vacuole membrane under autophagy conditions which is very similar to the localization of Atg18p^{Wt} observed in Δ*vac7* cells.

Therefore it now becomes quite important to note the localization of Atg18p^{H244R} in Δ*fab1* cells, in order to discriminate between Atg18p-PtdIns(3,5)P_2 dependent and Atg18p-PtdIns3*P* dependent localization? (Figure 3.2.13)

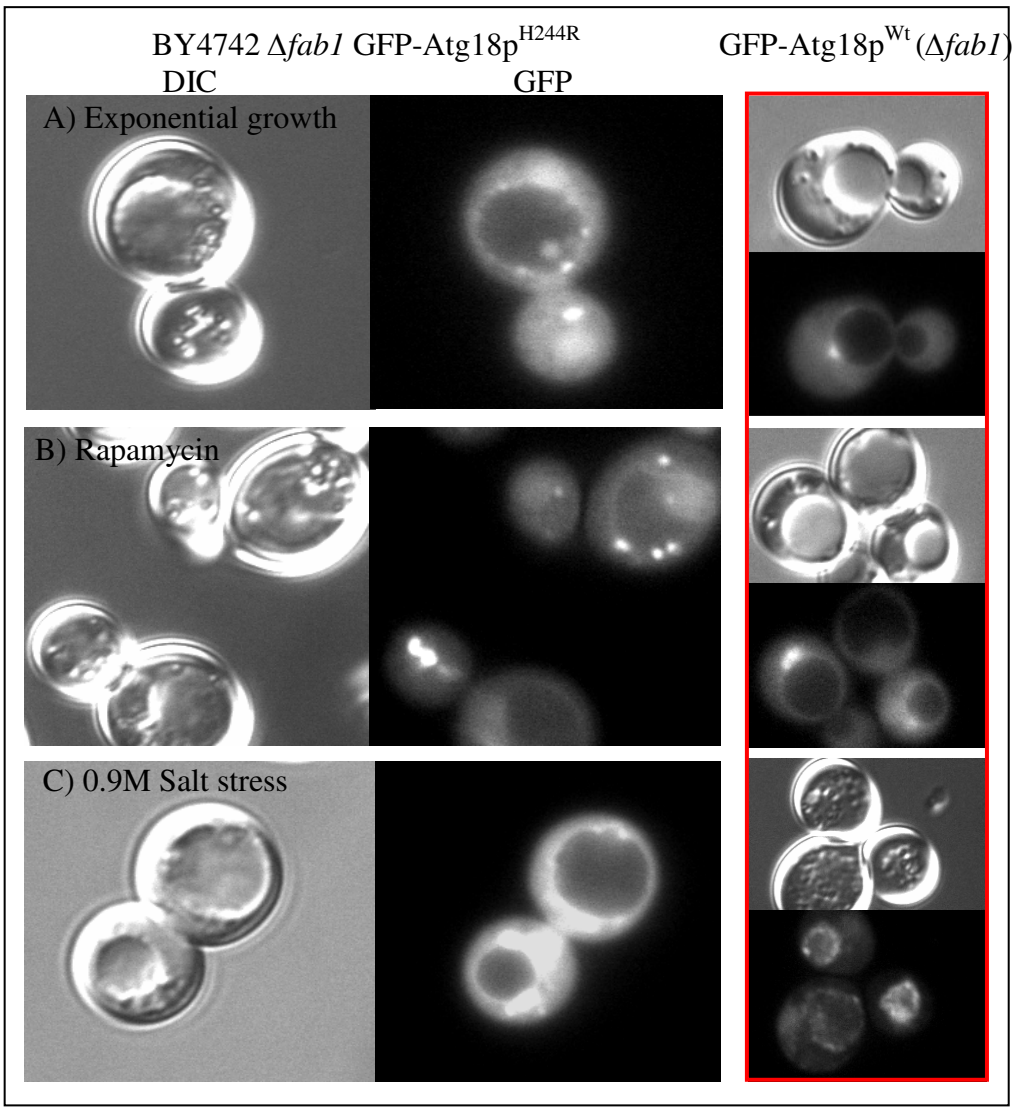

Figure 3.2.13: *In vivo* localization of GFP-Atg18p^{H244R} in Δ*fab1* cells.

BY4742 *fab1::KAN* pUG36-*ATG18*^{H244R} cells were grown overnight in SC-Ura-Meth medium with 2% glucose to 0.6 OD_{600nm}. This cell culture was then split into 3 fractions. Fraction A was resuspended in MES buffer (pH 5.6) with 2% glucose, Fraction B was subjected to Nitrogen-starvation media with (0.2µg/ml) rapamycin and incubated at 25°C in the respective media for 4 hours. Fraction C was subjected to 0.9M salt stress. Fractions A and B were washed once in fresh media and resuspended in MES buffer pH 5.6 while Fraction C was visualized in saline using DIC and GFP fluorescence microscopy. The images were processed on Photoshop. Photomicrographs in the left panel (highlighted by red) are only included as a reference to localization of Atg18p^{Wt} in Δ*fab1* cells, under specified conditions, but not to cell size.

Interestingly during autophagy, Atg18p^{H244R} loses its vacuolar localization in Δ*fab1* cells unlike in Δ*atg18* cells. This reinstates the finding that Atg18p punctae

localization under autophagy conditions depends on its interaction with PtdIns3*P*, and not Fab1p and/or PtdIns(3,5)P_2.

Atg18p^{H244R} partially localizes to the vacuole membrane in Δ*fab1* cells but fails to fragment the vacuole in a normal fashion.

Hence it becomes important to determine the nature of Atg18p^{H244R} punctae under exponential growth conditions in Δ*fab1* cells (Figure 3.2.14).

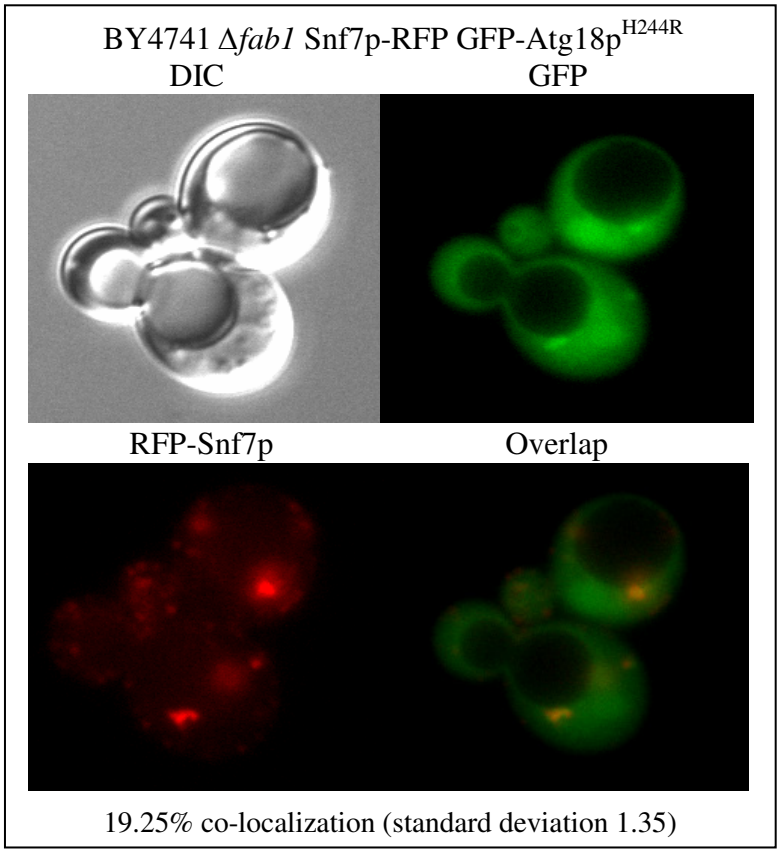

Figure 3.2.14: *In vivo* co-localization of GFP-Atg18p^{H244R} with RFP-Snf7p in Δ*fab1* cells.

BY4741 *SNF7-RFP::KAN* Δ*fab1::LEU2* pUG36-*ATG18*^{H244R} cells were grown overnight in SC-Ura-Meth-Leu medium with 2% glucose to 0.6 OD_{600nm}. The cell culture was washed once in fresh media and resuspended in MES buffer pH 5.6 and visualized using RFP and GFP fluorescence microscopy. The images were processed on Photoshop.

Figure 3.2.14 shows that Atg18p^{H244R} co-localize with RFP-Snf7p in Δ*fab1* cells, indicating that despite a significant increase in cytosolic localization, the punctae structures are indeed PVEs. The available data therefore suggests that Atg18p^{H244R} displays near normal PtdIns3*P* and Vac7p binding but possess compromised PtdIns(3,5)P_2 binding.

The localization of Atg18p^{A263R} mutant was investigated next (Figure 3.2.15).

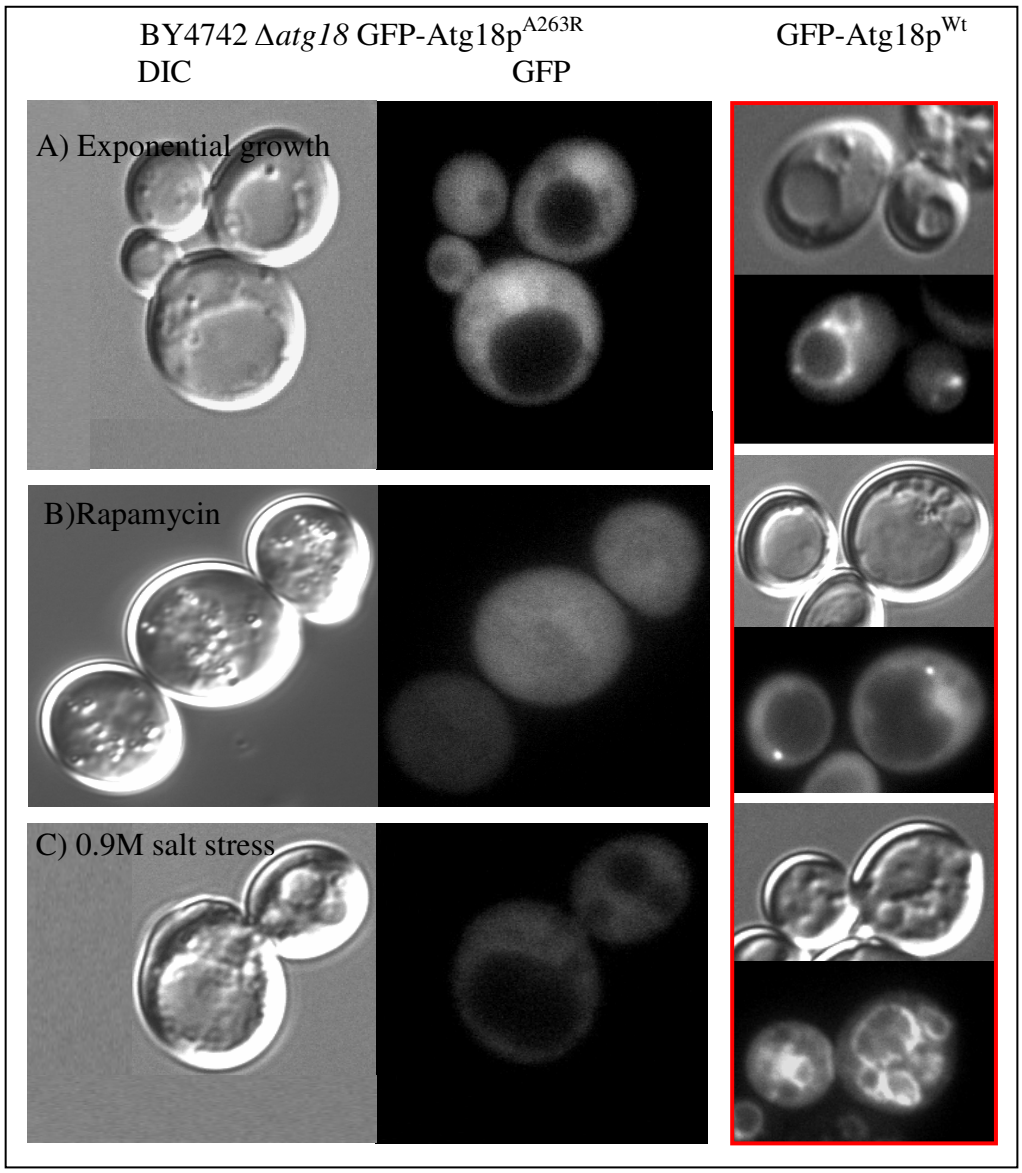

Figure 3.2.15: *In vivo* localization of GFP-Atg18p^{A263R}.

BY4742 *atg18::KAN* pUG36-*ATG18*^{A263R} cells were grown overnight in SC-Ura-Meth medium with 2% glucose to 0.6 OD_{600nm}. This cell culture was then split into 3 fractions. Fraction A was resuspended in MES buffer (pH 5.6) with 2% glucose, Fraction B was subjected to Nitrogen-starvation media with (0.2µg/ml) rapamycin and incubated at 25°C in the respective media for 4 hours. Fraction C was subjected to 0.9M salt stress. Fractions A and B were washed once in fresh media and resuspended in MES buffer pH 5.6 while Fraction C was visualized in saline using DIC and GFP fluorescence microscopy. The images were processed on Photoshop. Photomicrographs in the left panel (highlighted by red) are only included as a reference to localization of Atg18p^{Wt} in Δ*atg18* cells, under specified conditions, but not to cell size.

A loss of localization of Atg18p^{A263R} is possibly due to its instability hence its localization in any other mutant was not investigated.

The localization of Atg18p^{K266T} mutant was investigated next (Figure 3.2.16).

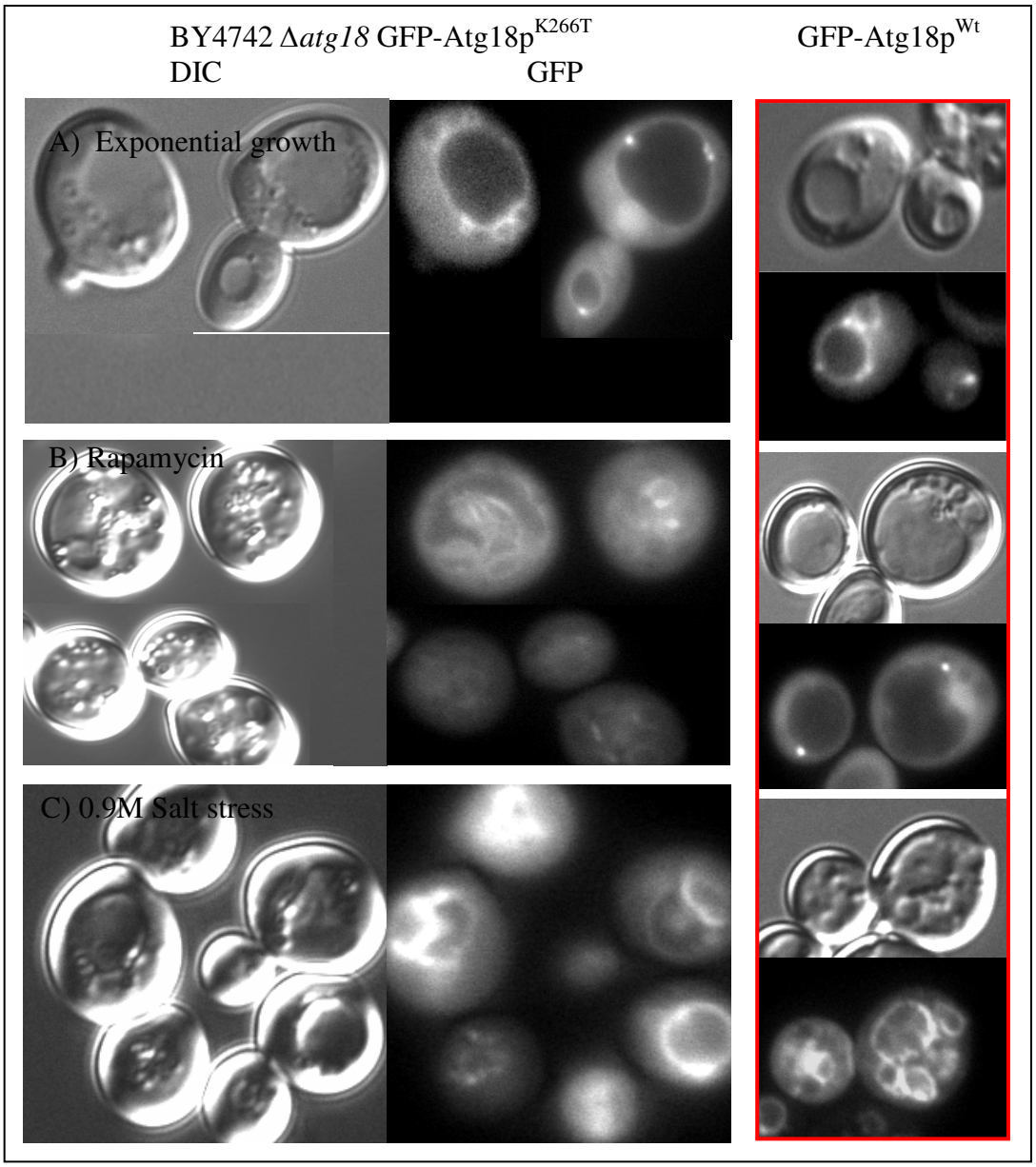

Figure 3.2.16: *In vivo* localization of GFP-Atg18p^{K266T}.

BY4742 *atg18::KAN* pUG36-*ATG18*^{K266T} cells were grown overnight in SC-Ura-Meth medium with 2% glucose to 0.6 OD_{600nm}. This cell culture was then split into 3 fractions. Fraction A was resuspended in MES buffer (pH 5.6) with 2% glucose, Fraction B was subjected to Nitrogen-starvation media with (0.2µg/ml) rapamycin and incubated at 25°C in the respective media for 4 hours. Fraction C was subjected to 0.9M salt stress. Fractions A and B were washed once in fresh media and resuspended in MES buffer pH 5.6 while Fraction C was visualized in saline using DIC and GFP fluorescence microscopy. The images were processed on Photoshop. Photomicrographs in the left panel (highlighted by red) are only included as a reference to localization of Atg18p^{Wt} in Δ*atg18* cells, under specified conditions, but not to cell size.

Figure 3.2.16 shows that Atg18p^{K266T} localizes to membranous structures which accumulate during autophagy, in contrast to the distinct punctae formation and enlargement of the vacuole observed in wild type.

Vacuole fragmentation and localization is observed to be normal under osmotic shock, but Atg18p^{K266T} loses its vacuolar localization quite significantly and becomes slightly nuclear, while retaining its punctae localization under exponential growth conditions. The identity of these Atg18p^{K266T} punctae was investigated through co-localization of GFP-Atg18p^{K266T} with various RFP-tagged organelle markers under exponential growth conditions (Figure 3.2.17).

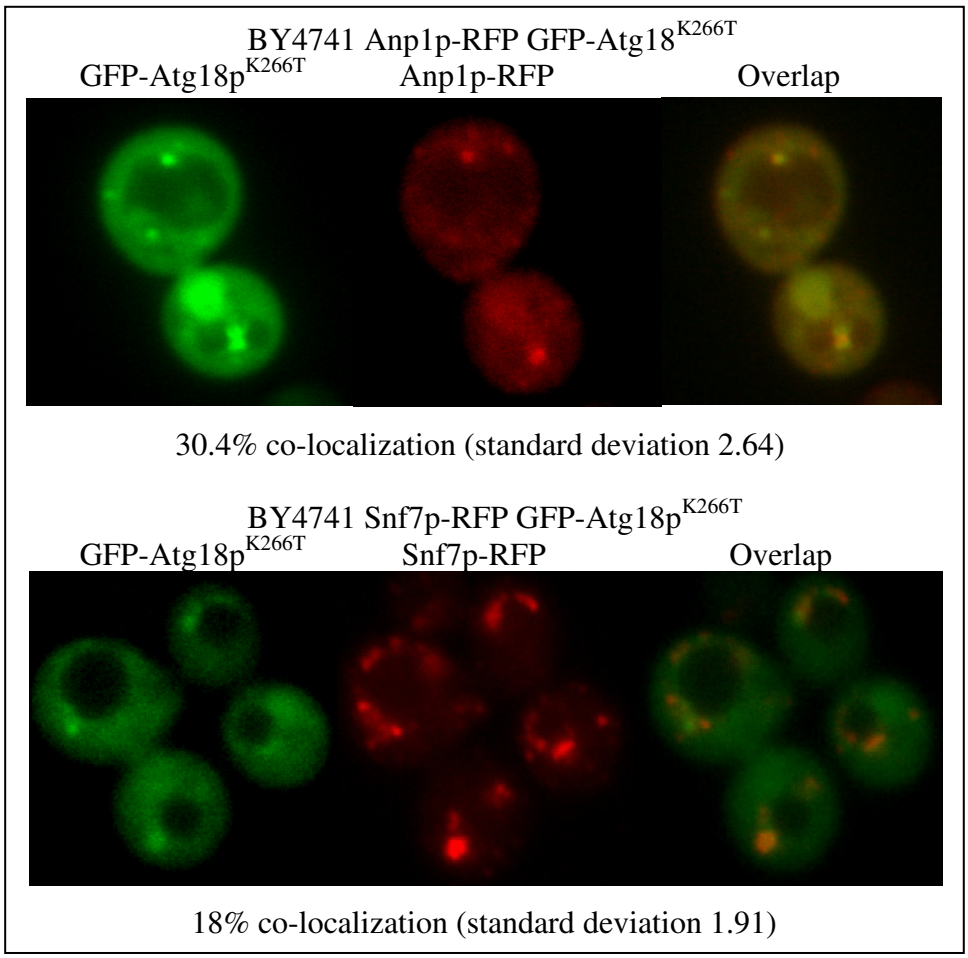

Figure 3.2.17: *In vivo* co-localization of Atg18p^{K266T} with RFP-Anp1p (TGN marker) and RFP-Snf7p (late endosome marker).

BY4741 *ANP1*-RFP::KAN pUG36-*ATG18*^{K266T} and BY4741 *SNF7*-RFP::KAN pUG36-*ATG18*^{K266T} cells were grown overnight in SC-Ura-Meth medium with 2% glucose to 0.6 OD_{600nm}. The cell culture was washed once in fresh media and resuspended in MES buffer pH 5.6 and visualized using RFP and GFP fluorescence microscopy. The images were processed on Photoshop.

Figure 3.2.17 shows that Atg18p^{K266T} punctae besides being localized to PVEs, are also much enriched on TGN. The TGN localization suggests that this mutant is failing to disengage from one of the membrane proteins with which it normally associates and is being recycled back to TGN; possibly via a Vac7p-Atg18p^{K266T} interaction? Nonetheless it indicates that K266 residue plays a crucial role in disassociation of Atg18p from membranes.

In order to determine whether PtdIns(3,5)P_2 binding plays any significant role in Atg18p^{K266T} localization, its *in vivo* localization was studied in Δ*fab1* cells (Figure 3.2.18).

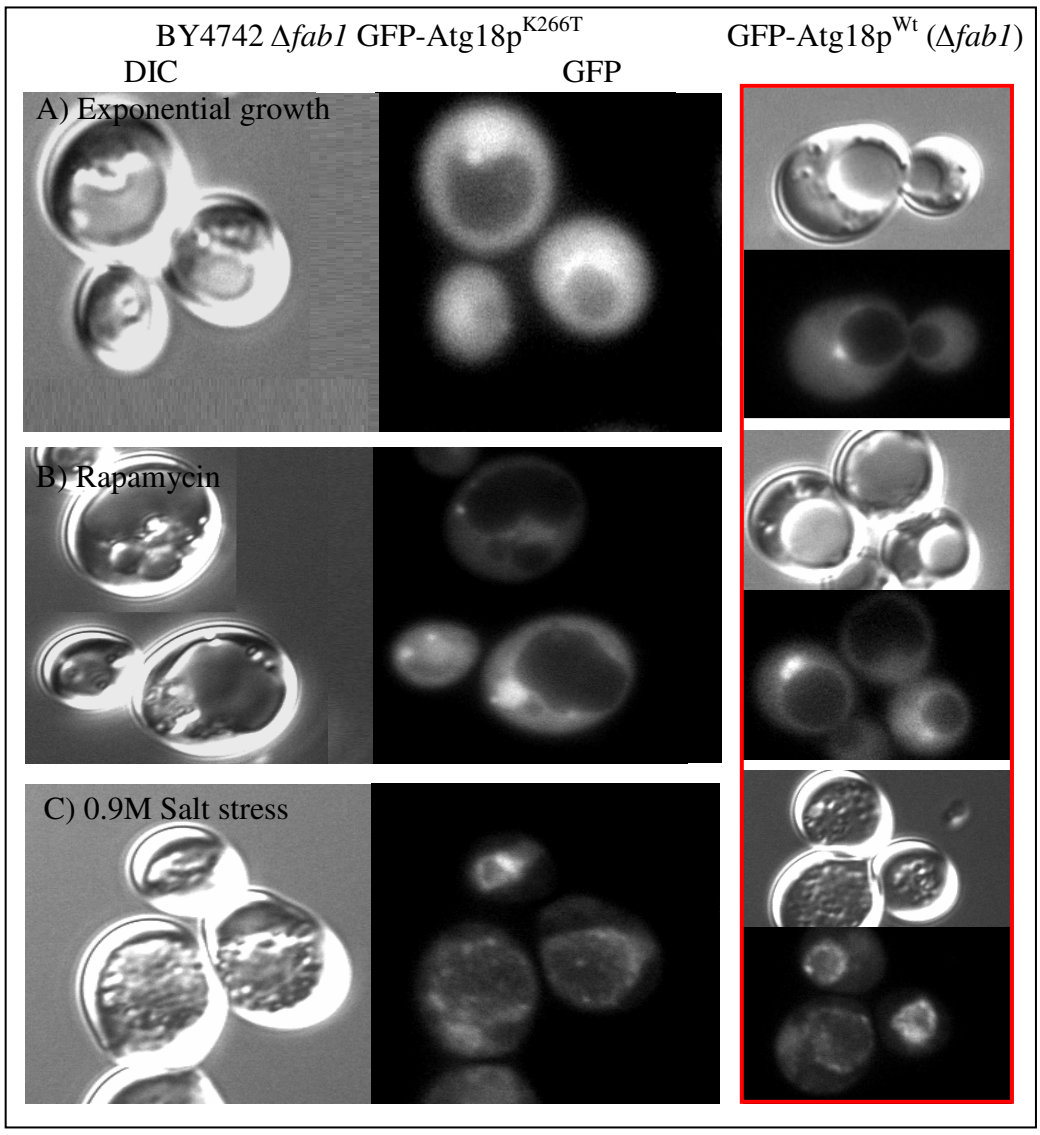

Figure 3.2.18: *In vivo* localization of GFP-Atg18p^{K266T} in Δ*fab1* cells.

BY4742 *fab1::KAN* pUG36-*ATG18*^{K266T} cells were grown overnight in SC-Ura-Meth medium with 2% glucose to 0.6 OD_{600nm}. This cell culture was then split into 3 fractions. Fraction A was resuspended in MES buffer (pH 5.6) with 2% glucose, Fraction B was subjected to Nitrogen-starvation media with (0.2µg/ml) rapamycin and incubated at 25°C in the respective media for 4 hours. Fraction C was subjected to 0.9M salt stress. Fractions A and B were washed once in fresh media and resuspended in MES buffer pH 5.6 while Fraction C was visualized in saline using DIC and GFP fluorescence microscopy. The images were processed on Photoshop. Photomicrographs in the left panel (highlighted by red) are only included as a reference to localization of Atg18p^{Wt} in Δ*fab1* cells, under specified conditions, but not to cell size.

Although Atg18p^{K266T} is cytosolic and punctae in Δ*atg18* cells, the punctae localization is lost in Δ*fab1* cells (Figure 3.2.18), indicating yet again that besides the vacuolar localization, the punctae localization is also affected by PtdIns(3,5)P_2 levels. It is also observed that Atg18p^{K266T} forms a few punctae under autophagy conditions and the accumulation of membranous structures (as in Δ*atg18* cells) is abolished.

During salt stress the mutant localizes to the vacuole indicating that either this mutant is recruited to the vacuole via protein interaction/s or more likely it is behaving in a similar manner as Atg18p^{Wt} in Δ*fab1* cells under similar conditions. Localization of mutant Atg18p^{T268R} was investigated next (Figure 3.2.19).

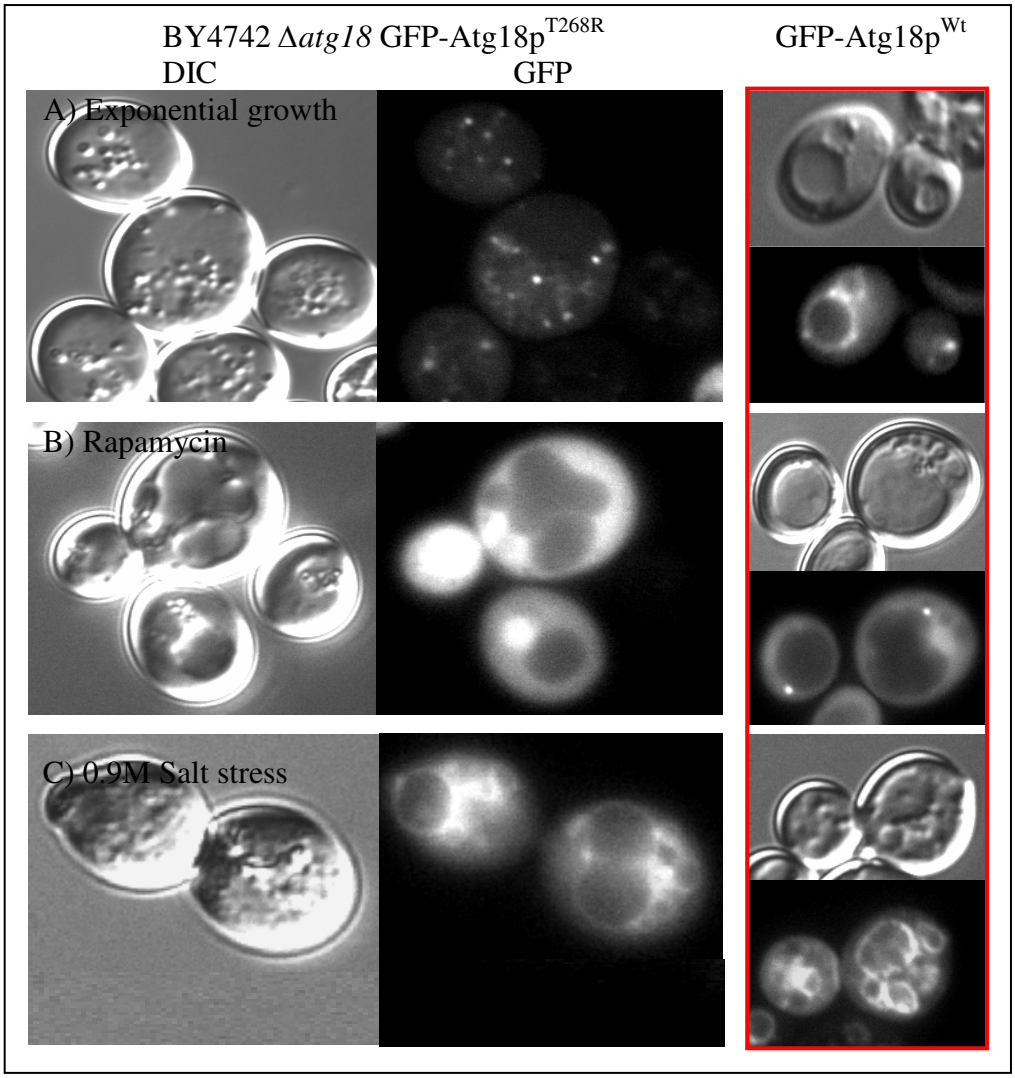

Figure 3.2.19: *In vivo* localization of GFP-Atg18p^{T268R}.

BY4742 *atg18::KAN* pUG36-*ATG18*^{T268R} cells were grown overnight in SC-Ura-Meth medium with 2% glucose to 0.6 OD_{600nm}. This cell culture was then split into 3 fractions. Fraction A was resuspended in MES buffer (pH 5.6) with 2% glucose, Fraction B was subjected to Nitrogen-starvation media with (0.2µg/ml) rapamycin and incubated at 25°C in the respective media for 4 hours. Fraction C was subjected to 0.9M salt stress. Fractions A and B were washed once in fresh media and resuspended in MES buffer pH 5.6 while Fraction C was visualized in saline using DIC and GFP fluorescence microscopy. The images were processed on Photoshop. Photomicrographs in the left panel (highlighted by red) are only included as a reference to localization of Atg18p^{Wt} in Δ*atg18* cells, under specified conditions, but not to cell size.

Figure 3.2.19 shows that Atg18p^{T268R} forms punctae structures under exponential growth conditions, whereas the localization of this mutant under osmotic shock and consequent vacuole fragmentation are similar to Atg18p^{Wt}. Interestingly, under autophagy conditions Atg18p^{T268R} becomes completely cytosolic unlike wild type, which indicates a putative disruption of its interactions with other proteins during autophagy.

The localization of Atg18p^{T268R} was further investigated in Δ*fab1* cells (Figure 3.2.20).

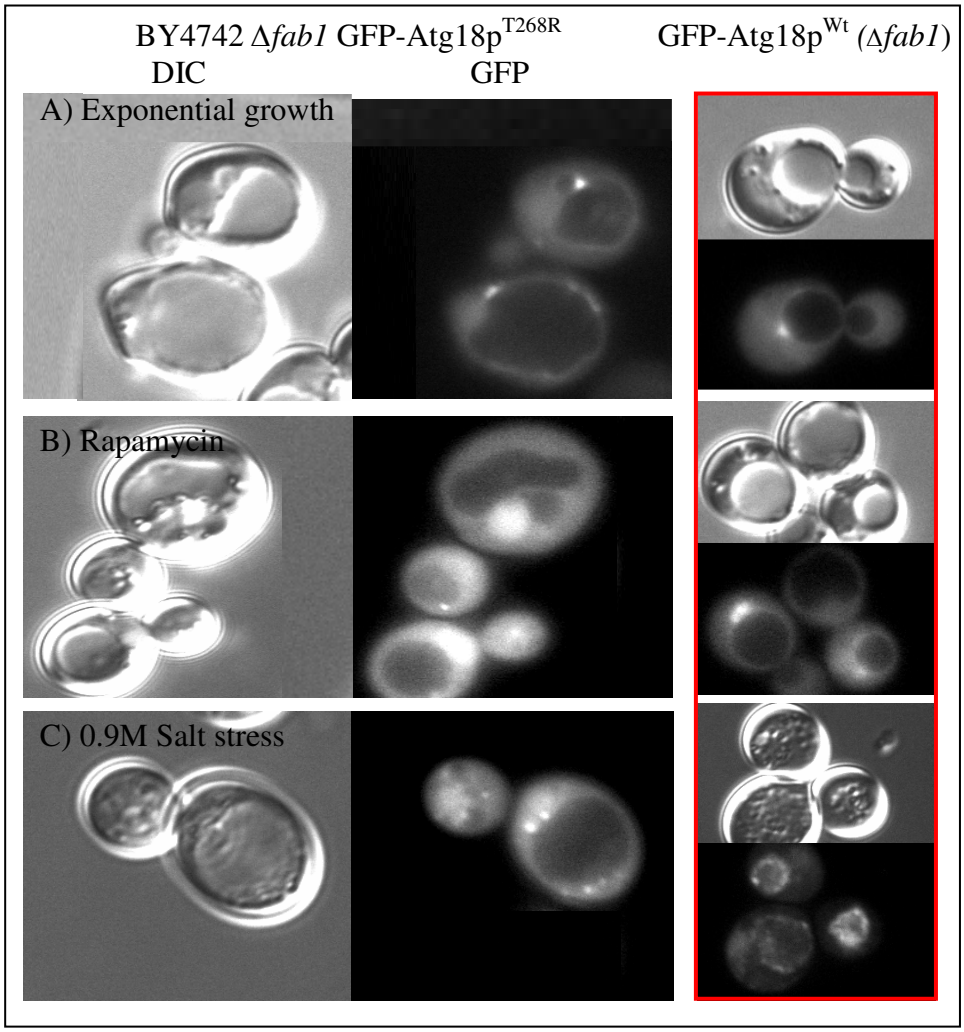

Figure 3.2.20: *In vivo* localization of GFP-Atg18p^{T268R} in Δ*fab1* cells.

BY4742 *fab1::KAN* pUG36-*ATG18*^{T268R} cells were grown overnight in SC-Ura-Meth medium with 2% glucose to 0.6 OD_{600nm}. This cell culture was then split into 3 fractions. Fraction A was resuspended in MES buffer (pH 5.6) with 2% glucose, Fraction B was subjected to Nitrogen-starvation media with (0.2µg/ml) rapamycin and incubated at 25°C in the respective media for 4 hours. Fraction C was subjected to 0.9M salt stress. Fractions A and B were washed once in fresh media and resuspended in MES buffer pH 5.6 while Fraction C was visualized in saline using DIC and GFP fluorescence microscopy. The images were processed on Photoshop. Photomicrographs in the left panel (highlighted by red) are only included as a reference to localization of Atg18p^{Wt} in Δ*fab1* cells, under specified conditions, but not to cell size.

The phenotype exhibited by Atg18p^{T268R} in Δ*fab1* cells is very similar to the one it exhibits in Δ*atg18* cells, therefore it could be reasoned that its behavior is largely unaffected by PtdIns(3,5)P_2 levels.

Another mutant, Atg18p^{R271T} was investigated subsequently for its *in vivo* localization (Figure 3.2.21).

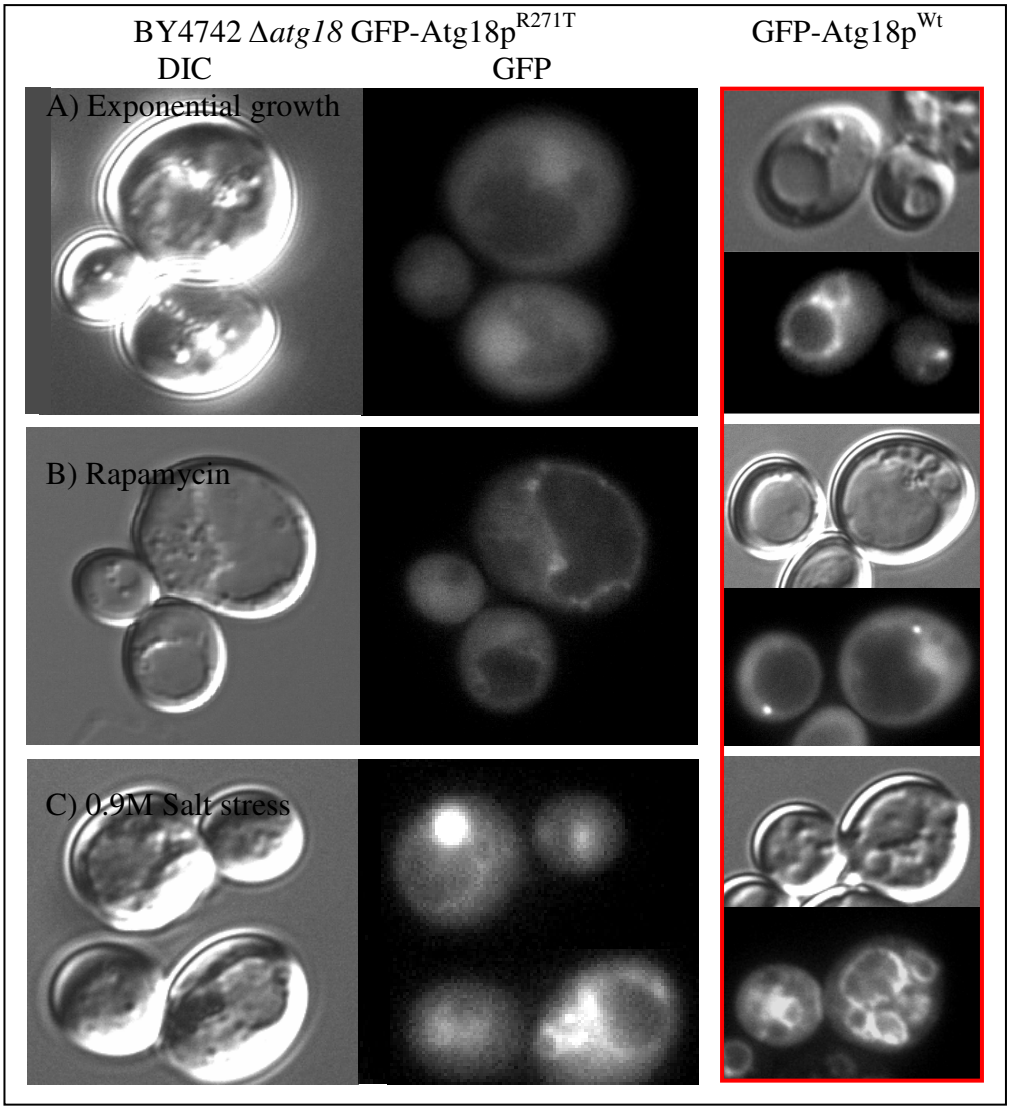

Figure 3.2.21: *In vivo* localization of GFP-Atg18p^{R271T}.

BY4742 *atg18::KAN* pUG36-*ATG18*^{R271T} cells were grown overnight in SC-Ura-Meth medium with 2% glucose to 0.6 OD_{600nm}. This cell culture was then split into 3 fractions. Fraction A was resuspended in MES buffer (pH 5.6) with 2% glucose, Fraction B was subjected to Nitrogen-starvation media with (0.2µg/ml) rapamycin and incubated at 25°C in the respective media for 4 hours. Fraction C was subjected to 0.9M salt stress. Fractions A and B were washed once in fresh media and resuspended in MES buffer pH 5.6 while Fraction C was visualized in saline using DIC and GFP fluorescence microscopy. The images were processed on Photoshop. Photomicrographs in the left panel (highlighted by red) are only included as a reference to localization of Atg18p^{Wt} in Δ*atg18* cells, under specified conditions, but not to cell size.

Figure 3.2.21 shows that Atg18p^{R271T} is mostly cytosolic under exponential growth conditions and slightly vacuolar under autophagy conditions, whereas the response and localization during osmotic shock is slightly defective.

Hence it was important to investigate the localization of this mutant in Δ*fab1* cells in order to check whether PtdIns(3,5)P_2 plays any role in its localization? (Figure 3.2.22 A/B)

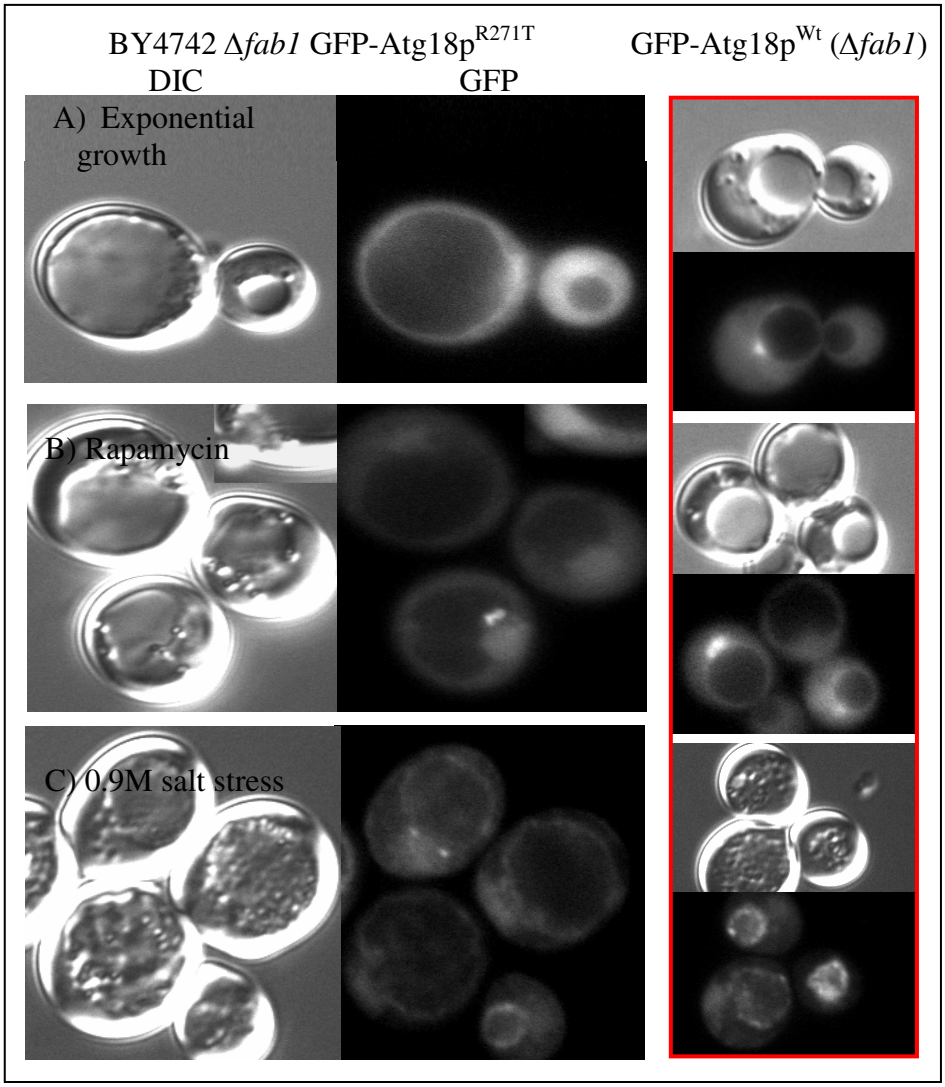

Figure 3.2.22 A: *In vivo* localization of Atg18p^{R271T} in Δ*fab1* cells.

BY4742 *fab1::KAN* pUG36-*ATG18*^{R271T} cells were grown overnight in SC-Ura-Meth medium with 2% glucose to 0.6 OD_{600nm}. This cell culture was then split into 3 fractions. Fraction A was resuspended in MES buffer (pH 5.6) with 2% glucose, Fraction B was subjected to Nitrogen-starvation media with (0.2µg/ml) rapamycin and incubated at 25°C in the respective media for 4 hours. Fraction C was subjected to 0.9M salt stress. Fractions A and B were washed once in fresh media and resuspended in MES buffer pH 5.6 while Fraction C was visualized in saline using DIC and GFP fluorescence microscopy. The images were processed on Photoshop. Photomicrographs in the left panel (highlighted by red) are only included as a reference to localization of Atg18p^{Wt} in Δ*fab1* cells, under specified conditions, but not to cell size.

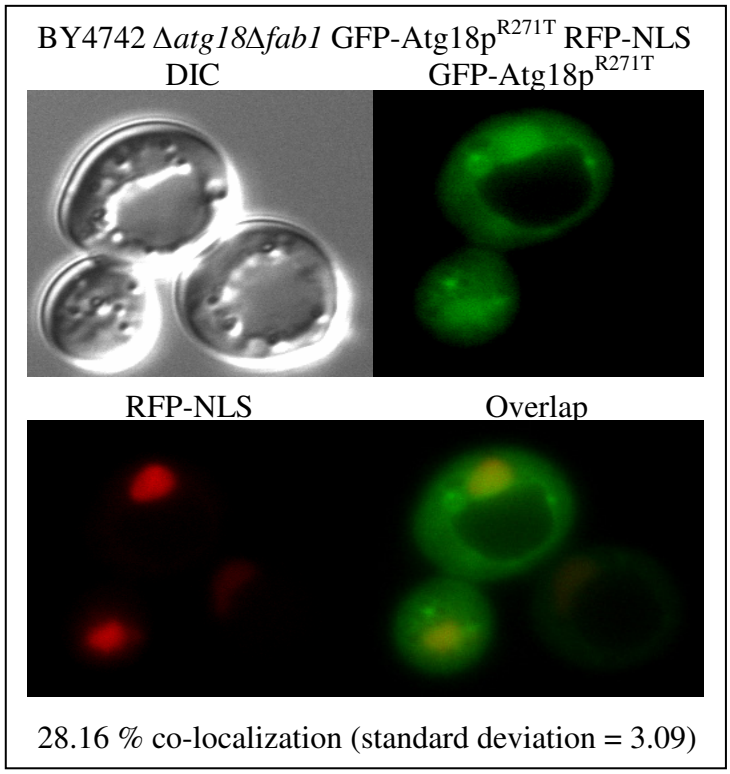

Figure 3.2.22 B: *In vivo* co-localization of GFP-Atg18p^{R271T} with RFP-NLS

BY4742 *fab1::KAN* pUG36-*ATG18*^{R271T} pUR34-NLS cells were grown overnight in SC-Ura-Meth-His medium with 2% glucose to 0.6 OD_{600nm}. The cell culture was washed once in fresh media and resuspended in MES buffer pH 5.6 and visualized using DIC and GFP fluorescence microscopy. The images were processed on Photoshop.

Figure 3.2.22A/B shows that the localization of Atg18p^{R271T} in Δ*fab1* cells is very similar to the one in Δ*atg18* cells under tested conditions, indicating that this mutant behaves in a similar fashion regardless of lipid binding, although an interesting observation is that this mutant also shows some nuclear localization in Δ*fab1* cells. Mutant Atg18p^{K280T} localization under various conditions was investigated next which is represented in Figure 3.2.23.

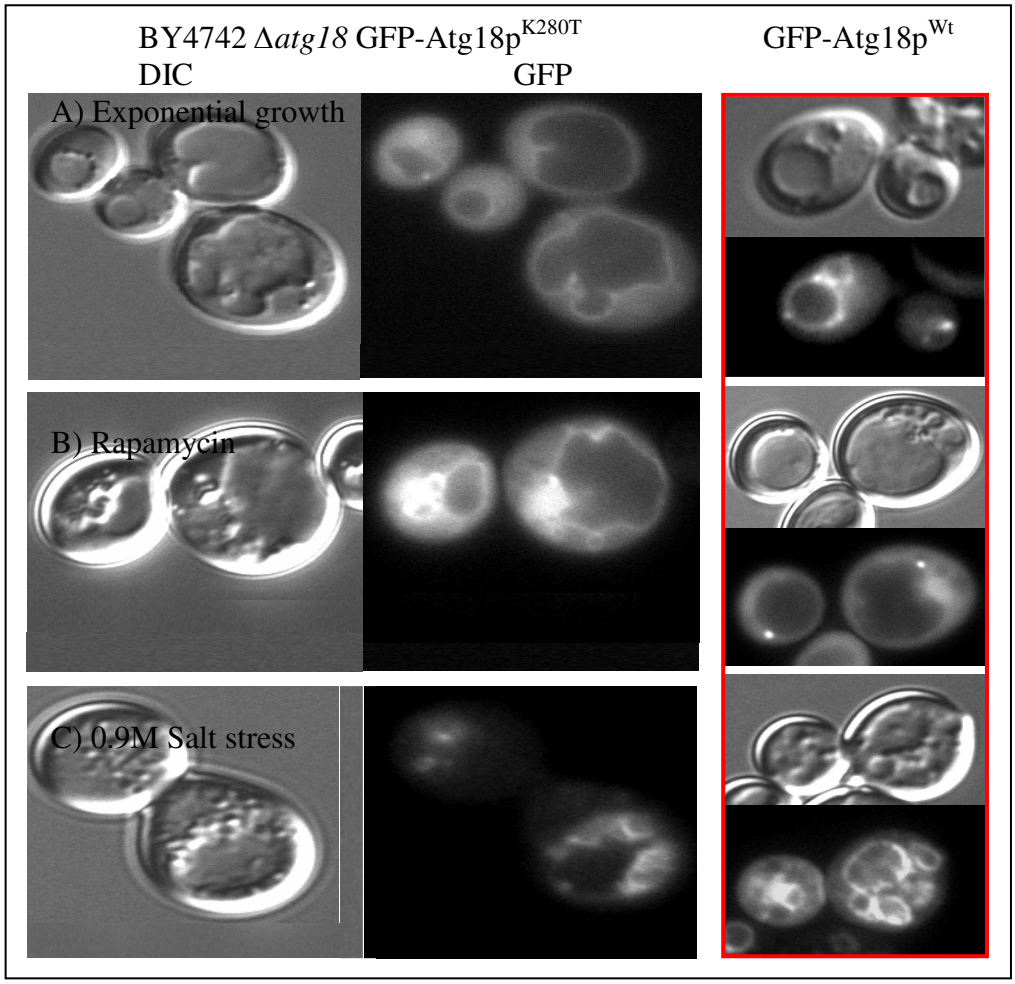

Figure 3.2.23: *In vivo* localization of GFP-Atg18p^{K280T}.

BY4742 *atg18::KAN* pUG36-*ATG18*^{K280T} cells were grown overnight in SC-Ura-Meth medium with 2% glucose to 0.6 OD_{600nm}. This cell culture was then split into 3 fractions. Fraction A was resuspended in MES buffer (pH 5.6) with 2% glucose, Fraction B was subjected to Nitrogen-starvation media with (0.2µg/ml) rapamycin and incubated at 25°C in the respective media for 4 hours. Fraction C was subjected to 0.9M salt stress. Fractions A and B were washed once in fresh media and resuspended in MES buffer pH 5.6 while Fraction C was visualized in saline using DIC and GFP fluorescence microscopy. The images were processed on Photoshop. Photomicrographs in the left panel (highlighted by red) are only included as a reference to localization of Atg18p^{Wt} in Δ*atg18* cells, under specified conditions, but not to cell size.

Figure 3.2.23 shows that Atg18p^{K280T} is vacuolar under exponential growth and autophagy conditions, which is unlike Atg18p^{Wt}, but this mutant behaves like wild type under osmotic shock. Therefore it was important to note the localization of this mutant in Δ*fab1* cells Figure 3.2.24 A/B).

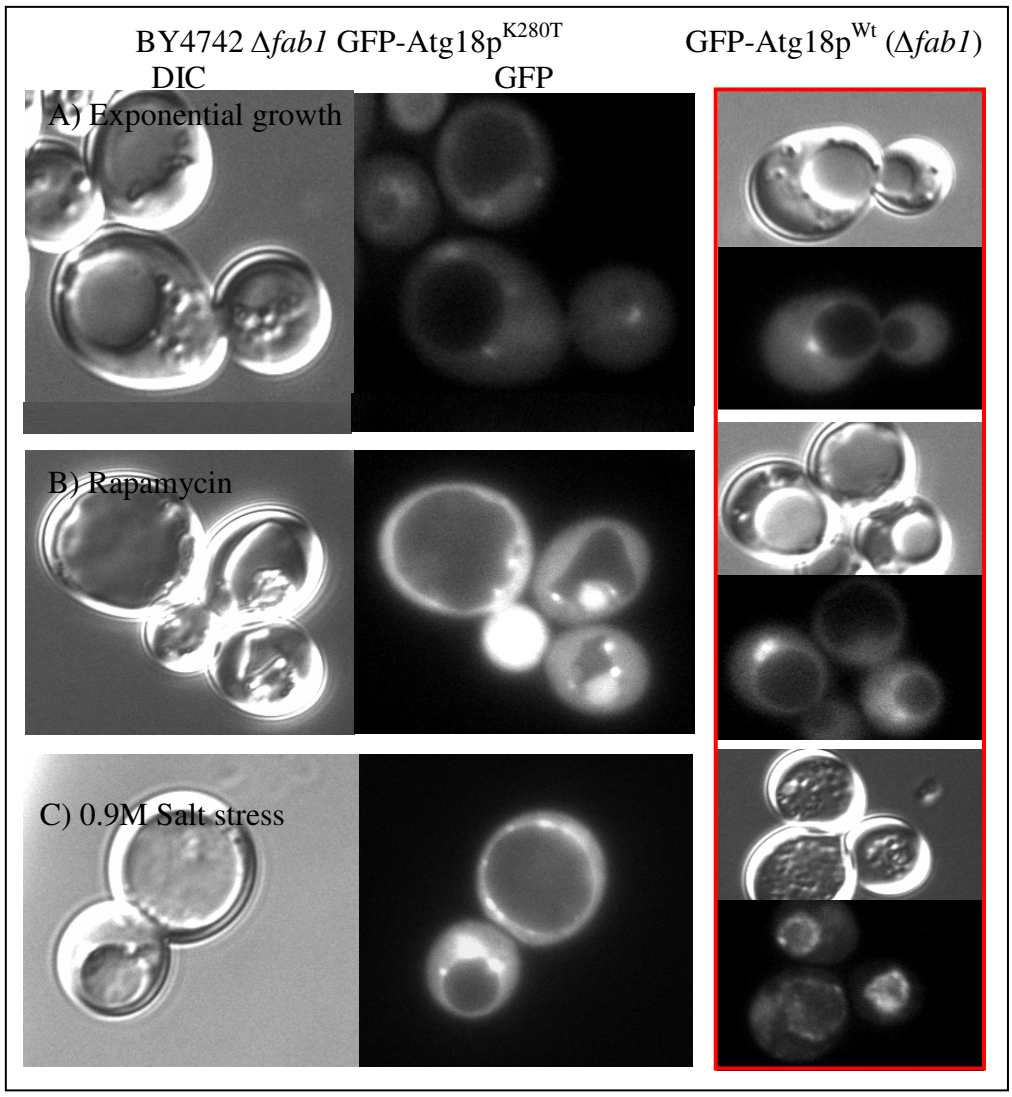

Figure 3.2.24A: *In vivo* localization of GFP-Atg18p^{K280T} in Δ*fab1* cells.

BY4742 *fab1::KAN* pUG36-*ATG18*^{K280T} cells were grown overnight in SC-Ura-Meth medium with 2% glucose to 0.6 OD_{600nm}. This cell culture was then split into 3 fractions. Fraction A was resuspended in MES buffer (pH 5.6) with 2% glucose, Fraction B was subjected to Nitrogen-starvation media with (0.2µg/ml) rapamycin and incubated at 25°C in the respective media for 4 hours. Fraction C was subjected to 0.9M salt stress. Fractions A and B were washed once in fresh media and resuspended in MES buffer pH 5.6 while Fraction C was visualized in saline using DIC and GFP fluorescence microscopy. The images were processed on Photoshop. Photomicrographs in the left panel (highlighted by red) are only included as a reference to localization of Atg18p^{Wt} in Δ*fab1* cells, under specified conditions, but not to cell size.

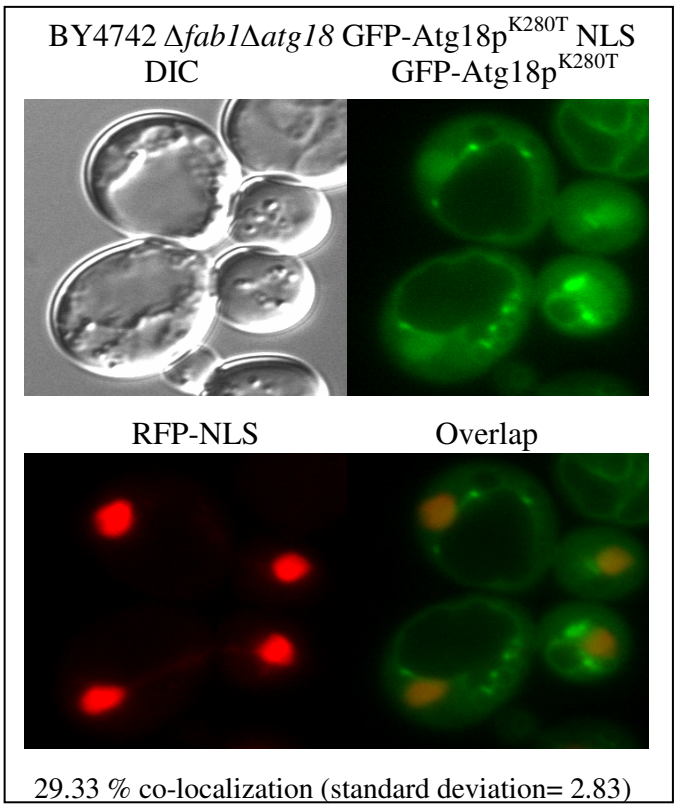

Figure 3.2.24B: *In vivo* co-localization of GFP-Atg18p^{K280T} with RFP-NLS in Δ*fab1* cells.

BY4742 *atg18::KAN fab1::LEU2* pUG36-ATG18^{H244R} pUR34-NLS cells were grown overnight in SC-Ura-Meth-Leu-His medium with 2% glucose to 0.6 OD_{600nm}. The cell culture was washed once in fresh media and resuspended in MES buffer pH 5.6 and was visualized using RFP and GFP fluorescence microscopy. The images were processed on Photoshop.

Figure 3.2.24A shows that this mutant loses its vacuolar localization under exponential growth and autophagy conditions in Δ*fab1* cells, unlike its behavior in Δ*atg18* cells, suggesting that PtdIns(3,5)P_2 binding plays a role in vacuolar localization of this mutant. Nonetheless, the behavior of this mutant under osmotic shock is comparable to wild type. Interestingly, this mutant also localizes to the nucleus in a similar fashion as Atg18p^{R271T} in Δ*fab1* cells (Figure 3.2.24B).

Lastly, localization of mutant Atg18p^{Q283N} was studied *in vivo* (Figure 3.2.25).

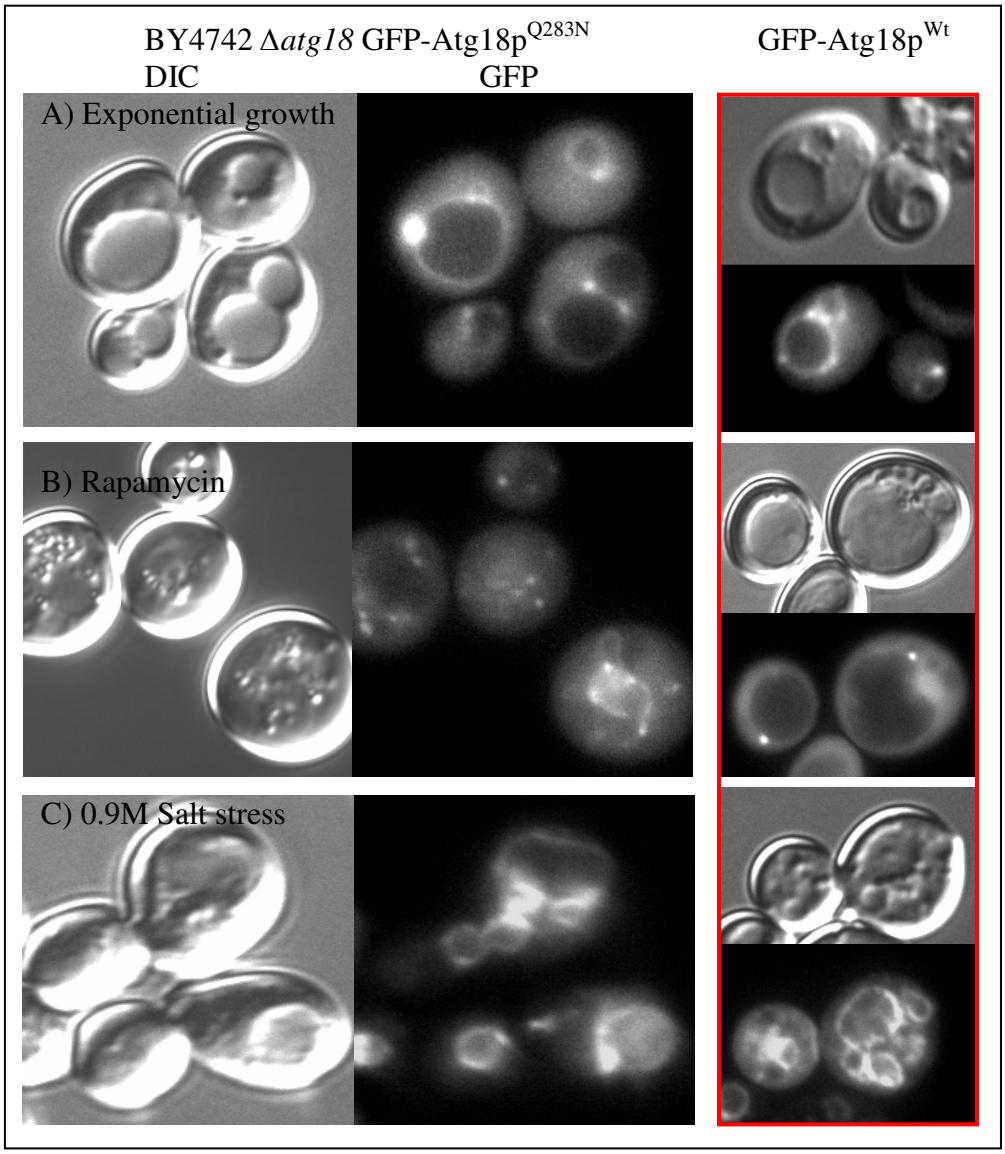

Figure 3.2.25: *In vivo* localization of GFP-Atg18p^{Q283N}.

BY4742 *atg18::KAN* pUG36-*ATG18*^{Q283N} cells were grown overnight in SC-Ura-Meth medium with 2% glucose to 0.6 OD_{600nm}. This cell culture was then split into 3 fractions. Fraction A was resuspended in MES buffer (pH 5.6) with 2% glucose, Fraction B was subjected to Nitrogen-starvation media with (0.2µg/ml) rapamycin and incubated at 25°C in the respective media for 4 hours. Fraction C was subjected to 0.9M salt stress. Fractions A and B were washed once in fresh media and resuspended in MES buffer pH 5.6 while Fraction C was visualized in saline using DIC and GFP fluorescence microscopy. The images were processed on Photoshop. Photomicrographs in the left panel (highlighted by red) are only included as a reference to localization of Atg18p^{Wt} in Δ*atg18* cells, under specified conditions, but not to cell size.

Figure 3.2.25 shows that although Atg18p^{Q283N} loses its vacuolar localization under exponential growth conditions yet its localization under autophagy and salt stress conditions is very similar to wild type. Therefore in order to check whether PtdIns(3,5)P_2 binding plays a significant role in its *in vivo* localization, the phenotype exhibited by this mutant in Δ*fab1* cells was investigated (Figure 3.2.26).

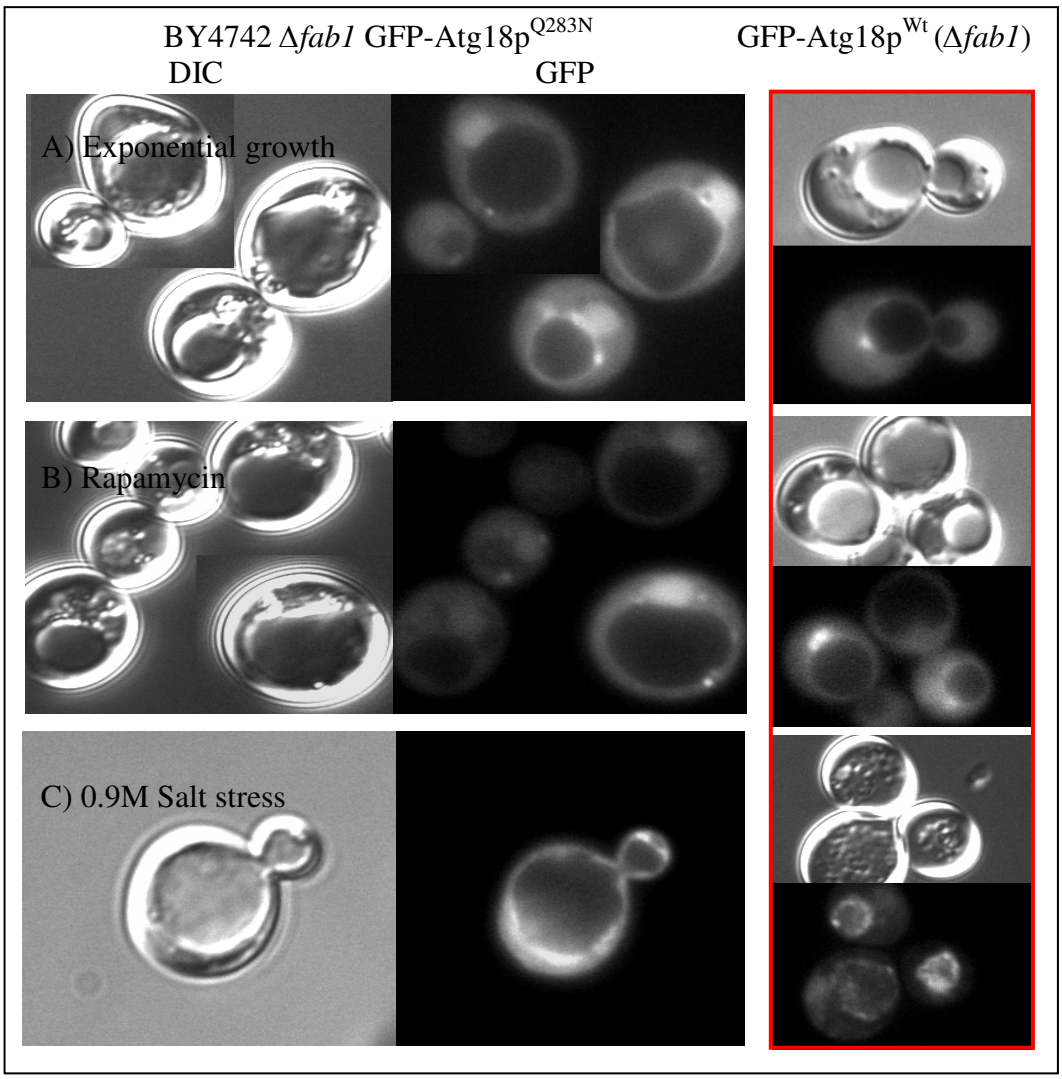

Figure 3.2.26: *In vivo* localization of GFP-Atg18p^{Q283N} in Δ*fab1* cells.

BY4742 *fab1::KAN* pUG36-*ATG18*^{Q283N} cells were grown overnight in SC-Ura-Meth medium with 2% glucose to 0.6 OD_{600nm}. This cell culture was then split into 3 fractions. Fraction A was resuspended in MES buffer (pH 5.6) with 2% glucose, Fraction B was subjected to Nitrogen-starvation media with (0.2µg/ml) rapamycin and incubated at 25°C in the respective media for 4 hours. Fraction C was subjected to 0.9M salt stress. Fractions A and B were washed once in fresh media and resuspended in MES buffer pH 5.6 while Fraction C was visualized in saline using DIC and GFP fluorescence microscopy. The images were processed on Photoshop. Photomicrographs in the left panel (highlighted by red) are only included as a reference to localization of Atg18p^{Wt} in Δ*fab1* cells, under specified conditions, but not to cell size.

Figure 3.2.26 shows that Atg18p^{Q283N} does not lose its punctae localization under exponential growth and autophagy conditions in Δ*fab1* cells. Atg18p^{Q283N} localization in response to osmotic shock in Δ*fab1* cells is also different from its

response in Δ*atg18* cells; in Δ*atg18* cells it localizes to the vacuole, but in Δ*fab1* cells Atg18p^{Q283N} is mostly cytosolic and fails to create vacuolar invaginations, typical of all the other mutants investigated. Since it is hypothesized during this study that the recruitment of Atg18p to the vacuole and PVEs is Vac7p dependent, it seemed important to investigate the localization of Atg18p^{Q283N} in Δ*vac7* cells (Figure 3.2.27).

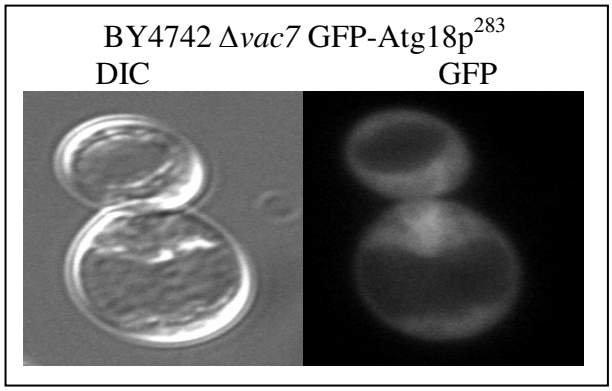

Figure 3.2.27: *In vivo* localization of GFP-Atg18p^{Q283N} in Δ*vac7* cells.

BY4742 *vac7::KAN* pUG36-*ATG18*^{Q283N} cells were grown overnight in SC-Ura-Meth medium with 2% glucose to 0.6 OD_{600nm}. The cell culture was washed once in fresh media and resuspended in MES buffer pH 5.6 and visualized using DIC and GFP fluorescence microscopy. The images were processed on Photoshop.

Figure 3.2.27 shows a loss of localization by Atg18p^{Q283N} in Δ*vac7* cells, yet again confirming that Atg18p localization is widely influenced by its interaction with Vac7p and intriguingly of all the mutants, Atg18p^{Q283N} was the only mutant which exhibited such a behavior in Δ*vac7* cells.

Table 3.2.1 summarizes the phenotypes of Atg18p point mutants in Δ*atg18* and Δ*fab1* cells.

Mutation	GFP Localization			Vacuole morphology			Lipid binding	
	Normal	**Salt stress**	**Autophagy**	**Normal**	**Salt stress**	**Autophagy**	**PI3*P***	**PI(3,5)P_2**
Wt	Punctae, vacoular	Vacoular	Puntae	Normal	Fragmented	Slightly enlarged	Yes	Yes
H244R	Punctae, vacoular	Punctae, vacuolar	Punctae, vacuolar	Slightly enlarged	Defective fragmentation	Fragmented	Yes	Yes
A263R	Diffused, nuclear	Diffused, nuclear	Diffused, nuclear	Large	Defective fragmentation	Slightly enlarged	No	No
K266T	Punctae, slightly vacuolar	Vacuolar	Vacuolar	Slightly enlarged	Fragmented	Fragmented	Yes	Yes
T268R	Punctae	Vacuolar	Diffused, nuclear	Normal	Fragmented	Slightly enlarged	Yes	Yes
R271T	Diffused	Punctae, slightly vacuolar	Diffused, partially vacuolar	Large	Defective fragmentation	Slightly enlarged	Yes	Yes
K280T	Partially vacuolar	Vacuolar	Vacuolar, Nuclear	Large	Fragmented	Slightly enlarged	Yes	Yes
Q283N	Punctae, vacoular	Vacuolar	Punctae, vacuolar	Slightly enlarged	Fragmented	Fragmented	Yes	Yes
R285T R286T	Diffused, nuclear	Punctae	Diffused, few punctae	Large	Large	Large	No	No

Table 3.2.1: A comparative summary of Atg18p point mutants.

As obvious by the study of these mutants, Atg18p regulates vacuole morphology both via its lipid binding and protein interactions, but it is reasonable to believe that Vac7p is not the only protein associating with Atg18p, besides neither Atg18p-Vac7p interaction nor Atg18p-PtdIns(3,5)P_2 binding completely explains regulation of vacuole fragmentation especially during salt stress. Hence an effort was made to identify other Atg18p interactions in order to acknowledge its role in membrane fission/fusion at the endo-lysosomal end.

Chapter 3; Results

3.3: Role of Atg18p in Vacuole fission/fusion.

Atg18p is involved in a number of processes like autophagy, regulation of vacuole morphology and the Cvt pathway, but the exact molecular details of its function in any of these processes are unknown.

Although Atg18p localization is attributed to its lipid binding, it is the protein-protein interactions at these loci which are primarily responsible to bring about any changes in vacuole morphology.

This section deals with some novel findings regarding protein interactions of Atg18p and hence highlights its role in regulation of vacuolar trafficking.

A link between Atg18p and Vps41p/Apl5p.

During a database search of proteins containing WD-40 like repeats with sequences similar to the repeat found in Atg18p responsible for lipid binding, it was noticed that the vacuolar protein Vps41p contained the following homologous stretch of amino acids that are also present in Atg18p.

***VPS41*: DGxxxATGSIDGTVII**
***ATG18*: DGxxxATAS-DKGTII**

This sequence is significant because mutation of this motif disrupts the interaction between Vps41p and the large subunit of the AP-3 adaptin complex Apl5p.

Vps41p is part of the HOPS complex that regulates vacuole-vacuole (homotypic) fusion. As the HOPS core complex of proteins is also part of the CORVET complex (Peplowska, Markgraf et al. 2007), that mediates vacuole fission and vacuole-

endosome fusion, this suggested a possible novel mechanism by which Atg18p might interact with the fission machinery.

The starting point for these studies was therefore to test if Atg18p binds Apl5p which was examined through Co-Immuno-Precipitation (Co-IP) of Atg18p^{Wt} and Apl5p^{Wt} (Figure 3.3.1).

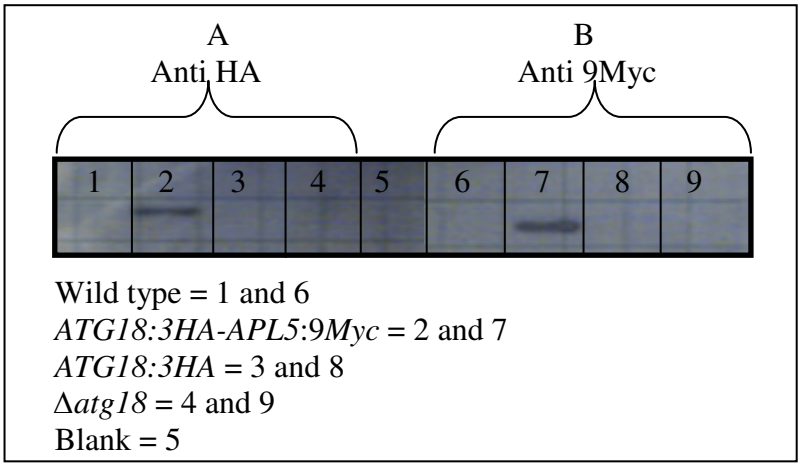

Figure 3.3.1: Western Blot for Atg18p-Apl5p CoIP.

50 ml of FY833^{Wt}, FY833 *ATG18-3HA*:HIS3 *APL5-9Myc*:TRP1, FY833 *ATG18-3HA*:HIS3 and BY4742 *atg18*::KAN cells were grown in suitable media at 30 ° C over night. The cells were washed once with fresh media and once with double distilled water and used for CoIP. Cell lysates were spin down and the supernatant collected in fresh tubes and incubated with A) Anti HA Antibody sepharose beads and B) Anti Myc Antibody sepharose beads and incubated at room temperature for 1 hour. The samples were run on 10 % SDS-PAGE and transferred to nitrocellulose membrane at 400 mAmp for 1 hour 15 minutes. Blot A was incubated with mouse Anti-Myc pIgG and blot B was incubated with Anti HA pIgG. Rabbit anti mouse HRP-IgG was used and the blots were visualized using chemiluminescence reagents A and B.

Figure 3.3.1 indicates that indeed Atg18p binds Apl5p *in vivo*. However it would also be interesting to check the binding of Atg18p point mutants with Apl5p, since the mutations were made in the region similar to Apl5p domain, known for Vps41p binding (Figure 3.3.2).

1	Atg18p^{H224R}
2	Atg18p^{A263R}
3	Atg18p^{K266T}
4	Atg18p^{T268R}
5	Atg18p^{R271T}
6	Atg18p^{K280T}
7	Atg18p^{Q283N}
8	Atg18p^{Wt}
9	Atg18p^{FTTG}

Figure 3.3.2: Western blot for Atg18p^{mutants} -Apl5p CoIP

FY833 *APL5-9Myc:TRP* pUG36-*ATG18* (wild type and mutants) cell lysates were used for Co-IP and transferred onto the blot where they were detected with mouse monoclonal anti-GFP and rabbit anti-mouse HRP antibody as per the same standards used for Atg18p^{Wt}/Apl5p^{Wt} Co-IP in the previous experiment.

Atg18p^{H244R}, Atg18p^{K263R}, Atg18p^{K266T}, and Atg18p^{Q283N} do not bind Apl5p while the rest of the mutants and wild type retain the ability to bind Apl5p with varying affinities.

If Atg18p binds Apl5p, then does it associate with Vps41p as well? This was investigated via Vps41pWt/Atg18p^{Wt} Co-IP (Figure 3.3.3).

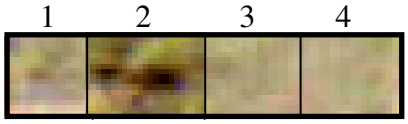

1	FY833 *ATG18-3HA:HIS3*
2	FY833 *ATG18-3HA:HIS3* pUG36-*VPS41*^{Wt}
3	FY833-WT
4	FY833 pUG3-*VPS41*^{Wt}

Figure 3.3.3: Western blot for Atg18p-Vps41p CoIP

50 ml of FY833 *ATG18-3HA:HIS3*, FY833 *ATG18-3HA:HIS3* GFP-*VPS41*^{Wt}, FY833^{Wt}, FY833 GFP-*VPS41*^{Wt} cells were grown in selective media and lysed using acid washed glass beads. The cell lysates were incubated with Anti-HA pIgG beads and 30 µl of the samples were run on SDS-PAGE and later transferred on to the nitrocellulose membrane. The proteins were detected using mouse monoclonal Anti-GFP IgG and Rabbit anti mouse IgG. The film was developed using chemiluminescence reagent on Agfa Xograph. The image was processed using Photoshop.

The blot reveals that Atg18p binds Vps41p *in vivo*, but is this binding in the same region as Apl5p binding? This was investigated by Co-IP of Atg18p point mutants with GFP-Vps41p (Figure 3.3.4).

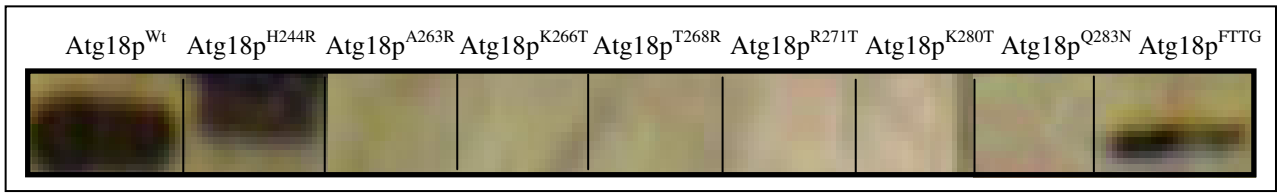

Figure 3.3.4: Western blot for Atg18p^{mutants}-Vps41p CoIP

50 ml of cell cultures (BY4742 *VPS41-3HA:HIS3* pUG36-*ATG18* wild type and mutants) were grown in selective media and lysed using acid washed glass beads. The cell lysates were incubated with Anti-HA pIgG beads and 30 µl of the samples were run on SDS-PAGE and later transferred on to the nitrocellulose membrane. The proteins were detected using mouse monoclonal Anti-GFP IgG and Rabbit anti mouse IgG. The film was developed using chemiluminescence reagent on Agfa Xograph. The image was processed using Photoshop.

Only Atg18p^{Wt}, Atg18p^{FTTG} and Atg18p^{H244R} bind Vps41p while the rest of the mutants do not bind Vps41p. Interestingly Atg18p^{FTTG} binds both Apl5p and Vps41p.

Since Vps41p, like Atg18p, is involved in regulation of vacuole morphology it was logical to first examine the *in vivo* localization of Vps41p^{Wt} in wild type cells, before establishing any link between Atg18p and Vps41p localizations (Figure/table 3.3.5).

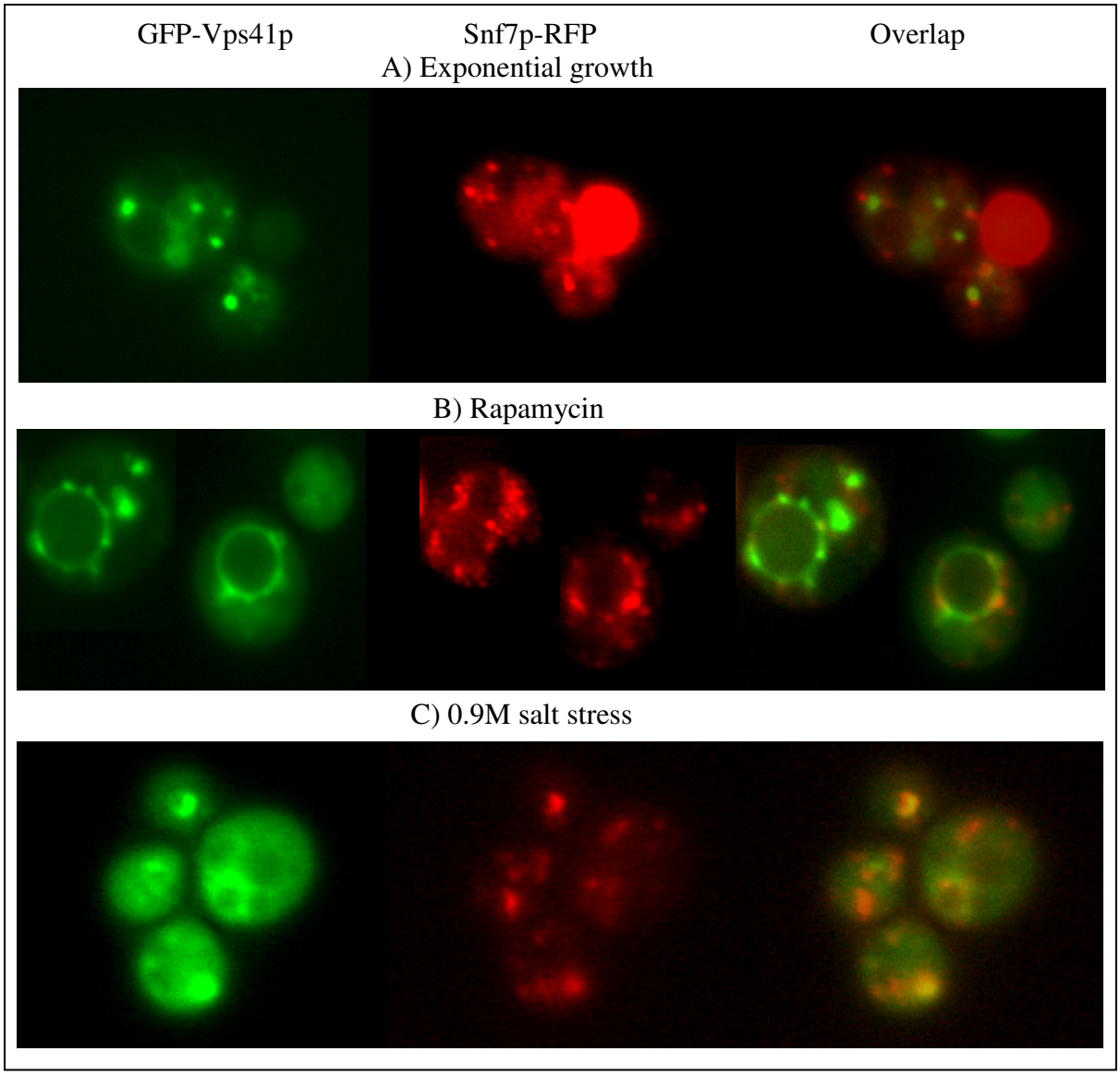

Figure 3.3.5: *In vivo* co-localization of GFP-Vps41p with RFP-Snf7p in wild type cells.

BY4741 cells with RFP-tagged Snf7p were transformed with pUG36-*VPS41*^{Wt} and grown on selective media for 4 days at 25 °C. The successful transformants were then grown in SC-Ura-Meth + 2 % glucose at 25 °C to 0.6 OD_{600nm}. 300 µl of this cell culture was mixed with 300 µl of fresh media and incubated further for 4 hours (Fraction A). 700 µl of the culture was spin down and the cells were resuspended in 1 ml N-starvation media + 0.2 µg/ml Rapamycin and incubated for further 4 hours at 25 °C (Fraction B). 100 µl of the cells grown in exponential growth media were subjected to 0.9 M salt stress (Fraction C) and examined immediately while the cells grown in exponential growth media and in N-starvation media were resuspended in MES buffer pH 5.6 and examined microscopically using a GFP and RFP filters. The images were processed using Photoshop.

	Exponential growth	Rapamycin	0.9 M salt-stress
Snf7p-RFP / GFP-Vps41p % co-localization	24.66	9.83	15
Standard deviation	3.91	0.93	3.74

Table 3.1: % co-localization of GFP-Vps41p with Snf7p-RFP.

Figure 3.3.5 shows that the localization of GFP-Vps41p in wild type cells changes during various conditions, from being punctae to cytosolic; although there is some co-localization with RFP-Snf7p (late endosome marker) under exponential growth conditions but this is lost significantly under autophagy conditions. This is in disagreement to the previous findings that HOPS complex does not traverse the endocytic pathway (Stamnes and Rothman 1993; Angers and Merz 2009), but supports Ungermann et al model (Cabrera, Ostrowicz et al. 2009).

Vps41p is also known to function in AP-3 pathway where it is recognized to bind the Apl5p sub-unit of the AP-3 complex. Apl5p is a peripheral protein recognized to (Angers and Merz 2009) partially co-localize and bind Vps41p (Figure 3.3.6/table 3.2).

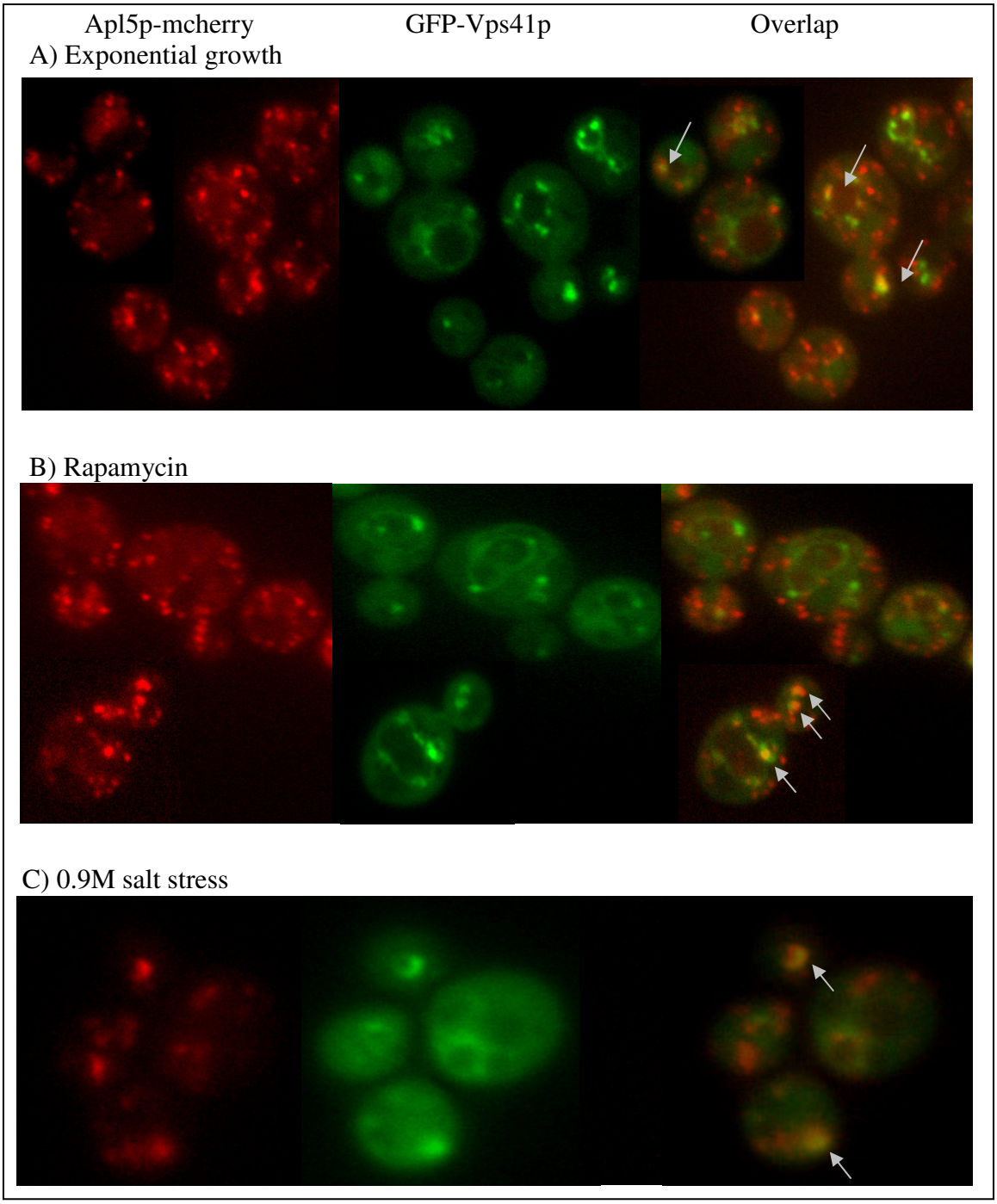

Figure 3.3.6: *In vivo* co-localization of Apl5p-mcherry with GFP-Vps41p

GFP-Vps41p was expressed in AMY632 *APL5-mcherry:Hyg* cells and grown on selective media at 25 °C to 0.6 OD_{600nm}. 300 µl of this cell culture was mixed with 300 µl of fresh media and incubated further for 4 hours. 700 µl of the culture was spin down and the cells were resuspended in N-starvation media with 0.2 µg/ml of Rapamycin and further incubated at 25 °C for 4 hours. 100 µl of the cells culture grown in exponential growth media was given 0.9 M salt stress and examined immediately while the cells grown in exponential growth or starvation media were then resuspended in MES buffer pH 5.6 and examined microscopically using a GFP and RFP filter. The images were processed using Photoshop. GFP-Vps41p/Apl5p:mcherry co-localization is represented by grey arrows.

	Exponential growth	Rapamycin	0.9 M salt-stress
Apl5p-mcherry / GFP-Vps41p % co-localization	49.58	19.58	10.08
Standard deviation	7.31	1.08	1.16

Table 3.2: % Co-localization of Apl5p-mcherry and GFP-Vps41p.

GFP-Vps41p co-localizes with Apl5p-mcherry under exponential growth conditions in accordance with the previous findings (Angers and Merz 2009) but an important thing to note here is that this co-localization is 'all or none' i.e some cells have perfect overlaps while others have no overlap.

Under rapamycin induced autophagy conditions, Vps41p is mostly enriched on the vacuole and the Apl5p-Vps41p co-localization is reduced, whereas under salt stress conditions, GFP-Vps41p is mostly cytosolic.

Since GFP-Vps41p co-localizes with Apl5p-mcherry under exponential growth conditions, it could be argued that this is due to the role of Vps41p in AP-3 pathway however it becomes important to note the localization of GFP-Vps41p in Δ*apl5* cells (Figure 3.3.7).

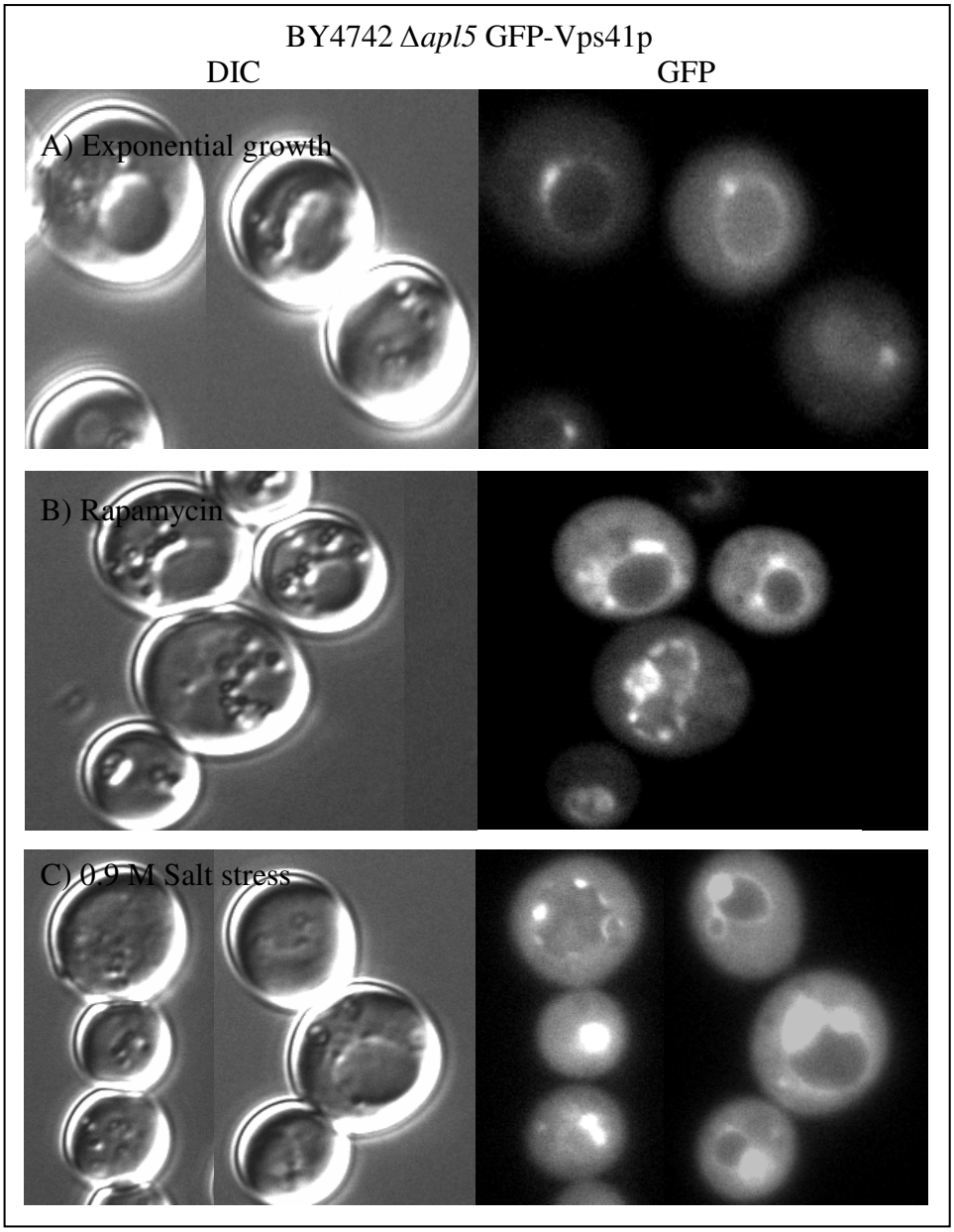

Figure 3.3.7: *In vivo* localization of GFP-Vps41p in Δ*apl5* cells.

BY4742 *apl5*::KAN cells were transformed with pUG36-*VPS41*^{Wt} and grown on selective media for 4 days at 25 °C. The successful transformants were then grown in SC-Ura-Meth + 2 % glucose at 25 °C to 0.6 OD_{600nm}. 300 µl of this cell culture was mixed with 300 µl of fresh media and incubated further for 4 hours (Fraction A). 700 µl of the cell culture was spin down and resuspended in 1 ml of N-starvation media + 0.2 µg / ml rapamycin for 4 hours at 25 °C (Fraction C). 100µl of cells growing in exponential growth media were given 0.9 M salt stress (Fraction C) and examined immediately while the cells grown in N-starvation media or exponential growth media were then resuspended in MES buffer pH 5.6 and examined microscopically using a GFP filter. The images were processed using Photoshop.

It is important to note that GFP-Vps41p vacuolar localization becomes slightly more prominent in Δ*apl5* cells as compared to wild type cells under exponential growth conditions. There is not much difference between the phenotypes exhibited by GFP-Vps41p in Δ*apl5* cells and wild type cells under autophagy conditions, but an important observation is that unlike wild type cells, the vacuolar association of GFP-Vps41p is not lost during hyper-osmotic shock in Δ*apl5* cells; besides, it is also noted that over-expression of Vps41p in these cells causes a slight increase in vacuole size.

HOPS complex sub-units Vps41p and Vps39p, are exchanged with the CORVET complex sub-units, Vps3p and Vps8p(Peplowska, Markgraf et al. 2007; Nickerson, Brett et al. 2009); to convert HOPS from a fusion promoting complex to CORVET. CORVET complex regulates vacuole fission and fusion of PVE with the vacuole. Nonetheless, if HOPS is required for fusion, it is important to investigate whether removal of Vps41p from the vacuole causes fragmentation or does this recycled Vps41p play a crucial role in regulating CORVET (especially Vps3p) activity at the PVE?

It would therefore be interesting to note the localization of Vps41p and Atg18p in Δ*vps3* and Δ*vps8* cells in order to check how the lack of such an exchange affects Vps41p and Atg18p localization (Figure 3.3.8/3.3.9)

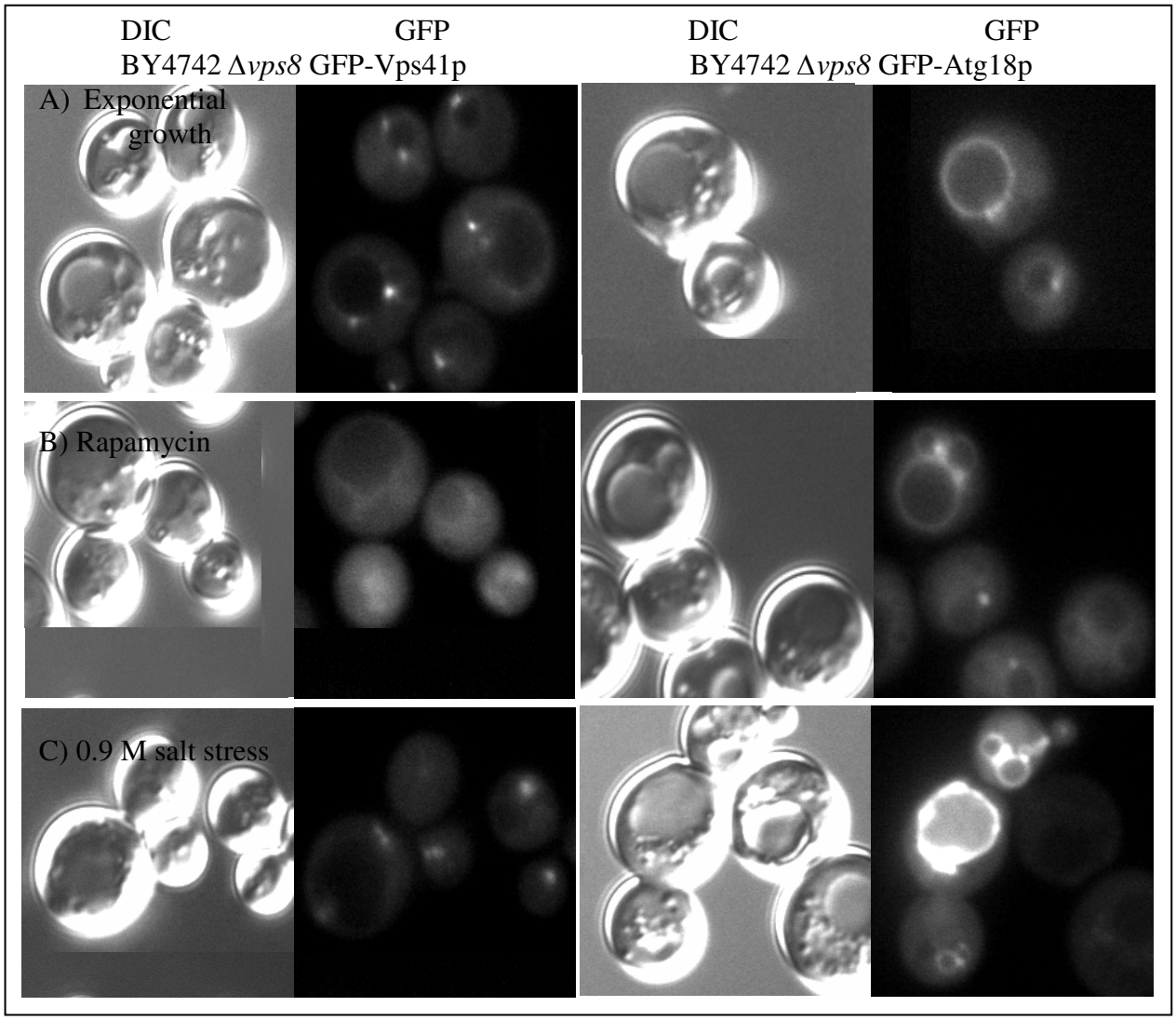

Figure 3.3.8: *In vivo* localization of Vps41p and Atg18p in Δ*vps8* cells.

BY4742 *vps8*::KAN cells were transformed with pUG36-*VPS41*^{Wt} and pUG36-*ATG18*^{Wt} and grown on selective media for 4 days at 25 °C. The successful transformants were then grown in SC-Ura-Meth + 2 % glucose at 25 °C to 0.6 OD_{600nm}. 300 µl of this cell culture was mixed with 300 µl of fresh media and incubated further for 4 hours (Fraction A). 700 µl of the cell culture was spin down and resuspended in 1 ml of N-starvation media + 0.2 µg / ml rapamycin for 4 hours at 25 °C (Fraction B). 100µl of cells growing in exponential growth media were given 0.9 M salt stress (Fraction C) and examined immediately while the cells grown in N-starvation media or exponential growth media were then resuspended in MES buffer pH 5.6 and examined microscopically using a GFP filter. The images were processed using Photoshop.

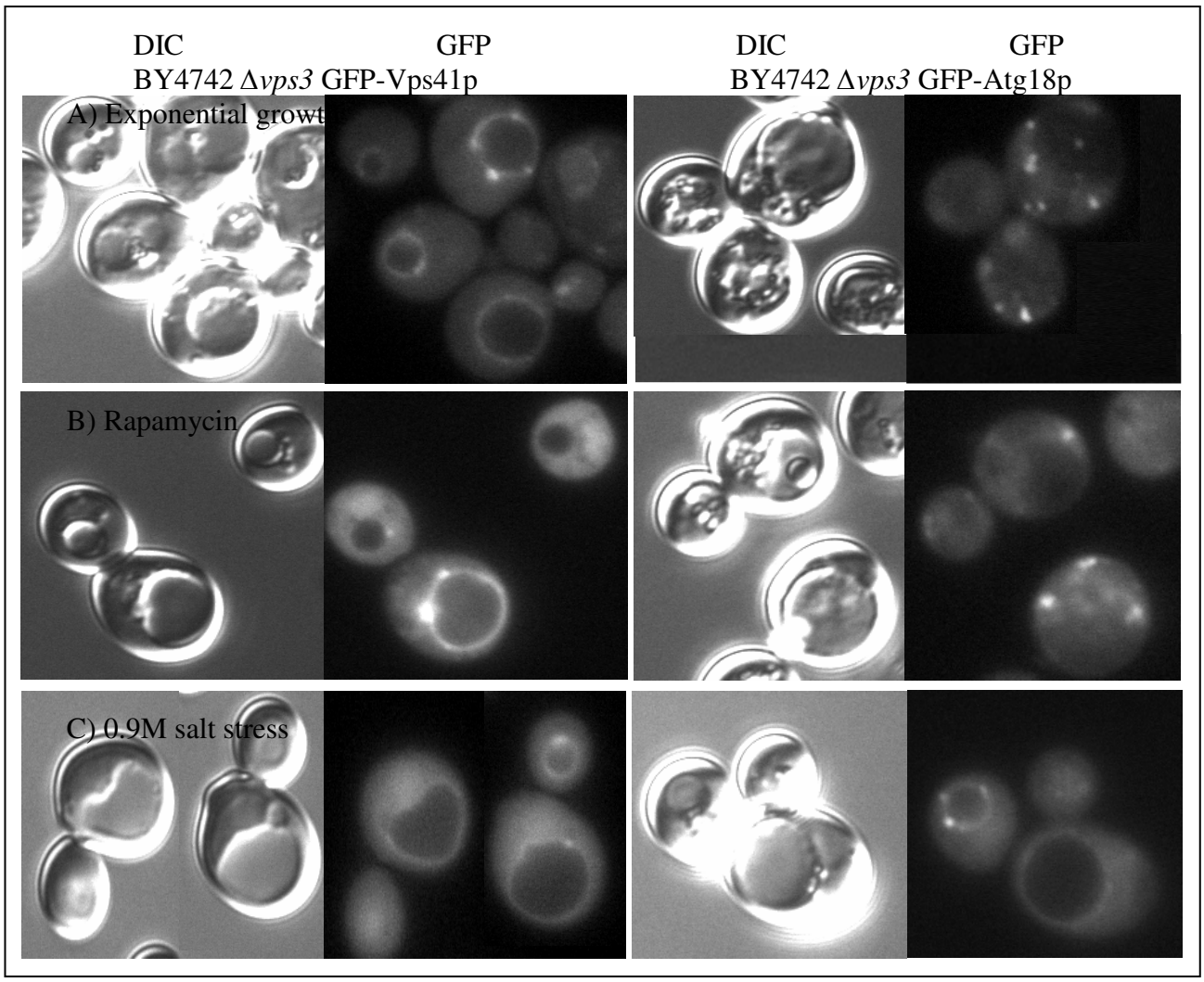

Figure 3.3.9*: In vivo* localization of GFP-Vps41p and GFP-Atg18p in Δ*vps3* cells.

BY4742 *vps8*::KAN cells were transformed with pUG36-*VPS41*^{Wt} and pUG36-*ATG18*^{WT} and grown on selective media for 4 days at 25 °C. The successful transformants were then grown in 1 ml SC-Ura-Meth + 2 % glucose at 25 °C to 0.5 OD_{600nm}. . 300 µl of this cell culture was resuspended in 300 µl of fresh media and incubated for 4 hours at 25 °C. 700 µl of the culture was incubated with 0.2 µg rapamycin / ml media for 4 hours at 25 °C and then washed once with fresh media and resuspended in MES buffer pH 5.7 and examined microscopically using a GFP filter. 100 µl of cell culture was given 0.9 M salt stress and examined immediately. The images were processed using Photoshop

Figure 3.3.8 shows that the localization of Atg18p and Vps41p in Δ*vps8* cells is comparable to wild type but during autophagy GFP-Vps41p is mostly cytosolic while Atg18p is on the vacuole rim. This is unlike wild type cells, indicating that Vps41p accumulation and Atg18p displacement from the vacuole (during autophagy) requires Vps8p. During salt stress Vps41p forms punctae while Atg18p localizes to the vacuole yet vacuole fragmentation defects are visible in Δ*vps8* cells.

In contrast, Figure 3.3.9 shows that GFP-Vps41p in Δ*vps3* cells only exhibits an aberrant phenotype under osmotic shock; it is observed to accumulate slightly on the vacuole. However Atg18p localization in Δ*vps3* cells is defective under exponential growth as well as osmotic shock conditions, accompanied with vacuole morphology defects.

Hence it gives a clear indication that putatively Vps8p arbitrates the localization of Vps41p and Atg18p under autophagy conditions while Vps3p regulates it during salt stress.

Nonetheless, Atg18p vacuolar localization during hyper osmotic-shock is reported to be due to an elevated PtdIns(3,5)P_2 level produced by activated Fab1p. However, if besides Fab1p and Atg18p, Vps41p also plays a significant role in regulation of vacuole morphology it would be interesting to note the localization of GFP-Vps41p in Δ*atg18* (Figure 3.3.10) and Δ*fab1* (Figure 3.3.11) cells; keeping in mind that Vps41p is known to bind a number of phosphoinositides *in vitro*, albeit in a very non-specific manner (Stroupe, Collins et al. 2006).

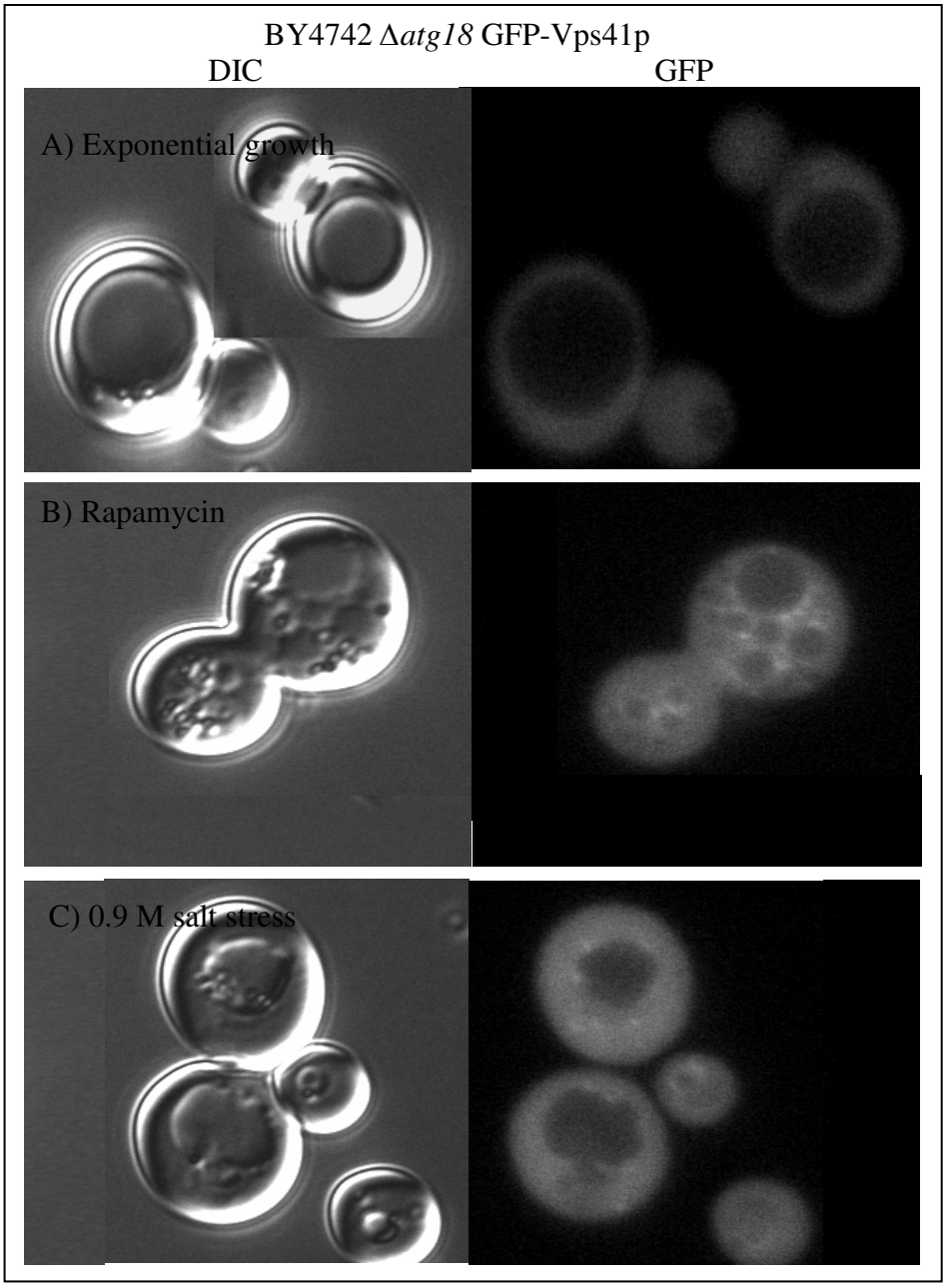

Figure 3.3.10: *In vivo* localization of GFP-Vps41p in Δ*atg18* cells.

BY4742 *atg18*::KAN cells were transformed with pUG36-*VPS41*^{Wt} and grown on selective media for 4 days at 25 °C. The successful transformants were then grown in SC-Ura-Meth + 2 % glucose at 25 °C to 0.6 OD_{600nm}. 300 µl of this cell culture was mixed with 300 µl of fresh media and incubated further for 4 hours (Fraction A). 700 µl of the cell culture was spin down and resuspended in 1 ml of N-starvation media + 0.2 µg / ml rapamycin for 4 hours at 25 °C (Fraction B). 100µl of cells growing in exponential growth media were given 0.9 M salt stress (Fraction C) and examined immediately while the cells grown in N-starvation media or exponential growth media were then resuspended in MES buffer pH 5.6 and examined microscopically using a GFP filter. The images were processed using Photoshop.

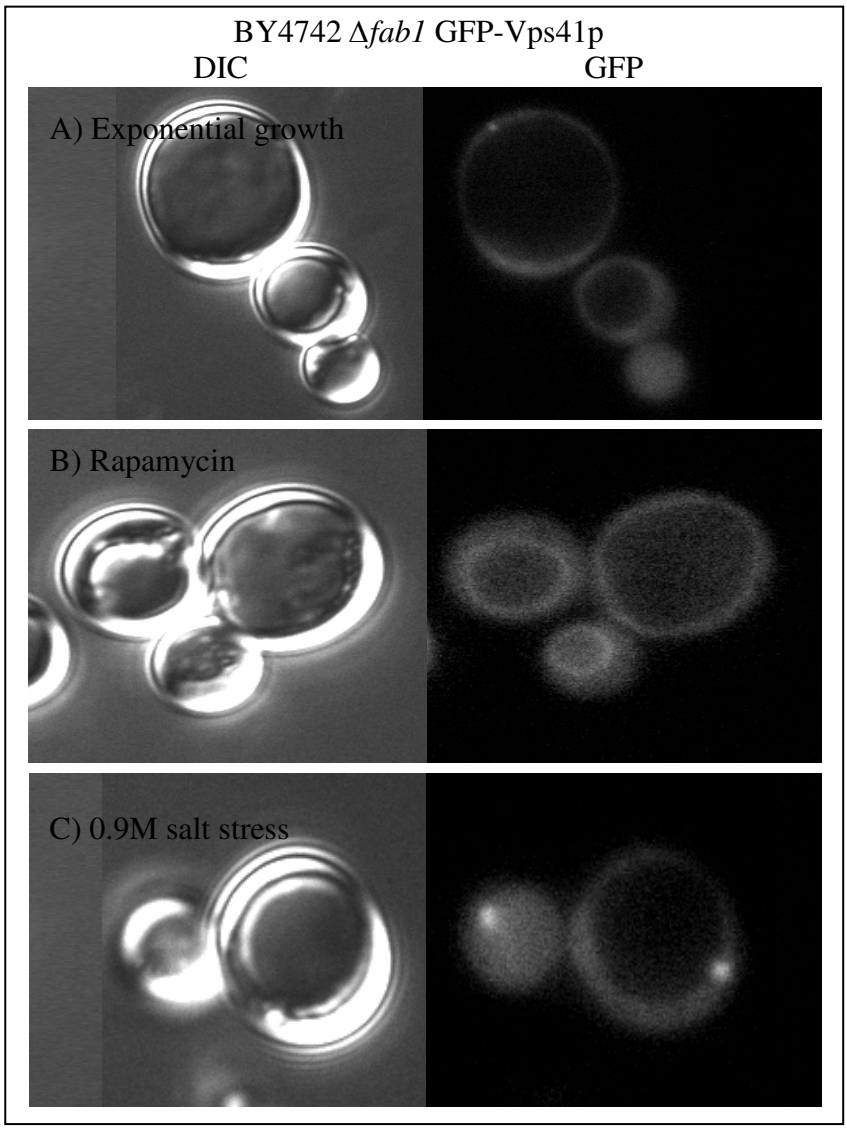

Figure 3.3.11: *In vivo* localization of GFP-Vps41p in Δ*fab1* cells.

BY4742 *fab1*::KAN pUG36-*VPS41*^{Wt} cells were grown in 1ml of SC-Ura-Meth + 2 % glucose at 25 °C to 0.6 OD_{600nm}. 300 µl of this cell culture was mixed with 300 µl of fresh media and incubated further for 4 hours (Fraction A). 700 µl of the cell culture was spin down and resuspended in 1 ml of N-starvation media + 0.2 µg / ml rapamycin for 4 hours at 25 °C (Fraction B). 100µl of cells growing in exponential growth media were given 0.9 M salt stress (Fraction C) and examined immediately while the cells grown in N-starvation media or exponential growth media were then resuspended in MES buffer pH 5.6 and examined microscopically using a GFP filter. The images were processed using Photoshop.

Figure 3.3.10/3.3.11 show that GFP-Vps41p is mis-localized and largely cytosolic in Δ*atg18* and Δ*fab1* (few Δ*fab1* cells exhibit few punctae) under exponential growth conditions.

During autophagy conditions, GFP-Vps41p localization in Δ*fab1* cells and wild type cells is comparable, but it fails to localize to the vacuole during autophagy in Δ*atg18* cells. This indicates a possible link between the regulation of vacuole morphology and Fab1 pathway; Vps41p can localize to the vacuole in absence of PtdIns(3,5)P_2 i.e in Δ*fab1* cells under autophagy conditions but not when PtdIns(3,5)P_2 levels are very high i.e in Δ*atg18* cells. Therefore it was important to test whether Vps41p is stable in Δ*fab1* and Δ*atg18* backgrounds? (Figure 3.3.12)

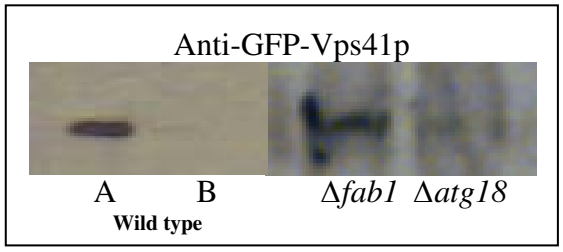

Figure 3.3.12: Stability blot for GFP-Vps41p in Δ*atg18* and Δ*fab1* cells..

BY4742 *atg18*::KAN GFP-Vps41p and BY4742 *fab1*::KAN GFP-Vps41p cells were grown in 10 ml SC-Ura-Meth + 2 % glucose at 25 °C to 0.7 OD_{600nm} along with wild type cells with (A) or without (B) GFP-Vps41p. 5 ml of the cell culture was used for alkaline lysis and boiled in SDS sample buffer. 40µl of sample was run on 10 % SDS-PAGE at 100 volts and later transferred to nitro-cellulose membrane for 1hour 10 minutes at 400 mAmp. The membrane was blocked with 3% milk protein to reduce non specific binding overnight at 4 °C. It was then incubated with mouse anti-GFP primary IgG and rabbit anti mouse secondary IgG. Washings were given thrice between the incubations with the antibodies and later before being treated with Chemiluminescence reagents. The film was processed using Xograph machine from Agfa.

As indicated by the blot, Vps41p is stable in Δ*fab1* but its stability is much reduced in Δ*atg18* background; possibly a result of hyperactive V-ATPase due to high PtdIns(3,5)P_2 levels in Δ*atg18* cells and consequent higher acidity of the cell lysates or due to increased vacuolar fragility during lysis.

Although Vps41p vacuolar localization could possibly be PtdIns3*P* dependent in Δ*fab1* cells, as it is known to bind PPIns, but its localization with regard to Atg18p is novel.

Another important observation is that numerous vesicles accumulate in the cytosol in Δ*atg18* cells and unlike wild type cells the vacuole does not become enlarged (Figure 3.3.13).

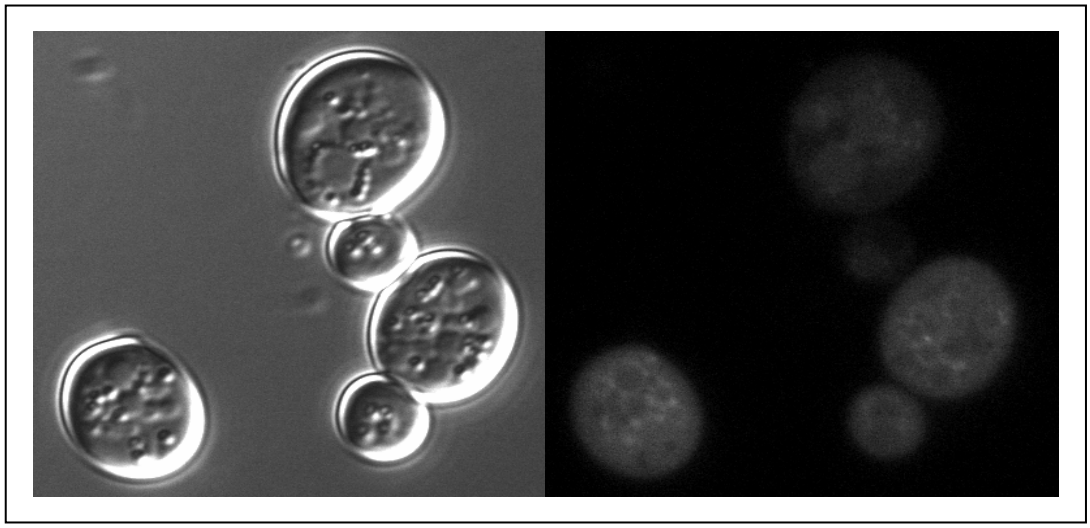

Figure 3.3.13: *In vivo* localization of GFP-Vps41p in Δ*atg18* cells under rapamycin induced autophagy.
BY4742 *atg18*::KAN pUG36-*VPS41*^{Wt} cells were grown on selective media in 1 ml SC-Ura-Meth + 2 % glucose at 25 °C to 0.6 OD_{600nm}. The cell culture was spin down and resuspended in 1 ml of N-starvation media + 0.2 µg / ml rapamycin for 4 hours at 25 °C. The cells were then resuspended in MES buffer pH 5.6 and examined microscopically using a GFP filter. The images were processed using Photoshop

A similar phenotype is also observed in Δ*vac7*, Δ*vps38* (Rapamycin) and Δ*atg18* cells (Rapamycin and cyclohexamide) over expressing Atg18p (results section 1).

Since in Δ*vps41* cells the vesicles originating from various trafficking pathways are unable to fuse to form a vacuole and accumulate in the cytosol, it could be argued that either Vps41p-lipid binding is responsible for Vps41p association/disassociation from a particular site through co-incidence detection and/or lipids mediate Rab activation which in turn leads to recruitment of Vps41p. It could also be postulated that Atg18p functions in such processes either indirectly through regulation of Fab1p activity and/or directly via displacing Vps41p from the vacuole and releasing it for next cycle of events.

Therefore, it becomes important to note the localization of Vps41p in Δ*vps34* cells with undetectable PtdIns3*P* and PtdIns(3,5)P_2 levels (Figure 3.3.14).

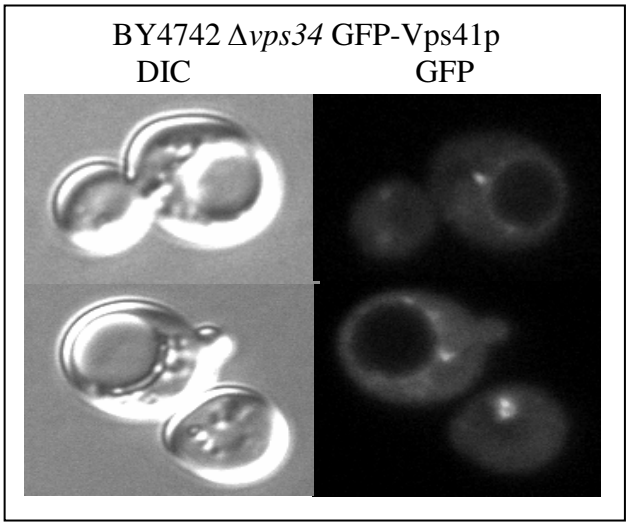

Figure 3.3.14: *In vivo* localization of GFP-Vps41p in Δ*vps34* cells.
BY4742 *vps34*::KAN pUG36-*VPS41*^{Wt} cells were grown in 1 ml SC-Ura-Meth + 2 % glucose at 25 °C to 0.5 OD_{600nm}. . 500 µl of this cell culture was spin down and resuspended in 1 ml of fresh media and incubated for 4 hours at 25 °C. The cells were then resuspended in MES buffer pH 5.6 and examined microscopically using a GFP filter. The images were processed using Photoshop

Figure 3.3.14 shows that although Vps41p loses most of its vacuolar localization in a lipid dependent manner but this does not seem to affect its punctae localization, indicating that Vps41p is not mis-localized in Δ*atg18* cells due to aberrant PtdIns3*P* and PtdIns(3,5)P_2 levels.

If this is true then Atg18p-Vps41p association could be required for regulation of vacuole morphology in terms of limiting vacuolar fusion and displacing Vps41p from the vacuole in response to lipid levels.

Chapter 3; Results

3.4: The role of Atg18p in MVB sorting

Cells constantly exchange materials via endocytosis/exocytosis, between organelles and from the environment forming an extensive trafficking system. Within the cells, proteins with at least one trans-membrane domain, bind their specific receptors and are incorporated into a vesicle by associating with a coat e.g clathrin or Adaptins. The sorting signal within the proteins or their modification, together with the specific SNAREs present on the vesicle membrane, determines the destination of the vesicle; though the default destination for membrane proteins with no sorting information is vacuole lumen.

Cargo specifically destined for vacuole (yeast) or lysosome (most other eukaryotes) via the endocytic system is sorted at the late endosomes (PVE in yeast) which matures into MVBs. Mono-ubiquitination acts as a tag for endocytic sorting of proteins destined for lysosomal/vacuolar degradation (Katzmann et al, 2002;Hicke and Dunn, 2003). Hence trafficking into the vacuole needs subsequent factors;

- Proteins of the ESCRT complexes and VPS proteins.
- Phosphoinositides.
- Ubiquitin, Ubiquitination and deubiquitination enzymes.
- HOPS, CORVET and VAM proteins.
- Cargo.

ESCRT proteins recognize the cargo through their Ubiquitin Binding Domains and are primarily involved in packaging the cargo into membranous vesicles through recognition of Phosphoinositide signaling; e.g Vps27p (ESCRT-0 complex) is

shown to bind PtdIns3*P* specifically and recruit ESCRT-I complex to this site (Katzmann, Stefan et al. 2003).

The exact details of ubiquitination of cargo through ligase enzymes like Rsp5p (yeast) are not yet clear but it is hypothesized that it takes place at multiple sites depending on the cargo (Lemmon and Traub 2000; Katzmann, Sarkar et al. 2004; Baxter, Abeliovich et al. 2005; Oestreich, Aboian et al. 2007; Kirkin, McEwan et al. 2009).

A number of biological molecules that act as cargo for MVB sorting are:

1. Endocytic cargo; down regulated receptors, nutrients and some lipophillic/hydrophobic dyes.
2. Biosynthetic cargo; resident vacuolar proteins like phosphatases, carboxypeptidases etc.
3. Degradative cargo; proteins which are mis-folded or no longer required by the cell.

It is known that low PtdIns(3,5)P_2 levels, as in Δ*fab1* and Δ*vac14* cells, cause aberrations in MVB sorting (Dove, McEwen et al. 2002). It was previously tested whether Atg18p plays any role in MVB sorting but in the case of Phm5p, a biosynthetic cargo, the answer was found to be that it did not. However, many proteins are now known that exhibit cargo specific effects on MVB sorting and so it was decided to test if Atg18p was one of these.

This was investigated by using 3 different cargo proteins, namely

- Sna3p, which can be sorted to the vacuole lumen in more than one way,
- Phm5p, which is a biosynthetic cargo and
- Ste3p, which is an endocytic cargo.

It is important to mention here that regardless of vacuole size, GFP signal within the vacuole is indicative of normal MVB sorting whereas any other phenotype is considered as anomalistic (Figure 3.4.1).

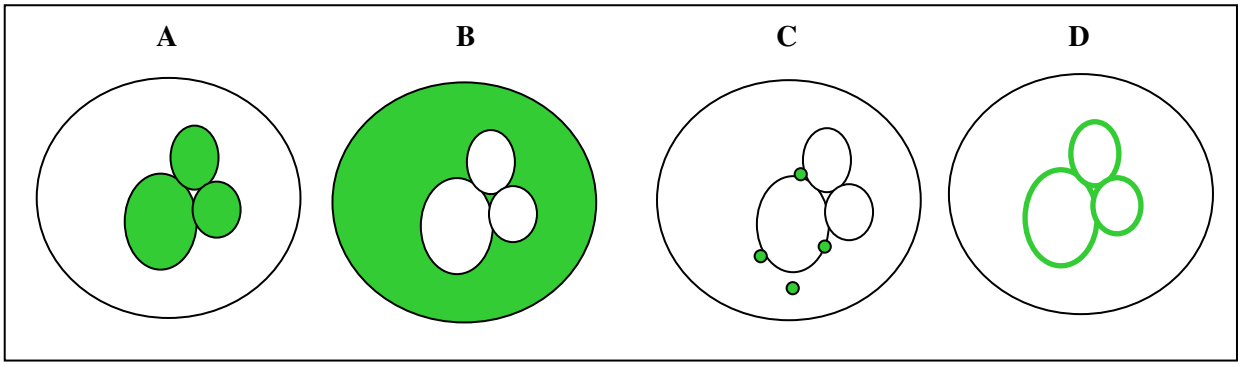

Figure 3.4.1: Localization of GFP signal in various null mutants involved in MVB sorting.

A) GFP-cargo in wild type cells indicating exponential growth MVB sorting, B and C) GFP-cargo in null mutants of the early acting factors indicating aberrant MVB sorting, D) GFP-cargo in null mutants of the late acting factors indicating aberrant MVB sorting.

As an initial reference point, BY4742^{Wt} cells expressing GFP-Phm5p (biosynthetic cargo), Ste3p (endocytic cargo) and Sna3p were investigated (Figure 3.4.2).

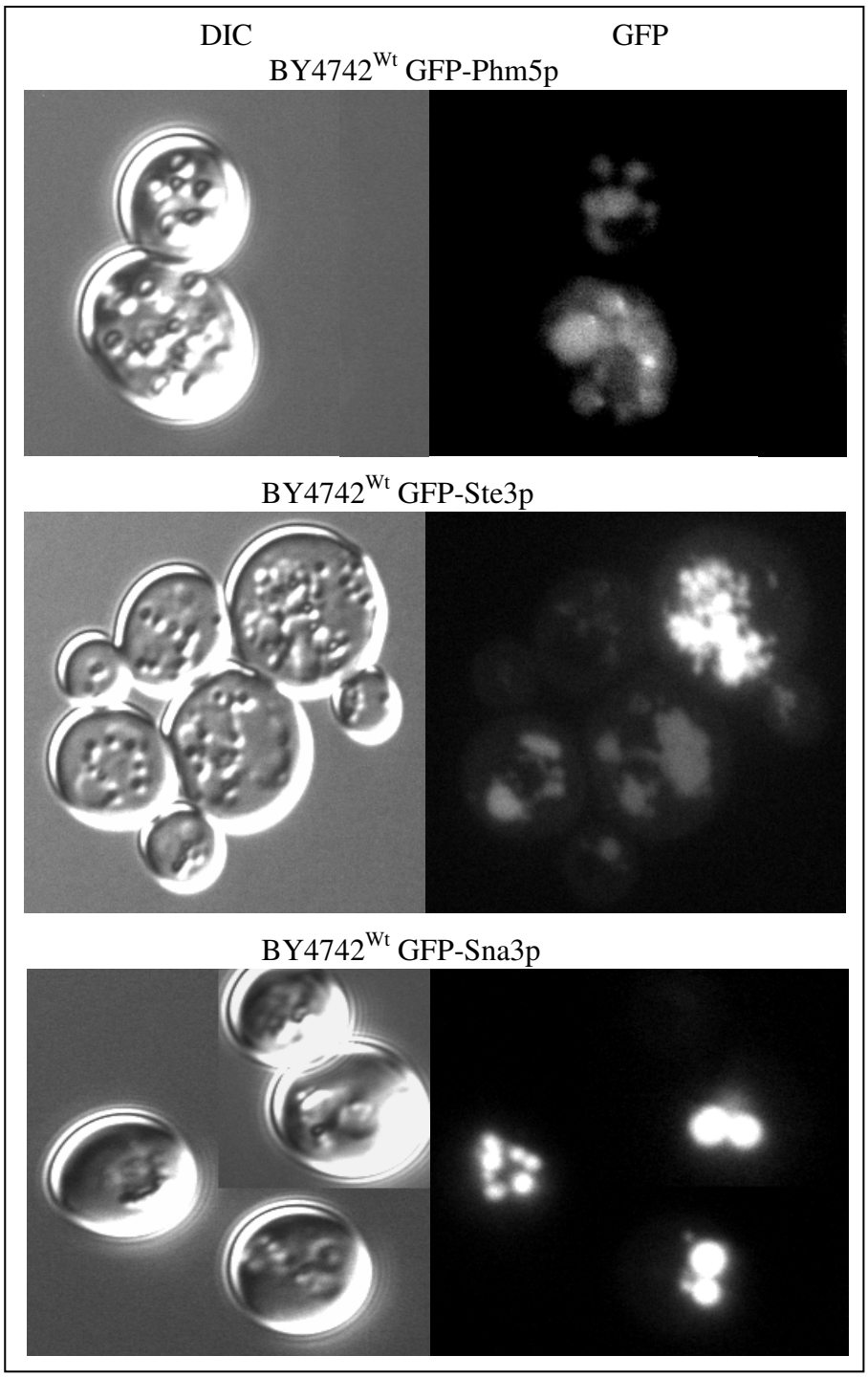

Figure 3.4.2: *In vivo* localization of GFP-Phm5p, GFP-Ste3p and GFP-Sna3p in wild type cells.

BY4742^{Wt} GFP-Phm5p, BY4742^{Wt} GFP-Ste3p and BY4742^{Wt} GFP-Sna3p cells were grown overnight in Selective media with 2% glucose to 0.6 OD_{600nm}. The cell culture was washed once in fresh media and resuspended in MES buffer pH 5.6 and visualized using DIC and GFP fluorescence microscopy. The images were processed on Photoshop.

As expected, all 3 types of MVB cargo are sorted correctly into the vacuole lumen in wild type cells. Since Fab1p/PtdIns(3,5)P_2 is previously shown to exhibit MVB sorting defects (Odorizzi, Babst et al. 1998), the *in vivo* localization of the cargo was investigated in Δ*fab1* cells (Figure 3.4.3).

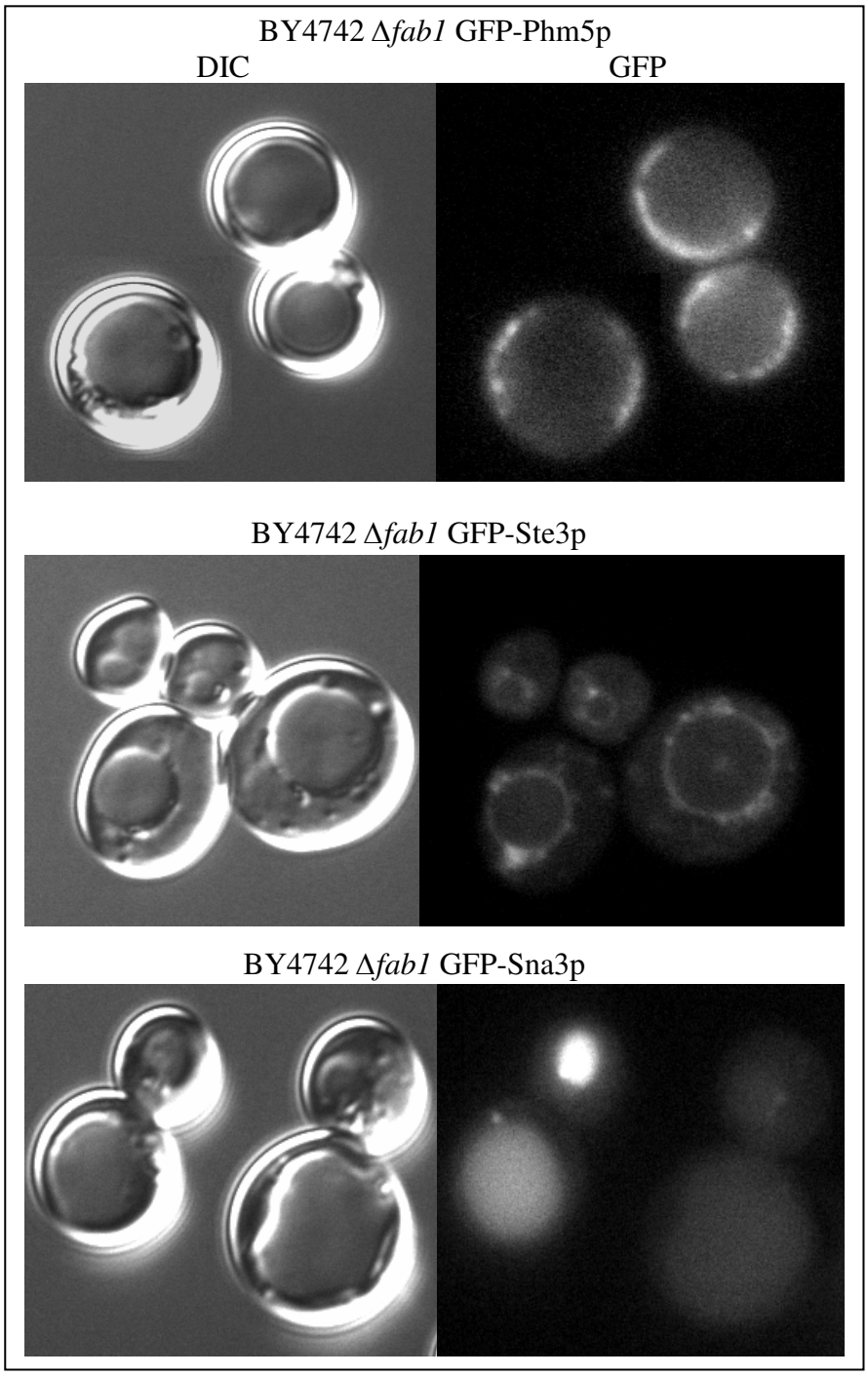

Figure 3.4.3: *In vivo* localization of GFP-Phm5p, GFP-Ste3p and GFP-Sna3p in Δ*fab1* cells.

BY4742 Δ*fab1* GFP-Phm5p, BY4742 Δ*fab1* GFP-Ste3p and BY4742 Δ*fab1* GFP-Sna3p cells were grown overnight in SC-Ura-Meth medium with 2% glucose to 0.6 OD_{600nm}. The cell culture was washed once in fresh media and resuspended in MES buffer pH 5.6 and visualized using DIC and GFP fluorescence microscopy. The images were processed on Photoshop.

Phm5p and Ste3p localization in Δ*fab1* cells is aberrant whereas Sna3p is correctly localized to the vacuole lumen as previously described(Macdonald, Stringer et al. ; Odorizzi, Babst et al. 1998; Phelan, Millson et al. 2006). This indicates that 1) sorting of various cargo is distinct and 2) Fab1p/PtdIns(3,5)P_2 plays a crucial role in Phm5p and Ste3p sorting but not Sna3p sorting.

The localization of these cargo proteins in Δ*atg18* cells was investigated next (Figure 3.4.4).

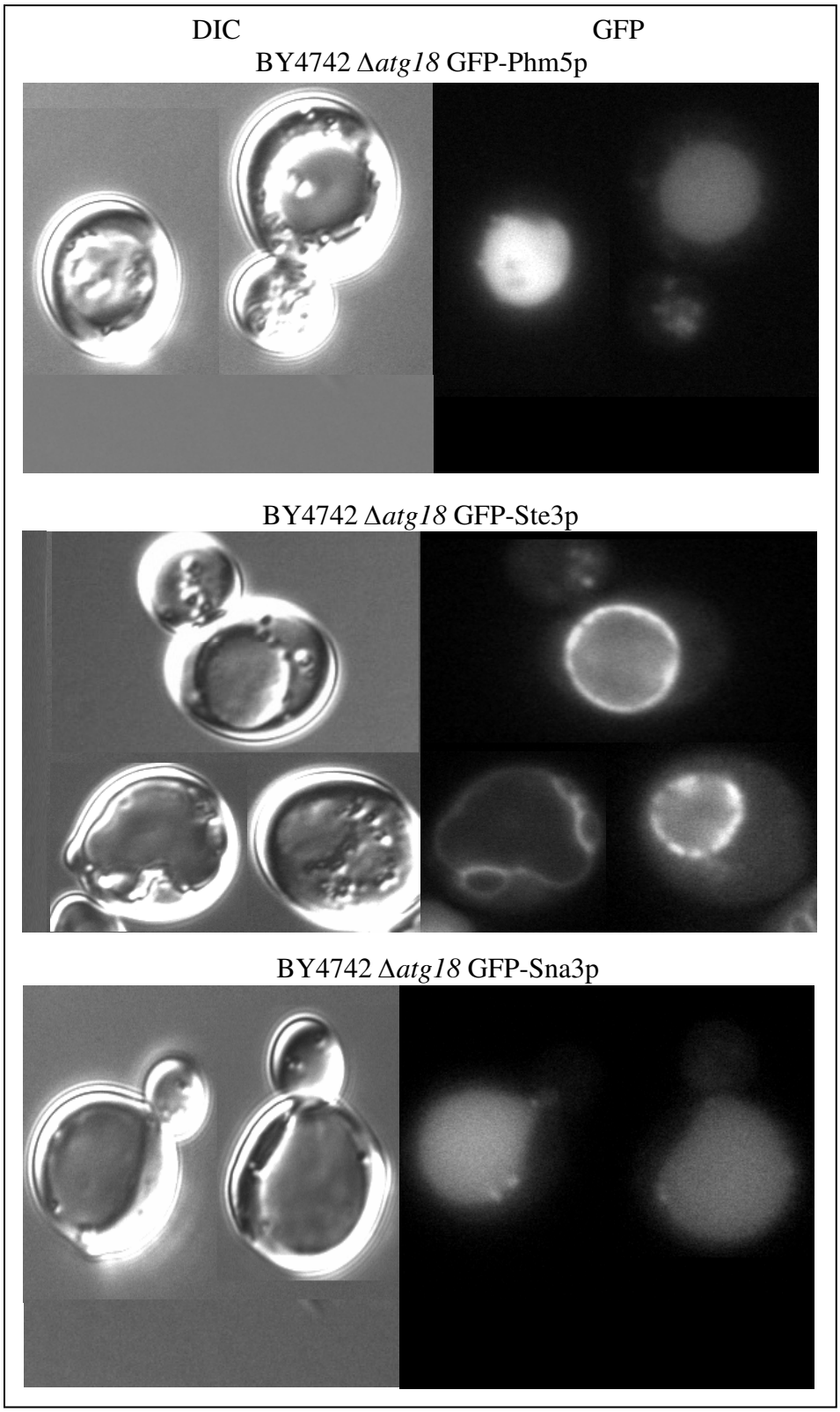

Figure 3.4.4: *In vivo* localization of GFP-Phm5p, GFP-Ste3p and GFP-Sna3p in Δ*atg18* cells.

BY4742 Δ*atg18* GFP-Phm5p, BY4742 Δ*atg18* GFP-Ste3p and BY4742 Δ*atg18* GFP-Sna3p cells were grown overnight in SC-Ura-Meth medium with 2% glucose to 0.6 OD_{600nm}. The cell culture was washed once in fresh media and resuspended in MES buffer pH 5.6 and visualized using DIC and GFP fluorescence microscopy. The images were processed on Photoshop.

Figure 3.4.4 indicates that Atg18p effects MVB sorting of Ste3p and not Phm5p. Although most of GFP-Sna3p is localized in the vacuole lumen in Δ*atg18* cells yet there are a few punctae in close proximity to the vacuole; this is similar to the phenotype observed in Δ*fab1* GFP-Sna3p cells.

Although the phenotype exhibited by GFP-Ste3p in Δ*atg18* cells is similar to the one exhibited in Δ*fab1* cells, it cannot logically be due to PtdIns(3,5)P_2 levels given that PtdIns(3,5)P_2 levels in Δ*fab1* cells are undetectable whereas they are 10 times higher than exponential growth in Δ*atg18* cells.

This is of course assumed that the PtdIns(3,5)P_2 in *Δatg*18 cells is accessible to the PVE-machinery; however it might all be on the vacuole, in which case the phenotypes of *Δfab1* and *Δatg18* could be related. Hence the newly identified role of Atg18p in displacing/recycling of Vps41p in a lipid dependent manner seems to fit in well; potentially Atg18p could regulate Vps41p localization, which in turn would affect CORVET activity and therefore fusion of MVB with the vacuole. However, if this were the mechanism then both Fab1p and Atg18p would be predicted to affect the MVB sorting of all cargo, and this is clearly not the case.

Since Ste3p endocytosis and consequent MVB sorting is constitutive, it seems possible that Atg18p-Vac7p interaction might play some role in selective recycling of an unidentified component of endocytic MVB sorting?

Therefore the localization of the GFP-tagged cargo was investigated in Δ*vac7* cells (3.4.5).

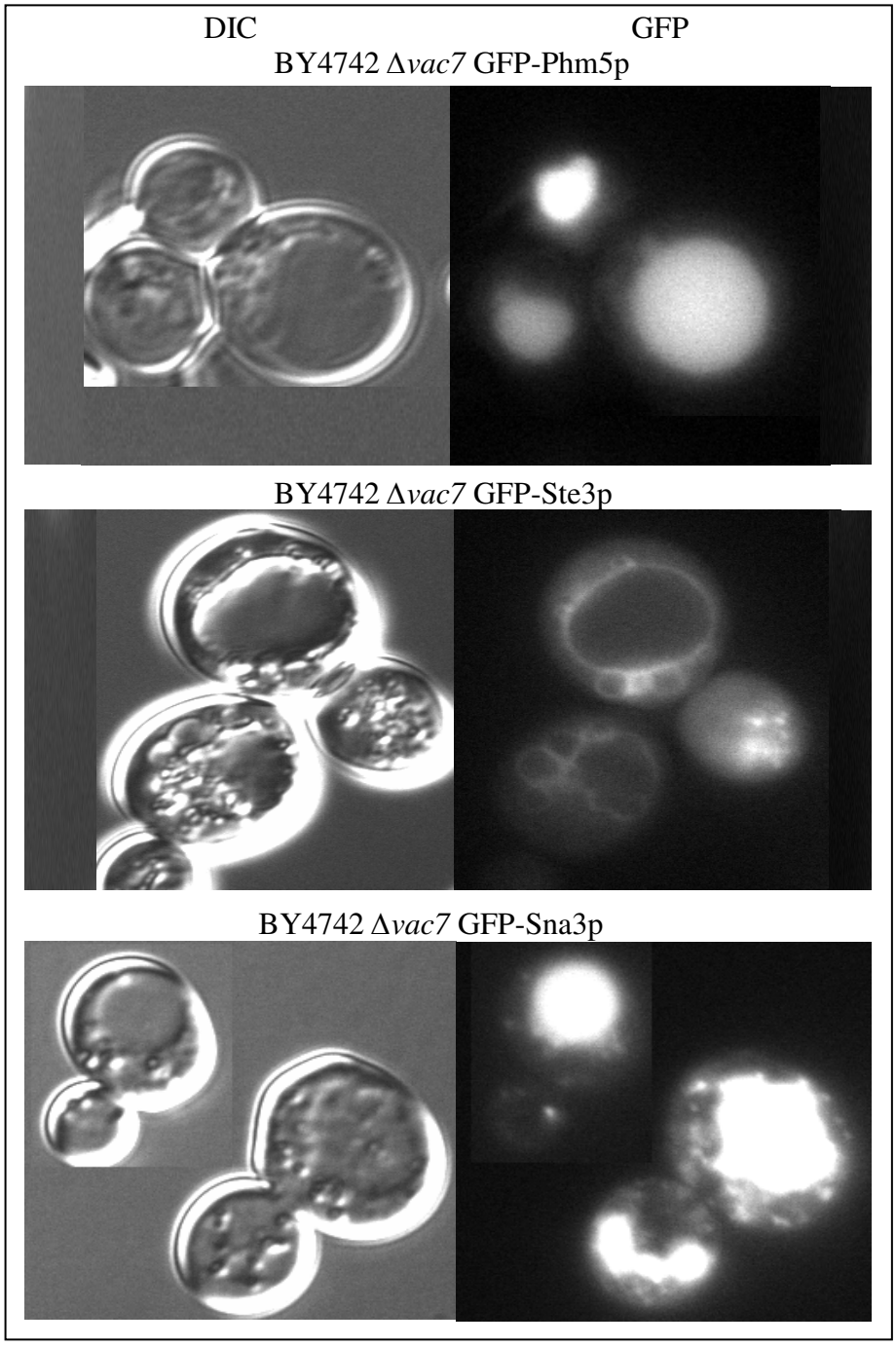

Figure 3.4.5: *In vivo* localization of GFP-Phm5p, GFP-Ste3p and GFP-Sna3p in Δ*vac7* cells.

BY4742 Δ*vac7* GFP-Phm5p, BY4742 Δ*vac7* GFP-Ste3p and BY4742 Δ*vac7* GFP-Sna3p cells were grown overnight in SC-Ura-Meth medium with 2% glucose to 0.6 OD_{600nm}. The cell culture was washed once in fresh media and resuspended in MES buffer pH 5.6 and visualized using DIC and GFP fluorescence microscopy. The images were processed on Photoshop.

Figure 3.4.5 shows that the localizations of GFP-Phm5p, GFP-Ste3p and GFP-Sna3p in Δ*vac7* cells is very similar to their localizations in Δ*atg18* cells. This clearly indicates that indeed both Atg18p and Vac7p are involved in recycling of essential components of the endocytic cargo only; if this phenotype would only be due to low PtdIns(3,5)P_2 levels in Δ*vac7* cells then Δ*vac7* cells should affect both Phm5p and Ste3p as is observed in Δ*fab1* cells.

Since Atg18p and Vac7p are implicated in retrograde trafficking from the vacuole to the PVE, it would be important to note the localization of these cargo proteins in Δ*vps38* cells. This would demarcate whether the recycled component is circulated between vacuole and PVE only or vacuole, PVE and TGN. The localization of these cargos was thus investigated in Δ*vps38* cells (Figure 3.4.6).

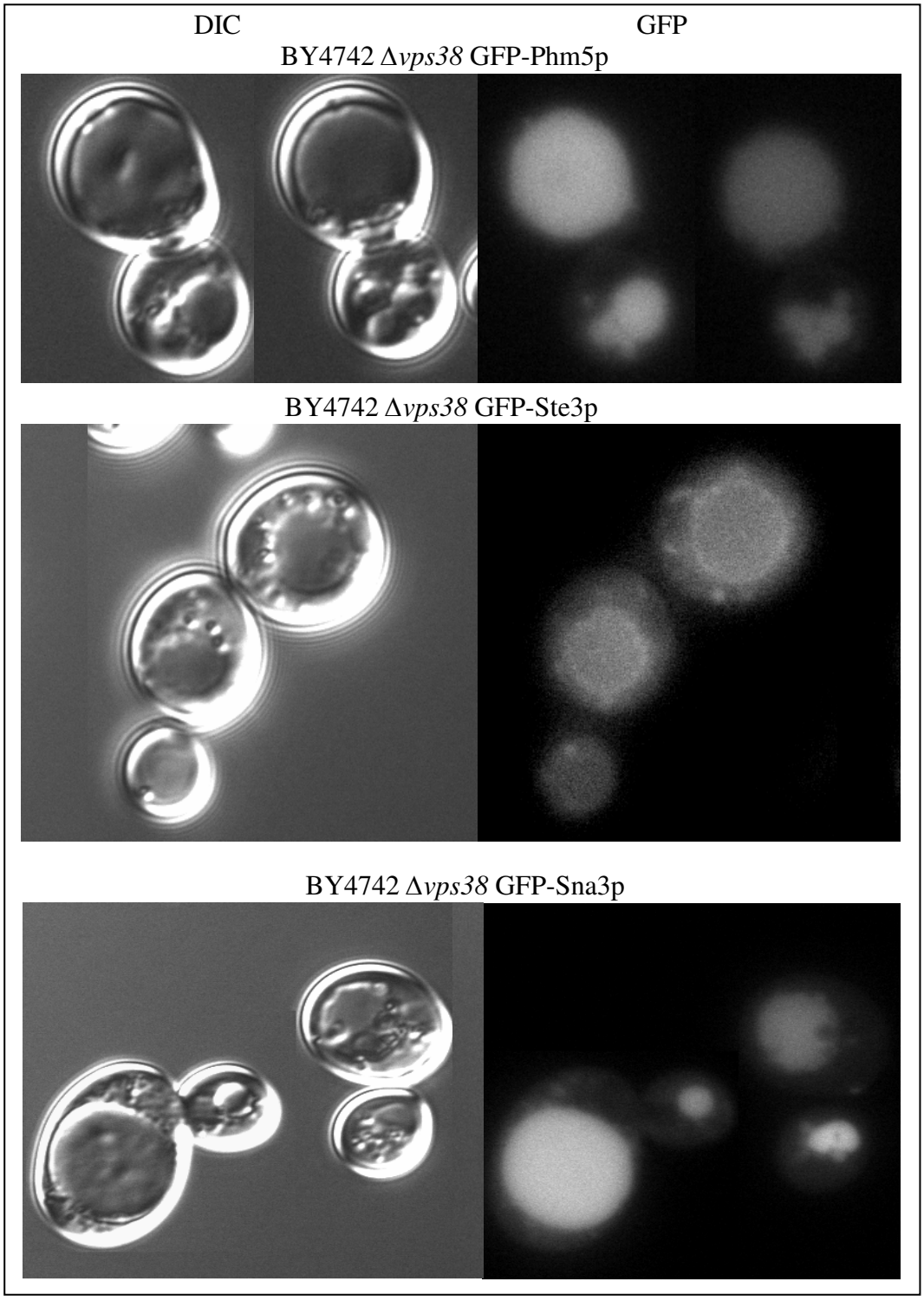

Figure 3.4.6: *In vivo* localization of GFP-Phm5p, GFP-Ste3p and GFP-Sna3p in Δ*vps38* cells.

BY4742 Δ*vps38* GFP-Phm5p, BY4742 Δ*vps38* GFP-Ste3p and BY4742 Δ*vps38* GFP-Sna3p cells were grown overnight in SC-Ura-Meth medium with 2% glucose to 0.6 OD_{600nm}. The cell culture was washed once in fresh media and resuspended in MES buffer pH 5.6 and visualized using DIC and GFP fluorescence microscopy. The images were processed on Photoshop.

Figure 3.4.6 shows 1) only a component of the endocytic sorting machinery is recycled via retrograde trafficking since only GFP-Ste3p is partially mis-localized to the vacuole membrane in Δ*vps38* cells, but not Phm5p or Sna3p and 2) possibly the recycled component is constantly exchanged between TGN, PVE and the vacuole membrane.

AP-3 pathway is crucial in regulating heterotypic fusion in 2 ways; 1) SNAREs, Vti1p and Vam3p are trafficked through this pathway and 2) Yck3p trafficking to the vacuole through this pathway results in phosphorylation of Vps41p and consequent disassociation.

Hence localization of cargo was investigated in Δ*apl5* cells (Figure 3.4.7) and Δ*apl5*Δ*vps38* cells (Figure 3.4.8).

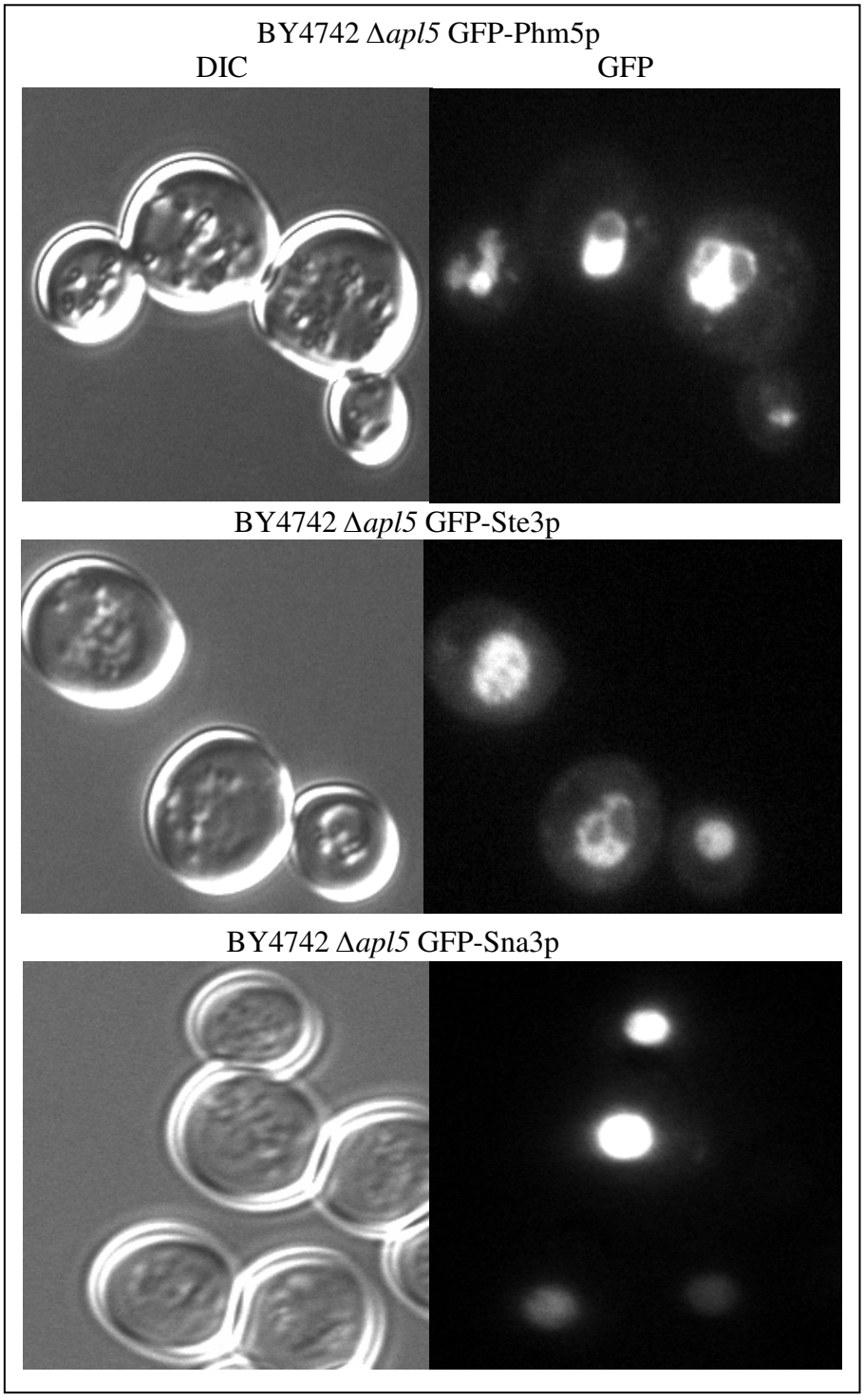

Figure 3.4.7: *In vivo* localization of GFP-Phm5p, GFP-Ste3p and GFP-Sna3p in Δ*apl5* cells.

BY4742 Δa*pl5* GFP-Phm5p, BY4742 Δ*apl5* GFP-Ste3p and BY4742 Δ*apl5* GFP-Sna3p cells were grown overnight in SC-Ura-Meth medium with 2% glucose to 0.6 OD_{600nm}. The cell culture was washed once in fresh media and resuspended in MES buffer pH 5.6 and visualized using DIC and GFP fluorescence microscopy. The images were processed on Photoshop.

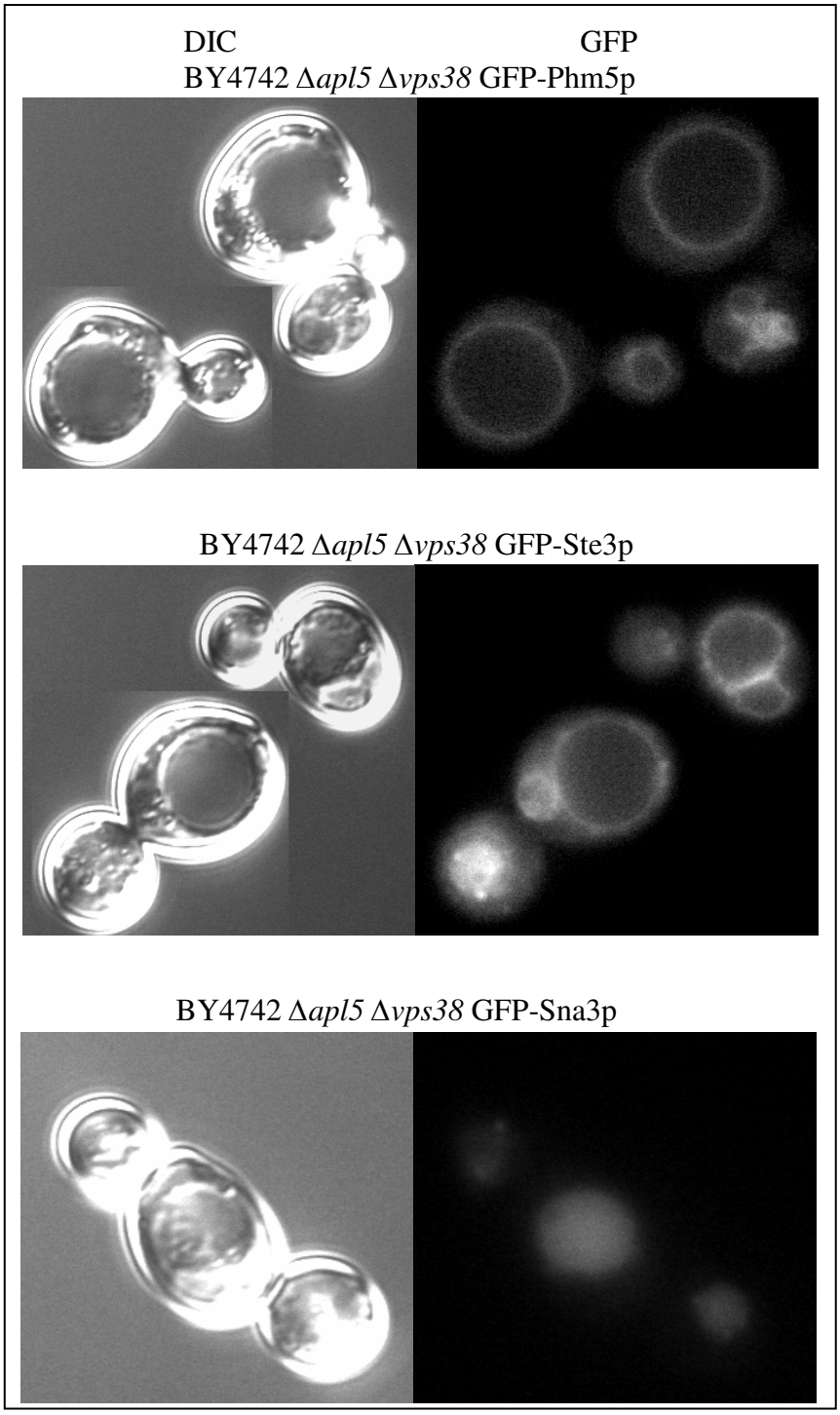

Figure 3.4.8: *In vivo* localization of GFP-Phm5p, GFP-Ste3p and GFP-Sna3p in Δ*apl5* Δ*vps38* cells.

BY4742 Δ*vps38* Δ*apl5* GFP-Phm5p, BY4742 Δ*vps38* Δ*apl5* GFP-Ste3p and BY4742 Δ*vps38* Δ*apl5* GFP-Sna3p cells were grown overnight in SC-Ura-Meth medium with 2% glucose to 0.6 OD_{600nm}. The cell culture was washed once in fresh media and resuspended in MES buffer pH 5.6 and visualized using DIC and GFP fluorescence microscopy. The images were processed on Photoshop.

Although vacuole size in Δ*apl5* cells is small, GFP-Phm5p and GFP-Ste3p mis-localization in Δ*apl5* cells is obvious (where the GFP is observed on the vacuole membrane rather than the vacuole lumen).

This becomes more prominent in Δ*apl5* Δ*vps38* cells due to the vacuole size, where GFP-Ste3p and GFP-Phm5p but not GFP-Sna3p, localize to the vacuole membrane rather than the lumen. This indicates 1) Sna3p sorting is distinct from Phm5p and Ste3p and 2) MVB sorting of Sna3p is not under the influence of any regulatory proteins influencing PtdIns(3,5)P_2 levels.

Since Sna3p is believed to be an Rsp5p adapter protein (Macdonald, Stringer et al.) and it is not yet certain whether Sna3p MVB sorting depends on its ubiquitination or not, it would be interesting to observe the localization of GFP-Sna3p, GFP-Ste3p and GFP-Phm5p in Δ*doa4* cells in order to establish whether the differences observed are due to the differences in their ubiquitination or not? (Figure 3.4.9)

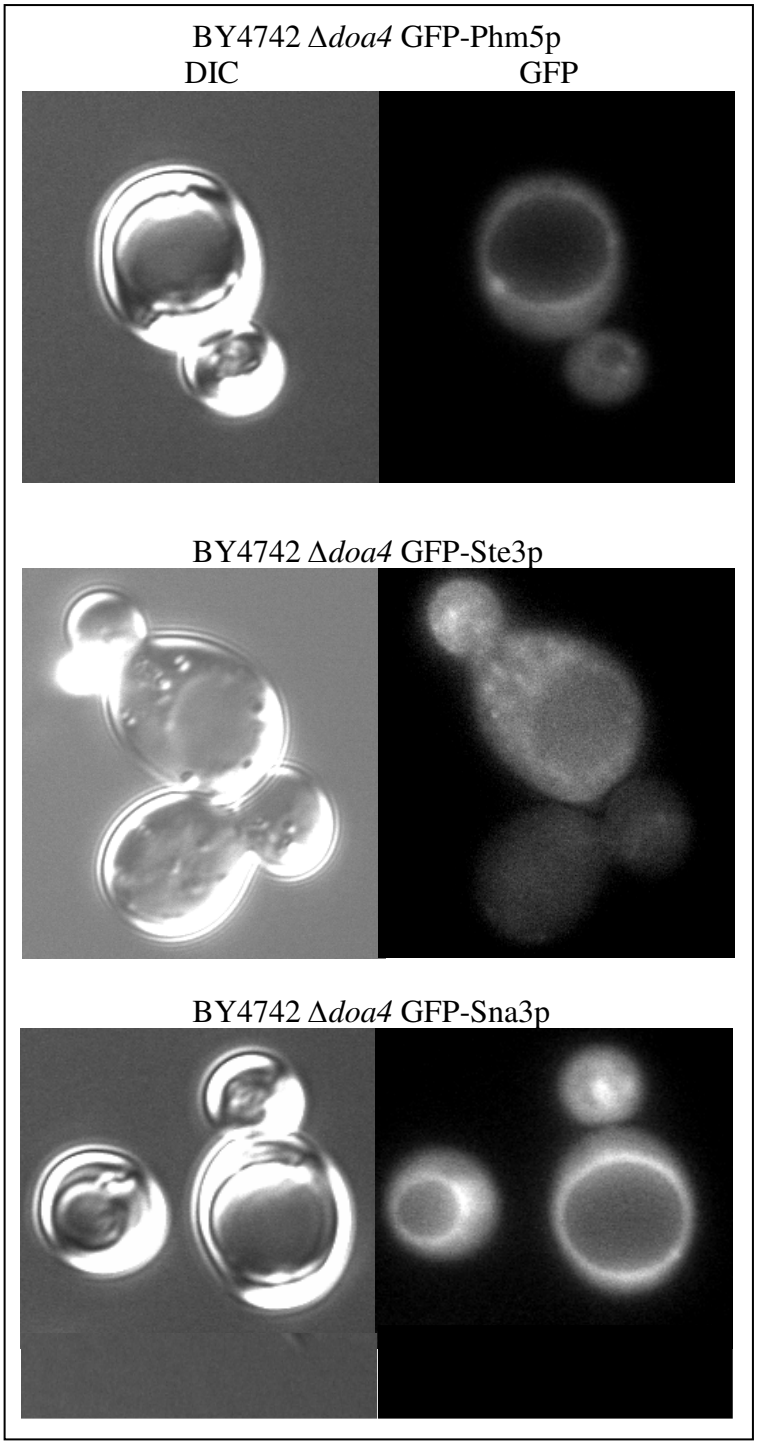

Figure 3.4.9: *In vivo* localization of GFP-Phm5p, GFP-Ste3p and GFP-Sna3p in Δ*doa4* cells

GFP-Phm5p, GFP-Ste3p and GFP-Sna3p was expressed in BY4742 *doa4*::KAN cells and successful transformants were grown in SC-Ura-Meth + 2 % glucose to 0.6 OD_{600nm} and washed once in fresh media and resuspended in MES buffer pH5.6 and examined microscopically using GFP-filter.

Figure 3.4.9 shows that Δ*doa4* cells exhibit defects in MVB sorting of all 3 cargo proteins indicating that 1) deubiquitination of cargo is crucial for efficient MVB sorting 2) possibly a very high turnover/degradation of Ubiquitin in Δ*doa4* cells leads to such defects and 3) Ste3p relies on Doa4p for its sorting in multiple ways whereas Phm5p and Sna3p are possibly mis-sorted due to high Ubiquitin turn-over.

Since most previous findings indicate that 1) PtdIns(3,5)P_2 levels are involved in regulating a complex which acts at a later stage in MVB sorting (Odorizzi, Babst et al. 1998), 2) Δ*fab1* cells are suggested to show premature deubiquitination (Stringer and Piper), and 3) Doa4p is a deubiqutinating enzyme, which is particularly and specifically involved in MVB sorting and localizes to PVE (Ren, Pashkova et al. 2008), therefore Doa4p becomes one of the most likely candidates for PtdIns(3,5)P_2 dependent regulation of MVB sorting. Hence co-localization of GFP-Doa4p with RFP-Snf7p in wild type and Δ*fab1* cells was investigated in order to verify this hypothesis (Figure 3.4.10).

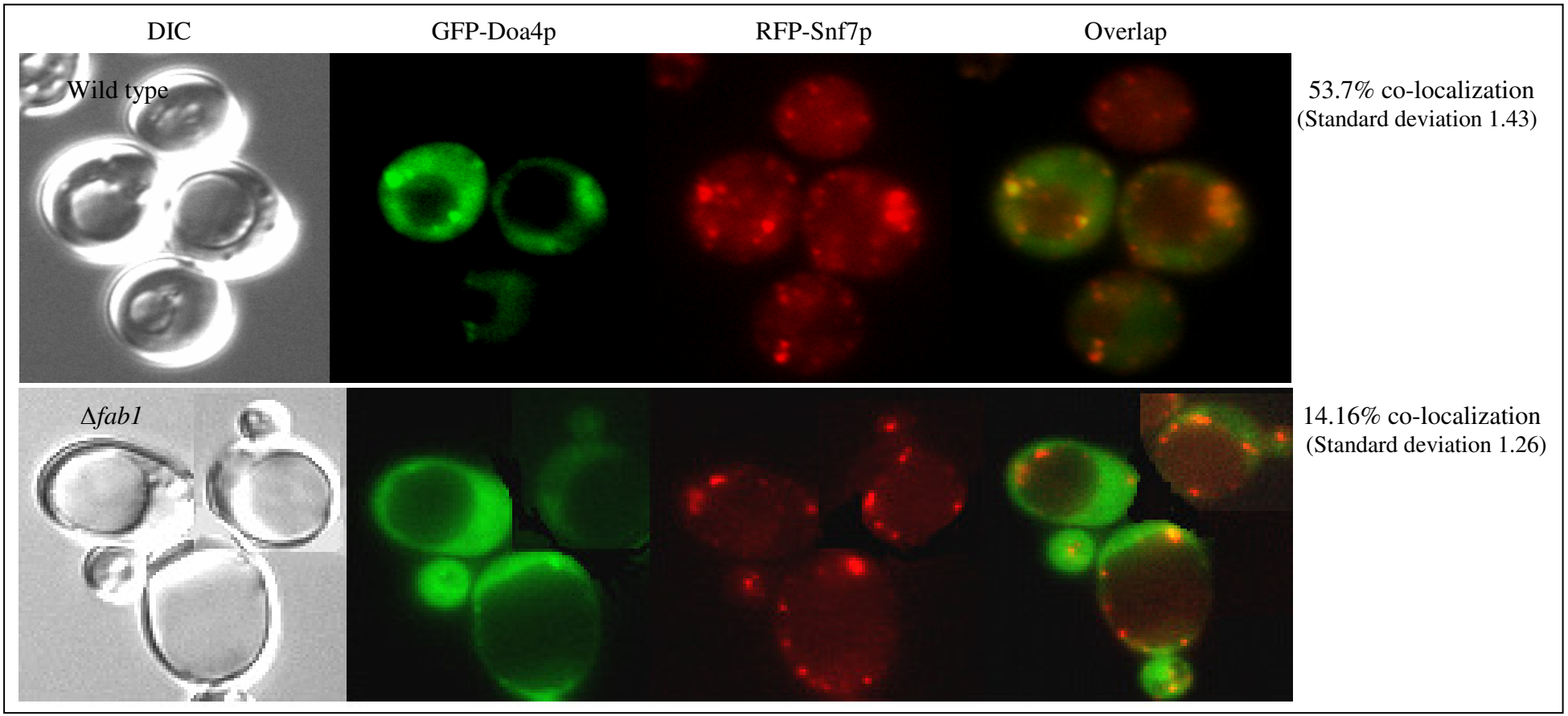

Figure 3.4.10: *In vivo* co-localization of RFP-Snf7p with GFP-Doa4p in wild type and Δ*fab1* cells.

BY4742 RFP-Snf7p GFP-Doa4p and BY4742 Δ*fab1* RFP-Snf7p GFP-Doa4p cells were grown in selective media + 2 % glucose to 0.6 OD_{600nm} and washed once in fresh media and resuspended in MES buffer pH5.6 and examined microscopically using GFP-filter. The images were processed in Photoshop.

Figure 3.4.10 indicates that GFP-Doa4p co-localizes with RFP-Snf7p in wild type cells whereas most of GFP-Doa4p is cytosolic in Δ*fab1* cells; although few very faint GFP-Doa4p punctae which co-localize with RFP-Snf7p are observed. This indicates that possibly Doa4p localization depends on other proteins (a protein complex?) requiring PtdIns(3,5)P_2 for their localization/s subsequently resulting in protein-protein interactions essential for MVB sorting.

If this is true then PtdIns(3,5)P_2 requirement cannot be bypassed by redundant levels of the lipid as in Δ*vac7* cells; therefore localization of GFP-Doa4p was investigated in Δ*vac7* cells (3.4.11A). Nonetheless, in order for this hypothesis to be true, it was also important to note the localization of GFP-Doa4p in Δ*atg18* cells, where PtdIns(3,5)P_2 levels are very high (3.4.11B).

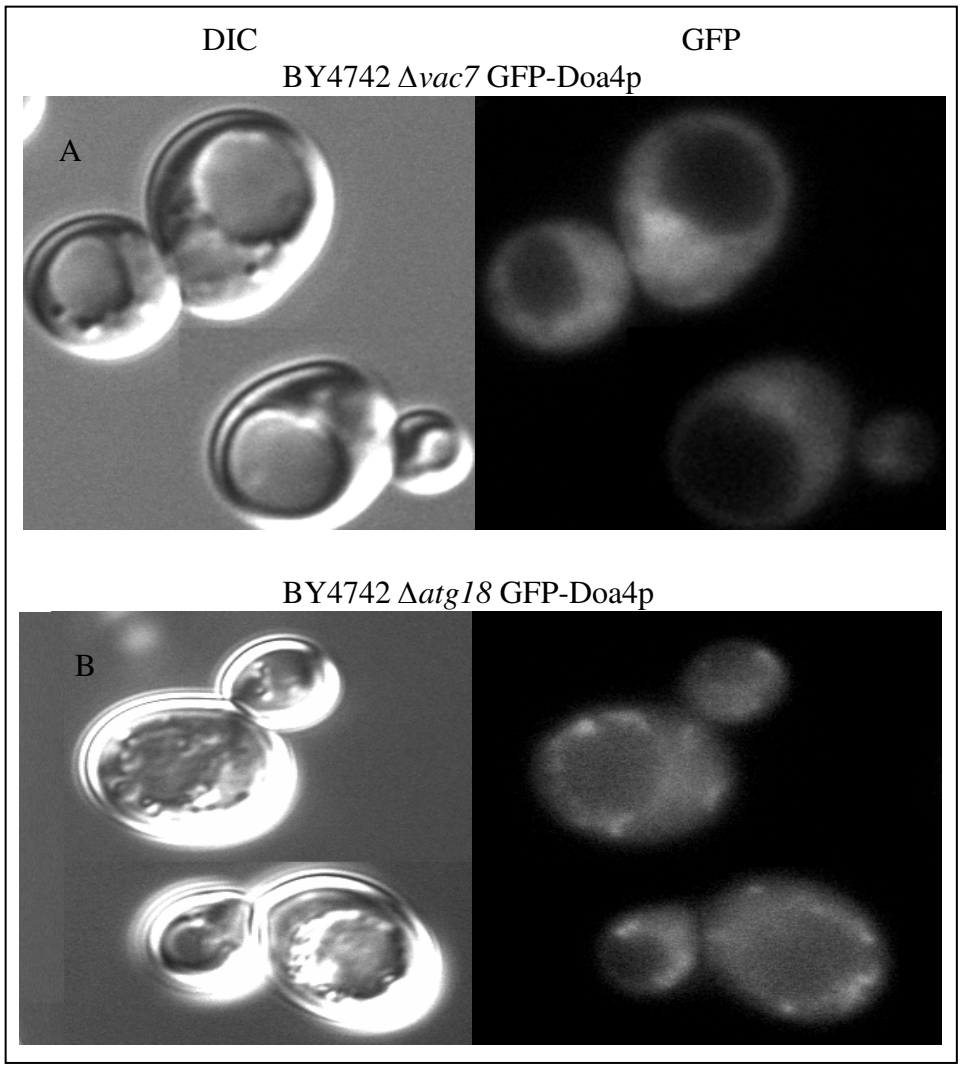

Figure 3.4.11 A/B: *In vivo* localization of GFP-Doa4p in Δ*vac7* and Δ*atg18* cells.

GFP-Doa4p was expressed in BY4742 *vac7*::KAN and BY4742 *atg18*::KAN cells and successful transformants were grown in SC-Ura-Meth + 2 % glucose to 0.6 OD_{600nm} and washed once in fresh media and resuspended in MES buffer pH 5.6 and examined microscopically using GFP-filter.

Figure 3.4.11A/B shows that GFP-Doa4p localization is similar to wild type in Δ*atg18* cells and its localization is similar in Δ*fab1* and Δ*vac7* cells, therefore it is likely that Fab1p/PtdIns(3,5)P_2 regulates the Doa4p complex which effects MVB sorting, whereas Atg18p-Vac7p interaction on Ste3p sorting is not mediated through Doa4p. This suggests that PtdIns(3,5)P_2 dependent regulation of MVB sorting in *S. cerevisiae* occurs at multiple, distinct steps.

Chapter 4; Discussion

4.1 Localization of Atg18p

At the start of this project, Atg18p had been isolated in multiple studies, and was hypothesized to have biological roles in vacuole homeostasis, starvation induced autophagy, the Cvt pathway, and a number of other, less well defined processes that often centered around starvation responses (Dove, Piper et al. 2004; Proikas-Cezanne, Waddell et al. 2004; Xiong, Contento et al. 2005; Efe, Botelho et al. 2007; Obara, Sekito et al. 2008).

The only known molecular functions for Atg18p at that time were PtdIns(3,5)P_2 and PtdIns3*P* binding and protein-protein interactions with Vac7p and Atg2p (Efe, Botelho et al. 2007; Obara, Sekito et al. 2008). Since much of the available evidence emerging in 2008-9 was contradictory; especially with regard to phosphoinositide binding, it was decided to re-examine all earlier claims in our experimental systems, in order to try to reconcile the differences in the *in vivo* and *in vitro* binding preferences of Atg18p for phosphoinositides; *in vitro*, PtdIns(3,5)P_2 was clearly the preferred ligand whereas the *in vivo* localization of Atg18p seemed dominated by PtdIns3*P*.

Under various conditions, Atg18p localizes to PVEs (exponential growth and autophagy), vacuole membrane (exponential growth and salt stress), distinct punctae sites possibly autophagosomes (autophagy) and segregation structure (during vacuole inheritance).

Such a wide distribution, as well as the pleiotrophic phenotypes exhibited by the *Δatg18* strain always suggested that Atg18p participates in multiple apparently distinct processes; but that possibly, like the general trafficking machinery, this protein is likely to be regulating one mechanistically similar step in each of these processes.

Although the localization of Atg18p has been investigated in many studies (Dove, Piper et al. 2004; Krick, Henke et al. 2008) yet most have catalogued the changes in localization that occur, without providing any insight into the mechanism of such shifts.

The aim of this study was to try and resolve this issue, and to find novel binding partners for Atg18p that may shed further light on this protein's actual role.

In 2008-9 a fairly simple model was emerging for Atg18p function; PtdIns(3,5)P_2, which is present at levels approximating 0.1% of total Inositol lipids in unstressed, exponentially growing yeast cells, allowed Atg18p to interact dynamically with the vacuole membrane whereby much of the protein was on the tonoplast but a substantial pool was also found in the cytosol (Dove, Piper et al. 2004; Efe, Botelho et al. 2007; Krick, Henke et al. 2008).

In *fab1* mutants, this vacuolar pool was abolished; and the same was true of *vac7* and *vac14* mutants. These latter observations were initially no surprise since both Vac7p and Vac14p had long been known as essential co-factors for normal Fab1p activity; however, when the Emr group dimerised Atg18p artificially, they

discovered that the Atg18p-Atg18p homodimer could stably interact with the vacuole membrane in the absence of PtdIns(3,5)P_2 or PtdIns3*P*, but only provided that Vac7p was still present on the tonoplast (Efe, Botelho et al. 2007). This suggested a direct protein-protein interaction between Atg18p and Vac7p existed and this was later confirmed by physical interaction tests.

Later studies suggested that the GFP-Atg18p punctate structures in exponentially growing cells were Snf7p positive PVEs; an endosomal compartment usually situated adjacent to the vacuole. Localization to these compartments was largely thought to be the result of binding to PtdIns3*P* because these punctae were retained in a *Δfab1* strain but lost in a *Δvps34* mutant (Proikas-Cezanne, Ruckerbauer et al. 2007; Proikas-Cezanne and Pfisterer 2009). It is also important to note that even the best co-localizations suggest only ~40-50% of the GFP-Atg18p punctae to be PVEs; the identity of the other ~50% has never been resolved, though Atg18p's association with these unidentified structures is also PtdIns3*P* dependent as they are lost in *Δvps34* mutants.

Under starvation conditions, Atg18p loses its vacuolar localization, and the number of punctate structures was reported to increase but change from Snf7p positive endosomes to Atg8p positive PAS (Obara, Sekito et al. 2008). This shift from vacuolar to PAS localized Atg18p was found to require Atg14p, because this protein re-directs some of the PtdIns 3-kinase Vps34p from the sites where PtdIns3*P* is made in exponentially growing cells (TGN, PVEs and the vacuole) towards PAS. This relocalization of Atg18p also coincides with the 'shutting off' of the Fab1p pathway; levels of PtdIns(3,5)P_2 slightly decline in starved cells, though not enough

to explain the loss of membrane binding of Atg18p. In addition, during starvation mode, Fab1p no longer responds to hyper-osmotic stress with the massive increases in PtdIns(3,5)P_2 that can be observed to occur in exponentially growing cells, where PtdIns(3,5)P_2 levels can rise as much as 30 fold within 10 minutes, beginning seconds after the initiation of a salt shock. Neither the mechanism of the relocation of Atg18p to the PAS nor the 'switching off' of Fab1p have ever been understood but what is observed at the whole cell level is that vacuoles of starved cells often lose their 'bunch of grapes' morphology and merge together to become one single, unlobed structure.

This study of Atg18p localizations have largely confirmed the above model but have extended it in two important ways.

The first novel observation made in this study is the data suggesting that Atg18p can be recruited to the vacuole during osmotic stress, largely independently of PtdIns(3,5)P_2 (Figure 3.1.9C) and possibly also of PtdIns3*P* (Figure 3.1.11C).

Since osmotic shock is relatively lightly studied with respect to Atg18p, as most work has focussed on autophagy, this has never been reported before and is surprising since it has widely been anticipated that the main function of the vast elevation in PtdIns(3,5)P_2 levels that follow hyper-osmotic stress, is to drive Atg18p to the vacuole membrane to carry out the rapid scission one observes during the yeast response to salt stress. To find that Atg18p only partially requires lipid-binding is puzzling.

Although one caveat to the data in this study should be stated immediately; the GFP constructs used here are capable of dimerising because of a known interfacial association between pairs of GFP-molecules. Since homodimerization of GFP would also dimerise the attendant Atg18p molecules, and given that Atg18p dimerization is known to allow this PROPPIN to bypass the need for PPIn in order to interact with membranes, it is possible that this data is artefactual. However, since true dimerization of Atg18p leads to constitutive vacuolar association, even in unstressed cells (note that this was not observed in this study Figure 3.1.9A) it can reasonably be said that the dimerization is not happening substantially in unstressed cells. The situation in stressed cells is not quite so simple; the dehydration of yeast by the external osmolarity might increase the effective concentration of GFP to the extent where homodimers are more favoured, leading to vacuolar binding in the absence of PPIn. However since the binding of Atg18p to vacuole during salt stress fails to occur in *Δvac7* cells (Figure 3.1.15), caution is needed in interpreting these data.

The second important finding to emerge from this study is the discovery that Vac7p trafficks away from the vacuole during autophagy (Figure 3.1.16) to reside in the Golgi. This is important, because, as was stated earlier, Vac7p is both a Fab1p activator and is required for Atg18p to associate with the vacuole. Since both Fab1p activity and Atg18p vacuolar localization are somehow 'switched off' by unknown means during autophagy, this observation offers a single explanation for both phenomena. As Vac7p is absolutely required for full Fab1p activity, especially in response to hyper-osmotic stress, its partitioning away from Fab1p, into a different compartment offers an immediate mechanism for the down-regulation of both

constitutive and stress inducible Fab1p activity that is observed in starved cells or cells in the G_0 phase of the cell cycle.

In addition, the loss of vacuolar membrane association of Atg18p during autophagy has also never been adequately explained because starved cells retain substantial levels of PtdIns(3,5)P_2 when measured at the level of the whole cell. The only uncertainty surrounding this latter statement is whether this residual PtdIns(3,5)P_2 in starved cells is vacuolar or not? This question won't be fully answered until a proper probe for this lipid is established. However, what is clear is that vacuolar association of Atg18p is an example of co-incidence detection, where neither PtdIns(3,5)P_2 nor Vac7p binding alone is of sufficient strength to confer tonoplast localization to Atg18p, but that together the protein-lipid and protein-protein interactions provide an avidity effect that drives the protein to the membrane. The data in this study also shows that Vac7p leaves the vacuolar compartment during autophagy, simultaneously lowering PtdIns(3,5)P_2 levels and removing an important protein ligand for Atg18p from the vacuole surface. The inevitable consequence of these changes would be predicted to be a loss of vacuolar association of Atg18p and its relocation to the PtdIns3*P* rich PAS and PVEs; exactly what is observed (Figure 3.1.5/6).

What causes Vac7p translocation during autophagy is not clear from this work, though it appears to revolve around PtdIns3*P* synthesis, since Atg18p remains vacuolar in *Δatg14* cells (Figure 3.1.13), Δ*vps38* cells (Figure 3.1.14) and Δ*ymr1* cells (Figure 3.1.20) as in Δ*vac7* cells (Figure 3.1.15).

The data also indicates that the loss of vacuolar association of Vac7p during autophagy occurs via recycling from vacuole to PVE and from PVE to Golgi, which is blocked in *Δvps34* cells (Figure 3.1.18) and Δ*vps38* cells (Figure 3.1.14), suggesting that Vac7p takes the Fab1p mediated retrograde pathway away from the vacuole and then is sorted back to the Golgi via a retromer like step. Low levels of PtdIns(3,5)P_2 (50% less) in *AP-1* deletions reciprocate this hypothesis (Cowles, Odorizzi et al. 1997; Panek, Stepp et al. 1997).

Intriguingly, one of the Atg18p point mutants isolated in this study; Atg18p^{K266T} also appears to relocalize to the Golgi, but this time under exponential growth conditions (Figure 3.2.17). Could this be a hint that although the steady-state localization of Vac7p is vacuolar, it continuously recycles between the vacuole and the Golgi and this mutant is somehow failing to disassociate from it; further work is needed to resolve this suggestion?

It is also indicated by this study that Vps41p displacement from the vacuole could also be affected by any such Vac7p recycling or Atg18p-Vac7p interactions especially in response to stress signals, which helps to explain vacuole morphology during these processes (discussed separately in section 4.5).

Atg18p modification in response to various stress signals and its lipid binding in response to this modification could be another indicator towards understanding the regulation of vacuole morphology in a Atg18p mediated fashion (discussed separately in section 4.2)

Figure 5.1 represents a putative cycle of Atg18p localizations under autophagy and salt stress conditions.

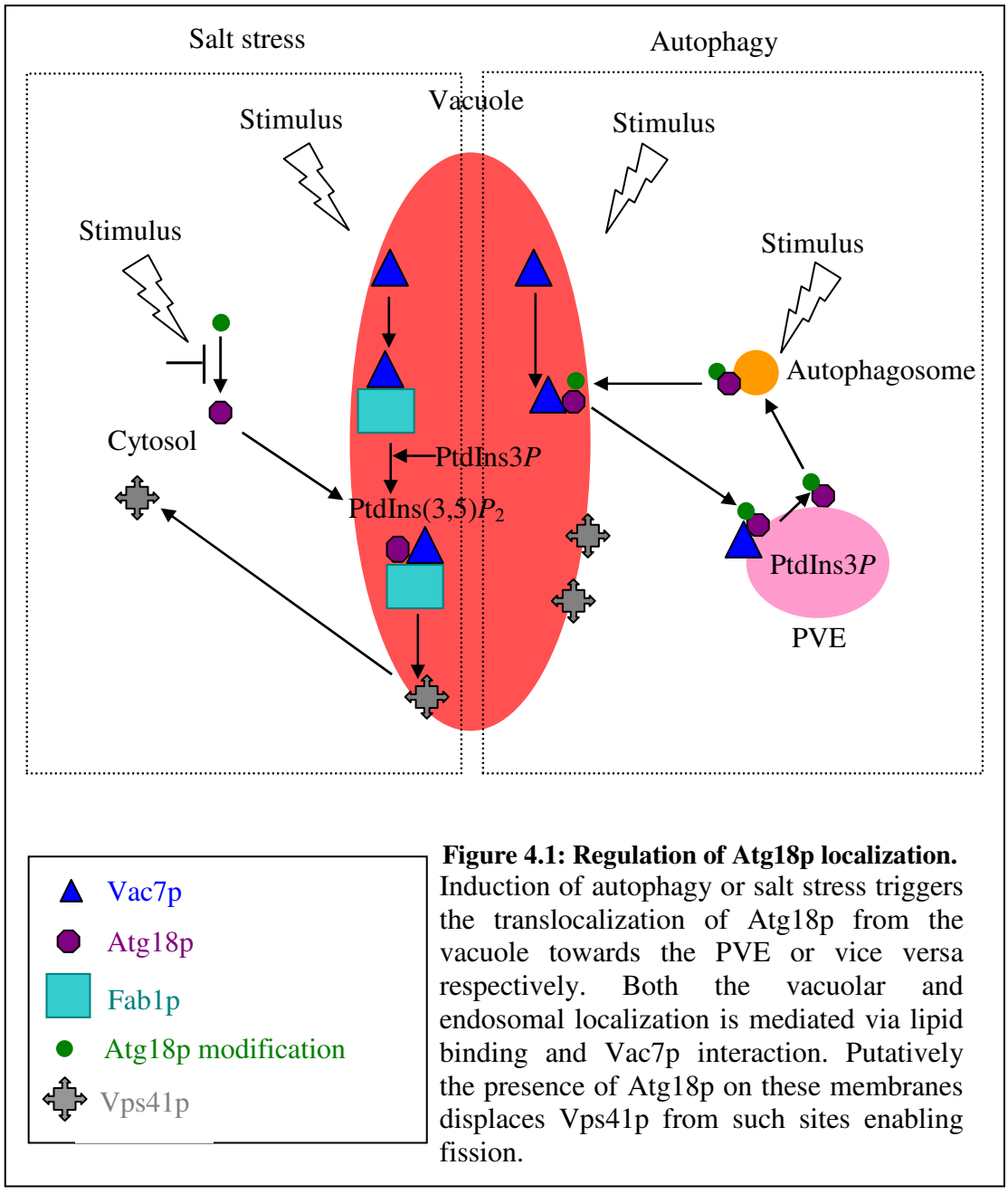

Figure 4.1: Regulation of Atg18p localization. Induction of autophagy or salt stress triggers the translocalization of Atg18p from the vacuole towards the PVE or vice versa respectively. Both the vacuolar and endosomal localization is mediated via lipid binding and Vac7p interaction. Putatively the presence of Atg18p on these membranes displaces Vps41p from such sites enabling fission.

Chapter 4; Discussion

4.2 Atg18p Lipid binding motifs

Atg18p is a WD β-propeller PROPIN protein and hence a bonafide Phosphoinositide binding protein which binds PtdIns(3,5)P_2 and PtdIns3*P*. The FRRG motif is a known component candidate of the lipid binding motif in Atg18p; 1) due to being highly conserved in all PROPPINs (Dove, Piper et al. 2004), 2) its disruption/mutation leads to a complete loss of membrane localization of Atg18p 3) >40 fold decrease *in vitro* lipid binding by the mutant protein and 4) defects in regulation of vacuole morphology as indicated by a large vacuole phenotype exhibited by the mutant.

In this study it was observed that Atg18p^{FTTG} is cytosolic and partly nuclear, accompanied by a large vacuole (Figure 3.2.2/3.2.3).

As vacuole morphology defects are unanimously reported, it is quite possible that either Atg18p^{FTTG} sequesters an unidentified protein within the cytosol, resulting in increased fusion and decreased retrograde trafficking from the vacuole, and/or putatively up-regulates Vps41p enrichment on the vacuole resulting in increased fusion. Nonetheless, it was observed that Atg18p^{FTTG} formed a few punctae during rapamycin induced autophagy.

This is also reported in other studies and these sites are postulated to be PAS(Obara, Sekito et al. 2008), indicating that some residual autophagic activity still persists in FTTG mutants. Since lipid binding is disrupted in this mutant this reminiscent

punctae localization could be a result of Atg18p-Atg8p binding which is acknowledged to be independent of lipid binding (Stromhaug, Reggiori et al. 2004).

However, the effects of this mutation on Cvt pathway are controversial (Stromhaug, Reggiori et al. 2004; Krick, Muehe et al. 2008), which could invariably be due to experimental conditions rather then the specific lipid binding of the mutant or more plausibly due to differences in nature of Atg18p interactions in both the processes.

Nonetheless, Atg18p^{FTTG} also forms punctae under salt stress, indicating that formation of such complexes involved in regulation of vacuole morphology (on the vacuole membrane or else where) is triggered by PtdIns(3,5)P_2 synthesis and possibly due to lack of lipid binding by FTTG mutant, it is not recruited correctly to the destined membrane. This also affirms the hypothesis that Atg18p^{FTTG} possibly sequesters another protein/s in a lipid mediated fashion.

On the contrary, Atg18p^{FTTG}-FYVE is vacuolar and punctae under exponential growth conditions, becomes patchy with no apparent vacuole during autophagy, and attains punctae localization in the cytosol with no vacuole fragmentation under salt stress conditions (Figure 3.2.5).

If Atg18p-PtdIns3*P* binding is required for the putative shuttling of the membrane protein Atg9p (Reggiori et al., 2004) during autophagy then, in the absence of the Atg18p-PtdIns3*P* interaction, the delivery of membrane to the growing autophagosomes is impeded resulting in autophagy defects.

This holds valid for Atg18p^{Wt} in Δ*atg14* cells (Figure 3.2.5) where a substantial decrease in punctae formation is observed, however Atg18p^{FTTG}-FYVE appears to localize on membranous structures in these Δ*atg14* cells (Figure 3.2.6). If these membranous structures are vacuoles then it indicates that Atg18p shift off the vacuole requires Atg14p mediated PtdIns3*P* synthesis whereas if these are PAS sites then it suggests that this chimeric is unable to disengage from PAS due to the attached FYVE domain; however further work is required to derive a conclusion.

Since autophagy proteins are required to disassociate from PAS for an efficient fusion of autophagosome with the vacuole, it can be envisioned that Atg18p^{FTTG}-FYVE possibly also fails to do so which partially explains the reduced vacuole size in these cells unlike wild type cells.

However the disassociation of autophagy proteins is linked to PtdIns3*P* turnover once the autophagosome has formed (Cebollero, van der Vaart et al.), in which case it is more likely that Atg18p^{FTTG}-FYVE localization is possibly linked to Atg18p-Atg8p interaction. However unlike Atg18p^{FTTG}, this chimeric is putatively interacting with other PtdIns3*P* rich sites due to the attached FYVE domain and hence localizes aberrantly. This could also explain the large vacuole in Atg18p^{FTTG} (Δ*atg18* cells) but a rather lack of visible vacuole in Atg18p^{FTTG}-FYVE (Δ*atg18* cells).

Punctae formation within the cytosol during salt stress in Δ*atg18* cells by both Atg18p^{FTTG}FYVE (Figure 3.2.5C) and Atg18p^{FTTG} (Figure 3.2.2C) indicates that these mutants are possibly modified in a similar fashion in compliance with cell's

response to salt stress, but fail to localize correctly and hence show defects in vacuolar fragmentation; indicating that Atg18p-PtdIns(3,5)P_2 binding is a prerequisite for vacuolar fragmentation.

Hurley et al (2012) report 2 separate PtdIns3*P* and PtdIns(3,5)P_2 binding sites in *K. lactis* Hsv2p, a PROPPIN sharing approximately 70% homology with Atg18p. These 2 sites span blades 5 and 6 and interestingly the 2 Arginines in the FRRG motif mediate 2 distinct lipid binding pockets. His178, Asn180, Ser198, Thr202, Arg205, Glu217, and Arg219 of propeller blade 5 contribute to site 1 whereas Arg220, Ser243, Lys245, Thr247, and His249 in blade 6 make up site 2. Independent mutations, R219A (site 1) and R220A (site 2) result in complete loss of PtdIns3*P* binding while mutations in Site 1 show no effect on PtdIns(3,5)P_2 binding (despite elimination of PtdIns3*P* binding). However, site 2 mutation R220A completely perturbs PtdIns(3,5)P_2 binding whereas mutations K285D/K288D, which adjoin site 2, show decreased membrane binding (Baskaran, Ragusa et al.).

If this is true then why does FTTG mutant, with disrupted PtdIns3*P* and PtdIns(3,5)P_2 binding sites, retain much reduced yet partial PtdIns(3,5)P_2 binding *in vitro*? (Dove, Piper et al. 2004)

This could be explained on the basis of structural differences between *S.cerevisiae* Atg18p and *K.lactis* Hsv2p and taken into account that possibly the rest of the residues in these 2 sites and the hydrophobic C-terminal residues Tyr367, Tyr381 and Phe398 (crucial for membrane residence) participate in arbitrating the residual PtdIns3*P* and PtdIns(3,5)P_2 binding in Atg18p; a residual autophagic activity which

is reported in case of double mutants (Δsite1 Δsite2) (Baskaran, Ragusa et al.) also supports this hypothesis.

It is also important to note that according to Hurley et al integrity of both binding sites is more important for PtdIns3*P* binding than PtdIns(3,5)P_2 binding, which largely relies on binding site 2.

Sequence homology between Atg18p and Hsv2p for sites 1 and 2 is depicted in Figure 4.2.1.

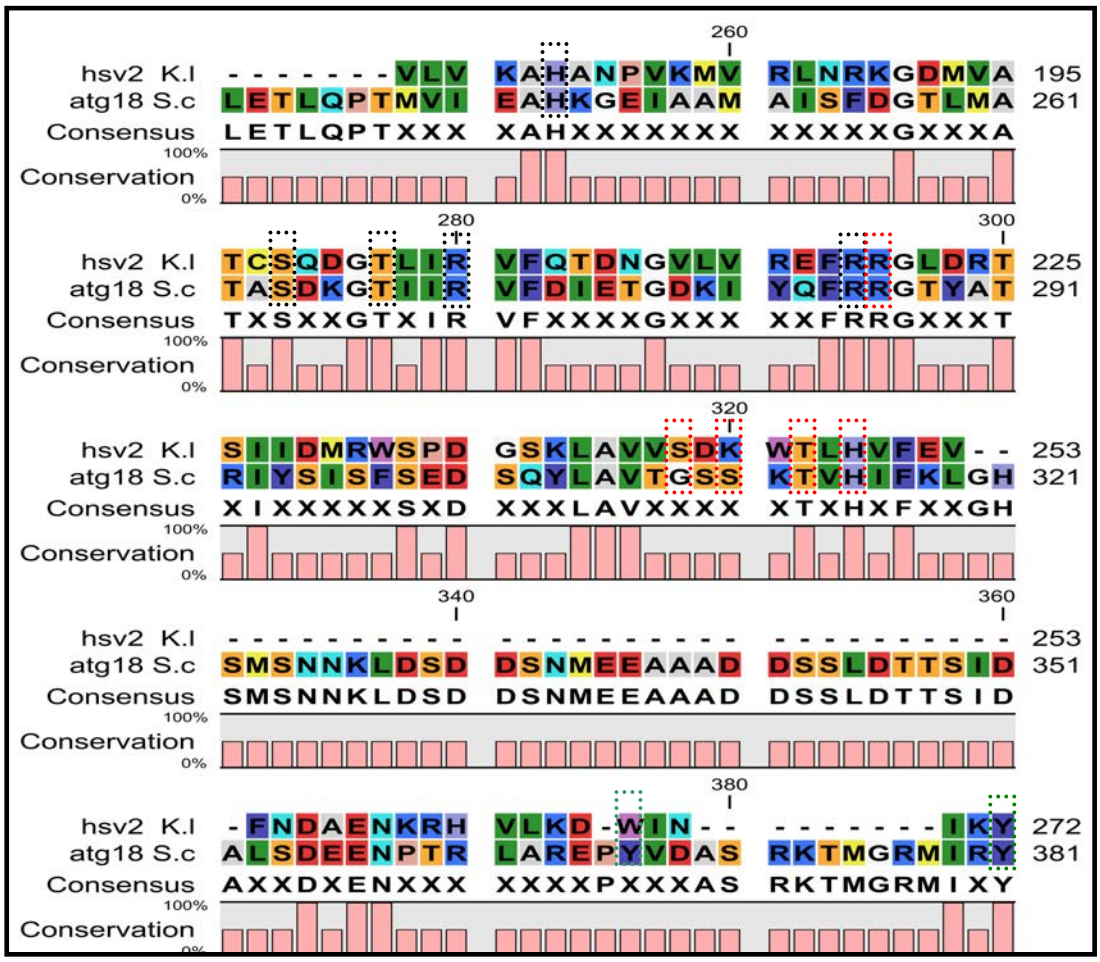

Figure 4.2.1: Homology mapping between Atg18p (*S.cerevisiae*) and Hsv2p (K.lactis)

Homologous residues contributing to Site 1 are circled in black while residues contributing to site 2 are circled in red. The hydrophobic residues known for membrane residence are circled green.

During this study the *in vivo* localizations (under various conditions) and *in vitro* lipid binding of Atg18p mutants (in the 5D β-sheet, close to FRRG motif) were studied and Figure 4.2.2 depicts these mutated residues in Atg18p and their corresponding residues in Hsv2p (*K.lactis*).

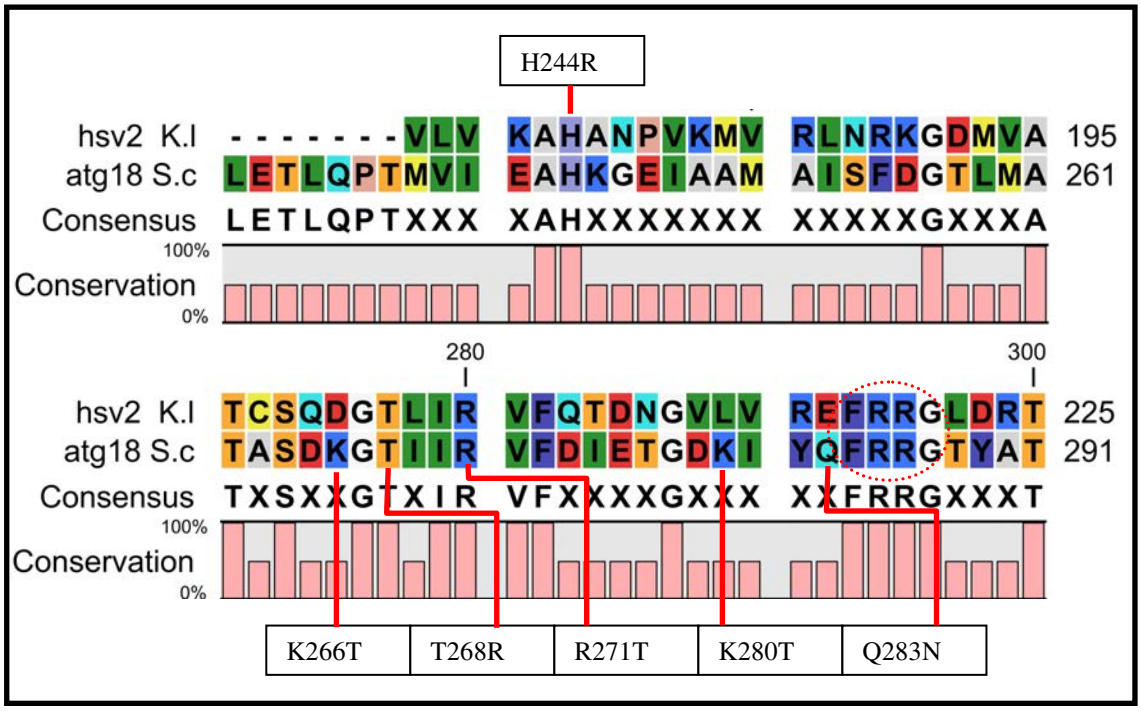

Figure 4.2.2: Atg18p point mutants.

Amino-acids mutated are denoted in boxes, whereas the FRRG motif is circled.

In vitro affinity of Atg18p^{FTTG} towards both PtdIns3*P* and PtdIns(3,5)P_2 is substantially reduced as obvious from the lipid dot blot assay (Figure 3.2.9) (in accordance with previous findings (Krick, Tolstrup et al. 2006) and Hurley et al model) (Baskaran, Ragusa et al.) yet this cannot be attributed to instability of FTTG mutant (Figure 3.2.8).

Hurley et al shows that mutations H244A and R271A (site 1) and R286A and H315A (site2) disrupt lipid binding in Atg18p and result in autophagy defects

Where as triple null mutants of sites 1, 2 and hydrophobic residues results in an additional complete loss of vacuolar localization. This indicates that membrane residence and protein-protein interactions of Atg18p can still persist in absence of its lipid binding, though to a much decreased level. This supports the observation that some residual Atg18p vacuolar localization is observed during salt stress in Δ*fab1* cells.

Hurley et al model also points out that Atg18p vacuolar localization is not much effected by disruption of lipid binding site 1. In compliance to this, mutant H244R (this study) shows much reduced *in vitro* PtdIns3*P* binding, as compared to the wild type, whereas mutants K266T, T268R, R271T, and K280T show increased PtdIns(3,5)P_2 binding (Figure 3.2.9).

Hurley et al also describes R271 to be important for lipid binding in site 1. This is in accordance with mis-localization of Atg18p^{R271T} (under exponential growth conditions) (Figure 3.2.21) but dot blot assay does not show substantial loss in PtdIns3*P* binding. Since Atg18p^{R271T} response to salt stress is only partially defective, whereas Atg18p^{H244R} (Figure 3.2.10C) has a much pronounced vacuole fragmentation defect, it indicates that despite both positions i.e H244 and R271 being described crucial for formation of site 1 (PtdIns3*P* binding), possibly position H244 is more critical for full osmotic response, or putatively there may be some differences between *K.lactis* and *S.cerevisiae* PtdIns3*P* binding sites.

If it is argued that PtdIns3*P* binding is necessary for Atg18p localization on PVE while PtdIns(3,5)P_2 binding is required for vacuolar recruitment of Atg18p, then

mutants H244R and R271T with reduced PtdIns3*P* binding should show defects reflecting this hypothesis.

Indeed, both these mutants do not disassociate from the vacuole membrane during autophagy reflecting defects in PtdIns3*P* binding. However, only Atg18p^{R271T} loses its punctae localization during exponential growth conditions (Figure 3.2.21) but not Atg18p^{H244R} (Figure 3.2.10); which does not lose its punctae localization in either Δ*atg18* or Δ*fab1* cells (Figure 3.2.13). This indicates that the affect of these mutations on lipid binding are slightly distinct.

Since both these mutants also show defects in vacuole fragmentation during salt stress, it indicates that either PtdIns(3,5)P_2 binding alone is not sufficient for vacuolar fragmentation or else these residues mediate protein-protein interactions in Atg18p.

Contrary to this, point mutants K266T, T268R, K280T and Q283N exhibit comparable to wild type, *in vitro* PtdIns(3,5)P_2 binding (Figure 3.2.9) and a large vacuole (except for mutant T268R where the vacuole is normal in size (Figure 3.2.19).

The large vacuole in these mutants could possibly be due to interactions of these proteins with some other protein affecting vacuole morphology.

Nonetheless, all of these mutants show normal response to salt stress in Δ*atg18* cells but not Δ*fab1* cells. Lack of fragmentation can be attributed to lack of PtdIns(3,5)P_2

in Δ*fab1* cells but reminiscent vacuolar localization of these mutants under such conditions suggests that these mutants also behave like wild type Atg18p.

Mutating hydrophilic residue to basic i.e T268R leads to punctae localization under exponential growth conditions in Δ*atg18* cells, although very faint vacuolar localization is also apparent. This mutant has a normal vacuole size and also exhibits normal response to osmotic shock (Figure 3.2.19). This position corresponds to T202 (site 1) in Hsv2p (*K.lactis*) but is described to have a lesser effect on lipid binding, justifying only a partial loss of localization by Atg18p^{T268R}.

On the contrary, this mutant in Δ*fab1* cells does not localize to the tonoplast during salt stress (Figure 3.2.20), unlike wild type and other mutants, which suggests that possibly protein interactions are more affected than lipid binding by this mutation.

According to Hurley et al, besides amino-acid residues bordering the FRRG motif (serving to anchor the D-3 of PtdIns3*P* and/or D-3 and D-5 of the PtdIns(3,5)P_2), the hydrophobic residues and the distance between the singly bonded, membrane-distal phosphoryl group and the membrane core also play a key role in determination of lipid binding; e.g putative D-5 binding to a PROPPIN would depend on the sequence variability in the loop harboring these hydrophobic residues. This could serve as an additional level of regulation and specificity. Hence Atg18p's specificity towards PtdIns(3,5)P_2 could infact depend on this loop (to accommodate the D-5 position) as well as its distance from the hydrophobic residues.

K. lactis Hsv2p is 339 whereas Atg18p is 500 amino-acids long, but residues making site 1 are spaced similarly amongst the 2 proteins, indicating that PtdIns3*P* binding pocket is much alike. Nonetheless, residues N180 and E217 in Hsv2p site 1, do not match up with residues in Atg18p, whereas S243 and K245 in Hsv2 site 2 have G309 and S311 in Atg18p respectively with neighboring S310 and K312 respectively (Figure 4.2.3).

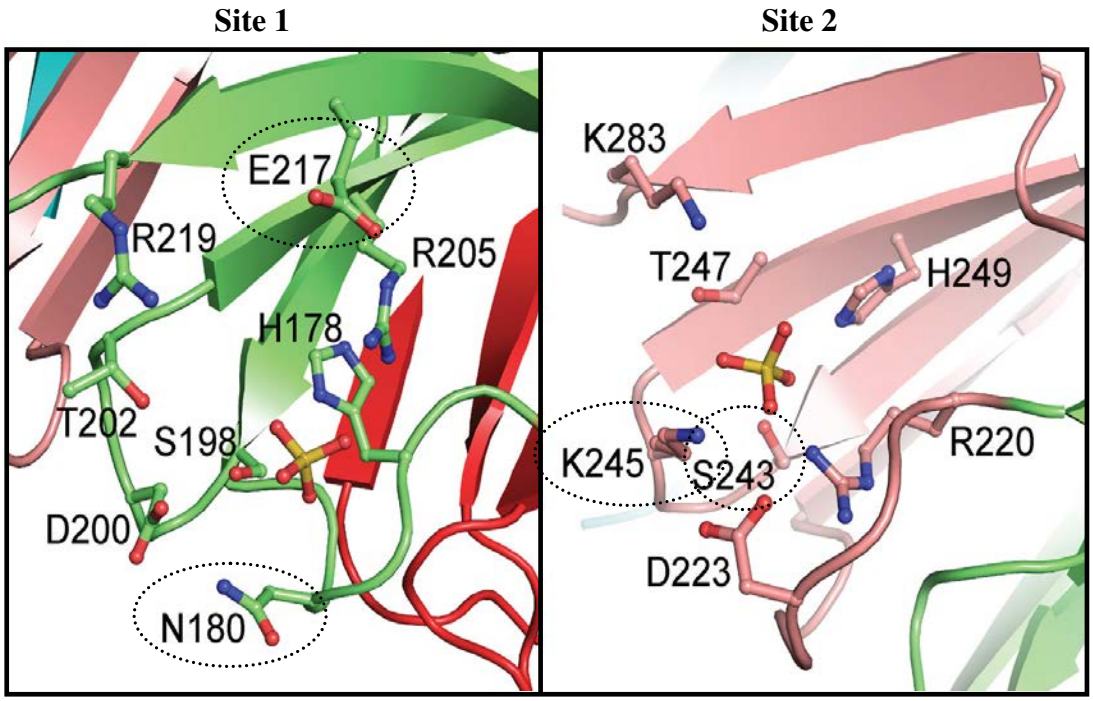

Figure 4.2.3: *K. lactis* Hsv2p lipid binding sites 1 and 2 (Baskaran, Ragusa et al. 2012).
The amino-acid residues which differ between Atg18p and Hsv2p binding sites 1 and 2 are circled.

These differences in real term would mean that lipid binding sites in Atg18p are slightly different from Hsv2p sites. As both residues (K245 and S243) are in a position to manipulate the bound phosphate, it is highly likely that shifting these 2 residues one place further could facilitate and render increased PtdIns(3,5)P_2 binding specificity.

Besides Hurley et al model, the best known PtdIns3*P* binding domains, namely FYVE domain [D-3 binding pocket (R(R/K)(R/K)HHCR)] and PX domain [D-3 binding pocket ((R/K) (R/K) (F/Y)] (Stahelin 2009) comprise of basic residues surrounded by hydrophobic residues, known to be crucial for membrane residence of such proteins.

Hence it is important to analyze the surrounding residues and their significance in such lipid binding interactions in Atg18p in order to make a comparison. The boxed letters in Figure 4.2.4 represent the 2 highly conserved basic motifs in Atg18p.

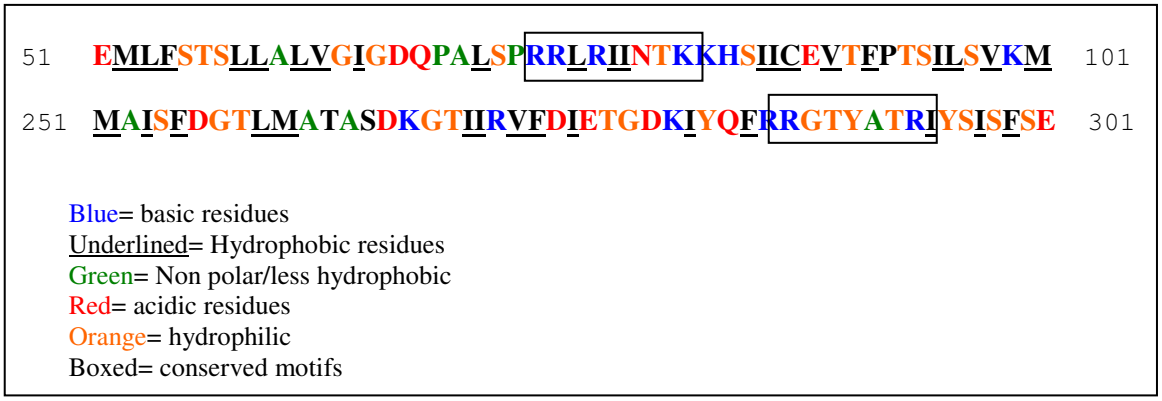

Figure 4.2.4: Atg18p sequence surrounding the 2 conserved basic motifs.

It is quite obvious that both the FRRG and SPRRLR motifs in Atg18p also lie in hydrophobic regions, which could facilitate membrane residence and therefore is not much discerning. But PtdIns3*P* itself is comparatively more hydrophobic than PtdIns(3,5)P_2. Hence more hydrophobic amino-acids immediately neighboring the basic residues in the PtdIns3*P* binding pocket would allow increased interaction between the protein and the lipid.

Atg18p^{SPSSLS} mutant localizes on tonoplast and as punctae under exponential growth conditions, although the localization is much reduced as compared to wild type. The punctae formation is also reduced during autophagy, but interestingly this mutant does not localize to the vacuole during salt stress (Figure 3.2.7). As SPRRLR motif is also a conserved motif in most PROPPINs it could be argued that it plays some role in lipid binding, specifically PtdIns(3,5)P_2.

If an analogy is made between Atg18p^{FTTG}-FYVE, Atg18p^{SPSSLS} and Atg18p^{FTTG} during salt stress, it is noted that they all localize as punctae, with defective vacuolar fragmentation under osmotic shock. Since the *in vitro* lipid binding of this mutant is reported to be only slightly reduced (Dove, Piper et al. 2004) therefore this motif either works in conjunction with FRRG motif (sites 1 and 2) or possibly it is a modification site responsible for modulation of FRRG binding sites 1 and 2.

This also aids in understanding the role of Atg18p in regulation of vacuole morphology in terms of blocking/displacing PtdIns3*P* binding proteins like Vam3p, from the vacuole during vacuolar fission/fusion cycles in response to a stimulus (discussed separately).

LC-CID-FT-MS data of Atg18p^{Wt} and Atg18p^{FTTG} indicates that both FRRG and SPRRLR sites lie in putative phosphorylation regions (Figure 4.2.5A and 4.2.5B). This is in accordance with FRRGT motif being postulated as a potential PKA phosphorylation site (Budovskaya, Stephan et al. 2005).

Locations (AA)	Phosphorylated Sites	HMM Bit Score	E-value	Catalytic Kinases	Predictive Models	
					HMMs	Logo
71	QPALSPRRL	5.3	1	Other-MDD	HMM	
71	QPALSPRRL	-6.5	58	MAPK	HMM	
288	FRRGTYATR	2.3	2.5	PKA	HMM	
289	RRGTYATRI	-2.6	23	PKA	HMM	

Figure 4.2.5A: ICMS data on putative Phosphorylation sites in Atg18p

Atg18p wild-type

MSDSSPTINFINFNQTGTCISLGTSKGFKIFNCEPFGKFYSEDSGGYAIVEMLFSTSLLALVGIGDQ
PALSPRRLRIINTKKHSIICEVTFPTSILSVKMNKSRLVVLLQEQIYIYDINTMRLLHTIETN
PNPRGLMAMSPSVANSYLVYPSPPKVINSEIK**AHATTNNITLSVGGNTETSFK**R**DQQ**
DAGHSDISDLDQYSSFTKR**DDADPTSSNGGNSSIIKNGDVIVFNLETL**
QPTMVIEAHKGEIAAMAISFDGTLMATASDKGTIIRVFDIETGDKIYQ**FRRGTYATR**IY
SISFSEDSQYLAVTGSSKTVHIFKLGHSMSNNKLDSDDSNMEEAAADDSSLDTTSIDALSDEENPTR
LAREPYVDASRKTMGRMIRYSSQKLSRR**A**AR**TLGQIFPIKVTSLLESSR**HFASLKLPVET
NSHVMTISSIGSPIDIDTSEYPELFETGNSASTESYHEPVMKMVPIRVVSSDGYLYNFVMDPERGGD
CLILSQYSILMD

Atg18p FTTG Mutant

MSDSSPTINFINFNQTGTCISLGTSKGFKIFNCEPFGKFYSEDSGGYAIVEMLFSTSLLALVGIGDQ
PALSPRRLRIINTKKHSIICEVTFPTSILSVKMNKSRLVVLLQEQIYIYDINTMRLLHTIETN
PNPRGLMAMSPSVANSYLVYPSPPKVINSEIK**AHATTNNITLSVGGNTETSFK**R**DQQ**
DAGHSDISDLDQYSSFTKRDDADPTSSNGGNSSIIKNGDVIVFNLETL
QPTMVIEAHKGEIAAMAISFDGTLMATASDKGTIIRVFDIETGDKIYQFTTGTYATRIY
SISFSEDSQYLAVTGSSKTVHIFKLGHSMSNNKLDSDDSNMEEAAADDSSLDTTSIDALSDEENPTR
LAREPYVDASRKTMGRMIRYSSQKLSRRAAR**TLGQIFPIKVTSLLESSR**HFASLKLPVET
NSHVMTISSIGSPIDIDTSEYPELFETGNSASTESYHEPVMKMVPIRVVSSDGYLYNFVMDPERGGD
CLILSQYSILMD

Figure 4.2.5 B: ICMS predicted phosphorylation sites in Atg18p^{Wt} and Atg18p^{FTTG}

Putative primary phosphorylation sites are shown in red, secondary phosphorylation sites are shown in brown whereas sites which do not show phosphorylation are underlined.

It is quite possible that in response to a stimulus, Atg18p gets phosphorylated which alters its binding to PtdIns3*P* and/or PtdIns(3,5)P_2.

FRRG site is postulated to be PKA target site, and PKA activates TOR (Chiang and Abraham 2005) whereas mTORC1 component, Raptor, is known to directly interact with PtdIns(3,5)P_2 and regulate mTORC1 localization (Bridges, Ma et al.) via lipid bidning. Hence phosphorylation of Atg18p by PKA in response to starvation putatively inhibits Atg18p-PtdIns(3,5)P_2 binding while still allowing PtdIns(3,5)P_2 dependent TOR localization.

Since *K.lactis* Hsv2p does not have a SPRRLR motif, a STKKEL motif which lies in the region could act as potential substitute and/or this motif could be responsible for Atg18p's additional specificity towards PtdIns(3,5)P_2 via serving as a modulation site (Figure 4.2.6).

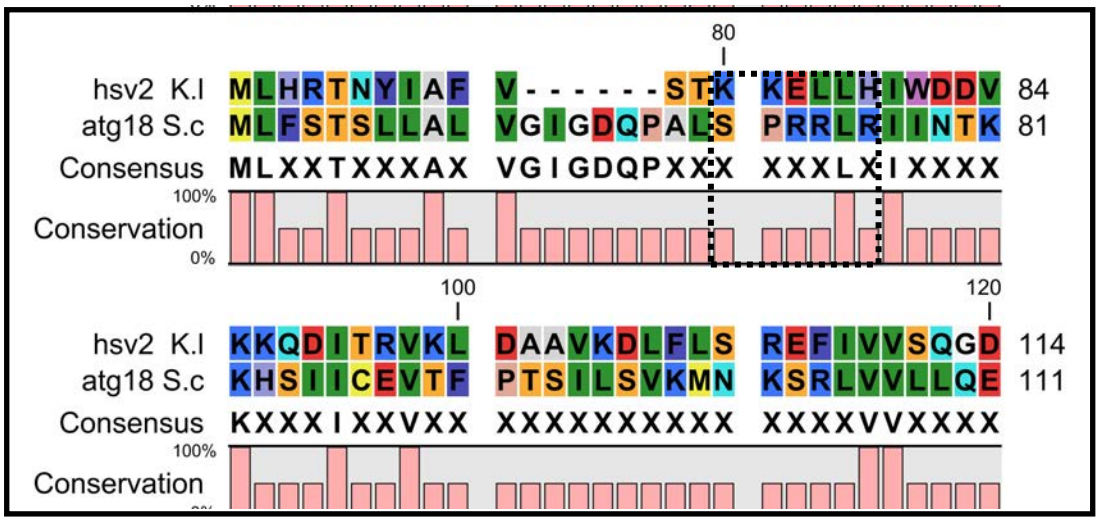

Figure 4.2.6: Homology mapping between Atg18p (S.cerevisiae) and Hsv2p (K.lactis)

Hence SPRRLR stands out as a strong candidate for allosteric regulation of PtdIns(3,5)P_2 binding, in Atg18p because:

1. PtdIns(3,5)P_2 binding is slightly decreased in SPSSLS mutant under exponential growth conditions.
2. It is a putative phosphorylation site according to LC-CID-FT-MS analysis.
3. SPSSLS mutant exhibits similar defects as Atg18p^{FTTG} and Atg18p^{FTTG}FYVE mutants under salt stress.
4. Hurley et al model does not predict this site to be a lipid binding site.
5. Although Hsv2p (*K. lactis*) does not harbor this motif but does have similar residues in the region in terms of charge.
6. SPRRLR and FRRG sites are topographically distal, following the pattern of allosteric modulation sites.
7. Lipid binding by Atg18p^{Wt} and SPSSLS follows a Monod-Wyman-Changeux (MWC) sigmoid curve pattern (Dove, Piper et al. 2004).
8. Atg18p^{Wt}-PtdIns(3,5)P_2 binding requires Mg^{++} (Dove, Piper et al. 2004).

Hurley et al also describes the importance of 3 hydrophobic residues in Atg18p namely, Y367, F398 and Y381, contributing towards increased membrane residence (Baskaran, Ragusa et al. 2012).

However it is quite possible that these C terminal residues could also be involved in interacting with other trans-membrane proteins like Vac7p or membrane protein complexes like Fab1 (in case of Atg18p).

5D β-sheet i.e the one harboring FRRG motif in Atg18p is also identified to be the Ubiquitination site (Pashkova, Gakhar et al.) (Figure 4.2.7)

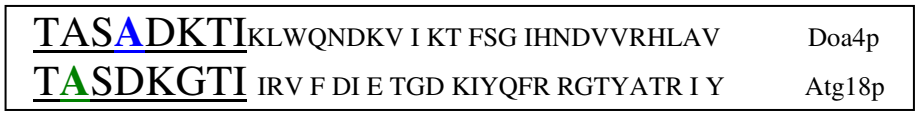

Figure 4.2.7: Ubiquitination sites in Doa4p and Atg18p.

Mutating A158E blocks Ub binding in Doa4p (represented in blue). A263 represented in green denotes a point mutation created in Atg18p during this study.

A mutation in Atg18p at position i.e Atg18p^{A263R} causes it to become unstable (Figure 3.2.8) and since this position is similar to the one designated as ubiquitination site in Doa4p, it could be hypothesized that A263 dependent ubiquitination of Atg18p provides stability to the protein.

Chapter 4; Discussion

4.3 Atg18p-Vps41p and Atg18p-Apl5p binding

Atg18p was initially tested for Apl5p binding because of homology between a blade of the β-propeller like domain of Vps41p that interacts Apl5p (Darsow, Katzmann et al. 2001), as shown below, and a corresponding blade of the β-propeller of the PROPPIN; indeed the very blade that is responsible for lipid binding. It took such a bioinformatic approach to motivate such a study because there is no known link between the AP-3 pathway and the Fab1p pathway. The site of a mutation in Vps41p that was found to disrupt its interaction with Apl5p is indicated (underlined) below. Intriguingly, there is also a ubiquitination site in Atg18p in this potential Apl5p binding motif (also underlined) that is exactly the homologous residue to that mutated in the *vps41* allele that fails to bind Apl5p, suggesting a possible mode of regulation of this interaction.

VPS41: **DGxxxATGSIDGTVII**

ATG18: **DGxxxATAS-DKGTII**

As shown in the results, Atg18p was found to bind, not only Apl5p (Figure 3.3.1), but also surprisingly to Vps41p itself (Figure 3.3.3). This binding was detected by an *in vivo* Co-IP and so it is theoretically possible that in fact Atg18p only binds Apl5p directly, with Vps41p being pulled out as a result of its own interaction with Apl5p in a co-complex. However, this explanation is unlikely because a study of *ATG18* point mutants in this study has showed that whilst Atg18p^{A263R}, Atg18p^{T268R}, Atg18p^{R271T}, Atg18p^{K280T} and Atg18p^{FTTG} all retain an interaction with Apl5p, only Atg18p^{FTTG} of these mutants also binds Vps41p. Indeed, Atg18p^{FTTG} is the only mutant in the whole

study that retains binding to both of these proteins. This is not what would be predicted if Apl5p and Vps41p were pulled out as a co-complex, with only Apl5p directly interacting with Atg18p; in that case it would be expected that all the Atg18p mutants would either bind Apl5p and Vps41p or they would bind neither of them. Indeed, Atg18p^{H244R} also appears to bind Vps41p without being able to interact with Apl5p, adding further weight to the assertion that both interactions, if not being direct are at least independent.

The data from the Atg18p^{FTTG} mutant also adds further information to this discussion; as it not only interacts with both Apl5p and Vps41p (Figure 3.3.2), but it does so despite being unable to associate with membranes (Figure 3.2.2), suggesting that both of these interactions can occur free in the cytosol.

The binding of Atg18p to Vps41p was initially surprising because this protein is a subunit of the HOPS complex, that is responsible for homotypic vacuole fusion, rather than the fission processes with which PtdIns(3,5)P_2 is usually associated. However, it seems that Vps41p localization is influenced by both Atg18p and Fab1p (Figure 3.3.10/11), as might have been expected, given the interaction that is uncovered.

The association between a subunit of the AP-3 complex and Atg18p may be significant, because AP-3 is postulated to represent a protein coat and no coat proteins are yet associated with PtdIns(3,5)P_2 dependent vacuole to PVE trafficking. Further work will be needed to determine if some of the AP-3 machinery in fact participates in retrograde vacuole to PVE trafficking but the fact that the vacuole is

not quite as grossly enlarged in *Δapl5* cells as it is in *Δatg18* cells does suggest that the hypothesis is not entirely correct (data not shown).

Perhaps more significant, are the findings that Atg18p vacuolar localization depends upon the CORVET subunit, Vps3p; a complex intimately associated with vacuolar fission (Figure 3.3.9).

Therefore, Atg18p interaction with Vps41p partially explains its role in regulation of vacuole morphology but further investigations i.e Atg18p binding to other HOPS and CORVET sub-units will reveal the exact details of the process.

Chapter 4; Discussion

4.4 Regulation of Vacuole morphology

Yeast vacuole is a functional equivalent of mammalian lysosome and is involved in processes like autophagic turn over, storage and osmo-regulation. A very fine balance between vacuole morphology and its functions is maintained via sets of proteins localized on the vacuole membrane. Most of these proteins are continuously recycled back to the endocytic compartments and/or cytosol to retain compartment identity as well as ensure apt trafficking, while others like Fab1p reside on the vacuole membrane and are switched on or off in response to upstream signaling.

Fab1p synthesizes PtdIns(3,5)P_2, which acts directly in regulation for vacuole morphology by recruiting proteins through lipid binding and indirectly by sequestering PtdIns3*P*.

A number of PtdIns(3,5)P_2 effecter proteins are known, yet ill-characterized; Atg18p being one of them. Since Δ*atg18* cells have large vacuoles it could be postulated that it participates in either enabling fission and/or limiting fusion.

The fission-fusion cycle operates as counteracting and counter-balancing in the following manner:

1) Priming: Sec18p (NSF)-ATPase increases PtdIns3*P* availability by releasing Sec17p (α-SNAP) resulting in release of Vam3p and dis-assembly of the previous cis-SNARE.

2) Docking: $Ypt7p^{GTP}$ recruits Vps41p (HOPS) which interacts with Vam7p for tethering and trans-SNARE pair up.

3) Tethering/vertex ring formation: Ca^{++} efflux from the vacuole, V_0 interaction with the SNAREs.

4) Fusion: lipid mixing is fast and prior to content mixing, which is slow.

5) Once, one round of fusion is complete Sec17p binds Sec18p which decreases the availability of PtdIns3*P* and displaces HOPS from the vertex (Boeddinghaus, Merz et al. 2002; Thorngren, Collins et al. 2004; Stroupe, Collins et al. 2006) and disassembles Vps1p (polymeric form) releasing Vam3p and HOPS for later rounds of fusion (Bryant, Piper et al. 1998). On the contrary, if Vps1p binds Vam3p then it results in fission (Smaczynska-de, Allwood et al.).

This enables the cell to use same components in different conFigureurations for regulation of fusion/fission of all pathways converging at the vacuole while maintaining integrity (Piper, Bryant et al. 1997).

Over-expression of FYVE domain inhibits re-association of Vam7p with the vacuole therefore it can be reasoned that any protein with the ability to bind PtdIns3*P* and consequently increase the availability of Sec17p at the vacuole would block the re-association of Vam7p, resulting in delayed fusion and increased fission.

Atg18p binds both PtdIns3*P* and PtdIns(3,5)P_2 with much specificity, hence it has the potential to block Vam7p re-association when PtdIns3*P* levels are high as well as blocking HOPS when PtdIns(3,5)P_2 levels are high. This would give a dual control over vacuole fission/fusion machinery depending on the lipid levels.

It was observed during this study that Atg18p binds Vps41p and Apl5p, making it much easier to understand its role in various processes with regard to its lipid binding.

The main identified function of Vps41p is as a Rab-effector which brings about fusion. Vps41p binds Ypt7p (yeast Rab7 homologue) in its GTP bound form for enabling fusion (Stroupe, Collins et al. 2006) while its Yck3p dependent phosphorylation on the vacuole leads to its disassociation from the vacuole (Cabrera, Ostrowicz et al. 2009). This results in vacuole fragmentation, but also increases vacuolar Vam3p content (SNARE which acts in homotypic fusion) which triggers the next round of fusion. Hence the pathway acts in a self-limiting cyclic manner.

Vps41p is mostly cytosolic during salt stress in wild type cells but during autophagy it is observed to accumulate on the vacuole (Figures 3.3.6/3.3.5). It would be logical to believe that there exists a means to prevent Vps41p association with PVEs while encouraging it to accumulate on the vacuole without being phosphorylated during autophagy.

Atg18p fits into the role perfectly; 1) it binds PtdIns3*P* on the PVEs and autophagosomes during autophagy in order to block Vps41p association with these sites and 2) since it loses its vacuolar localization during autophagy, putatively Atg18p-Apl5p binding does not take place which possibly slows down Yck3p and Vam3p release on the vacuole due to decreased Apl5p recycling and encourages Vps41p vacuolar accumulation. This is also supported by the fact that *WIPI49* null

mutants have a mis-localized γ-adaptin (Jeffries, Dove et al. 2004; Krick, Henke et al. 2008; Krick, Muehe et al. 2008).

However once normal conditions are restored Atg18p redistributes and equilibrates itself between the vacuole and the PVEs and hence Vps41p localization is also altered accordingly.

CORVET complex is involved in vacuole fission and vacuole-endosome fusion. Over expression of Vps3p causes vacuole fragmentation. Since both HOPS and CORVET complexes exist in equilibrium, therefore it could be argued that partial mis-localization of Vps41p in Δ*vps3* (under osmotic shock; Figure 3.3.9) and Δ*vps8* cells (under autophagy conditions; Figure 3.3.8), is one of the reasons behind a reciprocating Atg18p mis-localization in these cells. This is also in accordance with the finding that Rab5p over-expression leads to mis-localization of WIPI49(Jeffries, Dove et al. 2004; Proikas-Cezanne and Pfisterer 2009).

Nevertheless, an important thing to note is that both Atg18p and Vps41p are mis-localized in opposing manner to one another and in each null mutant. Although this supports the hypothesis that Atg18p displaces Vps41p from a particular membrane yet it also indicates that Vps3p and Vps8p effect Vps41p localization differentially and possibly their interaction with Atg18p is pivotal which should be explored in future. This is also supported by Roswitha et al model where Atg18p is hypothesized to replace Vps8p/Vps41p from the vacuole and/or endosome with Vps45p/Vac1p complex; coupling fusion/fission with retrograde trafficking (Krick, Henke et al. 2008). This is further supported by the fact that PMN degradation is affected in

Δvps41, *Δatg18* and *Δvam3* cells. Since PMN rates depend on PtdIns3*P* and not PtdIns(3,5)P_2 it clearly indicates that Atg18p dependent Vps41p displacement/localization and Vam3p release is a prerequisite for regulation of all pathways converging at the vacuole.

Chapter 4; discussion

4.5 Role of Atg18p in MVB sorting and autophagy.

MVB sorting is a unique trafficking event because the budding of vesicles is topologically different from any other, occurring away from the cytosol and towards the lumen of the organelle.

This process appears to have evolved to allow the sorting of membrane proteins into the lumen of degradative compartments like the vacuole (or lysosome in higher eukaryotes) where they can be destroyed by proteolytic enzymes. Hence the intra lumenal vesicles (ILVs) of the MVB are the default destination for any integral membrane protein in the cell that possesses no other sorting information. Indeed, this is the way that cells destroy misfolded membrane proteins; preventing them from aggregating and causing programmed cell death.

Odorizzi et al (1998) first described that *fab1*mutants displayed defects in the sorting of both biosynthetic and endocytic cargoes. These defects do not seem to involve aberrant localization of any of the components of the ESCRT complexes; indeed the sorting of the tetraspanin-like protein, Sna3p into the ILVs of MVBs was found to occur normally in *fab1* cells at the same time as cargoes like Cps1p (biosynthetic) and Ste2p (endocytic) cargoes failed to enter these same ILVs (Figure 3.4.3). This was an important observation because it demonstrated that ILVs form normally in *fab1* mutants, and that it is the sorting of proteins into the ILVs that is defective in cells lacking PtdIns(3,5)P_2. This places *fab1* into a unique group of MVB sorting mutants, as in all of the so-called 'Class E VPS mutants' that define

the components of the ESCRT complexes, ILV formation or fusion of the MVB with the vacuole were always found to be defective.

Indeed, the role of *fab1* in cargo sorting into ILVs was further highlighted when Reggiori et al discovered that when Cps1p was expressed as an in frame fusion with non-hydrolysable ubiquitin tag, it resulted in this cargo being sorted normally in *fab1* mutants (Phelan, Millson et al. 2006). Since ubiquitination of cargoes was found to be normal in *fab1* mutants this led to the suggestion that the defect in cells deficient in PtdIns(3,5)P_2 was that the cargo was deubiquitinated before it had been sorted into the ILV and not after. Removal of ubiquitin from all cargoes was known to occur based on the fact that ubiquitin turnover in wild-type cells is very slow indeed, demonstrating that ubiquitin never enters the vacuole/lysosome, despite being tagged to most cargoes sorted via MVBs.

This focused attention on the ubiquitin isopeptidase Doa4p that is known to be responsible for all MVB cargo deubiquitination (Amerik, Nowak et al. 2000). It was reported that *Δdoa4* cells display the same MVB cargo sorting phenotype (Ren, Pashkova et al. 2008) as *fab1* mutants whereby ubiquitin dependent cargoes fail to sort properly whereas expression of ubiquitin tagged cargoes (like Ub-Phm5p or Ub-Cps1p) bypasses the defect and allows normal MVB cargo sorting in this mutant (Katzmann, Babst et al. 2001). This is probably because, in *Δdoa4* cells, ubiquitin is not removed from cargoes and so is destroyed along with them in the vacuole/lysosome. Since ubiquitin transcription is slow, ubiquitin levels in *Δdoa4* drop dramatically, and this prevents subsequent rounds of MVB sorting from proceeding properly, because cargo ubiquitination is then affected.

However, the matter has never progressed beyond that point because no-one has found evidence for premature deubiquitination in *fab1* cells. Ubiquitin levels in *fab1* mutants are not low like in *Δdoa4* cells because over-expression of ubiquitin fails to rescue the MVB sorting defects in these mutants, whereas it does restore sorting in *Δdoa4* cells (Dr S.K. Dove pers comm). Neither had any mechanism for defects in Doa4p activity or localization in *fab1* cells ever been found prior to this study.

What is demonstrated in this work is that Doa4p localization is aberrant in *fab1* mutants, with the enzyme no longer bound to the forming MVB (Figure 3.4.10). It is tempting to speculate that when bound in complex with PtdIns(3,5)P_2, Doa4p activity is under strict temporal and spatial regulation whereas when the enzyme is not in its proper complex (e.g. in *fab1* mutants), it is free to attack newly arriving cargo at the forming MVB, removing the ubiquitin tag before the cargo has been properly sorted into ILVs. Further work is needed to prove this assertion but it remains the only testable model yet suggested for how *fab1* mutants control cargo sorting at the MVB.

As PtdIns(3,5)P_2 was involved in MVB sorting, it was natural to seek an effector. If the above model is correct, then Doa4p itself is a potential effector protein and may bind PtdIns(3,5)P_2 directly. However, prior to this study members of the Vps24p family were suggested as PtdIns(3,5)P_2 effectors(Whitley, Reaves et al. 2003) but these proteins do not display very stringent PtdIns(3,5)P_2 binding and the properties of *vps24* mutants are typical 'Class E' rather than displaying the same phenotype as *fab1* mutants. The discovery of Atg18p shed no light on the mechanism of PtdIns(3,5)P_2 mediated MVB sorting because most studies, using only biosynthetic

cargoes like Phm5p and Cps1p, both of which are actually vacuole resident enzymes, sort normally in *Δatg18* cells.

What this study shows is that although Atg18p plays no role in the sorting of biosynthetic cargo, it somehow affects sorting of at least one endocytic cargo; the pheromone receptor Ste3p. The evidence presented in this work suggests that the defect in Ste3p sorting is fundamentally different from that present in *fab1* cells because *Δatg18* cells sort Phm5p normally and also because Doa4p localization is normal in these mutants (Figure 3.3.4 and 3.3.10). This suggests that PtdIns(3,5)P_2 does indeed regulate MVB sorting, but at multiple and distinct steps.

Future work to directly test if lipid binding was required for Atg18p to carry out this role using the Atg18p$^{FTTG\text{-}FYVE}$ construct would reveal valuable information. However, it is tempting to speculate that the defects in MVB sorting in *Δatg18* cells might relate to the high levels of PtdIns(3,5)P_2 found in these mutants and the the effects this might have on acidity of the PVE; PtdIns(3,5)P_2 is known to control acidity of the vacuole through TRP-like channels (Zhang, Li et al.).

However, this model is made less likely by the observation that *Δvac7* cells have a fundamentally similar MVB sorting defect to *Δatg18* cells but not to *fab1* cells as might have been expected. This suggests another mechanism for the sorting defect because whilst PtdIns(3,5)P_2 is very high in *Δatg18* cells, they are very low in *Δvac7* cells. It indicates that the physical presence of the Atg18p protein is required on the MVB membrane for correct Ste3p sorting, as this could be similarly defective in both *Δatg18* and *Δvac7* cells.

Concluding remarks

The role of Atg18p in regulation of vacuolar trafficking, morphology and autophagy is putatively to displace or limit Vps41p association with the target membranes and hence to limit fusion which either directly or indirectly enhances fission.

Its lipid binding is slightly distinct from *K.lactis* Hsv2p and in contrast to earlier findings, Atg18p can partially localize to membranes even in absence of PtdIns(3,5)P_2.

PtdIns(3,5)P_2 affects the localization of Doa4p and hence MVB sorting, which could have a direct or an indirect affect on Atg18p localization.

Future prospects

1. Investigations of the interactions of Atg18p with individual sub-units of both HOPS and CORVET would decipher the exact mechanism of Atg18p's association with the 2 complexes and the affect of such interactions on fission and fusion processes. The investigation of role of Atg18p-lipid in any such interactions could also prove important in understanding the role of PtdIns(3,5)P_2 in regulating the activity of both these complexes directly or indirectly.
2. Investigating the affect of PtdIns(3,5)P_2 on Ubiquitination and deubiquitination via localization of Doa4p interacting proteins like Rsp5p and Bro1p could help explain the hypothesis presented herein i.e PtdIns(3,5)P_2 dependent localization of Doa4p regulates its activity and therefore deubiquitination/ubiquitination.

3. Investigation of the role of Atg18p-lipid binding on its function in MVB sorting would help reveal whether Atg18p function/s in MVB sorting are distinct from PtdIns(3,5)P_2 functions or not?
4. Investigation of Vac7p localization and its interaction with Atg18p at various sites would help understand and possibly identify the role of Vac7p in cellular trafficking.
5. Investigation of Atg18p lipid binding sites via mutations in site 1 and 2 would reveal the true nature of Atg18p lipid binding.
6. Investigation of Atg18p SPRRLR motif via specific point mutations would reveal (if any) whether the arginines in this site work together or behave distinctly as the arginines in the FRRG motif.

Appendix 1; List of Plasmids used in this study.

Plasmid	Obtained from	Yeast Marker	Bacterial marker	Plasmid type	Promoter
pGEX6P-1	ATCC		Amp, Chmp		
pGEX6P-T1	Dove Lab		Amp, Chmp		
pGFP-*DOA4*	M. Hochstrasser	URA3	Amp	CEN	
pGFP-*PHM5*	H. Pelham	URA3	Amp	CEN	
pRS316-*STE3*	K.Borrower	URA3	Amp	CEN	T7
pRS423	ATCC	HIS3	Amp	2 µ	T7
pUG36-*ATG18*	Dove Lab	URA3	Amp	CEN/ARS	Met 25
pUG36-*ATG18*^{SPSSLS}	Dove Lab	URA3	Amp	CEN/ARS	Met25
pUG36-*ATG18*^{FTTG}	Dove Lab	URA3	Amp	CEN/ARS	Met 25
pUG36	Dove Lab	URA3	Amp	CEN/ARS	Met 25
pUG36-*VAC7*	Dove Lab	URA3	Amp	CEN/ARS	Met 25
pUG36-*VPS41*	Dove Lab	URA3	Amp	CEN/ARS	Met 25
pUR34NLS	Dr. F. Rodrigues	HIS3	Amp	CEN/ARS	Met 25
pYM6	ATCC	TRP1	Amp	2 µ	T7
pRS316-*ATG18*^{FTTG}-GFP-HA-FYVE		URA3	Amp	CEN	T7
pGFP-*SNA3*	Dove lab	URA3	Amp		

Appendix 2; Yeast strains used in this study.

Parent strain	Knock out	Knock in	Genotype	Source
BY4742	All null/deletion mutants	None	*MATα;his3Δ1;leu2Δ0;lys2Δ0;ura3Δ0;**gene**::KAN*	EUROSCARF
BY4742	WT	None	*MATα;his3Δ1;leu2Δ0;lys2Δ0;ura3Δ0*	EUROSCARF
FY833	WT	None	*MATα;his3Δ;ura3Δ;leu2Δ;lys2Δ;trp1Δ;GAL2*	ATCC
FY833	None	*ATG18-3HA:HIS3*	*MATα;his3Δ;ura3Δ;leu2Δ;lys2Δ;trp1Δ;GAL2;ATG18-3HA:HIS3*	Dove Lab
FY833	None	*ATG18P-3HA:HIS3 APL5-9MYC:TRP*	*MATα;his3Δ;ura3Δ;leu2Δ;lys2Δ;trp1Δ;GAL2;ATG18-3HA:HIS3APL5-9MYC:TRP*	This study
BY4742	None	*VPS41-3HA:HIS3*	*MATα;his3Δ1;leu2Δ0;lys2Δ0;ura3Δ0VPS41-3HA:HIS3*	Dove Lab
BY4741	*fab1::LEU2*	*ANP1-RFP:KAN*	*MATa ; his3Δ1; leu2Δ0; met15Δ0; ura3Δ0 ANP1::ANP1-RFP fab1::LEU2*	This study
BY4741	*fab1::LEU2*	*CHC1-RFP:KAN*	*MATa ; his3Δ1; leu2Δ0; met15Δ0; ura3Δ0 COP1::COP1-RFP fab1::LEU2*	This study
BY4741	*fab1::LEU2*	*SNF7-RFP:KAN*	*MATa ; his3Δ1; leu2Δ0; met15Δ0; ura3Δ0 SNF7::SNF7-RFP fab1::LEU2*	This study
BY4741	None	*ANP1-RFP:KAN*	*MATa ; his3Δ1; leu2Δ0; met15Δ0; ura3Δ0 ANP1:: ANP1-RFP*	Erin'O'Shea
BY4741	None	*COP1-RFP:KAN*	*MATa ; his3Δ1; leu2Δ0; met15Δ0; ura3Δ0 COP1::COP1-RFP*	Erin'O'Shea
BY4741	None	*CHC1-RFP:KAN*	*MATa ; his3Δ1; leu2Δ0; met15Δ0; ura3Δ0 CHC1::CHC1-RFP*	Erin'O'Shea
BY4741	None	*PEX3-RFP:KAN*	*MATa ; his3Δ1; leu2Δ0; met15Δ0; ura3Δ0 PEX3::PEX3-RFP*	Erin'O'Shea
BY4741	None	*SEC3-RFP:KAN*	*MATa ; his3Δ1; leu2Δ0; met15Δ0; ura3Δ0 SEC3::SEC3-RFP*	Erin'O'Shea
BY4741	None	*SNF7-RFP:KAN*	*MATa ; his3Δ1; leu2Δ0; met15Δ0; ura3Δ0 SNF7::SNF7-RFP*	Erin'O'Shea

BY4742	*fab1*::*LEU2* *atg18*::KAN	None	*MATα;his3Δ1;leu2Δ0;lys2Δ0;ura3Δ0;fab1::LEU2;atg18::KAN*	This study
BY4742	*fab1*::LEU2 *vps34*::KAN	None	*MATα;his3Δ1;leu2Δ0;lys2Δ0;ura3Δ0fab1::LEU2;vps34::KAN*	This study
BY4742	*fab1*::LEU2 *Figure4*::KAN	None	*MATα;his3Δ1;leu2Δ0;lys2Δ0;ura3Δ0fab1::LEU2;Figure4::KAN*	This study
AMY6	*APL5-RFP:HYG*	None		Alex Merz
BY4742	*vps38::*KAN *atg14::*HIS3	None	*MATα;his3Δ1;leu2Δ0;lys2Δ0;ura3Δ0vps38::KAN;atg14::HIS3*	Dove Lab
BY4742	*vps38::KAN apl::HIS3*	None	*MATα;his3Δ1;leu2Δ0;lys2Δ0;ura3Δ0vps38::KAN;apl5::HIS3*	This study

Appendix 3; Preparation of *E. Coli* Competent cells

3 ml of innoculum in LB + G418 0.8 OD_{600nm} was added to 1L 'super competent media' (a proprietary bacterial growth media from BIO101) and incubated at 37°C for the culture to grow to 0.8 OD_{600nm}. The culture was cooled on ice for 20 minutes and centrifuged at 4°C, 4000 *xg*. The cell pellet was washed twice in 500 ml ice cold double distilled deionized water. The cell pellet was then resuspended in ice-cold 1 x Rubidium-$CaCl_2$ mixture (2.0 ml:BIO101) and incubated at 4°C over night. Cells were centrifuged at 1500 *xg* at 4°C and the cell pellet was resuspended in ice-cold x 1 Rubidium-$CaCl_2$ mixture (4 ml: BIO101) containing 20% (w:v) glycerol. The competent cells were divided into 100 µl aliquots and stored at -80°C till further use.

Appendix 4.1; Standard curve for cell number vs OD_{600nm} (based on an average of 4 values)

Volume of cell culture µl	Volume of water µl	Dilution factor	OD @ 600nm (Average of 4 readings)	cells / 0.1 µl (Average of 4 readings)	No of cells in 1 ml
500	500	0.5	1.275	361.3	1806500 ($1x10^6$)
500	1000	0.33	1.132	325.5	1085000 ($1x10^6$)
400	1000	0.286	0.710	310.3	887458 ($8x10^5$)
350	1000	0.26	0.581	243	631800 ($6x10^5$)
300	1000	0.23	0.615	205.3	472190 ($4x10^5$)
250	1000	0.2	0.577	199.3	398600 ($3x10^5$)
200	1000	0.17	0.528	151.5	252500 ($2x10^5$)
100	1000	0.09	0.435	129	117273 ($1x10^5$)
50	1000	0.05	0.312	110	55000 ($5x10^4$)
25	1000	0.03	0.173	52.5	15750 ($1x10^4$)
12.5	1000	0.012	0.077	25.75	3090 ($3x10^3$)
6.25	1000	0.006	0.036	14.5	870 ($8x10^2$)

Appendix 4.2 Standard curve of cell number vs OD_{600nm} (4 individual values)

Dilution factor	Cells / ml	OD at 600nm	Cells / ml	OD at 600nm	Cells / ml	OD at 600nm	Cells / ml	OD at 600nm
0.5	1735000	1.221	1765000	1.264	1840000	1.306	1885000	1.312
0.33	1020000	1.063	1099000	1.173	1049000	1.097	1125000	1.197
0.286	1001000	0.787	778000	0.612	858000	0.699	912000	0.744
0.26	616000	0.384	634000	0.682	624000	0.511	652000	0.747
0.23	467000	0.579	450800	0.599	480700	0.638	489900	0.642
0.2	400000	0.589	400000	0.576	382000	0.531	412000	0.611
0.17	238000	0.483	265200	0.549	256700	0.521	270300	0.559
0.09	108000	0.389	122400	0.509	117900	0.432	116100	0.411
0.05	52500	0.294	56500	0.312	59000	0.356	52000	0.287
0.03	17100	0.187	14400	0.154	15300	0.166	16200	0.183
0.012	2500	0.049	3120	0.071	3480	0.099	3240	0.087
0.006	90	0.037	66	0.024	114	0.053	78	0.031

Appendix 5; List of reagents and buffers

5.1 Chemiluminescence reagents A and B

Solution A

100 mM Glycine pH 10 (with NaOH) + 0.4 mM luminol + 8 mM 4-iodophenol in double distilled deionized water. The solution was stored at 4°C in an amber bottle.

Solution B

0.12% (w/w) hydrogen per oxide in double distilled deionized water. It was stored at 4°C.

Equal quantities of solution A and B were mixed immediately before use.

5.2 Cyclohexamide stock solution

28mg cyclahexamide / 10ml of DMSO = 10 mM

5.3 EDTA stock solution

0.5M solution of EDTA was prepared in double distilled deionized water using 1M NaOH solution to increase the solubility of EDTA in water.

5.4 Elution buffer

50 mM Tris HCl, 150 mM NaCl, 1mM PMSF. Stored at -20°C.

20mM Glutathione was added prior to use.

5.5 IPTG stock solution

200 mg of IPTG was dissolved in 1ml double distilled deionized water and stored at -20°C till further use.

5.6 Lysis buffer

100 mM HEPES/KOH pH 7.5, 150 mM NaCl, 1 mM PMSF. 30 mg/ml Lysozyme was added prior to use.

5.7 1x MES buffer

50 mM Tris base, 50 mM 3Â-(NÂ-Morpholino propanesulfonic acid), 1mM EDTA, 0.01% SDS was dissolved in double distilled deionized water. The pH was adjusted to 7.3 and the buffer stored at 4°C in a dark place. 2% glucose was added prior to use.

5.8 PBS Buffer

PBS tablets (NaCl 8%, KCl 0.2 %, Na_2HPO_4 1.15%, KH_2PO_4 0.2% w/w) from oxoid were used to prepare PBS buffer. 1 tablet was added to 100ml of double

distilled water and autoclaved for 10 minutes at 120°C and later stored at room temperature till further use.

0.5 % v/v Tween 20 was added prior to use, if/when required.

5.9 PMSF solution

100 mM PMSF in Isopropanol was made fresh prior to use.

5.10 10x SDS-PAGE running buffer

250 mM Tris-Base, 2.5 M Glycine, 1% SDS (w:v) in double distilled deionized water.

5.11 5x SDS sample buffer

250 mM Tris-HCl pH 6.8, 10% (v/v) SDS, 30% Glycerol (v/v), 5% beta-meracaptoethanol or 0.5 M DTT, 0.02% bromophenol blue. The buffer was stored at -20°C.

5.12 TBS Buffer

50 mM Tris, 150 mM NaCl. The pH was adjusted with HCl to pH 7.6.

0.5% (v/v) Tween 20 was added when/if required.

5.13 TNE Buffer

50 mM Tris HCl pH 7.4, 150 mM NaCl, 7.5 mM EDTA.

5.14 Towbin's buffer

30.3 g (25 mM) Tris, 144 g (192M) Glycine, 10% SDS in 1L double distilled water (stock solution). 1X Towbin's buffer was prepared as: 200ml methanol+ 100ml 10x Towbin's stock buffer solution and the volume made up to 1L with double distilled deionized water.

5.15 1M Tris stock solution

1L of 1M Tris solution was made in double distilled deionized water and filter sterilized. The pH was adjusted to 7.5 or 8 or 8.5 with HCl / NaOH.

5.16 Wash buffer

100 mM HEPES / KOH pH 7.5, 150 mM NaCl, 1mM PMSF, 5 mM Benzimidine was made in double distilled deionized water and pH adjusted to 7.5. It was stored at 4 °C.

Appendix 6; Media used in this study

6.1 LB

10 g Tryptone, 5 g yeast extract, 10 g NaCl / 1L double distilled deionized water. pH was adjusted to 7. Autoclaving was carried out for 15 minutes at120°C. 2% glucose was added prior to use or prior to autoclaving in case of plates. 20g agar was used for making LB plates. 0.1 mg/ml Ampicillin was added prior to use/pouring the plates.

The media was stored at room temperature in a dark cabinet, while the plates were stored at 4°C.

6.2 YEPD/YETD

20 g Bacto peptone/tryptone, 10 g yeast extract, 100 mg adenine, 100 mg uracil / 1L double distilled deionized water. Autoclaved for 15 minutes at 120°C. 2 % glucose was added to media prior to use. In case of plates, 20 g agar was added prior to autoclaving and 2 % glucose was added prior to pouring the plates. The plates and media were stored at room temperature in a dark cabinet.

6.3 Nitrogen starvation media

1.7 % YNB in double distilled deionized water was autoclaved for 15 minutes at 120 °C and stored at room temperature. 2 % glucose was added prior to use.

6.4 Amino-acid mixture

Adenine 2.03 g

Alanine 2.08 g

Arginine 1.99 g

Aspartic acid 2.11 g

Glutamic acid 2.01 g

Glycine 1.99 g

Isoleucine 2 g

Phenylalanine 2.06 g

Proline 2.09 g

Serine 2.01 g

Threonine 2.02 g

Valine 2.07 g

The powder mixture was milled for 1 minute and stored at 4°C till further use.

6.5 Synthetic complete media/selective media

1.7 g YNB, 3 g $(NH_4)_2SO_4$, 1 g glutamine, 1 g amino acid stock mixture, 100 mg each of Leucine, Lysine, Tryptophan, Histidine, Uracil and Methionine. pH was adjusted to 5.7.

The appropriate amino acid, Uracil and/or Methionine (depending on the strain) was not added in case of selective / drop out media. Autoclaving was done for 15 minutes at 120°C. 2 % glucose was added prior to use.

Incase of plates 20 g agar was added prior to autoclaving and 2% glucose was added prior to pouring the plates. The plates and media were stored at room temperature in a dark cabinet.

6.6 Saline stock solution for induction of osmotic stress

2 M NaCl solution was prepared and autoclaved for 15 minutes at 120°C and stored at room temperature.

6.7 SOB

20 g Bactotryptone, 5 g yeast extract, 0.5 g NaCl, 0.186 g KCl / 1L double distilled deionized water. pH was adjusted to 7.

6.8 SOC

0.01 M $MgCl_2$, 1 M glucose in 20 ml SOB. Stored at -20°C.

6.9 Ampicillin stock solution

50 mg of G418 was dissolved in 1 ml of double distilled deionized water and stored at -20°C till further use.

6.10 Chloramphenicol stock solution

34 mg of chloramphenicol was added to 1 ml of double distilled deionized water and stored at -20°C.

Nomenclature

Gene	Alias	Mammalian homologue	Description and function
AKT1			
AMS1	None	*MAN2C1*	Vacuolar alpha mannosidase, involved in free oligosaccharide (fOS) degradation; delivered to the vacuole in a novel pathway distinct from the secretory pathway.
ANP1	*GEM3 , MNN8*	*ALG2*	Type II membrane protein and a subunit of the alpha-1,6 mannosyltransferase complex. Used in this study as a TGN marker.
APE1	*YSC1, API, LAP4*	*APEX1*	Vacuolar aminopeptidase yscI; zinc metalloproteinase that belongs to the peptidase family M18; often used as a marker protein in studies of autophagy and cytosol to vacuole targeting (CVT) pathway.
APL5	*YKS4*	*APL5*	Delta adaptin-like subunit of the clathrin associated protein complex AP-3, which functions in the transport of alkaline phosphatase to the vacuole.
APM3	*YKS6*	*APM3*	Mu3-like subunit of the clathrin associated protein complex AP-3, which functions in transport of alkaline phosphatase to the vacuole.
ATG1	*AUT3, CVT10, APG1*	*ULK1*	Protein ser/thr kinase required for vesicle formation in autophagy and the cytoplasm-to-vacuole targeting (Cvt) pathway; structurally required for phagophore assembly site formation; during autophagy forms a complex with Atg13p and Atg17p.
ATG2	*SPO72 , AUT8, APG2*	*ATG2*	Peripheral membrane protein required for vesicle formation during autophagy, pexophagy, and the cytoplasm-to-vaucole targeting (Cvt) pathway; involved in Atg9p cycling between the phagophore assembly site and mitochondria.
ATG8	*APG8, CVT5, AUT7*	*ATG8*	Component of autophagosomes and Cvt vesicles; undergoes conjugation to phosphatidylethanolamine (PE); Atg8p-PE is anchored to membranes, is involved in phagophore expansion, and may mediate membrane fusion

			during autophagosome formation.
ATG9	*AUT9, CVT7, APG9*	*ATG9*	Transmembrane protein involved in forming Cvt and autophagic vesicles; cycles between the phagophore assembly site (PAS) and other cytosolic punctate structures, not found in autophagosomes; may be involved in membrane delivery to the PAS.
ATG14	*CVT12 , APG14*	*ATG14*	Autophagy-specific subunit of phosphatidylinositol 3-kinase complex I (along with Vps34p/Vps15p/Vps30p). Atg14p targets complex I to the phagophore assembly site (PAS) and is required for localizing additional ATG proteins to the PAS. Its human homolog is Barkor-protein.
ATG18	*NMR1, CVT18, AUT10*	*WIPI1*	Yeast WD-40 repeat protein predicted to fold as a β-propeller and hence listed as a PROPPIN protein. Its mammalian homologs are the WIPI proteins.
ATG21	*MAL1, HSV1*	*WIPI2*	Phosphoinositide binding protein required for vesicle formation in the cytoplasm-to-vacuole targeting (Cvt) pathway; binds both Phosphatidylinositol (3,5)-bisphosphate and Phosphatidylinositol 3-phosphate; WD-40 repeat protein.
ATG6	*APG6, VPT30 , VPS30*	*BECN1*	Subunit of Phosphatidylinositol (PtdIns) 3-kinase complexes.
BRO1		*ALIX*	
CCZ1	*CVT16*		Protein involved in vacuolar assembly, essential for autophagy and the cytoplasm-to-vacuole pathway.
CHC1	*SWA5*	*RCC1*	Subunit of the major Clathrin heavy chain coat protein involved in intracellular protein transport and endocytosis. Used here as a Golgi to vacuole vesicle marker.
CHS3	*CAL1, CSD2, DIT101, KTI2*		Chitin synthase III, catalyzes the transfer of N-acetylglucosamine (GlcNAc) to chitin; required for synthesis of the majority of cell wall chitin, the chitin ring during bud emergence, and spore wall chitosan.
COP1	*SEC3 , RET1,*	*RFWD2*	Alpha subunit of COPI vesicle

	SOO1		coatomer complex, which surrounds transport vesicles in the early secretory pathway. Used here as a marker for Golgi to ER vesicles.
DNM1	None	*DRP1*	Dynamin-related GTPase required for mitochondrial fission and morphology; assembles on the cytosolic face of mitochondrial tubules at sites at which division will occur; also participates in endocytosis and regulating peroxisome abundance
DOA4	*DOS1, MUT4, NPI2, SSV7, UBP4*	*UBPY*	Ubiquitin isopeptidase, required for recycling ubiquitin from proteasome-bound ubiquitinated intermediates, acts at the late endosome/PVE compartment to recover ubiquitin from ubiquitinated membrane proteins en route to the vacuole.
EEA1			
ENT3	None	*SLC29A3*	Protein containing an N-terminal epsin-like domain involved in clathrin recruitment and traffic between the Golgi and endosomes; associates with the clathrin adaptor Gga2p.
ENT5	None	*EPSINR*	Protein containing an N-terminal epsin-like domain involved in clathrin recruitment and traffic between the Golgi and endosomes; associates with the clathrin adaptor Gga2p, clathrin adaptor complex AP-1, and clathrin.
FAB1	*SVL7*	*PIP5-K3 PIKFYVE*	Sole identified yeast vacuolar 1-phosphatidylinositol-3-phosphate 5-kinase.
FIG4	None	*FIG4*	Identified as Phosphatidylinositol 3,5-bisphosphate (PtdIns(3,5)P_2) phosphatase.
GGA1	None	*GGA1*	Golgi-localized protein with homology to gamma-adaptin, interacts with and regulates Arf1p and Arf2p in a GTP-dependent manner in order to facilitate traffic through the late Golgi.
GGA2	None	*GGA2*	Protein that interacts with and regulates Arf1p and Arf2p in a GTP-dependent manner to facilitate traffic through the late Golgi; binds Phosphatidylinositol 4-phosphate,

			which plays a role in TGN localization; has homology to gamma-adaptin.
HSE1	None	*STAM*	Subunit of the endosomal Vps27p-Hse1p complex required for sorting of ubiquitinated membrane proteins into intralumenal vesicles prior to vacuolar degradation, as well as for recycling of Golgi proteins and formation of lumenal membranes.
HSV2	None		Yeast Phosphatidylinositol 3,5-bisphosphate-binding PROPPIN protein.
INP52	*SJL2*	*SYNJ1*	Polyphosphatidylinositol phosphatase, dephosphorylates a number of phosphatidylinositols (PIs) to PI; involved in endocytosis; hyperosmotic stress causes translocation to actin patches; synaptojanin-like protein with a Sac1 domain.
INP53	*SJL3, SOP2*	*SYNJ2*	Polyphosphatidylinositol phosphatase, dephosphorylates multiple phosphatidylinositols; involved in trans Golgi network-to-early endosome pathway; hyper-osmotic stress causes translocation to actin patches; contains Sac1 and 5-ptase domains.
IVY1	None		Phospholipid-binding protein that interacts with both Ypt7p and Vps33p, may partially counteract the action of Vps33p and vice versa, localizes to the rim of the vacuole as cells approach stationary phase.
MGM1	*MNA1*	*OPA1*	Mitochondrial GTPase, present in complex with Ugo1p and Fzo1p; required for mt morphology and genome maintenance; exists as long and short form with different distributions; homolog of human OPA1 involved in autosomal dominant optic atrophy.
MON1	*AUT12*	*MON1*	Protein required for fusion of cvt-vesicles and autophagosomes with the vacuole; associates, as a complex with Ccz1p, with a peri-vacuolar compartment; potential Cdc28p substrate.
MSS4	None	*PIP5K1B*	Phosphatidylinositol-4-phosphate 5-

			kinase.
MTM1	None		Mitochondrial protein of the mitochondrial carrier family, involved in activating mitochondrial Sod2p.
MYO2	*CDC66*	*MYOSIN V*	One of two type V myosin motors (along with MYO4) involved in actin-based transport of cargos; required for the polarized delivery of secretory vesicles, the vacuole, late Golgi elements, peroxisomes, and the mitotic spindle.
MUP1	None		High affinity methionine permease, integral membrane protein with 13 putative membrane-spanning regions; also involved in cysteine uptake.
NHX1	*VPS44, NHA2, VPL27*	*NHA2*	Na+/H+ and K+/H+ exchanger, required for intracellular sequestration of Na+ and K+; located in the vacuole and late endosome compartments; required for osmo-tolerance to acute hypertonic shock and for vacuolar fusion
PEP1	*VPS10, YPT1*	*NSG1*	Type I transmembrane sorting receptor for multiple vacuolar hydrolases; cycles between the late-Golgi and pre-vacuolar endosome-like compartments.
PEP12	*VPL6, VPS6 , VPT13*	*SNX16*	Target membrane receptor (t-SNARE) for vesicular intermediates traveling between the Golgi apparatus and the vacuole; controls entry of biosynthetic, endocytic, and retrograde traffic into the pre-vacuolar compartment; syntaxin.
PEX3	*PAS3*	*PEX3*	Peroxisomal membrane protein (PMP) required for proper localization and stability of PMPs. Used here as peroxisomes marker.
PGD1	*HRS1, MED3*	*hHRS1*	Subunit of the RNA polymerase II mediator complex; associates with core polymerase subunits to form the RNA polymerase II holoenzyme; essential for basal and activated transcription; direct target of Cyc8p-Tup1p transcriptional corepressor.
PHO8	None	*ALPL*	Repressible vacuolar alkaline phosphatase; regulated by levels of Pi and by Pho4p, Pho9p, Pho80p,

			Pho81p and Pho85p; dephosphorylates phosphotyrosyl peptides; contributes to NAD+ metabolism by producing nicotinamide riboside from NMN.
RSP5	*MDP1 , MUT2, NPI1, UBY1, SMM1*	*NEDD4L*	E3 ubiquitin ligase of the NEDD4 family; involved in regulating many cellular processes including MVB sorting, heat shock response, transcription, endocytosis, and ribosome stability; human homolog is involved in Liddle syndrome; mutant tolerates aneuploidy; ubiquitylates Sec23p.
RUFY1			
SEC13	*ANU3*	*SEC13, SEH1L*	Component of the Sec13p-Sec31p complex of the COPII vesicle coat, and the SEA (Seh1-associated) complex. It is required for vesicle formation in ER to Golgi transport. Used here as a ER to Golgi vesicle marker.
SEC17	*RNS3*	*α-SNAP*	Peripheral membrane protein required for vesicular transport between ER and Golgi, the 'priming' step in homotypic vacuole fusion, and autophagy; stimulates the ATPase activity of Sec18p; has similarity to mammalian alpha-SNAP.
SEC18	*ANU4*	*NSF*	ATPase required for vesicular transport between ER and Golgi, the 'priming' step in homotypic vacuole fusion, autophagy, and protein secretion; releases Sec17p from SNAP complexes; has similarity to mammalian NSF.
SNF7	*DID1, VPS32, RNS4, VPL5*	*hSNF7*	One of four subunits of the endosomal sorting complex ESCRT-III. It is involved in the sorting of transmembrane proteins into the multi-vesicular body (MVB) pathway and is recruited from the cytoplasm to endosomal membranes. Used here as a late endosome/MVB marker.
SNX3	*GRD19*	*SNX3*	Sorting nexin required to maintain late-Golgi resident enzymes in their proper location by recycling molecules from the pre-vacuolar

			compartment; contains a PX domain and sequence similarity to human Snx3p.
TLG1	None	*SNX6*	Essential t-SNARE that forms a complex with Tlg2p and Vti1p and mediates fusion of endosome-derived vesicles with the late Golgi; binds the docking complex VFT (Vps fifty-three) through interaction with Vps51p.
TLG2	None	*SNX16*	Syntaxin-like t-SNARE that forms a complex with Tlg1p and Vti1p and mediates fusion of endosome-derived vesicles with the late Golgi; binds Vps45p, which prevents Tlg2p degradation and also facilitates t-SNARE complex formation; homologous to mammalian SNARE protein syntaxin 16 (Sx16).
TOR1	*DRR1*	*mTOR*	PIK-related protein kinase and rapamycin target; subunit of TORC1, a complex that controls growth in response to nutrients by regulating translation, transcription, ribosome biogenesis, nutrient transport and autophagy; involved in meiosis
VAC14	*SVP2*	*VAC14*	Protein involved in regulated synthesis of PtdIns(3,5)P_2, and trafficking of some proteins to the vacuole lumen via the MVB, and in maintenance of vacuole size and acidity. It is known to interact with Fig4p and forms a complex with Fab1p.
VAC7	None		Integral vacuolar membrane protein involved in vacuole inheritance and morphology. It activates Fab1p kinase activity under basal conditions and also after hyper-osmotic shock.
VAM3	*PTH1*	*SNX 3A*	Syntaxin-like vacuolar t-SNARE that functions with Vam7p in vacuolar protein trafficking; mediates docking/fusion of late transport intermediates with the vacuole; has an acidic di-leucine sorting signal and C-terminal transmembrane region.
VAM7	*VPS43, VPL24*	*SNAP-25*	Vacuolar SNARE protein that functions with Vam3p in vacuolar

			protein trafficking; has an N-terminal PX domain (phosphoinositide-binding module) that binds PtdIns-3-P and mediates membrane binding; SNAP-25 homolog.
VPS1	*GRD1*, *LAM1*, *SPO15*, *VPL1*, *VPT26*	*DNM1L*	Dynamin-like GTPase required for vacuolar sorting; also involved in actin cytoskeleton organization, endocytosis, late Golgi-retention of some proteins, regulation of peroxisome biogenesis.
VPS15	*GRD8, VAC4, VPL19, VPS40*	*PIK3R4*	Myristoylated serine/threonine protein kinase involved in vacuolar protein sorting. It functions as a membrane-associated complex with Vps34p, where the active form recruits Vps34p to the Golgi membrane and interacts with the GDP-bound form of Gpa1p.
VPS17	*PEP21, VPT3*	*SNX1*	Subunit of the membrane-associated retromer complex essential for endosome-to-Golgi retrograde protein transport; peripheral membrane protein that assembles onto the membrane with Vps5p to promote vesicle formation.
VPS24	*DID3, VPL26*	*VPS24*	One of the four subunits of the endosomal sorting complex ESCRT-III. It forms an ESCRT-III subcomplex with Did4p and is involved in the sorting of transmembrane proteins into the multi-vesicular body (MVB) pathway.
VPS27	*GRD11, SSV17, VPL23, VPT27, DID7*	*HRS1*	Endosomal protein that forms a complex with Hse1p. It is required for recycling of Golgi proteins, forming lumenal membranes and sorting ubiquitinated proteins destined for degradation. It is known to have a Ubiquitin Interacting Motifs which bind ubiquitin.
VPS3	*PEP6 , VPL3, VPT17*	*VPS3*	Component of CORVET tethering complex. It is a cytosolic protein required for the sorting and processing of soluble vacuolar proteins, acidification of the vacuolar lumen, and assembly of the vacuolar H^+ ATPase.
VPS33	*CLS14, MET27,*	*VPS33A,*	ATP-binding protein that is a subunit

	PEP14, SLP1, VAM5, VPL25, VPT33	*VPS33B*	of the HOPS complex and of the CORVET tethering complex; essential for protein sorting, vesicle docking and fusion at the vacuole.
VPS34	*END12, PEP15, VPL7, VPT29 , STT8, VPS7*	*PIK3C3*	Phosphatidylinositol 3-kinase responsible for the synthesis of Phosphatidylinositol 3-phosphate and a core subunit of all the Vps34 complexes.
VPS38	*VPL17*	*UVRAG*	Part of a Vps34p Phosphatidylinositol 3-kinase complex that functions in carboxypeptidase Y (CPY) sorting at the endosome.
VPS39	*CVT4, VPL18, VPL22, VAM6*	*VPS39*	Vacuolar protein that plays a critical role in the tethering steps of vacuolar membrane fusion by facilitating guanine nucleotide exchange on small guanosine triphosphatase, Ypt7p.
VPS4	*CSC1, END13, GRD13, VPL4, VPT10, DID6*	*VPS4A, DID6*	AAA-ATPase involved in multi-vesicular body (MVB) protein sorting, ATP-bound Vps4p localizes to endosomes and catalyzes ESCRT-III disassembly and membrane release; ATPase activity is activated by Vta1p; regulates cellular sterol metabolism.
VPS41	*CVT8, FET2, SVL2, VAM2, VPL20*	*VPS41*	Vacuolar membrane protein that is a subunit of the homotypic vacuole fusion and vacuole protein sorting (HOPS) complex. It is essential for membrane docking and fusion at the Golgi-to-endosome and endosome-to-vacuole stages of protein transport.
VPS45	*STT10 , VPL28*	*VPS45*	Protein of the Sec1p/Munc-18p family. It is essential for vacuolar protein sorting and is required for the function of Pep12p and the early endosome/late Golgi SNARE Tlg2p. It is also essential for fusion of Golgi-derived vesicles with the pre-vacuolar compartment.
VPS5	*GRD2 , PEP10 , VPT5*	*SNX1*	Nexin-1 homolog required for localizing membrane proteins from a pre-vacuolar/late endosomal compartment back to the late Golgi apparatus; structural component of the retromer membrane coat

			complex; forms a retromer sub-complex with Vps17p.
VPS8	*FUN15 , VPT8 , VPL8*	*VPS8*	Membrane-associated, RING finger motif protein that interacts with Vps21p to facilitate soluble vacuolar protein localization. It is a component of the CORVET complex and is required for localization and trafficking of the CPY sorting receptor.
VTI1	None	*VTI1A, VTI1B*	Protein involved in cis-Golgi membrane traffic; v-SNARE that interacts with two t-SNARES, Sed5p and Pep12p; required for multiple vacuolar sorting pathways.
YMR1	None	Myotubularin	Phosphatidylinositol 3-phosphate (PI3P) phosphatase; involved in various protein sorting pathways, including CVT targeting and endosome to vacuole transport; has similarity to the conserved myotubularin dual specificity phosphatase family.

http://www.yeastgenome.org/, http://www.ihop-net.org/UniPub/iHOP/,

References

Abeliovich, H. and D. J. Klionsky (2001). "Autophagy in yeast: mechanistic insights and physiological function." Microbiol Mol Biol Rev **65**(3): 463-479, table of contents.

Acharya, J. K., P. Labarca, et al. (1998). "Synaptic defects and compensatory regulation of inositol metabolism in inositol polyphosphate 1-phosphatase mutants." Neuron **20**(6): 1219-1229.

Allaoui, A., R. Menard, et al. (1993). "Characterization of the Shigella flexneri ipgD and ipgF genes, which are located in the proximal part of the mxi locus." Infect Immun **61**(5): 1707-1714.

Amerik, A. Y., J. Nowak, et al. (2000). "The Doa4 deubiquitinating enzyme is functionally linked to the vacuolar protein-sorting and endocytic pathways." Mol Biol Cell **11**(10): 3365-3380.

Anderson, R. A., I. V. Boronenkov, et al. (1999). "Phosphatidylinositol phosphate kinases, a multifaceted family of signaling enzymes." J Biol Chem **274**(15): 9907-9910.

Angers, C. G. and A. J. Merz (2009). "HOPS interacts with Apl5 at the vacuole membrane and is required for consumption of AP-3 transport vesicles." Mol Biol Cell **20**(21): 4563-4574.

Baars, T. L., S. Petri, et al. (2007). "Role of the V-ATPase in regulation of the vacuolar fission-fusion equilibrium." Mol Biol Cell **18**(10): 3873-3882.

Babst, M., B. Wendland, et al. (1998). "The Vps4p AAA ATPase regulates membrane association of a Vps protein complex required for normal endosome function." EMBO J **17**(11): 2982-2993.

Baek, S. H., E. K. Kim, et al. (2009). "Insulin withdrawal-induced cell death in adult hippocampal neural stem cells as a model of autophagic cell death." Autophagy **5**(2): 277-279.

Balla, T. (2005). "Inositol-lipid binding motifs: signal integrators through protein-lipid and protein-protein interactions." J Cell Sci **118**(Pt 10): 2093-2104.

Balla, T. and K. J. Catt (1994). "Phosphoinositides and calcium signaling New aspects and diverse functions in cell regulation." Trends Endocrinol Metab **5**(6): 250-255.

Balla, T., Z. Szentpetery, et al. (2009). "Phosphoinositide signaling: new tools and insights." Physiology (Bethesda) **24**: 231-244.

Baskaran, S., M. J. Ragusa, et al. "Two-Site Recognition of Phosphatidylinositol 3-Phosphate by PROPPINs in Autophagy." Mol Cell **47**(3): 339-348.

Baskaran, S., M. J. Ragusa, et al. (2012). "How Atg18 and the WIPIs sense phosphatidylinositol 3-phosphate." Autophagy **8**(12).

Baxter, B. K., H. Abeliovich, et al. (2005). "Atg19p ubiquitination and the cytoplasm to vacuole trafficking pathway in yeast." J Biol Chem **280**(47): 39067-39076.

Begley, M. J., G. S. Taylor, et al. (2003). "Crystal structure of a phosphoinositide phosphatase, MTMR2: insights into myotubular myopathy and Charcot-Marie-Tooth syndrome." Mol Cell **12**(6): 1391-1402.

Behnia, R. and S. Munro (2005). "Organelle identity and the signposts for membrane traffic." Nature **438**(7068): 597-604.

Berwick, D. C., G. C. Dell, et al. (2004). "Protein kinase B phosphorylation of PIKfyve regulates the trafficking of GLUT4 vesicles." J Cell Sci **117**(Pt 25): 5985-5993.

Bethoney, K. A., M. C. King, et al. (2009). "A possible effector role for the pleckstrin homology (PH) domain of dynamin." Proc Natl Acad Sci U S A **106**(32): 13359-13364.

Bhaskar, P. T. and N. Hay (2007). "The two TORCs and Akt." Dev Cell **12**(4): 487-502.

Black, M. W. and H. R. Pelham (2000). "A selective transport route from Golgi to late endosomes that requires the yeast GGA proteins." J Cell Biol **151**(3): 587-600.

Blagoveshchenskaya, A., F. Y. Cheong, et al. (2008). "Integration of Golgi trafficking and growth factor signaling by the lipid phosphatase SAC1." J Cell Biol **180**(4): 803-812.

Blagoveshchenskaya, A. and P. Mayinger (2009). "SAC1 lipid phosphatase and growth control of the secretory pathway." Mol Biosyst **5**(1): 36-42.

Blero, D., F. De Smedt, et al. (2001). "The SH2 domain containing inositol 5-phosphatase SHIP2 controls phosphatidylinositol 3,4,5-trisphosphate levels in CHO-IR cells stimulated by insulin." Biochem Biophys Res Commun **282**(3): 839-843.

Blondeau, F., J. Laporte, et al. (2000). "Myotubularin, a phosphatase deficient in myotubular myopathy, acts on phosphatidylinositol 3-kinase and phosphatidylinositol 3-phosphate pathway." Hum Mol Genet **9**(15): 2223-2229.

Blondel, M. O., J. Morvan, et al. (2004). "Direct sorting of the yeast uracil permease to the endosomal system is controlled by uracil binding and Rsp5p-dependent ubiquitylation." Mol Biol Cell **15**(2): 883-895.

Boeddinghaus, C., A. J. Merz, et al. (2002). "A cycle of Vam7p release from and PtdIns 3-P-dependent rebinding to the yeast vacuole is required for homotypic vacuole fusion." J Cell Biol **157**(1): 79-89.

Bonangelino, C. J., N. L. Catlett, et al. (1997). "Vac7p, a novel vacuolar protein, is required for normal vacuole inheritance and morphology." Mol Cell Biol **17**(12): 6847-6858.

Bonangelino, C. J., J. J. Nau, et al. (2002). "Osmotic stress-induced increase of phosphatidylinositol 3,5-bisphosphate requires Vac14p, an activator of the lipid kinase Fab1p." J Cell Biol **156**(6): 1015-1028.

Boronenkov, I. V., J. C. Loijens, et al. (1998). "Phosphoinositide signaling pathways in nuclei are associated with nuclear speckles containing pre-mRNA processing factors." Mol Biol Cell **9**(12): 3547-3560.

Botelho, R. J., J. A. Efe, et al. (2008). "Assembly of a Fab1 phosphoinositide kinase signaling complex requires the Fig4 phosphoinositide phosphatase." Mol Biol Cell **19**(10): 4273-4286.

Bravo, J., D. Karathanassis, et al. (2001). "The crystal structure of the PX domain from p40(phox) bound to phosphatidylinositol 3-phosphate." Mol Cell **8**(4): 829-839.

Brice, S. E., C. W. Alford, et al. (2009). "Modulation of sphingolipid metabolism by the phosphatidylinositol-4-phosphate phosphatase Sac1p through regulation of phosphatidylinositol in Saccharomyces cerevisiae." J Biol Chem **284**(12): 7588-7596.

Bridges, D., J. T. Ma, et al. "Phosphatidylinositol 3,5-bisphosphate plays a role in the activation and subcellular localization of mechanistic target of rapamycin 1." Mol Biol Cell **23**(15): 2955-2962.

Bridges, D., J. T. Ma, et al. (2012). "Phosphatidylinositol 3,5-bisphosphate plays a role in the activation and subcellular localization of mechanistic target of rapamycin 1." Mol Biol Cell **23**(15): 2955-2962.

Bryant, N. J. and D. E. James (2001). "Vps45p stabilizes the syntaxin homologue Tlg2p and positively regulates SNARE complex formation." EMBO J **20**(13): 3380-3388.

Bryant, N. J., R. C. Piper, et al. (1998). "Traffic into the prevacuolar/endosomal compartment of Saccharomyces cerevisiae: a VPS45-dependent intracellular route and a VPS45-independent, endocytic route." Eur J Cell Biol **76**(1): 43-52.

Bryant, N. J., R. C. Piper, et al. (1998). "Retrograde traffic out of the yeast vacuole to the TGN occurs via the prevacuolar/endosomal compartment." J Cell Biol **142**(3): 651-663.

Budovskaya, Y. V., H. Hama, et al. (2002). "The C terminus of the Vps34p phosphoinositide 3-kinase is necessary and sufficient for the interaction with the Vps15p protein kinase." J Biol Chem **277**(1): 287-294.

Budovskaya, Y. V., J. S. Stephan, et al. (2005). "An evolutionary proteomics approach identifies substrates of the cAMP-dependent protein kinase." Proc Natl Acad Sci U S A **102**(39): 13933-13938.

Burda, P., S. M. Padilla, et al. (2002). "Retromer function in endosome-to-Golgi retrograde transport is regulated by the yeast Vps34 PtdIns 3-kinase." J Cell Sci **115**(Pt 20): 3889-3900.

Cabrera, M., C. W. Ostrowicz, et al. (2009). "Vps41 phosphorylation and the Rab Ypt7 control the targeting of the HOPS complex to endosome-vacuole fusion sites." Mol Biol Cell **20**(7): 1937-1948.

Carricaburu, V., K. A. Lamia, et al. (2003). "The phosphatidylinositol (PI)-5-phosphate 4-kinase type II enzyme controls insulin signaling by regulating PI-3,4,5-trisphosphate degradation." Proc Natl Acad Sci U S A **100**(17): 9867-9872.

Cebollero, E., A. van der Vaart, et al. "Phosphatidylinositol-3-phosphate clearance plays a key role in autophagosome completion." Curr Biol **22**(17): 1545-1553.

Chang-Ileto, B., S. G. Frere, et al. (2012). "Acute manipulation of phosphoinositide levels in cells." Methods Cell Biol **108**: 187-207.

Cheever, M. L., T. K. Sato, et al. (2001). "Phox domain interaction with PtdIns(3)P targets the Vam7 t-SNARE to vacuole membranes." Nat Cell Biol **3**(7): 613-618.

Chiang, G. G. and R. T. Abraham (2005). "Phosphorylation of mammalian target of rapamycin (mTOR) at Ser-2448 is mediated by p70S6 kinase." J Biol Chem **280**(27): 25485-25490.

Choudhury, R. R., N. Hyvola, et al. (2005). "Phosphoinositides and membrane traffic at the trans-Golgi network." Biochem Soc Symp(72): 31-38.

Chow, C. Y., J. E. Landers, et al. (2009). "Deleterious variants of FIG4, a phosphoinositide phosphatase, in patients with ALS." Am J Hum Genet **84**(1): 85-88.

Chow, C. Y., Y. Zhang, et al. (2007). "Mutation of FIG4 causes neurodegeneration in the pale tremor mouse and patients with CMT4J." Nature **448**(7149): 68-72.

Chu, E. C. and A. S. Tarnawski (2004). "PTEN regulatory functions in tumor suppression and cell biology." Med Sci Monit **10**(10): RA235-241.
Chung, J. K., F. Sekiya, et al. (1997). "Synaptojanin inhibition of phospholipase D activity by hydrolysis of phosphatidylinositol 4,5-bisphosphate." J Biol Chem **272**(25): 15980-15985.
Clarke, J. H., A. J. Letcher, et al. (2001). "Inositol lipids are regulated during cell cycle progression in the nuclei of murine erythroleukaemia cells." Biochem J **357**(Pt 3): 905-910.
Cleves, A. E., P. J. Novick, et al. (1989). "Mutations in the SAC1 gene suppress defects in yeast Golgi and yeast actin function." J Cell Biol **109**(6 Pt 1): 2939-2950.
Collins, K. M., N. L. Thorngren, et al. (2005). "Sec17p and HOPS, in distinct SNARE complexes, mediate SNARE complex disruption or assembly for fusion." EMBO J **24**(10): 1775-1786.
Cooke, F. T., S. K. Dove, et al. (1998). "The stress-activated phosphatidylinositol 3-phosphate 5-kinase Fab1p is essential for vacuole function in S. cerevisiae." Curr Biol **8**(22): 1219-1222.
Corda, D., C. Iurisci, et al. (2002). "Biological activities and metabolism of the lysophosphoinositides and glycerophosphoinositols." Biochim Biophys Acta **1582**(1-3): 52-69.
Corvera, S. (2000). "Signal transduction: stuck with FYVE domains." Sci STKE **2000**(37): pe1.
Corvera, S., A. D'Arrigo, et al. (1999). "Phosphoinositides in membrane traffic." Curr Opin Cell Biol **11**(4): 460-465.
Costaguta, G., M. C. Duncan, et al. (2006). "Distinct roles for TGN/endosome epsin-like adaptors Ent3p and Ent5p." Mol Biol Cell **17**(9): 3907-3920.
Cote, J. F. and K. Vuori (2009). "Cell biology. Two lipids that give direction." Science **324**(5925): 346-347.
Cowles, C. R., G. Odorizzi, et al. (1997). "The AP-3 adaptor complex is essential for cargo-selective transport to the yeast vacuole." Cell **91**(1): 109-118.
Cowles, C. R., W. B. Snyder, et al. (1997). "Novel Golgi to vacuole delivery pathway in yeast: identification of a sorting determinant and required transport component." EMBO J **16**(10): 2769-2782.
Cremona, O. and P. De Camilli (2001). "Phosphoinositides in membrane traffic at the synapse." J Cell Sci **114**(Pt 6): 1041-1052.
Darsow, T., D. J. Katzmann, et al. (2001). "Vps41p function in the alkaline phosphatase pathway requires homo-oligomerization and interaction with AP-3 through two distinct domains." Mol Biol Cell **12**(1): 37-51.
Demaurex, N. (2002). "pH Homeostasis of cellular organelles." News Physiol Sci **17**: 1-5.
Denu, J. M. and J. E. Dixon (1998). "Protein tyrosine phosphatases: mechanisms of catalysis and regulation." Curr Opin Chem Biol **2**(5): 633-641.
Dong, X. P., D. Shen, et al. (2010). "PI(3,5)P(2) controls membrane trafficking by direct activation of mucolipin Ca(2+) release channels in the endolysosome." Nat Commun **1**: 38.
Dove, S. K., F. T. Cooke, et al. (1997). "Osmotic stress activates phosphatidylinositol-3,5-bisphosphate synthesis." Nature **390**(6656): 187-192.
Dove, S. K., K. Dong, et al. (2009). "Phosphatidylinositol 3,5-bisphosphate and Fab1p/PIKfyve underPPIn endo-lysosome function." Biochem J **419**(1): 1-13.
Dove, S. K. and Z. E. Johnson (2007). "Our FABulous VACation: a decade of phosphatidylinositol 3,5-bisphosphate." Biochem Soc Symp(74): 129-139.
Dove, S. K., C. W. Lloyd, et al. (1994). "Identification of a phosphatidylinositol 3-hydroxy kinase in plant cells: association with the cytoskeleton." Biochem J **303 (Pt 2)**: 347-350.
Dove, S. K., R. K. McEwen, et al. (1999). "Phosphatidylinositol 3,5-bisphosphate: a novel lipid that links stress responses to membrane trafficking events." Biochem Soc Trans **27**(4): 674-677.
Dove, S. K., R. K. McEwen, et al. (2002). "Vac14 controls PtdIns(3,5)P(2) synthesis and Fab1-dependent protein trafficking to the multivesicular body." Curr Biol **12**(11): 885-893.
Dove, S. K. and R. H. Michell (2009). "Inositol lipid-dependent functions in Saccharomyces cerevisiae: analysis of phosphatidylinositol phosphates." Methods Mol Biol **462**: 59-74.
Dove, S. K., R. C. Piper, et al. (2004). "Svp1p defines a family of phosphatidylinositol 3,5-bisphosphate effectors." Embo J **23**(9): 1922-1933.
Dowler, S., G. Kular, et al. (2002). "Protein lipid overlay assay." Sci STKE **2002**(129): pl6.
Duex, J. E., F. Tang, et al. (2006). "The Vac14p-Fig4p complex acts independently of Vac7p and couples PI3,5P2 synthesis and turnover." J Cell Biol **172**(5): 693-704.
Dumas, J. J., E. Merithew, et al. (2001). "Multivalent endosome targeting by homodimeric EEA1." Mol Cell **8**(5): 947-958.
Efe, J. A., R. J. Botelho, et al. (2005). "The Fab1 phosphatidylinositol kinase pathway in the regulation of vacuole morphology." Curr Opin Cell Biol **17**(4): 402-408.

Efe, J. A., R. J. Botelho, et al. (2007). "Atg18 regulates organelle morphology and Fab1 kinase activity independent of its membrane recruitment by phosphatidylinositol 3,5-bisphosphate." Mol Biol Cell **18**(11): 4232-4244.
Ellson, C., K. Davidson, et al. (2006). "PtdIns3P binding to the PX domain of p40phox is a physiological signal in NADPH oxidase activation." EMBO J **25**(19): 4468-4478.
Emr, S. D. and V. V. Malhotra (1997). "Membranes and sorting." Curr Opin Cell Biol **9**(4): 475-476.
Erdman, S., L. Lin, et al. (1998). "Pheromone-regulated genes required for yeast mating differentiation." J Cell Biol **140**(3): 461-483.
Erdmann, K. S., Y. Mao, et al. (2007). "A role of the Lowe syndrome protein OCRL in early steps of the endocytic pathway." Dev Cell **13**(3): 377-390.
Eugster, A., E. I. Pecheur, et al. (2004). "Ent5p is required with Ent3p and Vps27p for ubiquitin-dependent protein sorting into the multivesicular body." Mol Biol Cell **15**(7): 3031-3041.
Ferguson, C. J., G. M. Lenk, et al. (2012). "Neuronal expression of Fig4 is both necessary and sufficient to prevent spongiform neurodegeneration." Hum Mol Genet **21**(16): 3525-3534.
Foti, M., A. Audhya, et al. (2001). "Sac1 lipid phosphatase and Stt4 phosphatidylinositol 4-kinase regulate a pool of phosphatidylinositol 4-phosphate that functions in the control of the actin cytoskeleton and vacuole morphology." Mol Biol Cell **12**(8): 2396-2411.
Friant, S., E. I. Pecheur, et al. (2003). "Ent3p Is a PtdIns(3,5)P2 effector required for protein sorting to the multivesicular body." Dev Cell **5**(3): 499-511.
Fry, M. J. (1994). "Structure, regulation and function of phosphoinositide 3-kinases." Biochim Biophys Acta **1226**(3): 237-268.
Futerman, A. H. and G. van Meer (2004). "The cell biology of lysosomal storage disorders." Nat Rev Mol Cell Biol **5**(7): 554-565.
Gary, J. D., T. K. Sato, et al. (2002). "Regulation of Fab1 phosphatidylinositol 3-phosphate 5-kinase pathway by Vac7 protein and Fig4, a polyphosphoinositide phosphatase family member." Mol Biol Cell **13**(4): 1238-1251.
Gary, J. D., A. E. Wurmser, et al. (1998). "Fab1p is essential for PtdIns(3)P 5-kinase activity and the maintenance of vacuolar size and membrane homeostasis." J Cell Biol **143**(1): 65-79.
Gaullier, J. M., A. Simonsen, et al. (1998). "FYVE fingers bind PtdIns(3)P." Nature **394**(6692): 432-433.
Gillooly, D. J., I. C. Morrow, et al. (2000). "Localization of phosphatidylinositol 3-phosphate in yeast and mammalian cells." EMBO J **19**(17): 4577-4588.
Gilman, A. G. (1987). "G proteins: transducers of receptor-generated signals." Annu Rev Biochem **56**: 615-649.
Godi, A., A. Di Campli, et al. (2004). "FAPPs control Golgi-to-cell-surface membrane traffic by binding to ARF and PtdIns(4)P." Nat Cell Biol **6**(5): 393-404.
Gozani, O., P. Karuman, et al. (2003). "The PHD finger of the chromatin-associated protein ING2 functions as a nuclear phosphoinositide receptor." Cell **114**(1): 99-111.
Guan, J., P. E. Stromhaug, et al. (2001). "Cvt18/Gsa12 is required for cytoplasm-to-vacuole transport, pexophagy, and autophagy in Saccharomyces cerevisiae and Pichia pastoris." Mol Biol Cell **12**(12): 3821-3838.
Halstead, J. R., M. Roefs, et al. (2001). "A novel pathway of cellular phosphatidylinositol(3,4,5)-trisphosphate synthesis is regulated by oxidative stress." Curr Biol **11**(6): 386-395.
Han, B. K. and S. D. Emr (2011). "Phosphoinositide [PI(3,5)P2] lipid-dependent regulation of the general transcriptional regulator Tup1." Genes Dev **25**(9): 984-995.
He, J., M. Vora, et al. (2009). "Membrane insertion of the FYVE domain is modulated by pH." Proteins **76**(4): 852-860.
Helmkamp, G. M., Jr. (1990). "Transport and metabolism of phosphatidylinositol in eukaryotic cells." Subcell Biochem **16**: 129-174.
Herman, P. K. and S. D. Emr (1990). "Characterization of VPS34, a gene required for vacuolar protein sorting and vacuole segregation in Saccharomyces cerevisiae." Mol Cell Biol **10**(12): 6742-6754.
Herman, P. K., J. H. Stack, et al. (1991). "A novel protein kinase homolog essential for protein sorting to the yeast lysosome-like vacuole." Cell **64**(2): 425-437.
Herman, P. K., J. H. Stack, et al. (1991). "A genetic and structural analysis of the yeast Vps15 protein kinase: evidence for a direct role of Vps15p in vacuolar protein delivery." EMBO J **10**(13): 4049-4060.
Hickinson, D. M., J. M. Lucocq, et al. (1997). "Association of a phosphatidylinositol-specific 3-kinase with a human trans-Golgi network resident protein." Curr Biol **7**(12): 987-990.

Hill, E. V., C. A. Hudson, et al. (2010). "Regulation of PIKfyve phosphorylation by insulin and osmotic stress." Biochem Biophys Res Commun **397**(4): 650-655.
Hirst, J., S. E. Miller, et al. (2004). "EpsinR is an adaptor for the SNARE protein Vti1b." Mol Biol Cell **15**(12): 5593-5602.
Hokin, L. E. and M. R. Hokin (1958). "The presence of phosphatidic acid in animal tissues." J Biol Chem **233**(4): 800-804.
Homma, K., S. Terui, et al. (1998). "Phosphatidylinositol-4-phosphate 5-kinase localized on the plasma membrane is essential for yeast cell morphogenesis." J Biol Chem **273**(25): 15779-15786.
Hope, H. R. and L. J. Pike (1996). "Phosphoinositides and phosphoinositide-utilizing enzymes in detergent-insoluble lipid domains." Mol Biol Cell **7**(6): 843-851.
Hu, G., M. Hacham, et al. (2008). "PI3K signaling of autophagy is required for starvation tolerance and virulenceof Cryptococcus neoformans." J Clin Invest **118**(3): 1186-1197.
Hughes, W. E., F. T. Cooke, et al. (2000). "Sac phosphatase domain proteins." Biochem J **350 Pt 2**: 337-352.
Hughes, W. E., R. Woscholski, et al. (2000). "SAC1 encodes a regulated lipid phosphoinositide phosphatase, defects in which can be suppressed by the homologous Inp52p and Inp53p phosphatases." J Biol Chem **275**(2): 801-808.
Hurley, J. H., E. Boura, et al. "Membrane budding." Cell **143**(6): 875-887.
Hyman, J., H. Chen, et al. (2000). "Epsin 1 undergoes nucleocytosolic shuttling and its eps15 interactor NH(2)-terminal homology (ENTH) domain, structurally similar to Armadillo and HEAT repeats, interacts with the transcription factor promyelocytic leukemia Zn(2)+ finger protein (PLZF)." J Cell Biol **149**(3): 537-546.
Ikezawa, H. (2002). "Glycosylphosphatidylinositol (GPI)-anchored proteins." Biol Pharm Bull **25**(4): 409-417.
Ikonomov, O. C., J. Fligger, et al. (2009). "Kinesin adapter JLP links PIKfyve to microtubule-based endosome-to-trans-Golgi network traffic of furin." J Biol Chem **284**(6): 3750-3761.
Ikonomov, O. C., D. Sbrissa, et al. (2007). "ArPIKfyve-PIKfyve interaction and role in insulin-regulated GLUT4 translocation and glucose transport in 3T3-L1 adipocytes." Exp Cell Res **313**(11): 2404-2416.
Ikonomov, O. C., D. Sbrissa, et al. (2002). "Functional dissection of lipid and protein kinase signals of PIKfyve reveals the role of PtdIns 3,5-P2 production for endomembrane integrity." J Biol Chem **277**(11): 9206-9211.
Irvine, R. F. (1987). "Inositol phosphates and calcium entry." Nature **328**(6129): 386.
Irvine, R. F. (1987). "The metabolism and function of inositol phosphates." Biochem Soc Trans **15**(1): 122-123.
Irvine, R. F. (1992). "Inositol phosphates and Ca2+ entry: toward a proliferation or a simplification?" FASEB J **6**(12): 3085-3091.
Irvine, R. F. and R. M. Dawson (1980). "The mechanism and function of phosphatidylinositol turnover [proceedings]." Biochem Soc Trans **8**(3): 376-377.
Irvine, R. F., A. J. Letcher, et al. (1984). "Phosphatidylinositol-4,5-bisphosphate phosphodiesterase and phosphomonoesterase activities of rat brain. Some properties and possible control mechanisms." Biochem J **218**(1): 177-185.
Ishihara, H., Y. Shibasaki, et al. (1996). "Cloning of cDNAs encoding two isoforms of 68-kDa type I phosphatidylinositol-4-phosphate 5-kinase." J Biol Chem **271**(39): 23611-23614.
Janke, C., M. M. Magiera, et al. (2004). "A versatile toolbox for PCR-based tagging of yeast genes: new fluorescent proteins, more markers and promoter substitution cassettes." Yeast **21**(11): 947-962.
Jefferies, H. B., F. T. Cooke, et al. (2008). "A selective PIKfyve inhibitor blocks PtdIns(3,5)P(2) production and disrupts endomembrane transport and retroviral budding." EMBO Rep **9**(2): 164-170.
Jeffries, T. R., S. K. Dove, et al. (2004). "PtdIns-specific MPR pathway association of a novel WD40 repeat protein, WIPI49." Mol Biol Cell **15**(6): 2652-2663.
Jin, N., C. Y. Chow, et al. (2008). "VAC14 nucleates a protein complex essential for the acute interconversion of PI3P and PI(3,5)P(2) in yeast and mouse." EMBO J **27**(24): 3221-3234.
Jones, A. T., I. G. Mills, et al. (1998). "Inhibition of endosome fusion by wortmannin persists in the presence of activated Rab5." Mol Biol Cell **9**(2): 323-332.
Jordens, I., M. Marsman, et al. (2005). "Rab proteins, connecting transport and vesicle fusion." Traffic **6**(12): 1070-1077.

Jourdain, I., Y. Gachet, et al. (2009). "The dynamin related protein Dnm1 fragments mitochondria in a microtubule-dependent manner during the fission yeast cell cycle." Cell Motil Cytoskeleton **66**(8): 509-523.
Kametaka, S., T. Okano, et al. (1998). "Apg14p and Apg6/Vps30p form a protein complex essential for autophagy in the yeast, Saccharomyces cerevisiae." J Biol Chem **273**(35): 22284-22291.
Kane, P. M. (2005). "Close-up and genomic views of the yeast vacuolar H+-ATPase." J Bioenerg Biomembr **37**(6): 399-403.
Karunakaran, S., T. Sasser, et al. (2012). "SNAREs, HOPS and regulatory lipids control the dynamics of vacuolar actin during homotypic fusion in S. cerevisiae." J Cell Sci **125**(Pt 7): 1683-1692.
Katzmann, D. J., M. Babst, et al. (2001). "Ubiquitin-dependent sorting into the multivesicular body pathway requires the function of a conserved endosomal protein sorting complex, ESCRT-I." Cell **106**(2): 145-155.
Katzmann, D. J., G. Odorizzi, et al. (2002). "Receptor downregulation and multivesicular-body sorting." Nat Rev Mol Cell Biol **3**(12): 893-905.
Katzmann, D. J., S. Sarkar, et al. (2004). "Multivesicular body sorting: ubiquitin ligase Rsp5 is required for the modification and sorting of carboxypeptidase S." Mol Biol Cell **15**(2): 468-480.
Katzmann, D. J., C. J. Stefan, et al. (2003). "Vps27 recruits ESCRT machinery to endosomes during MVB sorting." J Cell Biol **162**(3): 413-423.
Kihara, A., T. Noda, et al. (2001). "Two distinct Vps34 phosphatidylinositol 3-kinase complexes function in autophagy and carboxypeptidase Y sorting in Saccharomyces cerevisiae." J Cell Biol **152**(3): 519-530.
Kim, J., Y. Kamada, et al. (2001). "Cvt9/Gsa9 functions in sequestering selective cytosolic cargo destined for the vacuole." J Cell Biol **153**(2): 381-396.
Kim, S. A., P. O. Vacratsis, et al. (2003). "Regulation of myotubularin-related (MTMR)2 phosphatidylinositol phosphatase by MTMR5, a catalytically inactive phosphatase." Proc Natl Acad Sci U S A **100**(8): 4492-4497.
King, J. S., R. Teo, et al. (2009). "The mood stabiliser lithium suppresses PIP3 signalling in Dictyostelium and human cells." Dis Model Mech **2**(5-6): 306-312.
Kirkin, V., D. G. McEwan, et al. (2009). "A role for ubiquitin in selective autophagy." Mol Cell **34**(3): 259-269.
Klionsky, D. J. (2009). "Autophagy in mammalian systems, Part B. Preface." Methods Enzymol **452**: xxi-xxii.
Knodler, A., G. Konrad, et al. (2008). "Expression of yeast lipid phosphatase Sac1p is regulated by phosphatidylinositol-4-phosphate." BMC Mol Biol **9**: 16.
Kobayashi, T., K. Suzuki, et al. "Autophagosome formation can be achieved in the absence of Atg18 by expressing engineered PAS-targeted Atg2." FEBS Lett **586**(16): 2473-2478.
Kochendorfer, K. U., A. R. Then, et al. (1999). "Sac1p plays a crucial role in microsomal ATP transport, which is distinct from its function in Golgi phospholipid metabolism." Embo J **18**(6): 1506-1515.
Kotoulas, A., H. Kokotas, et al. (2011). "A novel PIKFYVE mutation in fleck corneal dystrophy." Mol Vis **17**: 2776-2781.
Krick, R., S. Henke, et al. (2008). "Dissecting the localization and function of Atg18, Atg21 and Ygr223c." Autophagy **4**(7): 896-910.
Krick, R., Y. Muehe, et al. (2008). "Piecemeal microautophagy of the nucleus requires the core macroautophagy genes." Mol Biol Cell **19**(10): 4492-4505.
Krick, R., J. Tolstrup, et al. (2006). "The relevance of the phosphatidylinositolphosphat-binding motif FRRGT of Atg18 and Atg21 for the Cvt pathway and autophagy." FEBS Lett **580**(19): 4632-4638.
Kunz, J., M. P. Wilson, et al. (2000). "The activation loop of phosphatidylinositol phosphate kinases determines signaling specificity." Mol Cell **5**(1): 1-11.
Lafourcade, C., K. Sobo, et al. (2008). "Regulation of the V-ATPase along the endocytic pathway occurs through reversible subunit association and membrane localization." PLoS One **3**(7): e2758.
Lawe, D. C., A. Chawla, et al. (2002). "Sequential roles for phosphatidylinositol 3-phosphate and Rab5 in tethering and fusion of early endosomes via their interaction with EEA1." J Biol Chem **277**(10): 8611-8617.

Lawe, D. C., V. Patki, et al. (2000). "The FYVE domain of early endosome antigen 1 is required for both phosphatidylinositol 3-phosphate and Rab5 binding. Critical role of this dual interaction for endosomal localization." J Biol Chem **275**(5): 3699-3705.

Lazar, T., D. Scheglmann, et al. (2002). "A novel phospholipid-binding protein from the yeast Saccharomyces cerevisiae with dual binding specificities for the transport GTPase Ypt7p and the Sec1-related Vps33p." Eur J Cell Biol **81**(12): 635-646.

Lee, J. O., H. Yang, et al. (1999). "Crystal structure of the PTEN tumor suppressor: implications for its phosphoinositide phosphatase activity and membrane association." Cell **99**(3): 323-334.

Lee, S. Y., M. R. Wenk, et al. (2004). "Regulation of synaptojanin 1 by cyclin-dependent kinase 5 at synapses." Proc Natl Acad Sci U S A **101**(2): 546-551.

Lemmon, M. A. (2003). "Phosphoinositide recognition domains." Traffic **4**(4): 201-213.

Lemmon, M. A. (2008). "Membrane recognition by phospholipid-binding domains." Nat Rev Mol Cell Biol **9**(2): 99-111.

Lemmon, M. A., K. M. Ferguson, et al. (1995). "Specific and high-affinity binding of inositol phosphates to an isolated pleckstrin homology domain." Proc Natl Acad Sci U S A **92**(23): 10472-10476.

Lemmon, M. A., K. M. Ferguson, et al. (1996). "PH domains: diverse sequences with a common fold recruit signaling molecules to the cell surface." Cell **85**(5): 621-624.

Lemmon, S. K. and L. M. Traub (2000). "Sorting in the endosomal system in yeast and animal cells." Curr Opin Cell Biol **12**(4): 457-466.

Lenk, G. M., C. J. Ferguson, et al. (2011). "Pathogenic mechanism of the FIG4 mutation responsible for Charcot-Marie-Tooth disease CMT4J." PLoS Genet **7**(6): e1002104.

Lichter-Konecki, U., L. W. Farber, et al. (2006). "The effect of missense mutations in the RhoGAP-homology domain on ocrl1 function." Mol Genet Metab **89**(1-2): 121-128.

Liscovitch, M. and L. C. Cantley (1995). "Signal transduction and membrane traffic: the PITP/phosphoinositide connection." Cell **81**(5): 659-662.

Lorenzo, O., S. Urbe, et al. (2005). "Analysis of phosphoinositide binding domain properties within the myotubularin-related protein MTMR3." J Cell Sci **118**(Pt 9): 2005-2012.

Luthi, A., G. Di Paolo, et al. (2001). "Synaptojanin 1 contributes to maintaining the stability of GABAergic transmission in primary cultures of cortical neurons." J Neurosci **21**(23): 9101-9111.

Macdonald, C., D. K. Stringer, et al. "Sna3 Is an Rsp5 Adaptor Protein that Relies on Ubiquitination for Its MVB Sorting." Traffic.

Markgraf, D. F., F. Ahnert, et al. (2009). "The CORVET subunit Vps8 cooperates with the Rab5 homolog Vps21 to induce clustering of late endosomal compartments." Mol Biol Cell **20**(24): 5276-5289.

Matthews, R. J., D. B. Bowne, et al. (1992). "Characterization of hematopoietic intracellular protein tyrosine phosphatases: description of a phosphatase containing an SH2 domain and another enriched in proline-, glutamic acid-, serine-, and threonine-rich sequences." Mol Cell Biol **12**(5): 2396-2405.

Mayinger, P. (2009). "Regulation of Golgi function via phosphoinositide lipids." Semin Cell Dev Biol **20**(7): 793-800.

Mayinger, P., V. A. Bankaitis, et al. (1995). "Sac1p mediates the adenosine triphosphate transport into yeast endoplasmic reticulum that is required for protein translocation." J Cell Biol **131**(6 Pt 1): 1377-1386.

McCrea, H. J., S. Paradise, et al. (2008). "All known patient mutations in the ASH-RhoGAP domains of OCRL affect targeting and APPL1 binding." Biochem Biophys Res Commun **369**(2): 493-499.

McDonald, B. and J. Martin-Serrano (2009). "No strings attached: the ESCRT machinery in viral budding and cytokinesis." J Cell Sci **122**(Pt 13): 2167-2177.

McEwen, R. K., S. K. Dove, et al. (1999). "Complementation analysis in PtdInsP kinase-deficient yeast mutants demonstrates that Schizosaccharomyces pombe and murine Fab1p homologues are phosphatidylinositol 3-phosphate 5-kinases." J Biol Chem **274**(48): 33905-33912.

Meijer, H. J., C. P. Berrie, et al. (2001). "Identification of a new polyphosphoinositide in plants, phosphatidylinositol 5-monophosphate (PtdIns5P), and its accumulation upon osmotic stress." Biochem J **360**(Pt 2): 491-498.

Michell, R. H., V. L. Heath, et al. (2006). "Phosphatidylinositol 3,5-bisphosphate: metabolism and cellular functions." Trends Biochem Sci **31**(1): 52-63.

Minagawa, T., T. Ijuin, et al. (2001). "Identification and characterization of a sac domain-containing phosphoinositide 5-phosphatase." J Biol Chem **276**(25): 22011-22015.
Mishra, A., S. Eathiraj, et al. (2010). "Structural basis for Rab GTPase recognition and endosome tethering by the C2H2 zinc finger of Early Endosomal Autoantigen 1 (EEA1)." Proc Natl Acad Sci U S A **107**(24): 10866-10871.
Misra, S. and J. H. Hurley (1999). "Crystal structure of a phosphatidylinositol 3-phosphate-specific membrane-targeting motif, the FYVE domain of Vps27p." Cell **97**(5): 657-666.
Morris, J. B., K. A. Hinchliffe, et al. (2000). "Thrombin stimulation of platelets causes an increase in phosphatidylinositol 5-phosphate revealed by mass assay." FEBS Lett **475**(1): 57-60.
Mruk, D. D. and C. Y. Cheng (2011). "The myotubularin family of lipid phosphatases in disease and in spermatogenesis." Biochem J **433**(2): 253-262.
Muller, O., M. J. Bayer, et al. (2002). "The Vtc proteins in vacuole fusion: coupling NSF activity to V(0) trans-complex formation." EMBO J **21**(3): 259-269.
Mund, T. and H. R. Pelham (2010). "Regulation of PTEN/Akt and MAP kinase signaling pathways by the ubiquitin ligase activators Ndfip1 and Ndfip2." Proc Natl Acad Sci U S A **107**(25): 11429-11434.
Myers, M. P., I. Pass, et al. (1998). "The lipid phosphatase activity of PTEN is critical for its tumor supressor function." Proc Natl Acad Sci U S A **95**(23): 13513-13518.
Nakamura, Y., Y. Hamada, et al. (2005). "Phospholipase C-delta1 and -delta3 are essential in the trophoblast for placental development." Mol Cell Biol **25**(24): 10979-10988.
Narayan, K. and M. A. Lemmon (2006). "Determining selectivity of phosphoinositide-binding domains." Methods **39**(2): 122-133.
Nemoto, Y., B. G. Kearns, et al. (2000). "Functional characterization of a mammalian Sac1 and mutants exhibiting substrate-specific defects in phosphoinositide phosphatase activity." J Biol Chem **275**(44): 34293-34305.
Nice, D. C., T. K. Sato, et al. (2002). "Cooperative binding of the cytoplasm to vacuole targeting pathway proteins, Cvt13 and Cvt20, to phosphatidylinositol 3-phosphate at the pre-autophagosomal structure is required for selective autophagy." J Biol Chem **277**(33): 30198-30207.
Nickerson, D. P., C. L. Brett, et al. (2009). "Vps-C complexes: gatekeepers of endolysosomal traffic." Curr Opin Cell Biol **21**(4): 543-551.
Nicot, A. S. and J. Laporte (2008). "Endosomal phosphoinositides and human diseases." Traffic **9**(8): 1240-1249.
Nieland, T. J., Y. Feng, et al. (2004). "Chemical genetic screening identifies sulfonamides that raise organellar pH and interfere with membrane traffic." Traffic **5**(7): 478-492.
Nishizuka, Y. (1995). "Protein kinase C and lipid signaling for sustained cellular responses." FASEB J **9**(7): 484-496.
Oancea, E. and T. Meyer (1998). "Protein kinase C as a molecular machine for decoding calcium and diacylglycerol signals." Cell **95**(3): 307-318.
Obara, K., T. Noda, et al. (2008). "Transport of phosphatidylinositol 3-phosphate into the vacuole via autophagic membranes in Saccharomyces cerevisiae." Genes Cells **13**(6): 537-547.
Obara, K. and Y. Ohsumi "PtdIns 3-Kinase Orchestrates Autophagosome Formation in Yeast." J Lipids **2011**: 498768.
Obara, K. and Y. Ohsumi (2008). "Dynamics and function of PtdIns(3)P in autophagy." Autophagy **4**(7): 952-954.
Obara, K. and Y. Ohsumi (2011). "Atg14: a key player in orchestrating autophagy." Int J Cell Biol **2011**: 713435.
Obara, K. and Y. Ohsumi (2011). "PtdIns 3-Kinase Orchestrates Autophagosome Formation in Yeast." J Lipids **2011**: 498768.
Obara, K., T. Sekito, et al. (2008). "The Atg18-Atg2 complex is recruited to autophagic membranes via phosphatidylinositol 3-phosphate and exerts an essential function." J Biol Chem **283**(35): 23972-23980.
Obara, K., T. Sekito, et al. (2006). "Assortment of phosphatidylinositol 3-kinase complexes--Atg14p directs association of complex I to the pre-autophagosomal structure in Saccharomyces cerevisiae." Mol Biol Cell **17**(4): 1527-1539.
Odorizzi, G., M. Babst, et al. (1998). "Fab1p PtdIns(3)P 5-kinase function essential for protein sorting in the multivesicular body." Cell **95**(6): 847-858.
Odorizzi, G., M. Babst, et al. (2000). "Phosphoinositide signaling and the regulation of membrane trafficking in yeast." Trends Biochem Sci **25**(5): 229-235.

Odorizzi, G., C. R. Cowles, et al. (1998). "The AP-3 complex: a coat of many colours." Trends Cell Biol **8**(7): 282-288.
Oestreich, A. J., M. Aboian, et al. (2007). "Characterization of multiple multivesicular body sorting determinants within Sna3: a role for the ubiquitin ligase Rsp5." Mol Biol Cell **18**(2): 707-720.
Ohsumi, Y. (2001). "Molecular dissection of autophagy: two ubiquitin-like systems." Nat Rev Mol Cell Biol **2**(3): 211-216.
Ohtaki, A., K. Noguchi, et al. (2010). "Structure and function of archaeal prefoldin, a co-chaperone of group II chaperonin." Front Biosci **15**: 708-717.
Ooms, L. M., C. G. Fedele, et al. (2006). "The inositol polyphosphate 5-phosphatase, PIPP, Is a novel regulator of phosphoinositide 3-kinase-dependent neurite elongation." Mol Biol Cell **17**(2): 607-622.
Ostrowicz, C. W., C. T. Meiringer, et al. (2008). "Yeast vacuole fusion: a model system for eukaryotic endomembrane dynamics." Autophagy **4**(1): 5-19.
Overmeyer, J. H., R. A. Erdman, et al. (1998). "Membrane targeting via protein prenylation." Methods Mol Biol **88**: 249-263.
Pagliarini, D. J., C. A. Worby, et al. (2004). "A PTEN-like phosphatase with a novel substrate specificity." J Biol Chem **279**(37): 38590-38596.
Panek, H. R., J. D. Stepp, et al. (1997). "Suppressors of YCK-encoded yeast casein kinase 1 deficiency define the four subunits of a novel clathrin AP-like complex." Embo J **16**(14): 4194-4204.
Parrish, W. R., C. J. Stefan, et al. (2004). "Essential role for the myotubularin-related phosphatase Ymr1p and the synaptojanin-like phosphatases Sjl2p and Sjl3p in regulation of phosphatidylinositol 3-phosphate in yeast." Mol Biol Cell **15**(8): 3567-3579.
Pashkova, N., L. Gakhar, et al. "WD40 repeat propellers define a ubiquitin-binding domain that regulates turnover of F box proteins." Mol Cell **40**(3): 433-443.
Payrastre, B., K. Missy, et al. (2001). "Phosphoinositides: key players in cell signalling, in time and space." Cell Signal **13**(6): 377-387.
Peplowska, K., D. F. Markgraf, et al. (2007). "The CORVET tethering complex interacts with the yeast Rab5 homolog Vps21 and is involved in endo-lysosomal biogenesis." Dev Cell **12**(5): 739-750.
Peters, C., T. L. Baars, et al. (2004). "Mutual control of membrane fission and fusion proteins." Cell **119**(5): 667-678.
Phelan, J. P., S. H. Millson, et al. (2006). "Fab1p and AP-1 are required for trafficking of endogenously ubiquitylated cargoes to the vacuole lumen in S. cerevisiae." J Cell Sci **119**(Pt 20): 4225-4234.
Phizicky, E. M. and S. Fields (1995). "Protein-protein interactions: methods for detection and analysis." Microbiol Rev **59**(1): 94-123.
Piper, R. C., N. J. Bryant, et al. (1997). "The membrane protein alkaline phosphatase is delivered to the vacuole by a route that is distinct from the VPS-dependent pathway." J Cell Biol **138**(3): 531-545.
Pizarro-Cerda, J. and P. Cossart (2004). "Subversion of phosphoinositide metabolism by intracellular bacterial pathogens." Nat Cell Biol **6**(11): 1026-1033.
Proikas-Cezanne, T. and S. G. Pfisterer (2009). "Assessing mammalian autophagy by WIPI-1/Atg18 puncta formation." Methods Enzymol **452**: 247-260.
Proikas-Cezanne, T., S. Ruckerbauer, et al. (2007). "Human WIPI-1 puncta-formation: a novel assay to assess mammalian autophagy." FEBS Lett **581**(18): 3396-3404.
Proikas-Cezanne, T., S. Waddell, et al. (2004). "WIPI-1alpha (WIPI49), a member of the novel 7-bladed WIPI protein family, is aberrantly expressed in human cancer and is linked to starvation-induced autophagy." Oncogene **23**(58): 9314-9325.
Rameh, L. E., K. F. Tolias, et al. (1997). "A new pathway for synthesis of phosphatidylinositol-4,5-bisphosphate." Nature **390**(6656): 192-196.
Razzini, G., A. Brancaccio, et al. (2000). "The role of the pleckstrin homology domain in membrane targeting and activation of phospholipase Cbeta(1)." J Biol Chem **275**(20): 14873-14881.
Reggiori, F. and H. R. Pelham (2001). "Sorting of proteins into multivesicular bodies: ubiquitin-dependent and -independent targeting." EMBO J **20**(18): 5176-5186.
Ren, J., N. Pashkova, et al. (2008). "DOA1/UFD3 plays a role in sorting ubiquitinated membrane proteins into multivesicular bodies." J Biol Chem **283**(31): 21599-21611.
Robinson, M. S. (2004). "Adaptable adaptors for coated vesicles." Trends Cell Biol **14**(4): 167-174.
Rohacs, T. (2007). "Regulation of TRP channels by PIP(2)." Pflugers Arch **453**(6): 753-762.

Rohacs, T. and B. Nilius (2007). "Regulation of transient receptor potential (TRP) channels by phosphoinositides." Pflugers Arch **455**(1): 157-168.
Roth, M. G. (2004). "Phosphoinositides in constitutive membrane traffic." Physiol Rev **84**(3): 699-730.
Rothman, J. H., I. Howald, et al. (1989). "Characterization of genes required for protein sorting and vacuolar function in the yeast Saccharomyces cerevisiae." EMBO J **8**(7): 2057-2065.
Rubino, M., M. Miaczynska, et al. (2000). "Selective membrane recruitment of EEA1 suggests a role in directional transport of clathrin-coated vesicles to early endosomes." J Biol Chem **275**(6): 3745-3748.
Rudge, S. A., D. M. Anderson, et al. (2004). "Vacuole size control: regulation of PtdIns(3,5)P2 levels by the vacuole-associated Vac14-Fig4 complex, a PtdIns(3,5)P2-specific phosphatase." Mol Biol Cell **15**(1): 24-36.
Sasaoka, T., H. Hori, et al. (2001). "SH2-containing inositol phosphatase 2 negatively regulates insulin-induced glycogen synthesis in L6 myotubes." Diabetologia **44**(10): 1258-1267.
Sbrissa, D., O. C. Ikonomov, et al. (2002). "Phosphatidylinositol 5-phosphate biosynthesis is linked to PIKfyve and is involved in osmotic response pathway in mammalian cells." J Biol Chem **277**(49): 47276-47284.
Sbrissa, D., O. C. Ikonomov, et al. (2012). "Functional dissociation between PIKfyve-synthesized PtdIns5P and PtdIns(3,5)P2 by means of the PIKfyve inhibitor YM201636." Am J Physiol Cell Physiol **303**(4): C436-446.
Sbrissa, D., O. C. Ikonomov, et al. (2002). "Phosphatidylinositol 3-phosphate-interacting domains in PIKfyve. Binding specificity and role in PIKfyve. Endomenbrane localization." J Biol Chem **277**(8): 6073-6079.
Scanga, S. E., L. Ruel, et al. (2000). "The conserved PI3'K/PTEN/Akt signaling pathway regulates both cell size and survival in Drosophila." Oncogene **19**(35): 3971-3977.
Schaletzky, J., S. K. Dove, et al. (2003). "Phosphatidylinositol-5-phosphate activation and conserved substrate specificity of the myotubularin phosphatidylinositol 3-phosphatases." Curr Biol **13**(6): 504-509.
Schorr, M., A. Then, et al. (2001). "The phosphoinositide phosphatase Sac1p controls trafficking of the yeast Chs3p chitin synthase." Curr Biol **11**(18): 1421-1426.
Schu, P. V., K. Takegawa, et al. (1993). "Phosphatidylinositol 3-kinase encoded by yeast VPS34 gene essential for protein sorting." Science **260**(5104): 88-91.
Seaman, M. N., E. G. Marcusson, et al. (1997). "Endosome to Golgi retrieval of the vacuolar protein sorting receptor, Vps10p, requires the function of the VPS29, VPS30, and VPS35 gene products." J Cell Biol **137**(1): 79-92.
Shisheva, A. (2008). "PIKfyve: Partners, significance, debates and paradoxes." Cell Biol Int **32**(6): 591-604.
Siegel, M. R. and H. D. Sisler (1963). "Inhibition of Protein Synthesis in Vitro by Cycloheximide." Nature **200**: 675-676.
Simonsen, A., R. Lippe, et al. (1998). "EEA1 links PI(3)K function to Rab5 regulation of endosome fusion." Nature **394**(6692): 494-498.
Smaczynska-de, R., II, E. G. Allwood, et al. "A role for the dynamin-like protein Vps1 during endocytosis in yeast." J Cell Sci **123**(Pt 20): 3496-3506.
Springer, S., A. Spang, et al. (1999). "A primer on vesicle budding." Cell **97**(2): 145-148.
Stack, J. H., D. B. DeWald, et al. (1995). "Vesicle-mediated protein transport: regulatory interactions between the Vps15 protein kinase and the Vps34 PtdIns 3-kinase essential for protein sorting to the vacuole in yeast." J Cell Biol **129**(2): 321-334.
Stack, J. H. and S. D. Emr (1994). "Vps34p required for yeast vacuolar protein sorting is a multiple specificity kinase that exhibits both protein kinase and phosphatidylinositol-specific PI 3-kinase activities." J Biol Chem **269**(50): 31552-31562.
Stahelin, R. V. (2009). "Lipid binding domains: more than simple lipid effectors." J Lipid Res **50 Suppl**: S299-304.
Stahelin, R. V., F. Long, et al. (2002). "Phosphatidylinositol 3-phosphate induces the membrane penetration of the FYVE domains of Vps27p and Hrs." J Biol Chem **277**(29): 26379-26388.
Stamnes, M. A. and J. E. Rothman (1993). "The binding of AP-1 clathrin adaptor particles to Golgi membranes requires ADP-ribosylation factor, a small GTP-binding protein." Cell **73**(5): 999-1005.
Stauffer, T. P., S. Ahn, et al. (1998). "Receptor-induced transient reduction in plasma membrane PtdIns(4,5)P2 concentration monitored in living cells." Curr Biol **8**(6): 343-346.

Stenmark, H., R. Aasland, et al. (2002). "The phosphatidylinositol 3-phosphate-binding FYVE finger." FEBS Lett **513**(1): 77-84.
Stolz, L. E., W. J. Kuo, et al. (1998). "INP51, a yeast inositol polyphosphate 5-phosphatase required for phosphatidylinositol 4,5-bisphosphate homeostasis and whose absence confers a cold-resistant phenotype." J Biol Chem **273**(19): 11852-11861.
Strachan, T. and A. P. Read (1999).
Stringer, D. K. and R. C. Piper "A single ubiquitin is sufficient for cargo protein entry into MVBs in the absence of ESCRT ubiquitination." J Cell Biol **192**(2): 229-242.
Stromhaug, P. E., F. Reggiori, et al. (2004). "Atg21 is a phosphoinositide binding protein required for efficient lipidation and localization of Atg8 during uptake of aminopeptidase I by selective autophagy." Mol Biol Cell **15**(8): 3553-3566.
Stroupe, C., K. M. Collins, et al. (2006). "Purification of active HOPS complex reveals its affinities for phosphoinositides and the SNARE Vam7p." EMBO J **25**(8): 1579-1589.
Takenawa, T. and T. Itoh (2001). "Phosphoinositides, key molecules for regulation of actin cytoskeletal organization and membrane traffic from the plasma membrane." Biochim Biophys Acta **1533**(3): 190-206.
Takenawa, T. and T. Itoh (2006). "Membrane targeting and remodeling through phosphoinositide-binding domains." IUBMB Life **58**(5-6): 296-303.
Tanemura, M., A. Saga, et al. (2009). "Rapamycin induces autophagy in islets: relevance in islet transplantation." Transplant Proc **41**(1): 334-338.
Thorngren, N., K. M. Collins, et al. (2004). "A soluble SNARE drives rapid docking, bypassing ATP and Sec17/18p for vacuole fusion." Embo J **23**(14): 2765-2776.
Vanhaesebroeck, B. and M. D. Waterfield (1999). "Signaling by distinct classes of phosphoinositide 3-kinases." Exp Cell Res **253**(1): 239-254.
Vazquez, F., S. R. Grossman, et al. (2001). "Phosphorylation of the PTEN tail acts as an inhibitory switch by preventing its recruitment into a protein complex." J Biol Chem **276**(52): 48627-48630.
Vazquez, F., S. Ramaswamy, et al. (2000). "Phosphorylation of the PTEN tail regulates protein stability and function." Mol Cell Biol **20**(14): 5010-5018.
Vazquez, F. and W. R. Sellers (2000). "The PTEN tumor suppressor protein: an antagonist of phosphoinositide 3-kinase signaling." Biochim Biophys Acta **1470**(1): M21-35.
Vida, T. A. and S. D. Emr (1995). "A new vital stain for visualizing vacuolar membrane dynamics and endocytosis in yeast." J Cell Biol **128**(5): 779-792.
Vieira, O. V., R. J. Botelho, et al. (2001). "Distinct roles of class I and class III phosphatidylinositol 3-kinases in phagosome formation and maturation." J Cell Biol **155**(1): 19-25.
Volinia, S., R. Dhand, et al. (1995). "A human phosphatidylinositol 3-kinase complex related to the yeast Vps34p-Vps15p protein sorting system." EMBO J **14**(14): 3339-3348.
Wada, T., T. Sasaoka, et al. (2001). "Overexpression of SH2-containing inositol phosphatase 2 results in negative regulation of insulin-induced metabolic actions in 3T3-L1 adipocytes via its 5'-phosphatase catalytic activity." Mol Cell Biol **21**(5): 1633-1646.
Walker, D. H., N. Dougherty, et al. (1988). "Purification and characterization of a phosphatidylinositol kinase from A431 cells." Biochemistry **27**(17): 6504-6511.
Walker, D. M., S. Urbe, et al. (2001). "Characterization of MTMR3. an inositol lipid 3-phosphatase with novel substrate specificity." Curr Biol **11**(20): 1600-1605.
Warrens, A. N., M. D. Jones, et al. (1997). "Splicing by overlap extension by PCR using asymmetric amplification: an improved technique for the generation of hybrid proteins of immunological interest." Gene **186**(1): 29-35.
Weiss, P., S. Huppert, et al. (2009). "Analysis of the dual function of the ESCRT-III protein Snf7 in endocytic trafficking and in gene expression." Biochem J **424**(1): 89-97.
Welch, H. C., W. J. Coadwell, et al. (2003). "Phosphoinositide 3-kinase-dependent activation of Rac." FEBS Lett **546**(1): 93-97.
Wemmer, M., I. Azmi, et al. "Bro1 binding to Snf7 regulates ESCRT-III membrane scission activity in yeast." J Cell Biol **192**(2): 295-306.
Whitley, P., B. J. Reaves, et al. (2003). "Identification of mammalian Vps24p as an effector of phosphatidylinositol 3,5-bisphosphate-dependent endosome compartmentalization." J Biol Chem **278**(40): 38786-38795.
Whitman, M., C. P. Downes, et al. (1988). "Type I phosphatidylinositol kinase makes a novel inositol phospholipid, phosphatidylinositol-3-phosphate." Nature **332**(6165): 644-646.

Whitters, E. A., A. E. Cleves, et al. (1993). "SAC1p is an integral membrane protein that influences the cellular requirement for phospholipid transfer protein function and inositol in yeast." J Cell Biol **122**(1): 79-94.
Wickner, W. and A. Haas (2000). "Yeast homotypic vacuole fusion: a window on organelle trafficking mechanisms." Annu Rev Biochem **69**: 247-275.
Wiradjaja, F., L. M. Ooms, et al. (2007). "Inactivation of the phosphoinositide phosphatases Sac1p and Inp54p leads to accumulation of phosphatidylinositol 4,5-bisphosphate on vacuole membranes and vacuolar fusion defects." J Biol Chem **282**(22): 16295-16307.
Workman, P., P. A. Clarke, et al. (2010). "Drugging the PI3 kinome: from chemical tools to drugs in the clinic." Cancer Res **70**(6): 2146-2157.
Wurmser, A. E., J. D. Gary, et al. (1999). "Phosphoinositide 3-kinases and their FYVE domain-containing effectors as regulators of vacuolar/lysosomal membrane trafficking pathways." J Biol Chem **274**(14): 9129-9132.
Wymann, M. P. and R. Schneiter (2008). "Lipid signalling in disease." Nat Rev Mol Cell Biol **9**(2): 162-176.
Xiong, Y., A. L. Contento, et al. (2005). "AtATG18a is required for the formation of autophagosomes during nutrient stress and senescence in Arabidopsis thaliana." Plant J **42**(4): 535-546.
Xu, H. and W. Wickner (2010). "Phosphoinositides function asymmetrically for membrane fusion, promoting tethering and 3Q-SNARE subcomplex assembly." J Biol Chem **285**(50): 39359-39365.
Yamamoto, A., D. B. DeWald, et al. (1995). "Novel PI(4)P 5-kinase homologue, Fab1p, essential for normal vacuole function and morphology in yeast." Mol Biol Cell **6**(5): 525-539.
Yamamoto, A., Y. Tagawa, et al. (1998). "Bafilomycin A1 prevents maturation of autophagic vacuoles by inhibiting fusion between autophagosomes and lysosomes in rat hepatoma cell line, H-4-II-E cells." Cell Struct Funct **23**(1): 33-42.
Yap, T. A., M. D. Garrett, et al. (2008). "Targeting the PI3K-AKT-mTOR pathway: progress, pitfalls, and promises." Curr Opin Pharmacol **8**(4): 393-412.
Yu, J. W. and M. A. Lemmon (2001). "All phox homology (PX) domains from Saccharomyces cerevisiae specifically recognize phosphatidylinositol 3-phosphate." J Biol Chem **276**(47): 44179-44184.
Zhang, X., X. Li, et al. "Phosphoinositide isoforms determine compartment-specific ion channel activity." Proc Natl Acad Sci U S A **109**(28): 11384-11389.
Zhong, Q., C. S. Lazar, et al. (2002). "Endosomal localization and function of sorting nexin 1." Proc Natl Acad Sci U S A **99**(10): 6767-6772.
Zhong, S., F. Hsu, et al. (2012). "Allosteric activation of the phosphoinositide phosphatase Sac1 by anionic phospholipids." Biochemistry **51**(15): 3170-3177.
Zieger, M. and A. Mayer "Yeast vacuoles fragment in an asymmetrical two-phase process with distinct protein requirements." Mol Biol Cell **23**(17): 3438-3449.
Zoncu, R., R. M. Perera, et al. (2009). "A phosphoinositide switch controls the maturation and signaling properties of APPL endosomes." Cell **136**(6): 1110-1121.